A proteomic investigation into the mechanisms of VEGF-adhesion crosstalk in endothelial cells.

A thesis submitted to the University of Manchester for the degree of Doctor of Philosophy in the Faculty of Biology, Medicine and Health

2017

Jenny A. James

School of Medical Sciences
Division of Cardiovascular Sciences

Contents

Word count: 51,511

List of Figures

List of Tables

Abstract

Adhesion of cells to the surrounding extra cellular matrix (ECM) is primarily mediated by integrin cell surface receptors, which mechanically link the ECM and actin cytoskeleton, enabling the positioning of cells within tissues. Upon integrin-ECM binding, signalling and adaptor proteins are recruited, leading to the formation of intracellular integrin adhesion complexes (IACs). These complexes and resulting integrin signalling pathways coordinate their activity with growth factor receptors and associated signalling pathways, regulating downstream processes such as adhesion, migration and proliferation. One example of crosstalk between growth factor and integrin mediated adhesion involves vascular endothelial growth factor (VEGF) in endothelial cells (ECs), and contributes to angiogenesis, the formation of new blood vessels from pre-existing vasculature. A better understanding of the factors and mechanisms involved in VEGF-adhesion crosstalk would enhance understanding of vascular development, and highlight ways that therapeutics can be used to treat angiogenic associated disorders.

The aim of this project was to identify mediators of VEGF-adhesion crosstalk in ECs. Initially, a protocol for human umbilical vein endothelial cell (HUVEC) IAC enrichment was optimised. Briefly, HUVECs were plated on fibronectin for two hours to allow IAC formation, followed by crosslinking to stabilise IACs, cell body removal, and collection of remaining IACs. Mass spectrometric analyses of enriched IACs defined, for the first time, the HUVEC IAC composition, a network of 297 proteins. This dataset was comparable to previously reported IAC composition datasets, confirming successful identification of IAC components. HUVEC IACs were then enriched following VEGF treatment, and proteomic analysis revealed that the abundance of only 1% of proteins changed ≥two-fold. A complementary phosphoproteomic strategy was adopted to analyse changes in protein phosphorylation within adhesion complexes following VEGF treatment. Phosphoproteomic analysis of VEGF-induced enriched IAC and total cell lysate samples revealed that over 18% of HUVEC IAC phosphopeptides identified changed greater that ≥two-fold. Together, these data suggested that, while adhesion complex composition remains largely unchanged during VEGF-adhesion crosstalk, changes and signalling events occur mainly through phosphorylation. From these proteomic and phosphoproteomic datasets, a range of protein-protein interaction networks were constructed, statistical analyses employed, and detailed kinase prediction analysis performed. A range of proteins were highlighted as potentially important in VEGF-adhesion crosstalk, including a role for Src kinase-mediated protein phosphorylation. To investigate a role for Src kinase, VEGF-induced migration assays were performed; Src and FAK inhibition reduced VEGF-induced migration of FN-plated HUVECs, with combined kinase inhibition showing greater effects.

This study presents one of the first to (1) perform a global proteomic analysis of EC IACs, and (2) investigate VEGF-adhesion crosstalk mechanisms using proteomic and phosphoproteomic workflows. The datasets derived in this study contain a great deal of information, which has been used here to define the HUVEC IAC protein composition and identify candidates that may contribute to VEGF-adhesion crosstalk. For example, Src kinase has been highlighted as a potential mediator of crosstalk, and future studies leading from this data may aid discovery of associated therapeutic targets. This study has the potential to provide a base for many future studies; for example there is unlimited potential for candidate selection and follow-up studies to be performed following on from the proteomic datasets generated here.

Declaration

No portion of the work referred to in the thesis has been submitted in support of an application for another degree or qualification of this or any other university or other institute of learning.

Copyright Statement

Acknowledgements

I would like to thank my supervisor, Professor Martin Humphries, for giving me the opportunity to work with his lab group, for the freedom to embark on my own project and for support and advice throughout my PhD. I would also like to thank my co-supervisor Professor Ann Canfield for advice and support throughout the project.

Thanks also go to my advisors Professor Catherine Kielty and Dr. Chiara Francavilla for their helpful advice and discussions, and Dr. Elizabeth Cartwright for genuine interest and support as PhD programme director.

I would also like to thank members of the Biological Mass Spectrometry facility, Dr. David Knight, Dr. Stacey Warwood for being available for advice, and for technical support regarding proteomic and phosphoproteomic mass spectrometry experiments and Julian Selley for bioinformatics support.

I would like to thank everyone I have worked with in the Humphries, Caswell and Lennon labs for their scientific advice and support, making the lab an enjoyable place to work, and providing a continuous supply of treats. Special appreciation and thanks also go to Dr. Jonathan Humphries for being available for discussion, help and advice whenever needed, and for thorough comments on the thesis.

I would like to thank the other students enrolled on the BHF PhD programme, in particular my friends Amy, Claire, Sophie and Tom for all the fun activities from day 1.

I also would like to thank my family and friends at home for their support and encouragement throughout my time at Manchester. Finally, I would like to thank Chris for always being there for me, for moving to Manchester with me, and for continued comments, support and guidance throughout my PhD and career.

The work referred to in this thesis was supported by the British Heart Foundation.

Abbreviations

ACN: Acetonitrile
AEBSF: 4-(2-aminoethyl)benzenesulfonylfluoride hydrochloride
AKT/PKB: Protein kinase B
AMBIC: Ammonium bicarbonate (NH_4HCO_3)
BAK: Bcl2-Antagonist/Killer
BCA: Bicinchoninic acid
BSA: Bovine serum albumin
CA: Consensus adhesome
Col: Collage- I
DAPI: 4',6-diamidino-2-phenylindole
DAVID: Database for Annotation, Visualisation and Integrated Discovery
DMEM: Dulbecco's modified Eagle's medium
DMEM-H: DMEM containing 25mM HEPES, 4.5mg/ml glucose, L-glutamine
DMSO: dimethyl sulfoxide
DOKR: Downstream of kinase related protein
DTBP: Dimethyl-3,3'dithiobispropionimidate 2HCl
DTT: Dithiothrietol
EC: Endothelial cell
ECM: Extra cellular matrix
EDTA: Ethylenediaminetetraacetic acid
EGF: Epidermal like growth factor
eNOS: Endothelial nitric oxide synthase
Erk: Extracellular signal–regulated kinase
ETS1: A transducer of proteolytic enzymes
FA: Formic acid
FAK: Focal adhesion kinase
FC: Flow cytometry
FCS: Foetal calf serum
FDA: Food and drug administration
FGF-2: Basic-FGF
FGF: Fibroblast growth factor
FGFR: Fibroblast growth factor receptor
FITC: fluorescein isothiocyanate
FN: Fibronectin
FRAP: fluorescence recovery after photobleaching
GIT: G protein-coupled receptor kinase-interacting target
Grb: Growth factor receptor-bound protein
GO: Gene ontology
HEPES: N-2-hydrozyethylpiperazine-N' 2-ethanesulphonic acid
HGF: Hepatocyte growth factor
HUVEC: Human umbilical vein endothelial cell
ILK: Integrin linked kinase
iTRAQ: isobaric tag for relative and absolute quantitation
kDa: Kilodalton
KEGG: Kyoto encyclopedia of genes and genomes

MARCKS: Myristoylated alanine-rich C-kinase substrate
MMP: Matrix metalloproteinase
Mol Wt: Molecular weight
IF: Immunofluorescence
IFNα/β/γ: Interferon-α, β and γ
IGF: Insulin like growth factor
IP-10: IFN-inducible protein-10
LASP1: LIM and SH3 protein 1
IL: Interleukin
LC: Liquid chromatography
LCA: Literature-curated adhesome
LC-MS/MS: Liquid chromatography coupled to tandem mass spectrometry
MA: Master adhesome
MAPK: Mitogen-activated protein kinase
MAKPAPK: MAPK-activated protein kinases
MEK: Mitogen-activated protein kinase kinase
MES: (2-N-morpholino)ethanesulfonic acid
MMP: Matrix metalloproteinases
Met: Hepatocyte growth factor receptor
MS: Mass spectrometry
MS/MS: tandem MS
NO: Nitric oxide
nSC: normalised spectral count
PAGE: Polyacrylamide gel electrophoresis
PBS-: Phosphate buffed saline without calcium and magnesium
PBS+: Phosphate buffered saline with 1mM calcium and 0.5mM magnesium
PDGF: Platelet-derived growth factor
PDGFR: Platelet-derived growth factor receptor
PFA: Paraformaldehyde
PKA: Protein kinase A
PKC: Protein kinase C
PL: Poly-D-Lysine
PLC: Phospholipase C
PKC: Protein kinase C
RGD: L-arginine-glycine-L-aspartic acid
PPM: parts per million
P13K: Phosphoinositide 3-kinase
RIPA: Radio-immunoprecipitation assay
Rpm: Revolutions per minute
SC: Spectral count
SDS: Sodium dodecylsulfate
SDS-PAGE: sodium dodecylsulphate-polyacrylamide gel electrophoresis
SFM: Serum free medium
SH2: Src homology 2
SILAC: stable isotope labelling with amino acids in cell culture
Sos: Son of sevenless

Stat5: Signal transducer and activator of transcription 5
TBST: Tris buffered saline with 0.01% tween
TCL: Total cell lysate
TFA: Trifluoroacetic acid
TFR: Transferrin receptor
TGF: Transforming growth factor
v: volume
VASP: vasodilator-stimulated phosphoprotein
VEGF: Vascular endothelial growth factor
VEGFR2: Vascular endothelial growth factor receptor-2
TiO_2: Titanium dioxidie
Ti-IMAC:
IMAC: Immobilised metal affinity chromatography
w: weight
WB: Western blot

Chapter 1: Introduction

1.1 Summary

Cell adhesion is essential for tissue formation and repair in multicellular life. Adhesion of cells to the surrounding extra cellular matrix (ECM) enables physical linking and positioning of cells within tissues. This link is primarily mediated by integrin cell surface receptors, which mechanically link the ECM and actin cytoskeleton (Byron et al. 2010;Hynes 1992). Upon integrin-ECM binding, signalling and adaptor proteins are recruited to the integrin cytoplasmic domain, leading to the formation of intracellular integrin adhesion complexes (IACs), (Brakebusch and Fässler 2003). These complexes and resulting integrin signalling pathways coordinate their activity with growth factor receptors and associated signalling pathways, regulating downstream processes such as cell adhesion, migration and proliferation. This crosstalk contributes to the maintenance of health and so, dysregulation can cause problems with associated biological functions, and often lead to disease (Eliceiri 2001;Streuli and Akhtar 2009).

One example of crosstalk between growth factor and integrin mediated adhesion involves vascular endothelial growth factor (VEGF) in endothelial cells (ECs), and contributes to angiogenesis, the formation of new blood vessels from pre-existing vasculature (Eliceiri 2001). To initiate angiogenesis, ECs are stimulated with growth factors, such as VEGF, initiating degradation of the surrounding ECM and formation of a provisional fibronectin-rich matrix. This allows ECs to proliferate and migrate, until they eventually form a stable blood vessel (Kalluri 2003). The angiogenic process is therefore mediated by growth factors, changes in surrounding ECM composition and hence, cell-ECM adhesion. Disrupted EC adhesion therefore has multiple associations with angiogenesis related disorders, such as cancer, atherosclerosis and macular degeneration (Folkman 2006).

Integrins and integrin ECM ligands influence angiogenesis in different ways. There is clear evidence indicating fibronectin-mediated integrin signalling, in part through coordinated VEGF activity, contribute to processes such as cell migration and proliferation, and hence angiogenesis (Kumar et al. 2012). Despite the apparent importance of this crosstalk, the mechanism by which fibronectin-induced integrin adhesion complexes and VEGF signalling coordinate their activities is largely unknown. Elucidating these mechanisms would improve overall understanding of the factors and mechanisms involved, would lead to a better understanding of vascular development as a whole, and highlight ways that therapeutics can be used to treat angiogenic associated diseases.

Integrin adhesion complex protein composition, collectively known as the ‘adhesome’, has been relatively well studied. Initially a literature-curated integrin adhesome (LCA) was compiled through scholarly analysis of proteins that localise to adhesions (Zaidel-Bar et al. 2007;Winograd-Katz et al.

2014). Complementary to this analysis, several laboratories have performed biochemical isolation of adhesion complexes, and subsequent mass spectrometry based analysis to determine their composition (Horton et al. 2015). However, the molecular composition of the EC adhesion is only recently starting to emerge (Atkinson et al. 2017), and a global unbiased study of EC adhesion-growth factor crosstalk is lacking. Biochemical isolation of EC adhesion complexes following growth factor stimulation, and subsequent proteomic analysis will provide an insight into the mechanisms of adhesion-growth factor receptor crosstalk. A better understanding of the factors and mechanisms involved would enhance understanding of vascular development, and highlight ways that therapeutics can be used to treat angiogenic associated disorders.

1.2 Cell adhesion

Cell adhesion, the attachment of cells to neighbouring cells or underlying ECM, via specialized multi-protein adhesive structures, is essential for tissue formation and repair in multicellular life (Byron et al. 2010;Hynes 1999). Cell adhesion is primarily mediated by families of cell surface adhesion receptors, including cadherins, immunoglobulins, selectins, syndecans and integrins, which enable linkage to neighbouring cells or ECM ligands (Juliano 2002;Morgan et al. 2007). This linkage of cells to the surrounding ECM permits their positioning within tissues (Brakebusch and Fässler 2003). Cell-ECM adhesion is primarily mediated via the integrin receptors, which upon ECM binding, recruit signalling and adaptor proteins to the integrin cytoplasmic domain, leading to the formation of intracellular adhesion complexes which can mediate adhesion signalling events. These complexes are termed integrin adhesion complexes (IACs); multimolecular structures that link integrins to the actin cytoskeleton, and contain over 200 reported components (Zaidel-Bar et al. 2007;Winograd-Katz et al. 2014;Horton et al. 2015;Horton et al. 2016a). Regulation of cell adhesion and associated signalling is fundamental to a range of developmental and pathological processes, and to understand the mechanisms that lead to disease in full, further insights into cell adhesion biology are essential.

1.2.1 Integrin adhesion receptors

Integrins are heterodimers, each containing one α and one β subunit. In mammals, 24 heterodimer combinations have been identified, formed via selective pairing of 18 α and eight β subunits (figure 1.1), (Humphries et al. 2006). The heterodimeric combination formed at the cell surface determines ligand specificity. These integrin heterodimers and can be divided into multiple classes depending on the mechanism of ligand binding. These include the Arg-Gly-Asp (RGD) binding, LDV binding, non-A-domain-containing β1 laminin-binding and the αA-domain-containing collagen-binding integrins. Most integrin heterodimers recognise several ligands. Likewise, many ECM components and cell surface adhesion proteins bind multiple integrin heterodimers, giving rise to numerous integrin-ligand combinations (figure 1.1) (Humphries et al. 2006;Hynes 2002a). For example, the

ECM proteins fibronectin and vitronectin contain an RGD peptide recognition motif, which is recognised by the RGD-binding integrins and collagen receptors with inserted I/A domains (α1, α2, α10, α11) bind collagens and laminins (Humphries et al. 2006;Hynes 2002a). On the cytoplasmic side of the membrane, the β-subunit cytoplasmic tail acts mainly as a binding site for intracellular adaptor proteins, which mediate integrin function and downstream signalling (Avraamides et al. 2008;Legate and Fässler 2009).

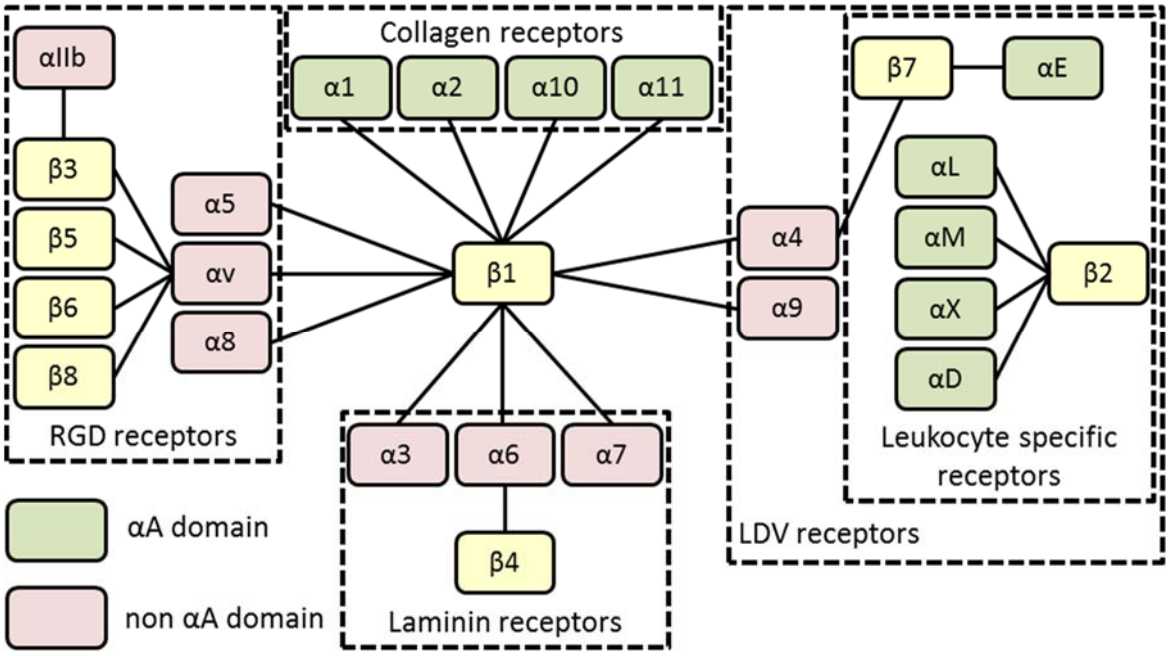

Figure 1.1. Integrin αβ heterodimer combinations. In mammals, 24 integrin heterodimer combinations have been identified, formed via selective pairing of 18 α and 8 β subunits. The heterodimeric combination formed at the cell surface determines ligand specificity. These heterodimers can be divided into multiple classes depending on the mechanism of ligand binding. These include the Arg-Gly-Asp (RGD), LDV, αA-domain-containing β1 collagen binding and the non-αA-domain containing laminin binding integrins. The αA-domain-containing integrins can bind both ECM proteins and Ig-superfamily cell surface receptors such as VCAM-1. α-subunits are coloured according to structural differences in the α-integrin subunit ligand binding region (green- αA-domain-containing integrins, pink- non-αA-domain-containing integrins). Figure adapted from Hynes, 2002 and Humphries et al., 2006.

Integrins link the ECM to the actin cytoskeleton, mediating bi-directional communication between the ECM and the cell interior. Integrins on the cell surface are conformationally regulated, and can be present in both 'inactive' and 'active' conformations (1.2a), (Luo and Springer 2006;Askari et al. 2009;Askari et al. 2010). In the most inactive form, which can be stabilised by binding of integrin inactivators, integrins are bent and have low affinity for their ligand (Pouwels et al. 2012). Unbending and elongation occurs following activation, which enables the head group to bind available ligands, and separation of cytoplasmic tail domains which allows interaction with intracellular proteins and activators. Integrins can be activated in two directions: by interaction of

intracellular proteins with the cytoplasmic domain (inside-out signalling), and ligand binding from the outside (outside-in signalling, figure 1.2) (Askari et al. 2009;Anthis and Campbell 2011).

During inside-out signalling, protein binding to the intracellular domain stabilises conformational changes in the head domain, regulating extracellular ligand affinity, and hence cell adhesion to the ECM. Integrin-ligand binding during outside-in signalling stabilises the active, high ligand affinity conformation, which induces integrin clustering, and recruitment of signalling and adaptor proteins to the cytoplasmic tails (Askari et al. 2009;Hu and Luo 2013). Adaptor proteins are first recruited to integrin cytoplasmic tails, and can provide a direct link to the actin cytoskeleton, for example via talin, a key integrin activator (Tadokoro et al. 2003;Anthis and Campbell 2011). A further layer of adaptor molecules strengthen these links, for example, talin interacts with vinculin, which also binds to actin (Zaidel-Bar and Geiger 2010;Zaidel-Bar et al. 2007). Signalling proteins are also recruited, either directly to the integrin tail or to associated proteins, and regulate the adhesion site itself, or feed into adhesion signalling pathways. For example kinases such as focal adhesion kinase (FAK) and Src are recruited and activated, leading to further recruitment, phosphorylation and activation of a range of adhesion associated proteins (figure 1.2), (Hu and Luo 2013;Zaidel-Bar and Geiger 2010). The protein complexes formed following integrin-ECM engagement are termed integrin adhesion complexes (IACs). Overall, it is regulation of protein recruitment to integrin adhesion sites, resulting intracellular changes such as phosphorylation, and activation of associated signalling components and pathways, which influences processes such as adhesion signalling, cell adhesion, migration, and proliferation (Vachon 2011;Stupack and Cheresh 2004;Cheresh and Stupack 2002).

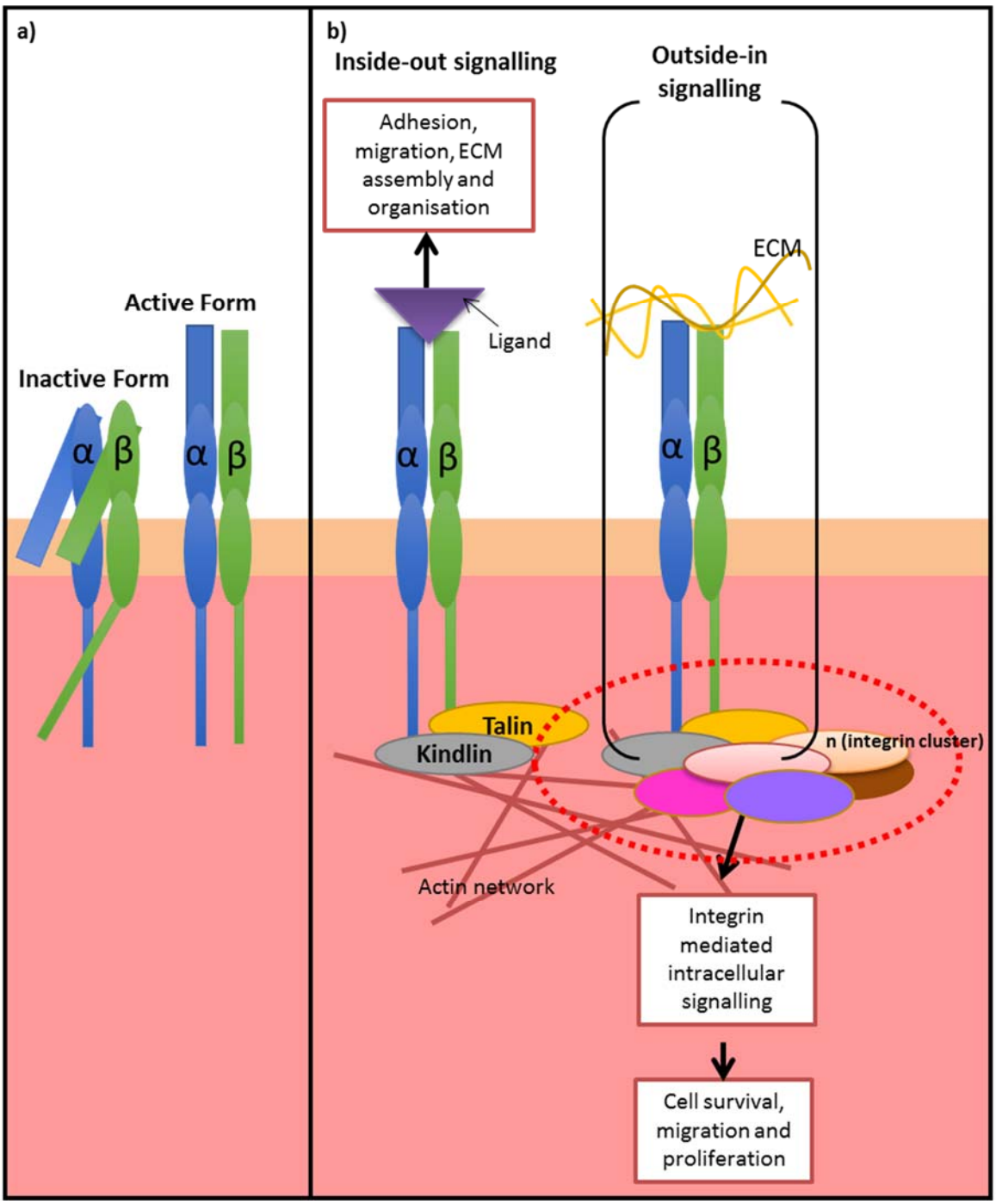

Figure 1.2. (a) Integrin activation states and (b) signalling mechanisms. (a) Low affinity or 'inactive' conformation integrins have their head group bent close to the cell membrane and their cytoplasmic tails closely associated. Unbending and elongation occurs following activation, which enables (1) the head group to bind available ligands, and (2) separation of the dimer cytoplasmic domains, allowing interaction with intracellular proteins and formation of adhesion complexes (Cheresh and Stupack 2002;Mould and Humphries 2004). (b) Signalling via 'inside-out 'mechanisms occurs when the intracellular activator talin and/or kindlin binds to the β subunit, cytoplasmic domain. This binding causes an increased affinity of the head domain for extracellular ligands, and so promotes ligand binding. Integrin-ECM ligand binding initiates 'outside-in' signalling. Binding leads to integrin clustering, activation of integrin mediated signalling cascades and formation of intracellular integrin adhesion complexes. (Cheresh and Stupack 2002;Geiger and Zaidel-Bar 2012;Calderwood et al. 2013). Figure adapted from Mas-Moruno, Rechenmacher et al.

1.2.2 Integrin adhesion complex composition

The integrin-cytoskeleton connection is dynamic, meaning IACs undergo continuous maturation, which involves both growth and compositional change, to modulate integrin signalling (Kuo et al. 2011;Morse et al. 2014). IACs are characterised by their size, location and lifetime. Classes include nascent adhesions, focal complexes, focal adhesions, fibrillar adhesions, invadopodia and podosomes. Each has a diverse role in processes such as adhesion-mediated signalling and cell migration. Nascent adhesions are the smallest structures seen in membrane lamellipodial protrusions, with a rapid rate of turnover (Sun et al. 2014). Fibrillar adhesions are more centrally located within the cell, mainly associated with fibronectin fibres, and when compared to focal adhesions have less mechanosensitivity. Focal adhesions are the best characterised class; they are fairly stable with a typical lifespan of over 10 minutes. Focal adhesions act as platforms for integrin signalling, strong anchors for actin linkage, and allow strong attachments to ECM substrates (Winograd-Katz et al. 2014;Geiger and Yamada 2011). Podosomes and invadopodia, have characteristics in common with focal adhesions, although degrade the ECM at membrane protrusions in invasive cells (Block et al. 2008).

The 3D molecular organisation of IACs has been investigated using super-resolution microscopy (Kanchanawong et al. 2010), which revealed a stratified localisation of adhesion proteins. This approach resulted in a model in which integrin cytoplasmic tails are positioned close to the plasma membrane, with signalling related proteins (e.g. FAK and paxillin) in an adjacent layer. The next, force regulatory layer, contains force-transducing adaptor proteins such as vinculin. The final layer overlaps with actin and contains actin regulators such as α-actinin, zyxin and vasodilator-stimulated phosphoprotein (VASP). Others studies using fluorescence cross-correlation spectroscopy and fluorescence recovery after photo bleaching (FRAP) to investigate IAC components suggest that some parts of the complex may pre-assemble in the cytoplasm prior to exchange with IACs (Hoffmann et al. 2014). Together, these studies demonstrate that high-resolution imaging methods can be used to gain insights into adhesion complex molecular structure.

In addition to the use of imaging methods to study IAC structure, literature-based analyses have been used to define the protein composition of IACs, termed ‘the adhesome’. Through extensive literature curation, this network has been defined, and redefined, consisting of all proteins that have been reported to locate to, or regulate, the adhesion complex. Over 200 proteins have been reported in the ‘literature-curated adhesome’ (LCA), comprising at least 742 interactions. Data used to compile this list of proteins comes from multiple adhesion classes and cell types (figure 1.3), (Zaidel-Bar et al. 2007;Winograd-Katz et al. 2014;Desgrosellier and Cheresh 2010;Kalluri 2003;Horton et al. 2016a).

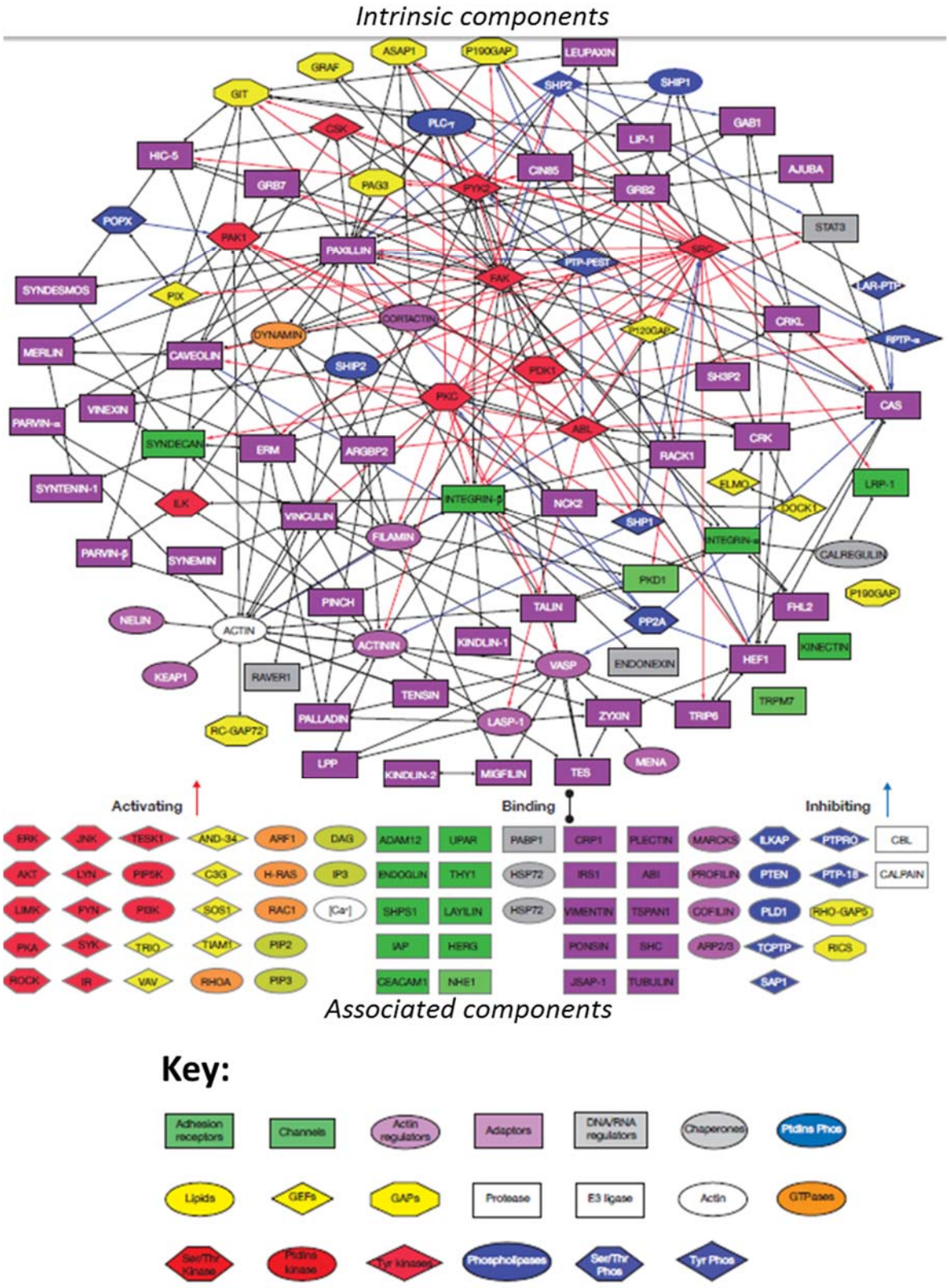

Figure 1.3. Literature-curated adhesome (LCA). A protein-protein interaction network of the known integrin-mediated adhesion complexes proteins, generated from an extensive literature search. The compiled literature-curated adhesome consists of 90 proteins that reside within the adhesion site, and a further 66 peripherally associated components. The network shows 690 links, which represents 213 directional activation interactions, 379 non-directional binding interactions, and 98 directional inhibitory interactions. Figure adapted from Zaidel-Bar 2007.

1.2.3 Proteomic analysis of integrin adhesion complex composition

Recently, several laboratories have developed protocols that allow enrichment of IAC proteins and subsequent proteomic analysis (Jones et al. 2015;Kuo et al. 2012;Schiller et al. 2011). Before this, mass spectrometry-based studies to analyse adhesion complex composition had been difficult due to problems associated with the instability and inaccessibility of such membrane-bound receptor complexes. The successful methods involve chemical crosslinking of cells to stabilise IACs and enrichment of IAC components by removal of the cell body and cytoplasmic proteins (Jones et al. 2015;Zaidel-Bar and Geiger 2010). Since development of these protocols, mass spectrometry has been used to identify IAC compositions for several cell types under a variety of culture conditions (Byron et al. 2012;Robertson et al. 2015;Ng et al. 2014;Kuo et al. 2011;Huang et al. 2014;Schiller and Fässler 2013;Schiller et al. 2011) .

Multiple proteomic datasets have been generated using a variety of different methods developed for IAC isolation. A 'meta adhesome' has been compiled, containing all proteins detected in seven of these datasets (2419 proteins), thereby providing an overview of all proteins that have been identified by this approach (Horton et al. 2015). These seven datasets were generated from mass spectrometry analysis of adhesion complex isolations using different cell types spread on fibronectin. As a further analysis of these datasets, a consensus adhesome has been put together, which includes adhesome components seen most robustly in adhesion complex datasets. This dataset includes 60 proteins, which are those seen in at least five out of seven selected IAC mass spectrometry datasets, thereby identifying 'essential' components that are nearly always found at adhesion sites, independent of cell type or conditions (Horton et al. 2015). Recently, further analysis integrating the consensus and literature-curated adhesomes was performed, resulting in an IAC network which comprises four broad signalling and actin-bridging axes (figure 1.4), (Horton et al. 2015;Horton et al. 2016a). This analysis aids interpretation of the mechanisms regulating IAC signalling (Horton et al. 2016a). Adhesion complex composition varies depending on cell type, integrin expression and the matrix protein that is engaged, meaning that not all identified components are expected to be at adhesion sites at any one time. In addition, only a limited number of cell types have been used for these analyses, indicating that that compiling data from other cell types may highlight further components, functions and cell type specificity of IACs. Together, these studies highlight the complexity of adhesion complex composition and function, and indicate that adhesion complexes may mediate multiple cellular processes.

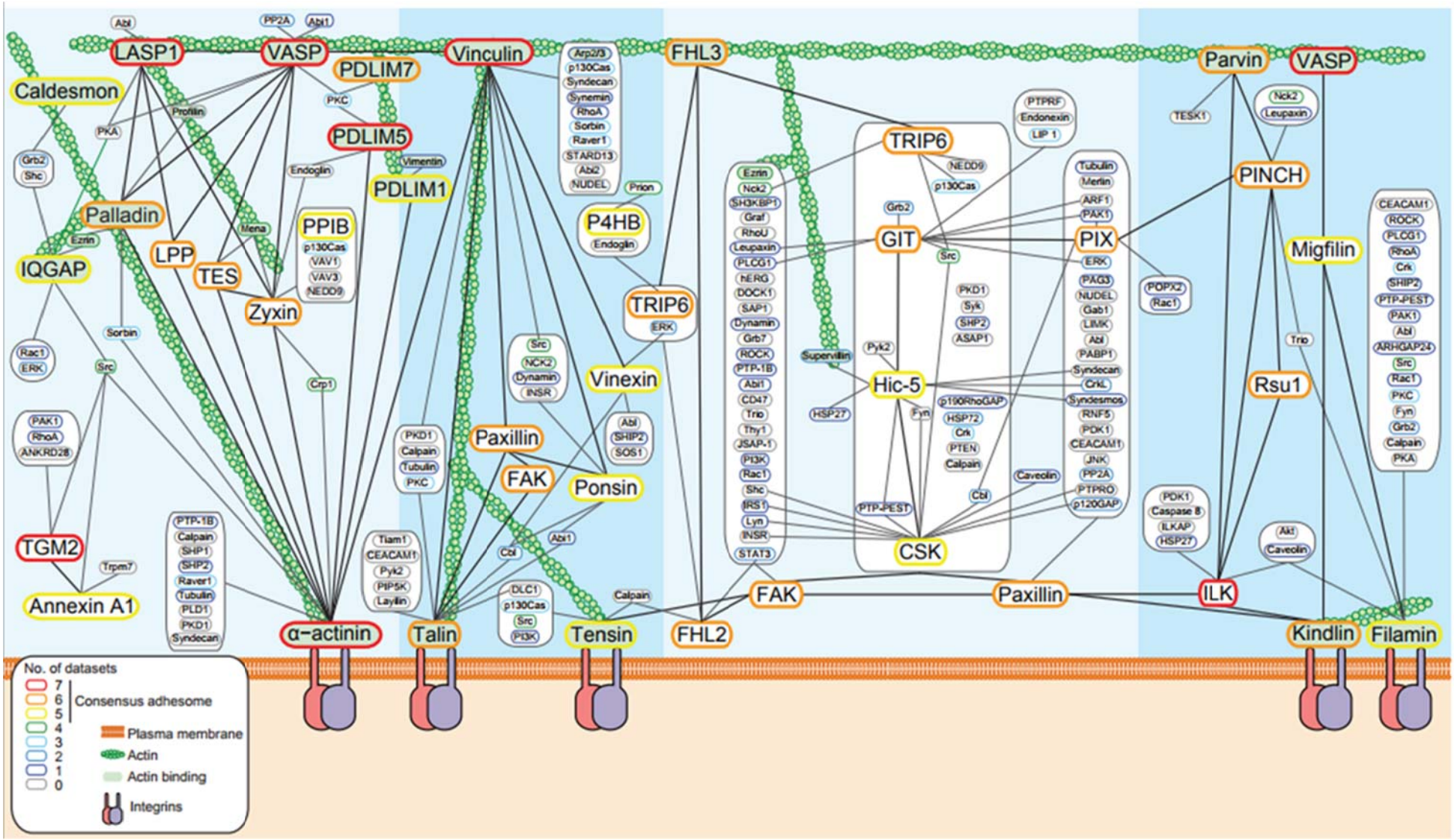

Figure 1.4. The integrin adhesome network at a glance. Protein-protein interaction network displaying the consensus adhesome integrated with the literature-curated adhesome. Figure adapted from Horton et al. (2016a).

1.2.4 Phosphoproteomic analysis of integrin adhesion complex composition

Phosphorylation plays critical roles in cellular responses and signalling pathways initiated by external stimuli, with a particular importance in integrin-mediated signalling and cell adhesion. Therefore, many kinases and phosphatases play important roles in integrin-mediated signalling. For example, phosphorylation of individual adhesion complex proteins, often in the context of integrin signalling, can be responsible for regulating cell behaviour in response to cell adhesion (Zaidel-Bar and Geiger 2010;Robertson et al. 2015). The key role played by phosphorylation in adhesion signalling is supported by data from a combination of studies. For example, multiple kinases and phosphatases localise to sites of IACs (Horton et al. 2015;Zaidel-Bar et al. 2007), and a high abundance of tyrosine phosphorylation is observed within adhesion complexes (Robertson et al. 2015;Zamir et al. 1999). Recent evidence also suggests that these kinase-dependent signals can propagate through IACs without gross changes in their protein composition (Horton et al. 2016b). These results indicate a separation between IAC composition and phosphorylation signalling, suggesting that altered dynamics of IAC signalling components mediates the relay of signalling through IACs (Horton et al. 2016b).

Protocols for global analyses of phosphorylation within IACs have recently been developed and performed using phosphoproteomics in human melanoma cells (Robertson et al. 2015;Robertson et al. 2017). The phosphoproteomic dataset produced in this Robertson et al. (2015) study was compared with components identified using proteomics, and contained a high number of adhesion complex proteins not identified by proteomic analysis of the corresponding samples. These data indicate that phosphoproteomic analysis of adhesion complex samples, alongside total protein proteomics, provides a more comprehensive and representative coverage of adhesion components than is possible by only proteomics (Robertson et al. 2015). In addition, follow up analysis performed as a result of this phosphoproteomic data highlighted an important role for phosphorylation events mediated by kinases such at CDK1, which are unlikely to be detected by proteomic studies alone (Robertson et al. 2015). Therefore, phosphoproteomics is an important tool, and may be used alongside proteomic approaches to address questions associated with phosphorylation signalling in IACs.

1.3 Adhesion-growth factor signalling crosstalk

Integrin-mediated cell adhesion and signalling is essential for tissue formation and repair. In addition to these integrin-mediated processes, growth factors can play an important role in integrin-dependent downstream processes. The integrin and growth factor receptor signalling systems are often studied as single systems which independently propagate signals. However, previous studies have shown that IACs and integrin signalling coordinate their activity with growth factor receptors and their associated signalling pathways (Eberwein et al. 2015;Streuli and Akhtar

2009;Eliceiri 2001;Tugues et al. 2013). Growth factor and integrin receptors recruit multiple proteins, constructing multi-layered signalling complexes (figure 1.5). Many factors can influence the cellular response to integrin-ligand binding, for example signal duration and strength, receptor expression, and feedback loops which may regulate the activity of multiple phosphatases and kinases (Schlessinger 2000). Crosstalk between adhesion and growth factor signalling may occur at multiple stages of these pathways, and at different cellular locations, affecting multiple downstream processes. This crosstalk is evident in a variety of cell types, regulating multiple signalling pathways. For example, specific ECM ligand-mediated IACs are a requirement for optimal signalling to epidermal growth factor (EGF), platelet-derived growth factor (PDGF), insulin, or VEGF (Eliceiri 2001). This synergy goes on to regulate downstream processes such as cell adhesion, migration and proliferation. The mechanisms by which this crosstalk occurs are poorly understood. Studying the synergy between integrin and growth factor receptor pathways will provide insights into these mechanisms, and how they contribute to cellular processes such as cell proliferation, adhesion, and migration (Eliceiri 2001). One example of crosstalk between growth factor- and integrin-mediated adhesion is the effects of VEGF in ECs: details of a selection of adhesion proteins involved in this crosstalk and associated phosphorylation events are shown in table 1.1. This crosstalk contributes to angiogenesis, the formation of new blood vessels from pre-existing vasculature, and will be discussed in detail in the following sections.

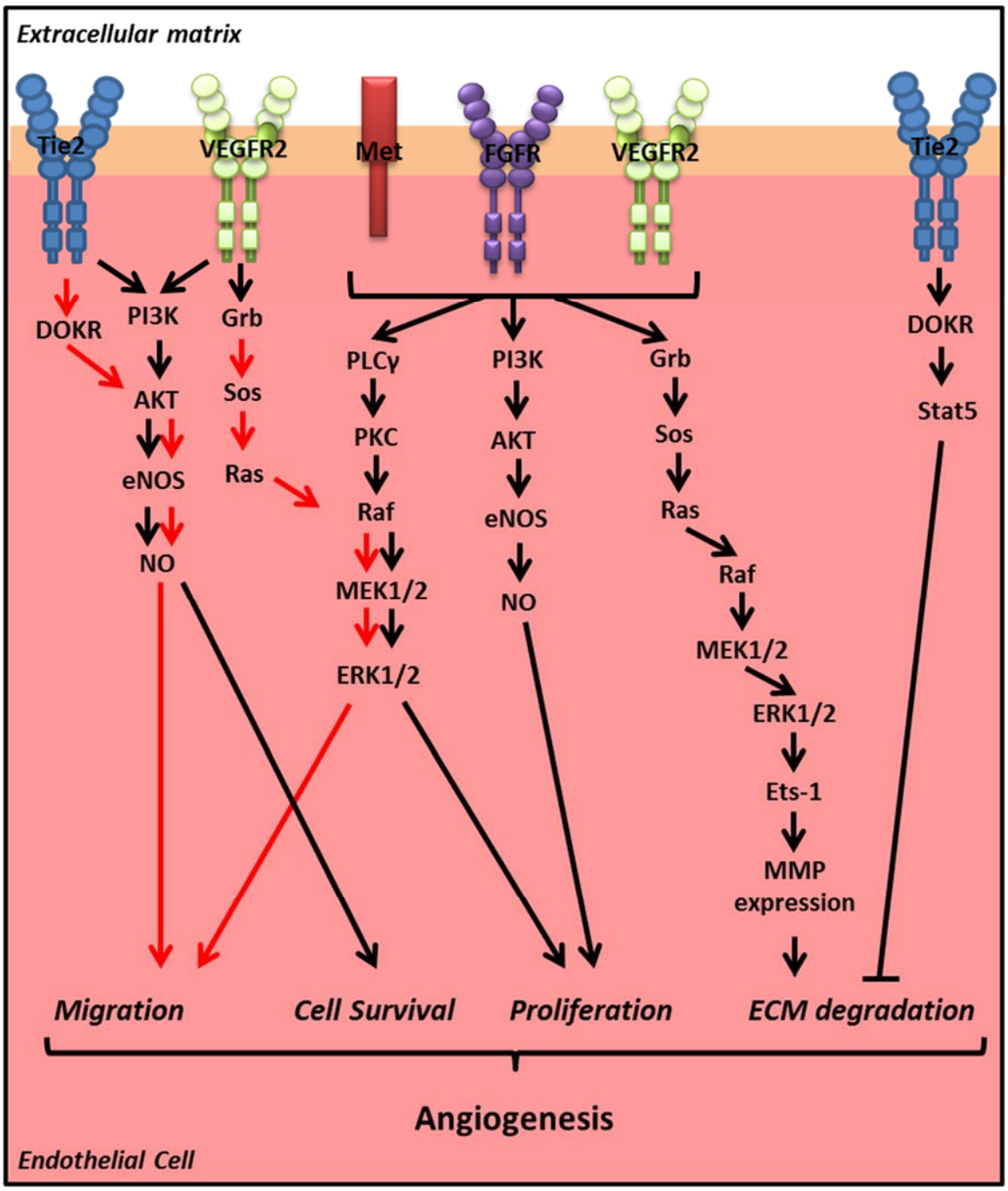

Figure 1.5. Angiogenic growth factor mediated signalling pathways. Angiogenic growth factor receptors such as VEGFR2 (activated by VEGF), FGFR (activated by FGF binding), Tie2 (activated by angiopoietin-1), and hepatocyte growth factor receptor (Met; activated by hepatocyte growth factor), can activate a range of signalling pathways. These pathways are involved in multiple downstream processes involving angiogenesis, such as endothelial cell migration, cell survival, proliferation and extracellular matrix degradation. For example, endothelial cell migration can be mediated by VEGFR2 (via Grb/ERK and p38 MAPK pathways) and Tie2 (via AKT mediated pathways). VEGFR2 and Tie2 can also induce activation of the PI3K signalling pathway, the main pathway involved in endothelial cell survival (Munoz-Chapuli et al. 2004). Proliferation of endothelial cells can be regulated by VEGFR2, FGFR and Met (via PI3K and ERK mediated pathways) and Tie2 (via the DOKR/Stat5 pathway). Extracellular matrix degradation is mediated by VEGFR2, FGFR and Met mediated pathways, via regulation of MMP expression. Abbreviations/definition: VEGFR2: vascular endothelial growth factor receptor 2, FGFR: fibroblast growth factor receptor, DOKR: Downstream of kinase related protein, PI3K: Phosphoinositide 3-kinase, AKT: protein kinase B, eNOS: endothelial Nitric oxide synthase, NO: Nitric oxide, Grb: Growth factor receptor-bound protein, Sos: Son of Sevenless , PLC: Phospholipase C, PKC: protein kinase C, Raf: serine/threonine-specific protein kinase, MEK: Mitogen-activated protein kinase kinase, ERK: extracellular signal-regulated kinases, Stat5: Signal Transducer and Activator of Transcription 5, ETS1: a transducer of proteolytic enzymes, MMP: matrix metalloproteinases, MAPK: mitogen-activated protein kinase, MAKPAPK: MAPK-activated protein kinases.

Table 1.1. A selection of integrin adhesion complex proteins, their protein function and association with VEGF signalling.

Protein	Gene name	Protein function	Association with VEGF signalling
Adaptors			
Paxillin	PXN	Multi-domain scaffold protein serving as a platform for recruitment of regulatory and structural proteins to cell adhesions. Phosphorylation of multiple tyrosine, serine and threonine sites controls these interactions (Deakin and Turner 2008).	VEGF-induces paxillin tyrosine phosphorylation in ECs (Abedi and Zachary 1997). Paxillin is required for VEGF-mediated adhesion, proliferation, migration and tube formation (Yang et al. 2015;Yang et al. 2017).
p130Cas	BCAR1	Adaptor protein, able to interact with multiple partners implicated in cell motility and survival, including Src, Crk, FAK and pyk2. p130Cas is a tyrosine kinase substrate which undergoes changes in phosphorylation downstream of integrin ligation. These phosphorylation events play an important role in downstream cellular processes. Src is the main mediator of phosphorylation (Geiger and Yamada 2011;Matsui et al. 2012).	VEGF treatment induces phosphorylation of p130Cas (Lesslie III et al. 2006). VEGF induces enrichment of actin dynamics and cell motility associated proteins to the p130Cas interactome (Evans et al. 2017).
Tyrosine kinases			
Src	Src	Tyrosine kinase, member of the Src family kinases (SFKs). Can be activated downstream of both integrins and growth factor receptors (Eliceiri 2001). Src associates with activated FAK, leading to a conformational change in Src, and formation of a Src-FAK signalling complex. Src activation involves autophosphorylation of the Src-Y416 in the kinase domain. Phosphorylation substrates include FAK, paxillin and p130Cas and mediate further signalling and interactions with sites of integrin adhesion. Src is negatively regulated by phosphorylation at the c-terminal domain Csk (c-Src terminal kinase), (Mitra et al. 2005;Playford and Schaller 2004).	Src pathway is required for VEGF induced angiogenesis and VEGF mediated FAK-Y861 phsophorylation (Abu-Ghazaleh et al. 2001;Eliceiri et al. 1999).
FAK	Ptk2	Non-receptor tyrosine kinase and scaffolding protein, playing a role in processes such as cell migration, survival and proliferation. Integrin-ECM engagement or growth factor-receptor binding leads to activation, which requires autophosphorylation (FAK-Y397), and forms a binding site for SH2 domain proteins such a Src. The focal adhesion targeting domain at the c-terminus interacts with the adaptor proteins talin and paxillin, facilitating recruitment of FAK to sites of adhesion (Sieg et al. 2000;Cox et al. 2006).	VEGF increases FAK-Y397, -Y407, and -Y861 phosphorylation (Abu-Ghazaleh et al. 2001;Herzog et al. 2011). VEGF also induces FAK-paxillin binding, localization to nascent adhesions and the formation of a FAK-αVβ5 integrin signalling complex (Eliceiri et al. 2002;Chen et al. 2012;Birukova et al. 2009;Avraham et al. 2003).
GAPs			
GIT1		G protein-coupled receptor kinase-interacting target (GIT) is a GAP, which undergoes complex interactions with proteins at sites of integrin adhesion. As many as 28 GIT1	GIT1 is an essential mediator of VEGF-induced podosome (section 1.2.2) formation and cell migration in ECs, which involves a signalling

		phosphorylation sites have been reported, playing a role in adhesion complex formation and signalling. For example, multiple phosphorylation sites in the C-terminal domain are required for paxillin binding. GIT1-S709 phosphorylation increases binding to paxillin, and is essential for GIT1 activity (Webb et al. 2006;Frank and Hansen 2008).	pathway with Src, GIT1 and PLCγ (Wang et al. 2009).
Actin binding			
Cortactin	CTTN	Molecular scaffold for actin assembly and organisation. Phosphorylated upon integrin adhesion to the ECM (Vuori 1998). Phosphorylation state can regulate its activity, for example CTTN-Y241, -Y466 and -Y482 phosphorylation reduce its ability to crosslink filamentous actin, whereas phosphorylation of S405 and S418 trigger actin polymerisation. Tyrosine phosphorylation can be mediated by multiple kinases, including Src. Phosphorylated in response to growth factor signalling (Huang et al. 1998;Kelley et al. 2010;Lua and Low 2005).	A signalling pathway involving cortactin (GEP100-Arf6-AMAP1-cortactin) is required for cell migration and tube formation. Blockage of this pathway inhibits VEGF induced angiogenesis (Hashimoto et al. 2011).

1.4 Angiogenesis

Angiogenesis, the formation of blood vessels through the expansion of pre-existing vasculature, involves a number of complex steps, which can be mediated by cell adhesion and growth factor signalling (figure 1.6). A key trigger of angiogenesis is hypoxia in poorly perfused tissues, which leads to secretion of growth factors such as VEGF-A. Resulting growth factor activity then initiates blood vessel formation, which restores the oxygen and nutrient supply to hypoxic areas (Wong 2017). Activation of angiogenesis involves growth factor stimulation of quiescent ECs, which rest on a mature ECM. Initiation involves specification of the activated ECs into tip and stalk cells and breakdown of ECM components by proteases such as matrix metalloproteinases. This ECM degradation causes vessels to become hyperpermeable to blood plasma proteins, causing leakage of ECM proteins such as fibrinogen, vitronectin and fibronectin, which form a provisional ECM together with pre-existing interstitial collagens. The transition from mature to provisional ECM plays many roles. For example, it allows detachment of pericytes which surround and support the vessel, promotes the proliferation and migration of ECs which invade the hypoxic tissue, and allows release of ECM-sequestered growth factors such as VEGF and FGF-2. The selected tip cells lead the sprout towards the established growth factor source, whereas the stalk cells proliferate, supporting sprout elongation. Eventually, a new mature ECM is formed, and ECs organize into tubes with functional lumens, a process known as vascular morphogenesis and stabilisation (figure 1.6), (Wong et al. 2017;Blanco and Gerhardt 2013;Senger and Davis 2011;Nussenbaum and Herman 2010;Kalluri 2003;Kumar et al. 2012;Papetti and Herman 2002). In addition to ECs, other cell types such as perivascular cells, fibroblasts and immune cells play an important role in angiogenesis

(Kalluri 2003;Bergers and Song 2005). Overall, the angiogenic process is mediated by growth factors, changes in surrounding ECM composition and hence, changes in EC cell-cell and cell-ECM adhesion (Strömblad and Cheresh 1996;Bischoff 1997).

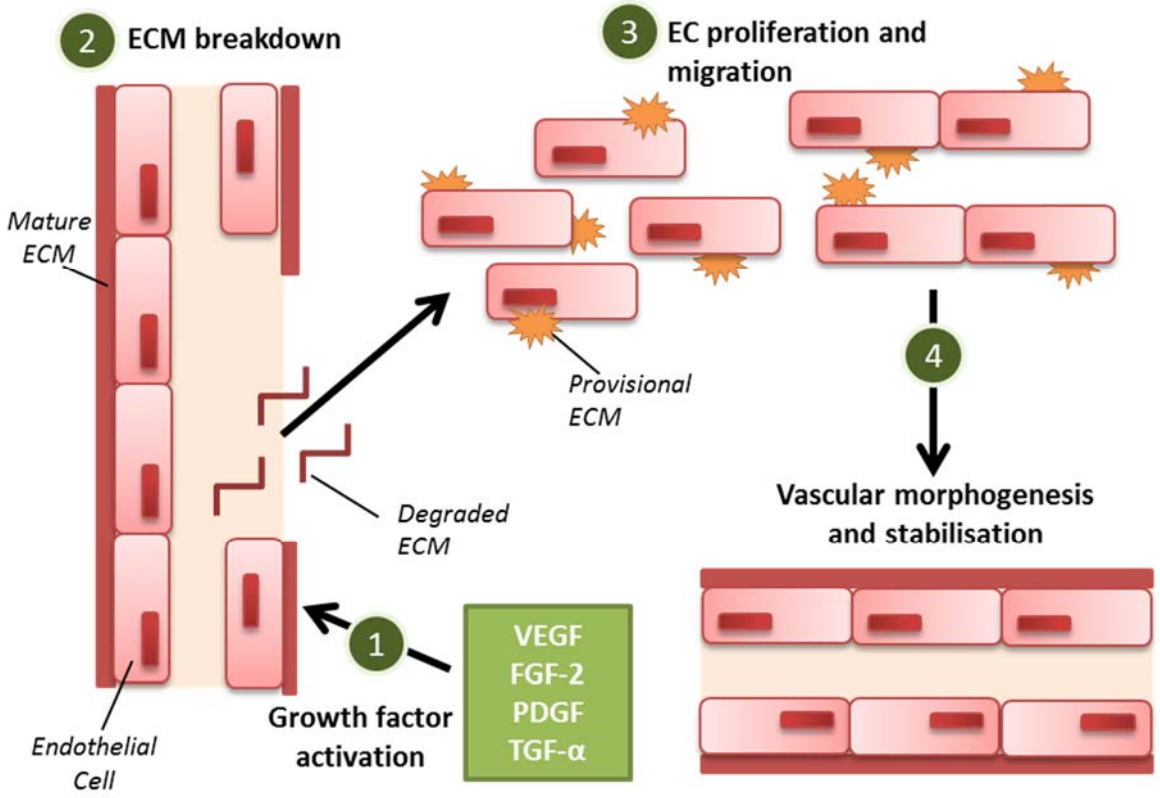

Figure 1.6. The stepwise process of angiogenesis. The process begins with vessel stimulation by growth factors (1). The mature extracellular matrix (ECM) is then degraded (2), leading to formation of the provisional ECM. This allows endothelial cells to proliferate and migrate (3), until they eventually form a stable blood vessel (4). The angiogenic process is therefore mediated by growth factors, changes in surrounding ECM composition and hence, changes in cell-cell and cell-ECM adhesion. Involvement of other cell types such as perivascular cells and fibroblasts have been omitted for clarity. Figure adapted from Kalluri 2003. Abbreviations; VEGF: vascular endothelial growth factor, FGF-2: basic fibroblast growth factor, PDGF: platelet-derived growth factor, TGF-α: transforming growth factor-alpha, ECM: extracellular matrix, EC: endothelial cell.

Angiogenesis is an essential process, playing a role in development through to adult life. An angiogenic vasculature is essential to supply oxygen and nutrients to tissues, supporting tissue function and growth (Nussenbaum and Herman 2010). However, abnormal or pathological angiogenesis can contribute to the development of pathological conditions, including cancer, atherosclerosis, arthritis and macular degeneration (Kalluri 2003;Moulton 2006;Folkman 2006). Angiogenesis under physiological and pathological conditions differ; the main difference is that pathological angiogenesis does not reach resolution upon the establishment of vascular perfusion (Seaman et al. 2007;Chung and Ferrara 2011). Extensive research has been directed towards defining the mechanisms of angiogenesis in both health and disease. This knowledge is

subsequently being used to develop pro- and anti- angiogenesis therapeutic strategies for pathologic conditions in which angiogenesis plays a role.

1.5 VEGF signalling

There are various activators and inhibitors that regulate angiogenesis. Of particular importance are angiogenic growth factors, which as described, initiate angiogenesis (Bergers and Benjamin 2003;Nussenbaum and Herman 2010;Stupack and Cheresh 2002;Sakurai and Kudo 2011). In particular, VEGF activity is essential for angiogenesis. There are seven VEGF family members, of which VEGF-A was the first to be discovered, and the most widely studied (Chung and Ferrara 2011;Simons et al. 2016). The requirement for VEGF-A in early vasculogenesis/angiogenesis is demonstrated by phenotypic lethality of mice lacking a single VEGF-A allele; mutants show disorganized blood vessels and ECs undergo delayed differentiation (Carmeliet et al. 1996;Ferrara and Kerbel 2005). Human VEGF-A has at least nine isoforms due to alternative splicing of a single gene. VEGF-A165 is the predominant isoform, and will be the VEGF isoform discussed for the remainder of this thesis. VEGFs bind with high affinity to the receptor tyrosine kinases VEGFR1, 2 & 3; VEGFR2 is the main VEGF receptor in ECs (Simons et al. 2016). VEGF acts via its receptor VEGFR2 on ECs to initiate its biological effects. VEGF-VEGFR2 binding induces receptor dimerization, which activates the VEGFR2 tyrosine kinase domain, leading to receptor autophosphorylation. The result is multiple VEGFR2 phosphotyrosine sites that create binding sites for Src homology 2 (SH2) domain-containing signalling proteins, which go on to initiate signalling pathways. These signalling cascades are mediated predominantly by phosphorylation events, and result in downstream biological effects (Koch and Claesson-Welsh 2012). For example, an important pathway in VEGFR2 signalling involves VEGFR2-Y1175/PLCγ-mediated activation of PKC (protein kinase C) and downstream induction of ERK, which leads to cell proliferation (Takahashi et al. 2001;Koch et al. 2011). In addition to that described above, many signalling pathways are activated in response to VEGF, such as ERK, p38/MAPK and Akt, the activation of which is regulated by phosphorylation (figure 1.5). Additionally, heparan sulfate proteoglycans (HSPGs) and neuropilins are co-receptors of the VEGF-VEGFR2 signalling axis (Simons et al. 2016;Ferrara et al. 2003). These signalling pathways promote and regulate processes such as EC proliferation, migration and survival, which act together to regulate angiogenesis (Zachary and Gliki 2001). A number of signalling pathways induced by some different angiogenic growth factors are shown in figure 1.5, illustrating the complexity of these processes.

1.6 Therapeutic targeting of angiogenesis

Therapeutic agents targeting angiogenesis are of increasing interest, due to the involvement of the process in a range of pathological conditions. Many anti-angiogenic approaches developed to date have targeted VEGF signalling, and have demonstrated that the concept is a viable therapeutic

option (Carmeliet 2005). Studies investigating the use of angiogenesis modulating agents have involved strategies to promote revascularization of ischaemic tissues, or to inhibit angiogenesis in diseases in which angiogenesis is enhanced. Administration of VEGF has been investigated as a pro-angiogenic approach, to promote revascularization of ischaemic tissues. However, clinical trials testing the potential of these agents produced disappointing results. For example, levels of VEGF were low after administration, off-target angiogenesis has been detected and side effects such as hypotension were observedagent (Simons 2005). In contrast, the development of anti-angiogenic therapies has had greater success, with a number being successfully developed and used for the treatment of pathological conditions in which angiogenesis is abnormally enhanced. For example, in cancer, the 'angiogenic switch' is a step in tumour development, which is required for exponential tumour growth. New blood vessels formed via angiogenesis provide the proliferating tumour with essential nutrients and oxygen. Therefore, the rationale behind anti-angiogenesis therapy for cancer is that, due to the dependence of tumour growth and metastasis on angiogenesis, depriving the tumour of vessels will prevent growth (De Palma et al. 2017;Folkman et al. 1971;Harmey and Bouchier-Hayes 2002).

The first anti-angiogenic drug to be approved by the Food and Drug Administration was a VEGF targeting monoclonal antibody, Avastin (Bevacizumab, Genentech), in 2004. Avastin is usually given in combination with other chemotherapeutic agents for a range of cancer types including metastatic colorectal cancer, metastatic breast cancer and advanced non-small cell lung cancer (Bellou et al. 2013;Hurwitz et al. 2004;Reck et al. 2010). Despite some success, the use of Avastin has not been as promising as originally expected. For example, use in untreated non-small cell lung cancer patients, in combination with chemotherapy, resulted in only moderate improvement in overall and progression free survival, and in the case of breast cancer, lack of improvement to overall survival caused approval to be revoked by the Food and Drug Administration in 2011 (Reck et al. 2010;Tanne 2011;Miles et al. 2010). Following approval of Avastin, a number of other anti-angiogenic agents have been approved. These mainly target VEGF signalling, although some target other signalling pathways. For example, a number of small molecule tyrosine kinase inhibitors have been approved, which often target multiple angiogenesis associated pathways (Bellou et al. 2013;Ivy et al. 2009). Increasing understanding of the mechanisms involved, and how different signalling systems work together to regulate angiogenesis will aid studies investigating angiogenesis targeting therapies.

As the role of integrin mediated adhesion in regulating angiogenesis is beginning to be elucidated (section 1.8), integrin-ECM interactions have been a focus of anti-angiogenic therapy. Integrins are attractive drug targets as they are easily accessible and using peptides, antibodies or

peptidomimetics, and can be readily inhibited (Hynes 2002b). For example, integrins αVβ3 and αVβ5 are upregulated in angiogenic and tumour endothelium, and so have been highlighted as attractive targets. Cilengitide is an RGD-based inhibitor of integrins αVβ3 and αVβ5, and has entered clinical trials for a range of cancer types (Smith et al. 1990;Beekman et al. 2006). However, studies suggest that long term treatment with Cilengitide may not be successful due to unwanted effects. For instance, compounds of this type have been shown to promote VEGF induced EC migration in mice, causing stimulation, rather than inhibition of angiogenesis and tumour growth (Reynolds et al. 2002). In addition, low levels of integrin antagonists can act as integrin agonists, and may therefore have an opposite response to that desired (Legler et al. 2001).

Although angiogenesis modulating therapies have shown great potential, disappointing results have suggested that the concept of anti-angiogenesis needs to be revaluated. For example, combination therapies involving angiogenic inhibition combined with other anti-cancer agents are likely to result in improved results (Cao 2016). In most cases, treatment with anti-angiogenic agents leads to only modest survival benefits for cancer patients (Cao 2016). In addition, anti-angiogenic agents can result in, (1) adverse side effects, (2) resistance to the agent (a result of compensatory mechanisms), and (3) increased risk of tumour metastasis and invasion, likely due to an anti-angiogenesis induced hypoxic microenvironment (Bellou et al. 2013;Shojaei 2012;Rapisarda and Melillo 2009). These problems, in combination, affect overall clinical outcome of the therapeutic, and suggest that novel ways to modulate angiogenesis for the treatment of cancer and other angiogenesis related disorders should be evaluated.

1.7 Phosphoproteomic analysis of growth factor signalling

Although knowledge of growth factor-activated pathways is continually increasing, the exact signalling nodes mediating growth-factor induced biological outcomes remain poorly defined. Mass spectrometry-based phosphoproteomics is a powerful tool that can be used to investigate growth factor signalling networks in an unbiased manner. The availability of phosphoproteomics has greatly advanced our knowledge of growth factor receptor signalling (Huang 2012); however, only a limited number of phosphoproteomic studies investigating VEGF signalling in ECs have been performed (Zhuang et al. 2013;Chidiac et al. 2016). For example, a study investigating temporal dynamics of VEGF-regulated protein phosphorylation in HUVECs used a phosphoproteomic approach. Subsets of phosphorylated proteins identified by phosphoproteomics were screened using small interfering RNA (siRNA) screens to investigate their function in VEGF-induced responses. This analysis identified the PI3K–mTORC2 (mammalian target of rapamycin complex 2) axis as being essential for VEGF-regulated phosphorylation and signalling (Zhuang et al. 2013). A more recent study performed phosphoproteomic profiling of both VEGF- and Ang1-treated bovine aortic ECs

using label-free quantification methods. This study identified 255 upregulated and nine downregulated phosphopeptides upon ten minutes of VEGF stimulation, and highlighted that a range of junctional proteins (ZO1, ZO2, JUP and p120-catenin) are phosphorylated in response to VEGF. Further targeted studies were performed, and revealed that downregulation of the identified junctional proteins led to activation of MAPK1 and increased VEGF- (but not Ang1-) induced proliferation (Chidiac et al. 2016). These global phosphoproteomic studies have revealed specific mechanisms by which VEGF signalling occurs in ECs and provide a basis for future investigations defining mechanisms of VEGF-induced signalling pathways.

In addition to the need to understand the specific phosphorylation and signalling events occurring in response to growth factor activation, the exact associations between receptor-induced signalling pathways and final biological outcome such as cell adhesion, migration, proliferation and angiogenesis are largely unknown. It appears, however, that each angiogenic growth factor regulates angiogenesis by different mechanisms, often involving crosstalk with other growth factor- and often adhesion-mediated signalling pathways (table 1.2 & figure 1.5). This crosstalk may be highlighted by the fact that each step in the angiogenic process is mediated by changes in both cell-cell and cell-ECM adhesion (figure 1.6). Hence, interplay between growth factors, integrin signalling and adhesion molecules has been shown to play an important role in the precise regulation of angiogenesis (Nussenbaum and Herman 2010;Moulton 2006;Carmeliet and Jain 2000;Simons et al. 2016;Silva et al. 2008).

1.8 Integrins in angiogenesis

Integrins have been implicated as essential regulators of EC biology, regulating processes such as EC migration, proliferation, adhesion and survival, all of which are important for angiogenesis. Hence, disrupted adhesion activity has many associations with angiogenesis and its related disorders. Collagen-, laminin-, vitronectin- and fibronectin-binding EC integrin heterodimers (α1β1, α2β1, α4β1, α5β1, α6β1, α6β4, α9β1, αVβ3 and αVβ5), have all been shown to play a role in angiogenesis (table 1.2), (Avraamides et al. 2008;Akalu et al. 2005;Silva et al. 2008). Expression and availability of integrins on quiescent and angiogenic ECs is highly coordinated to regulate interactions with the mature and provisional ECM, and neighbouring cells (figure 1.6). In situ analysis has demonstrated that quiescent vessels express a wide variety of integrin dimers, including α1β1, α2β1, α3β1, α5β1, α6β1 and /or α6β4, and αVβ5, which mostly bind basement membrane proteins, allowing EC anchorage to the vessel abluminal face. Although expressed in quiescent vessels at low levels, α5β1 and αVβ5 (fibronectin- and vitronectin-binding integrins, ligands present in the provisional ECM, figure 1.6) levels are increased in angiogenic vessels (Stupack and Cheresh 2002;Brooks et al. 1994;Kim et al. 2000a). For example, α5β1 expression was enhanced on blood vessels of human tumors and in VEGF or FGF-2 stimulated tissues, whereas

these molecules were minimally expressed on normal human vessels and on unstimulated tissues (Kim et al. 2000a) .

Table 1.2. Endothelial integrins and their role in angiogenesis. Evidence from genetically manipulated mice and the use of integrin blocking agents. Table modified from Avraamides et al., Garmy-Susini et al.

Integrin	Major ligand(s)	Evidence from genetically manipulated mice	Evidence from integrin blocking agents
α1β1	Collagen Laminin	α1 knockout: normal vascular development, reduced adult angiogenesis (Pozzi et al. 2000).	Function blocking antibodies: reduce VEGF induced angiogenesis (Senger et al. 1997).
α2β1	Collagen Laminin	α2 knockout: normal vascular development, enhanced tumour angiogenesis (Pozzi et al. 2000;Zhang et al. 2008).	Function blocking antibodies: reduce VEGF induced angiogenesis (Senger et al. 1997).
α4β1	Fibronectin VCAM1	α4 knockout: embryonic lethal (50% due to cardiovascular defects and 50% due to chorion–allantois fusion), (Yang et al. 1995).	Antagonists induce EC death and decrease tumour vascularisation and growth (Avraamides et al. 2008;Garmy-Susini et al. 2005).
α5β1	Fibronectin	α5 knockout: embryonic lethal, partially due to vascular defects (Yang et al. 1993).	Antagonists inhibit angiogenesis (Kim et al. 2000a;Umeda et al. 2006;Muether et al. 2007).
α6β1	Laminin	α6 knockout: embryonic lethal with no vascular defects (Georges-Labouesse et al. 1996).	α6 antagonists and small interfering RNAs inhibit angiogenesis (Lee et al. 2006).
α9β1	Fibronectin Collagen Laminin	α9 knockout: post-natal lethality due to a lymphatic defect (Huang et al. 2000b).	Blocking antibodies: inhibit angiogenesis (Vlahakis et al. 2007).
αVβ3	Fibronectin Vitronectin Osteopontin Developmental endothelial cell locus1 (DEL1)	αV knockout: enhanced angiogenesis, 80% embryonic lethal, 20% die due to brain haemorrhage (Bader et al. 1998). β3 knockout: 50% embryonic or post-natal lethal, surviving adults display enhanced angiogenesis (Hodivala-Dilke et al. 1999). β3 Y747F/Y759F knock-in: normal development, display reduced adult angiogenesis (Mahabeleshwar et al. 2006).	Antagonists block angiogenesis (Brooks et al. 1994).
αVβ5	Vitronectin Osteopontin DEL1	αV knockout: enhanced angiogenesis- 80% embryonic lethal, 20% die due to brain haemorrhage (Bader et al. 1998). β5 knockout: normal development, display reduced adult angiogenesis in response to angiogenic regulators (Bader et al. 1998;Huang et al. 2000a).	Antagonists block angiogenesis (Friedlander et al. 1995).
α6β4	Laminin 332	β4 knockout: normal vascular development, lethal due to skin defects. β4 Δ1355: normal development, reduced adult angiogenesis (Van Der Neut et al. 1996;Nikolopoulos et al. 2004).	α6 antagonists and small interfering RNAs inhibit angiogenesis (Lee et al. 2006).

Initial studies reporting a role for integrins in angiogenesis were published over two decades ago (Brooks et al. 1994). These studies have been followed by many studies aiming to further

understand the mechanisms by which integrins contribute to angiogenesis. Although these studies have provided further support for a role for integrins in angiogenesis and provided some mechanistic insights, studies using integrin blocking agents and genetically modified mouse models have resulted in conflicting theories of the mechanisms, details of which will be discussed in section 1.9. Therefore, the precise mechanisms by which integrins control EC behaviour, coordinate their activity with growth factors, and contribute to angiogenesis are poorly understood.

1.9 Adhesion-growth factor signalling crosstalk in angiogenesis

1.9.1 Role of αVβ3 and αVβ5 integrins in VEGF-mediated angiogenesis

Upon initial discovery of a role for integrins in angiogenesis, it quickly became apparent that integrins can coordinate their activity with growth factors to modulate angiogenic signalling (Brooks et al. 1994;Friedlander et al. 1995;Sheppard 2002). The first integrins shown to play a role in angiogenesis were integrin αVβ3 and αVβ5. These integrins both play a similar role in angiogenesis, although the two integrins act via distinct angiogenic signalling pathways. In vivo, antibody antagonists of integrin αVβ3 block FGF-2 induced angiogenesis, whereas αVβ5 antagonists block VEGF-mediated angiogenesis (Friedlander et al. 1995). Initial establishment of a role for integrin-growth factor crosstalk in angiogenesis was followed by many studies discovering further examples, and investigating the mechanisms involved. Although different growth factors have been shown to be involved in adhesion-growth factor crosstalk in angiogenesis, there is a huge amount of evidence suggesting a role for VEGF (Niland and Eble 2011;Eliceiri 2001;Somanath et al. 2009a).

Initial evidence for the role of integrins in angiogenesis was based on studies using antibodies and small molecule inhibitors to block integrin activity (Brooks et al. 1994;Friedlander et al. 1995). In general, integrin blocking agents inhibited or reduced angiogenesis (table 1.2), leading to the hypothesis that integrins are pro-angiogenic. However, studies using genetically modified animals have challenged this hypothesis. Integrin αV knockout mice display extensive vasculogenesis and angiogenesis (developing normally up until E9.5), (Bader et al. 1998), and integrin β3-deficient and double β3/β5-deficient mice are viable and fertile, displaying enhanced angiogenesis and tumour growth (Mas-Moruno et al. 2010;Reynolds et al. 2002). The results of these studies suggest that in vivo, αVβ3 and αVβ5 play a role in limiting angiogenesis (Reynolds et al. 2002). The enhanced angiogenic and tumour growth phenotype of β3-deficient mice may be explained by a compensatory mechanism, as ECs derived from β3-deficient mice display elevated VEGFR2 expression and activity. This enhanced activity is a requirement for enhanced VEGF-induced vascular permeability and increased tumour growth and angiogenesis in these β3-deficient mice (Reynolds et al. 2002;Reynolds et al. 2004;Robinson et al. 2004). Furthermore, in the heart of β3 knockout mice, capillaries fail to mature, and remain characteristic of immature or activated endothelium (Weis et al. 2007). This was a result of VEGF hypersensitivity in the β3 knockout,

demonstrated by antagonism of VEGFR2, which normalised the vascular abnormalities (Weis et al. 2007). Insights into the VEGFR2 compensatory mechanism in integrin β3-deficient mice have been provided by knock-in of mutant β3, which is unable to undergo tyrosine phosphorylation in the cytoplasmic domain. ECs from these mice have no enhanced VEGFR2 activity, and consistent with integrin antagonist studies, show impaired angiogenesis (Mahabeleshwar et al. 2006). Conflicting results from genetically manipulated mice and blocking agents demonstrate that results from such studies need to be interpreted with care. In addition, studies using different blocking reagents can exhibit differential responses. For example, tumstatin, an αVβ3 blocking peptide increases apoptosis and decreases proliferation in ECs, whereas blocking antibodies can initiate integrin clustering on the cell surface, resulting in a completely different signalling effect (Maeshima et al. 2002;Mould et al. 1998;Humphries 2004). Again, these results highlight that such results using blocking agents should be carefully evaluated.

Another example of VEGF-adhesion crosstalk is demonstrated by complex formation between αVβ3 and VEGFR2, which as demonstrated by multiple studies, appears to play an important role in angiogenesis. Evidence for this association comes from immunoprecipitation experiments, where β3 integrin co-immunoprecipitates with tyrosine phosphorylated VEGFR2 and immunohistochemistry, which shows co-localisation of the two receptors in vessels (Soldi et al. 1999;Mahabeleshwar et al. 2006;Mahabaleshwar and Byzova 2008;Somanath et al. 2009b). The mechanisms and functional consequences of this co-localisation are beginning to be elucidated. ECs permitted to spread on αVβ3 ligands vitronectin and fibrinogen display increased VEGFR2 phosphorylation in response to VEGF, in comparison to when plated on fibronectin and collagen (Soldi et al. 1999;Mahabaleshwar and Byzova 2008). Integrin αV and β3 blocking antibodies had no effect on adhesion to vitronectin, although both inhibit VEGF-induced VEGFR2 phosphorylation, whereas β1 blocking antibodies do not. These results indicate that it is αVβ3 that is important for this VEGF-induced VEGFR2 phosphorylation, rather than the ability of the cell to adhere to its substrate (Soldi et al. 1999;Mahabaleshwar and Byzova 2008). Another study also indicated that αVβ3 and VEGFR2 synergy is a requirement for full VEGFR2 phosphorylation (Masson-Gadais et al. 2003). This association is required to drive complete activation of migration pathways involving FAK and stress-activated protein kinase-2/p38 (SAPK2/p38). Activation of these pathways is HSP90-dependent; VEGFR2 is suggested to associate with αVβ3 integrin, which leads to FAK phosphorylation and recruitment of vinculin to VEGFR2 and adhesions (Masson-Gadais et al. 2003).

The phosphorylation status of VEGFR2 and αVβ3 integrin, as already suggested, plays an important role in their interaction, and is mediated by signalling proteins. Activation of either receptor, through αVβ3 adhesion and/or VEGF binding, leads to a conformational change of the integrin to the high affinity state, inducing β3 integrin phosphorylation at Y747 and Y759 on the cytoplasmic

tail (Mahabeleshwar et al. 2007). Studies using ECs expressing β3 integrin unable to undergo phosphorylation at these tyrosine residues, or peptides that target this cytoplasmic domain prevent formation of this complex and subsequent VEGF-induced angiogenic response, highlighting the importance of these phosphorylation events (Mahabeleshwar et al. 2006;Mahabeleshwar et al. 2007;West et al. 2012).

Many proteins regulate the synergy between VEGFR2 and αVβ3. One of the major kinases determined to be involved is Src, which mediates the physical and functional associations. VEGF induces Src association with, and phosphorylation of, β3 integrin, which is essential for formation of the VEGFR2-αVβ3 complex (Mahabeleshwar et al. 2007). Another recently identified mediator of the complex is sprouty-4, which negatively regulates VEGFR2-integrin crosstalk. The sprouty protein family was initially identified as inhibitors of receptor tyrosine kinase signalling pathways such as VEGF. Specifically, sprouty-4-deficient mice display enhanced angiogenesis, and overexpression results in deficient angiogenesis (Lee et al. 2001;Taniguchi et al. 2009). Subsequently, the signalling pathways involved were investigated; sprouty-4 inhibits Src induced integrin β3 phosphorylation, and thus, reduced VEGFR2-αVβ3 complex formation and angiogenesis (Gong et al. 2013). Another mediator of the VEGFR2-αVβ3 complex is gremlin. Gremlin is a non-canonical VEGFR2 ligand, which induces a pro-angiogenic phenotype. Gremlin acts by inducing formation of the VEGFR2-αVβ3 complex. In addition, gremlin-induced VEGFR2 activation and subsequent EC responses in vitro and in vivo are modulated by αVβ3 engagement with the ECM (Ravelli et al. 2013). Together, these data support a model in which the interaction of VEGFR2 and β3 integrin is required for activation of EC signalling pathways and VEGF-induced angiogenesis.

1.9.2 Role of fibronectin and fibronectin-binding integrins VEGF-mediated angiogenesis

During VEGF-induced angiogenesis, ECs come into contact with a range of ECM proteins. It is therefore not surprising that integrins in addition to αVβ3 and αVβ5, which have mainly been discussed so far, are also involved in crosstalk with VEGF signalling. For example, VEGF treatment of ECs can activate αVβ3, αVβ5, α5β1 and α2β1 to enhance EC adhesion and migration, and β1 integrin can interact with VEGFR2 in a similar way to that described for αVβ3 (Byzova et al. 2000;Chen et al. 2010;Tugues et al. 2013;Wijelath et al. 2002). The β1-VEGFR2 interaction is mediated by the tetraspanin CD63, which binds to both VEGFR2 and β1. Knockdown of CD63 in ECs in culture using siRNA prevents formation of the complex, disrupting VEGF signalling, adhesion, migration and tube formation (Tugues et al. 2013). Crosstalk also occurs between VEGF, FGF-2 and β1 integrin; FGF and VEGF stimulation of ECs leads to downregulation of a microRNA, miRNA-223, which targets β1 integrin. This micro RNA is usually expressed in ECs, and is anti-angiogenic, likely due to its targeting of β1 integrin (Shi et al. 2013). β1-VEGFR2 interactions also mediate differential signalling in response to ECM-bound and soluble VEGF in ECs. ECM-bound VEGF (but not soluble

VEGF) induces prolonged VEGFR2-Y1214 phosphorylation, enhancing activation of the p38/MAPK pathway. Inactivation of β1 prevents these downstream signalling responses, which are dependent on the β1-VEGFR2 association. In addition, matrix-bound, and not soluble VEGF induces β1 co-localisation with paxillin-positive adhesion complexes, shown by immunofluorescence staining (Chen et al. 2010). The evidence presented so far supports a role for integrin crosstalk with VEGF activity, with increasing evidence suggesting an important role of the ECM.

Angiogenesis is highly dependent on EC interaction with ECM proteins. ECs rest on a laminin-rich basement membrane under physiological conditions. Upon angiogenic stimulation, proliferating and migrating ECs form contacts with a fibronectin-rich, provisional matrix (figure 1.6). There is a vast amount of evidence supporting a role for fibronectin and endothelial fibronectin-binding integrins in modulating a range of EC functions associated with angiogenesis (Kumar et al. 2012). Mice lacking fibronectin die during embryogenesis due to defects in vascular network formation and/or maintenance (George et al. 1993;George et al. 1997;Francis et al. 2002). Mutations of the fibronectin binding sites for α5β1 and αVβ3/5 integrins lead to embryonic lethality due to vascular defects (Takahashi et al. 2007). Blockade of fibronectin assembly using inhibitors of fibronectin fibrillogenesis can also disrupt vascular network formation; further supporting a role for the fibronectin-based ECM in angiogenesis (Zhou et al. 2008). Studies involving fibronectin-binding integrin knockout mice also suggest an important role (table 1.2), with combined αV/α5 deletion showing a more severe phenotype than αV alone (Murphy et al. 2015;Yang et al. 1999). Together these genetic analyses have highlighted an important role for fibronectin in angiogenesis; however, a functional role for fibronectin and its associated integrins has been less well described.

One study revealed an important role for the central cell-binding domain of fibronectin; antibody antagonists of this domain blocked angiogenesis stimulated by VEGF and FGF-2, whilst these growth factors enhanced fibronectin expression (Kim et al. 2000a). However, antibody, peptide, and non-peptide antagonists of the fibronectin receptor α5β1 had minimal effects on angiogenesis induced by VEGF, while blocking angiogenesis stimulated by other growth factors; FGF-2-, TNFα- and IL8, indicating that fibronectin receptors other than α5β1 are important for VEGF mediated angiogenesis. These data suggest that both α5β1 and its ligand fibronectin contribute to an angiogenic signalling pathway distinct to that of VEGF, regulating the same pathway of angiogenesis to that of αVβ3 (Kim et al. 2000a).

Integrin α5β1 and αVβ3 have also been shown to coordinate their behaviours as a form of integrin-integrin crosstalk mediated by protein kinase A, the activity of which is suppressed by α5β1-fibronectin binding. Protein kinase A is an inhibitor of αVβ3-dependent focal adhesion formation, and hence, inhibiting α5β1 function reduces αVβ3-dependent adhesion complex formation, cell

migration and angiogenesis (Kim et al. 2000b). Protein kinase A can also activate caspase-8-dependent apoptosis in ECs, and therefore fibronectin-α5β1 interactions can prevent EC death, aiding angiogenesis in the presence of fibronectin (Kim et al. 2002). In addition, evidence from animal models has shown that α5β1 antagonists block tumour angiogenesis leading to tumour regression (Kim et al. 2000a).

As previously discussed (section 1.6), due to their role in angiogenesis, integrins and their ECM interactions are attractive drug targets. Therefore, knowledge of the role of fibronectin in angiogenesis led to the development of RGD mimetics, which inhibit these fibronectin-integrin interactions (Maubant et al. 2006). Preclinical studies using this class of drug have been promising, although clinical trials have led to questions about their mechanisms of action. For example, a phase three clinical trial of the RGD peptide mimetic Cilengitide as an anti-angiogenic cancer treatment, showed no clinical benefit (Reynolds et al. 2009). This lack of efficacy in humans is likely explained by the fact that low concentrations of αVβ3 and αVβ5 inhibitors can in fact promote angiogenesis induced by VEGF. Integrin inhibition alters αVβ3 integrin and VEGFR2 trafficking, promoting EC migration to VEGF, thereby promoting VEGF-induced angiogenesis (Reynolds et al. 2009). These studies provide further knowledge of the mechanisms that contribute to VEGF-adhesion crosstalk in a fibronectin dependent manner.

Whilst the studies highlighted above support a role for fibronectin binding integrins in angiogenesis, a recent study revealed that fibronectin and endothelial αV and α5 integrins are dispensable for tumour angiogenesis and growth (Murphy et al. 2015). The authors suggest that mechanisms other than a simple functional block may explain the promising, anti-angiogenic response seen using high dose RGD inhibitors and integrin blocking agents in preclinical studies (Reynolds et al. 2009). For example, inhibition of angiogenesis by antibodies or small molecules such as Cilengitite may occur through a dominant negative effect, rather than a functional block (Reynolds et al. 2009;Murphy et al. 2015). Together, these results highlight (1) the complexity of the mechanisms by which fibronectin-integrin interactions are involved in angiogenesis and (2) the need for a better understanding of these mechanisms in preclinical models, before progressing to clinical trials.

When combining evidence from individual studies, the importance of fibronectin-induced integrin-mediated adhesion to fibronectin in angiogenesis, in addition to VEGF activity has been highlighted. Coordination also occurs directly between the ECM and growth factors, in particular fibronectin and VEGF, to regulate adhesion-growth factor crosstalk and subsequent angiogenesis (Wijelath et al. 2006). Fibronectin contains a VEGF binding site; VEGF and α5β1 binding to their respective binding domains of fibronectin is required for maximal induction of VEGF-induced EC migration and proliferation. In addition, VEGF-fibronectin complexes lead to the physical association of VEGFR2

and α5β1, but not αVβ3 (Wijelath et al. 2006;Humphries et al. 2006). Another form of crosstalk involves a physical link in which the ECM brings together growth factors, growth factor receptors and integrins. For example, VEGF-fibronectin binding forms complexes which can enhance growth factor-integrin signalling, by inducing formation of VEGFR2 and integrin clusters (Martino et al. 2013;Martino et al. 2011). An engineered fibronectin fragment consisting of a fibrin-binding sequence, an integrin-binding domain and a growth factor binding domain was co-delivered with VEGF to ECs in vitro, and led to increased angiogenesis (Martino 2010). Therefore, growth factor signalling dynamics can depend on their surrounding ECM. Furthermore, co-delivery of growth factor VEGF and PDGF-BB with this fibronectin fragment in a mouse chronic wound model was able to induce angiogenesis at low doses, while growth factors delivered without the fibronectin fragment had no significant effect (Martino et al. 2011;Martino et al. 2015). Therefore, in addition to their crosstalk with integrins, growth factor signalling and availability are also influenced by binding to the ECM.

As described above, there is much evidence demonstrating a role for VEGF-adhesion crosstalk in angiogenesis. Of note, many of the mechanisms described in this introduction involve protein signalling and phosphorylation. However, the mechanisms by which this crosstalk occurs, and the factors that mediate this crosstalk appear to be extremely complex, and are not well understood. Therefore, a better understanding of the factors and mechanisms involved in VEGF-adhesion crosstalk would lead to a better understanding of vascular development, and highlight ways that therapeutics can be used to treat angiogenic associated diseases.

1.10 Proteomic techniques

In a typical proteomic experiment, trypsin is used to digest proteins into smaller peptides that can be identified by mass spectrometry analysis (Aebersold and Mann 2003). Due to the high complexity of proteomic samples, peptide samples are often fractionated by LC, usually reverse phase, which separates peptides based on their hydrophobicity, allowing peptides to be gradually eluted to the mass spectrometer. Peptides are then ionised in the ion source, transferred to the gas phase, and moved to a mass analyser where the first stage of separation (MS1) occurs based on the measured mass to charge ratio (m/z) of peptide (precursor) ions. A detector measures the intensity of ions collected at each m/z value, the results of which are presented as a m/z vs intensity plot known as a mass spectrum. In tandem mass spectrometry, a second mass spectrometry scan is performed (MS2), which selects the most abundant peptide precursor ions from MS1 analysis for further fragmentation. Spectra are then created from the resulting ion fragments, and provide information that allows specific peptide sequences to be derived. Database searching of information from the MS1 and MS2 spectra identifies peptide sequences, from which protein

identities can then be deduced (Domon and Aebersold 2010;Sadygov et al. 2004;Walther and Mann 2010).

1.10.1 Phosphoproteomics

Due to recent advancements, the ability to determine the phosphorylation status of proteins in a complex mixture by high resolution mass spectrometry has become possible. However, to use proteomic approaches for phosphorylation analysis, many technical issues need to be addressed. The main challenge is the low proportion of phosphopeptides in comparison to non-phosphorylated peptides in protein digests (usually less than 0.2%), leading to low signal intensities in the mass spectrometer (Kanshin et al. 2012). To facilitate the detection of phosphopeptides, enrichment of phosphorylated proteins or peptides from samples during the mass spectrometry sample preparation workflow is usually performed, for which many methodologies have been developed. Examples include immunoaffinity purification using phosphospecific antibodies, although this mainly limited to phosphotyrosine analysis (van der Mijn et al. 2015) and methods that enrich all phosphosites, such as immobilised metal affinity chromatography (IMAC) (Thingholm and Jensen 2009), and titanium dioxide (TiO_2) chromatography (Thingholm and Larsen 2009). The latter strategies rely on binding of phosphorylated amino acids (negatively charged) to immobilised cations at low pH. The specificity means that phosphopeptides bind preferentially, and can be eluted from the cations by increasing pH, resulting in a phosphopeptide-enriched sample that can be subsequently used for mass spectrometry analysis. Due to enhancement of technology, phosphoproteomic studies are being used increasingly to investigate growth factor (Ishihama and Imami 2014;Chidiac et al. 2016) and adhesion signalling (Robertson et al. 2015). However, VEGF signalling phosphoproteomic studies, and studies investigating growth factor-dependent phosphorylation in IACs, are limited (Paul 2014).

1.10.2 Quantification

Mass spectrometry-based proteomics can be used for quantification of proteins and peptides within a sample (Old et al. 2005;Liu et al. 2004). Relative quantification has been most commonly employed and can be subdivided into labelled and label-free methods (Old et al. 2005), both of which have been used to determine protein abundance differences between IAC samples (Byron et al. 2012;Robertson et al. 2015;Ng et al. 2014;Kuo et al. 2011;Huang et al. 2014;Schiller and Fässler 2013;Schiller et al. 2011). Labelling techniques usually involve labelling samples with different stable isotopes, mixing samples and performing the sample preparation and MS run on the mixed sample. Mixing ensures technical variation incurred through the analytical process is equal between samples, and the quantity of each differentially labelled peptide corresponds to a particular biological condition (Old et al. 2005). Label free approaches include spectral counting and ion

intensity analysis; for both methods samples from different experimental conditions are prepared and analysed by MS in parallel.

For spectral counting (Liu et al. 2004), each time a peptide ion is selected for MS2 analysis, a recording is made, termed a 'spectral count'. The number of spectral counts for each peptide can be used for peptide abundance. For measurement of protein abundance the spectral count of all measured peptides assigned to a particular protein are integrated to give an estimation of relative protein abundance. As more abundant peptides are more likely to be selected for MS2 analysis than those of lower abundance, a higher spectral count is representative of more abundant peptides. Therefore, the ratio between spectral count for each peptide or sum of all peptides belonging to an identified protein is used to estimate fold changes (Lundgren et al. 2010;Cifuentes 2013). The general principle of ion intensity quantification involves measurement of ion abundance at the MS1 stage of tandem mass spectrometry. For a particular peptide, which is eluted from chromatography over a short retention time window, several MS1 measurements are made, and are collectively termed a 'feature' or peptide ion with retention time and m/z value as coordinate values. Each peptide ion MS1 mass (or m/z) measurement has an associated ion intensity, which can be summed up over the feature to create an ion intensity value for the associated feature. For each peptide ion selected for MS2 analysis, MS2 scans confirm their sequence identity. Ion intensity values are representative of the abundance of the corresponding peptide, and can be compared between samples as a measure of relative quantification. This analysis requires specialised software, involving alignment and normalisation of MS1 data from different samples by their coordinates (retention time and m\z values) prior to identification using MS2 spectra. Alignment ensures each run in the experiment is perfectly aligned so that a particular ion in one run is in the same location as the matching ion in another run, allowing accurate comparison of peptide ions. In addition, if MS2 data were not obtained for a particular feature in one run, sequence data can be inferred from a feature with the same coordinates from another run. There are advantages to both label-free methods described. For example, spectral counting is relatively straightforward requiring no additional specialised software, and can be implemented in most current workflows. However it uses discrete data points, and low spectral count numbers can be unreliable for quantification. Ion intensity measurements are continuous, and provide a more accurate determination of fold changes, although more time and effort is required to process the data, and specific software is required (Old et al. 2005;Bantscheff et al. 2012;Cifuentes 2013).

1.11 Proteomics techniques in drug discovery

Proteomics can be used at many stages of drug discovery, and is increasingly becoming the method of choice. In particular, proteomics is commonly used to gain a better understanding how drugs

may be used to target proteins within cells of the human body. One of the main advantages of proteomic technologies is the unbiased (hypothesis free) nature, allowing thousands of proteins/phosphoproteins to be analysed per sample. Thus, these methods are inherently more amenable to discovering novel targets (Morris et al. 2014). Identification of potential targets involves finding proteins whose expression or activities change under certain biological conditions or disease states, which may serve as a potential therapeutic target. Although proteomics alone can provide a great deal of information, determining the phosphorylation status of proteins in relevant biological systems may also support drug discovery studies, as phosphorylation events are proximal to many disease-causing signalling mechanisms (Morris et al. 2014). For example, in the context of angiogenesis and growth factor signalling, changes that occur in both protein and protein phosphorylation may lead to hypotheses about potential drug targets relating to angiogenesis-related disorders such as cancer (section 1.6). Following target identification, proteomic methodologies can also support target validation, for example by testing the effects of targeting drugs on the cellular systems by looking at changes in protein and phosphorylation levels (Hughes et al. 2010; Kopec et al. 2005). Additional ways in which proteomics can be used include biomarker identification and investigations into drug action or toxicity mechanisms. Proteomics methodologies can also identify protein-protein interactions that may contribute to the disease state of interest and can lead to identification of potential drug targets (Morris et al. 2014). Overall, proteomics methodologies play a huge role in drug discovery and development, and in particular, may be used to identify drug targets that may have the potential to treat angiogenesis-associated diseases (section 1.6).

Chapter 2: Materials and methods

All chemicals were purchased from Sigma-Aldrich (Poole, UK), unless otherwise stated. All antibodies used in this study are detailed in table 2.1 and 2.2.

Table 2.1. Primary antibodies used in this study

Target protein	Clone number	Clonality	Species	Supplier	Use and dilution
Alpha 2 integrin	JA218	Monoclonal	Mouse	In house	FC: 1:100
Alpha 3 integrin	IA3	Monoclonal	Mouse	Abcam (Cambridge, UK)	FC: 1:25
Alpha 5 integrin	MAB16	Monoclonal	Rat	Gift	Integrin blocking antibody (scratch wound assays)
Alpha 5 beta 1 integrin	JBS5	Monoclonal	Mouse	Millipore Ltd (Watford, UK)	FC: 1:50
Alpha 6 integrin	GoH3	Monoclonal	Rat	Gift	FC: 1:20
Alpha V	17E6	Monoclonal	Mouse	Gift	FC: 1:50
Alpha V beta 3 integrin	LM609	Monoclonal	Mouse	Millipore	IF: 1:200
Alpha v beta 5 integrin	15F11		Mouse	Millipore	
ARHGAP24	-	Polyclonal	Rabbit	Abcam (Cambridge, UK)	IF: 1:200
BAK	-	Polyclonal	Rabbit	Sigma	WB 1:1000
Beta 1 integrin	9EG7	Monoclonal	Rat	In house	IF: 1:200
Beta 1 integrin	TS216	Monoclonal	Mouse	Gift	FC: 1:100
Beta 1 integrin	MAB13	Monoclonal	Rat	Gift	Integrin blocking antibody (scratch wound assays)
ERK1	-	Polyclonal	Rabbit	Santa Cruz (CA, USA)	WB 1:1000
ERK2	-	Polyclonal	Rabbit	Santa Cruz	WB 1:1000
ERK1/2 (p Thr202/Tyr204)	-	Polyclonal	Rabbit	Cell Signalling (Hitchin, UK)	WB 1:1000
FAK	77	Monoclonal	Mouse	BD Biosciences (Oxford, UK)	WB 1:1000
FAK-Y397	-	Polyclonal	Rabbit	Thermo Fisher Scientific (MA,	WB: 1:1000
Filamin A	PM6/317	Monoclonal	Mouse	Abcam	WB 1:1000
GIT1	-	Polyclonal	Rabbit	Proteintech (Manchester,	WB: 1:500
IgG Mouse		Polyclonal	Mouse	Abcam	FC: 1:50
IgG Rat	R3-34	Polyclonal	Rat	BD Biosciences	FC: 1:50
ILK	EPR1592	Monoclonal	Rabbit	Abcam	WB 1:1000
MARCKS	D88D11	Monoclonal	Rabbit	Cell signalling	IF: 1:200
Paxillin	349	Monoclonal	Mouse	BD Biosciences	WB 1:1000
Paxillin-Y118	-	Polyclonal	Rabbit	Thermo Fisher	WB: 1:1000
Src-Y416	-	Polyclonal	Rabbit	Cell signalling	WB: 1:1000
Talin	8D4	Monoclonal	Mouse	Sigma	WB 1:1000
Transferrin	H68.4	Monoclonal	Mouse	Invitrogen	WB 1:1000
VASP	-	Polyclonal	Rabbit	Proteintech	WB: 1:500
Vinculin	hVin1	Monoclonal	Mouse	Sigma	WB 1:1000

WB: Western blotting, IF: Immunofluorescence, FC: Flow cytometry.

Table 2.2. Secondary antibodies used in this study

Target protein	Conjugate	Supplier	Colnality	Species	Use and dilution
Mouse IgG	Alexa Fluor 680-conjugated	Invitrogen	Polyclonal	Goat	WB 1:5000
Rabbit IgG	Alexa Fluor 680-conjugated	Invitrogen	Polyclonal	Goat	WB 1:5000
Rat IgG	Alexa Fluor 680-conjugated	Invitrogen	Polyclonal	Goat	WB 1:5000
Mouse IgG	DyLight 800-conjugated	Cell Signalling Technology	Polyclonal	Goat	WB 1:5000
Rabbit IgG	DyLight 800-conjugated	Cell Signalling Technology	Polyclonal	Goat	WB 1:5000
Mouse IgG	Alexa-Fluor-488 conjugated	Invitrogen	Polyclonal	Donkey	IF: 1:400
Rat IgG	Alexa-Fluor-488 conjugated	Invitrogen	Polyclonal	Donkey	IF: 1:400
Mouse IgG	Alexa-Fluor-594 conjugated	Invitrogen	Polyclonal	Donkey	IF: 1:400
Rat IgG	Alexa-Fluor-594 conjugated	Invitrogen	Polyclonal	Donkey	IF: 1:400
Mouse IgG	FITC-conjugated	AbD Serotec (Oxford, UK)	Polyclonal	Rabbit	FC: 1:200
Rat IgG	FITC-conjugated	AbD Serotec	Polyclonal	Rabbit	FC: 1:200

WB: Western blotting, IF: Immunofluorescence, FC: Flow cytometry.

2.1 Kinase inhibitors

Inhibitors of FAK (AZ13256675, termed FAK [i]; Astra Zeneca, Macclesfield, UK) and Src (AZD0530, termed Src [i]; Astra Zeneca) were solubilised and stored in DMSO at 100 mM. Inhibitors were diluted to 10 mM in dimethyl sulfoxide (DMSO) and used at a dilution of 1:1000, unless otherwise stated. Where combined FAK [i] and Src [i] treatment was used, inhibitors were simultaneously applied to cells. MEK inhibitor (PD184352) and PKC inhibitor (Gö6983) was used at 1 µM.

2.2 HUVEC cell culture

HUVECs derived from pooled donors were purchased from PromoCell (Heidelberg, DE) and maintained in complete Endothelial Cell Growth Medium 2 (EGM2; PromoCell), at 37°C / 5% CO_2. Cells were passaged at approximately 90% confluence and used for experiments between passage 4 and 6. To passage, adherent cells were washed with phosphate-buffered saline without cations (PBS-) and detached with trypsin-ethylenediaminetetraacetic acid (EDTA). Full medium with addition of 10% foetal calf serum (FCS, Lonza Bioscience, Slough, UK) was then added to quench trypsin. HUVECs were collected by pelleting at 1100 revolutions per minute (RPM) for 3 minutes; cell pellets resuspended in complete EGM2 and distributed into attachment factor (Invitrogen) coated flasks at a dilution factor of approximately 1:4. For cryopreservation, cell pellets were resuspended in 90% FCS/ 10% DMSO and stored at -80°C (short term) or in liquid nitrogen (long term).

2.3 Cell spreading assays

Cell culture plates of 55- or 152 cm^2 (Corning, Amsterdam, NL), or round glass coverslips (13 mm diameter) were coated with 5, 15 or 1 mL respectively, of 10 µg/mL fibronectin (~ 1 µg/cm^2),

vitronectin or collagen-1 (BD Biosciences) diluted in phosphate-buffered saline containing 1 mM calcium and 0.5 mM magnesium (PBS+) for 60 minutes at room temperature or overnight at 4°C. For control conditions, plates/coverslips were coated with 10 µg/mL poly-D-lysine (poly-lysine or PL), apotransferrin or concanavalin A in the same way. Following aspiration of coating ligand, coated surfaces were incubated with 1% heat-denatured bovine serum albumin (BSA) in PBS- for 30-60 minutes to block non-specific binding sites. BSA was removed and plates/coverslips washed with PBS- to remove residual BSA.

Subconfluent HUVECs were harvested with trypsin and quenched with defined trypsin inhibitor (Invitrogen), washed and resuspended in Dulbecco's Modified Eagle's Medium (DMEM) containing 25 mM 4-(2-hydroxyethyl)-1-piperazineethanesulfonic acid (HEPES), 4.5 mg/mL glucose and L-glutamine (DMEM-H). Cells were then plated onto plates or coverslips at approximately 2-3 x 10^4 cells per cm^2. Plates/coverslips were incubated for 2 hours (unless otherwise stated) at 37°C in a 5% CO_2 incubator to allow cells to spread. For experiments involving Src or FAK kinase inhibition, HUVECs were spread on fibronectin for 1 hour and treated with DMSO, Src or FAK inhibitor at 10 µg/mL for 1 hour (section 2.1, unless otherwise stated). For experiments requiring VEGF treatment HUVECs were serum starved overnight in EGM2 basal serum free medium (SFM) prior to harvesting with trypsin (unless otherwise stated). Following spreading, medium was removed, and 5 mL SFM or SFM with 25 ng/mL VEGF (R and D systems, Minneapolis, USA) added for 7.5 minutes (unless otherwise stated).

For preparation of total cell lysates (TCL) following cell spreading assays, all medium was removed from cell culture plates, and cells washed with ice cold PBS-. Following removal of PBS-, lysis buffer was added to each plate on ice, and the surface of each dish scraped thoroughly to ensure full cell lysis. Cell lysis buffer composition was (150 mM NaCl, 25 mM tris(hydroxymethyl)methylamine (Tris), 2% (w/v) Triton X-100, pH 7.4) with addition of either Halt protease cocktail inhibitors (Thermo Fisher Scientific) or 0.5 mM 4-(2-aminoethyl)benzenesulfonylfluoride hydrochloride (AEBSF), 10 µg/ml leupeptin, 10 µg/ml aprotonin, 10 mM sodium fluoride and 2 mM sodium vanadate. Cell lysates were centrifuged at 4°C, 16,000g for 5 minutes to pellet non-solubilised material and the supernatant stored at -80°C until required for analysis.

2.4 Flow cytometry

Subconfluent HUVECs were detached using trypsin as described in section 2.2 with resuspension of cell pellets in PBS-. For each condition, 1 x 10^6 cells per condition were labelled with primary antibody (table 2.1) in 1% (v/v) FCS/0.01% (w/v) sodium azide in PBS- on ice for 1 hour. Cells were collected by centrifugation at 900g and washed with 1% FCS in PBS- (washing performed three times). After the final wash, cells were again collected by centrifugation and incubated with the

appropriate species-specific fluorescently-conjugated secondary antibodies (table 2.2) diluted in 1% FCS in PBS- on ice for 30 minutes. Cells were washed twice as performed previously, with a final wash in PBS-. After the final wash, cells were resuspended in 500 µL PBS- prior to flow cytometry analysis. Cell surface expression analysis was performed using a Dako CyAnTM ADP Analyser (Beckman Coulter, High Wycombe, UK).

2.5 Immunofluorescence microscopy

For immunofluorescence microscopy of HUVECs prepared by cell spreading assays, cell spreading was performed as described in section 2.3. Cells were either left intact on glass coverslips or processed for adhesion complex enrichment and complexes left attached to the plastic 55 cm^2 plate. For the latter, a small (13 mm diameter) section of the 55 cm^2 plate was processed for staining.

At the desired point, cells or enriched adhesion complexes were fixed in 4% w/v paraformaldehyde for 5-10 minutes and washed thoroughly in PBS- before staining. Samples were permeabilised with 0.5% Triton-X 100 (w/v), incubated in primary antibody (table 2.1) diluted in PBS- for 1 hour and washed thoroughly in PBS-. A secondary incubation was then performed with the appropriate secondary antibodies diluted in PBS- (table 2.2) and where indicated, Alexa Fluor-594 phalloidin (Invitrogen) for 1 hour. Samples were then washed in PBS-, counterstained with 4',6-diamidino-2-phenylindole (DAPI; 1 µg/mL) and mounted in ProLong Gold Antifade Reagent (Invitrogen). Images were then collected on an Olympus BX51 upright microscope using a 60x/0.65 - 1.25 UPlanFLN objective and captured using a Coolsnap EZ or HQ camera through MetaVue Software (Molecular Devices, Sunnyvale, USA). Specific band pass filter sets for DAPI, FITC and Texas red were used to prevent bleed through from one channel to the next. Images were processed using ImageJ.

2.6 Adhesion complex enrichment

Cell spreading was performed as described in section 2.3. After incubation, HUVECs were incubated with 6 mM (unless otherwise stated) dimethyl-3, 30-dithiobispropionimidate (DTBP, Sigma-Aldrich) diluted in DMEM-H for 5 minutes (unless otherwise stated). DTBP was then quenched using 1 M Tris, pH 8, for 2 minutes, after which the cells were transferred to ice and washed thoroughly with ice cold PBS-. Cell bodies were removed by a combination of cell lysis in RIPA buffer (50 mM Tris-HCl pH 7.6, 150 mM NaCl, 5 mM EDTA, 0.5% SDS (w/v), 1% Triton X-100 (w/v), 1% deoxycholate (w/v)) for 2 minutes and a 5 second high-pressure tap water wash. The remaining ligand bound complexes were washed with PBS- and recovered by scraping in recovery solution (40 µL per plate; 125 mM Tris-HCl, pH 6.8, 1% SDS (w/v), 150 mM dithiothrietol (DTT)). Following collection, samples were stored at -80°C until required for SDS-PAGE, western blotting, in-gel trypsin digestion (section 2.7) or phosphopeptide enrichment (section 2.8). For SDS–PAGE, western blotting and in-gel trypsin

digestion soluble protein was precipitated from solution by addition of four volumes of acetone, and incubated at -20°C overnight. After incubation, precipitated samples were centrifuged at 16,000g for 20 minutes at 4°C, and washed twice with ice cold acetone. The protein pellet was dried at room temperature and resuspended in the appropriate volume of reducing sample buffer (50 mM Tris-HCl [pH 6.8], 10% (w/v) glycerol, 4% (w/v) SDS, 0.004% (w/v) bromophenol blue, and 9% (v/v) β-mercaptoethanol) by shaking at 1400 RPM for 15 minutes at 70°C followed by incubation for 5 minutes at 95°C. Enriched adhesion complexes were then ready for analysis (SDS–PAGE, western blotting and in-gel trypsin digestion).

2.7 SDS-PAGE and western blotting

Samples to be analysed by SDS-PAGE were loaded into wells of a 4-12% (w/v) NuPAGE Novex Bis-Tris gel (Invitrogen) along with molecular weight markers (Precision Plus All Blue protein standards, Bio-Rad Laboratories, Hemel Hempstead, UK). Gels were run in (2-N-morpholino)ethanesulfonic acid (MES) running buffer at 200V for 50 minutes and processed for either Coomassie Blue staining or western blotting.

For Coomassie Blue staining proteins were visualised with InstantBlue (Expedeon, Harston, UK) stain, by incubation for 1 hour in stain, followed by destaining for at least 1 hour in water. For western blotting, proteins were transferred to a nitrocellulose membrane using XCell II blot modules (Invitrogen) according to the manufacturer's instructions. Proteins were transferred in transfer buffer (25 mM Tris-HCl, 190 mM glycine, 0.01% (w/v) SDS, 10% (v/v) methanol) at 30V for 90 minutes. Nitrocellulose membranes were blocked with casein blocking buffer (diluted in PBS-), probed with primary antibody (table 2.1) diluted in casein blocking buffer (dilute in Tris Buffered Saline containing 0.01% (v/v) Tween-20 (TBST)) for 1 hour at room temperature or overnight at 4°C. Membranes were then washed thoroughly in TBST followed by incubation with the appropriate fluorescent dye-conjugated secondary antibody (table 2.2) diluted in TBST for 45 minutes at room temperature protected from light. Membranes were washed thoroughly with TBST. Coomassie Blue stained gels and antibody probed membranes were scanned using the Odyssey infrared imaging system (LI-COR Biosciences, Nebraska, USA). Where required, relative band or region density quantification was performed using Odyssey software, which calculated the mean intensity of pixels in a border around a shape and subtracts that background from the shape.

2.8 In-gel trypsin digestion

Samples were resolved by SDS-PAGE as described in section 2.7 for 3 minutes. Proteins were then visualised by brief staining (approximately 15 minutes) with InstantBlue (Expedeon) protein stain, destained overnight, and protein bands cut out and transferred to wells of a perforated 96-well plate (Proxeon, Hemel Hempstead, UK). Gel slices were washed a minimum of two times (until gel

stain completely removed from gel slices) in 50% acetonitrile (ACN)/50% 25 mM NH_4HCO_3 (AMBIC) for 30 minutes at room temperature. Gel pieces were dehydrated twice in 100% ACN for 5 minutes at room temperature and then dried for 25 minutes under vacuum centrifuge at -118°C. Dried gel prices were then reduced in 10 mM DTT/25 mM AMBIC for 1 hour at 56°C and alkylated in 55 mM iodoacetamine/25 mM AMBIC for 45 minutes at room temperature protected from light. Gel pieces were then washed alternately with 25 mM AMBIC (to induce swelling) and ACN (to induce dehydration), these wash steps were repeated and the gel slices dried for 25 minutes under vacuum centrifuge at -118°C. Dried gel sliced were rehydrated in 0.6 µg trypsin (Promega, Southampton, UK) diluted in 25 mM AMBIC, overnight at 37°C, to achieve protein digestion. Following trypsinisation, peptides were collected by centrifugation into a collection plate and further extracted in 100% ACN (v/v)/0.2% formic acid (v/v) and then 50% ACN (v/v)/0.1% formic acid (v/v). Extracted peptides were dried by vacuum centrifugation, and peptides resuspended in 5% ACN (v/v)/0.1% formic acid (v/v) ready for analysis.

2.9 Phosphopeptide enrichment

TCL (section 2.3) or adhesion complex samples (section 2.6) were reduced with 10 mM DTT at 56°C for 1 hour, and alkylated with 15 mM iodoacetamide for 45 minutes at room temperature, protected from light. Proteins were precipitated as described in section 2.6, and pellets resuspended in 0.2% Rapigest (w/v; Waters, Elstree, UK) in 50 mM NH_4HCO_3. Trypsin (at 125 µg/mL) was then added at 1:20-1:50 (w/w) and incubated overnight at 37°C. Samples were acidified to 0.5% (v/v) trifluoroacetic acid (TFA) using a 10% TFA stock. Digested peptides were incubated for a further 45 minutes at 37°C and precipitated RapiGest within samples removed by centrifugation at 22,000g. Peptides were then desalted using Oasis HLB cartridges containing C18 media (Waters). For desalting, columns were first equilibrated with 50% ACN and washed with 0.1% formic acid. Peptides were loaded to the column, washed with 0.1% formic acid and bound peptides eluted into 200 µL binding solution (80% MeCN, 5% TFA, 1M glycolic acid). For enrichment using magnetic microspheres (Ti-IMAC or TiO_2; ReSyn Bioscience, Gauteng, South Africa), microspheres were washed according to manufacturer's instructions prior to phosphopeptide enrichment sample processing.

For enrichment using TopTip TiO_2 beads (Glygen, Maryland, USA), 10 mg beads in 50% (v/v) ACN were added to spin columns (Thermo Scientific Pierce) and washed through into a collecting tube by centrifugation at 11,000g for 1 minute. TiO_2 beads were then washed with binding solution (65% (v/v) ACN, 2% (v/v) TFA, saturated with glutamic acid). Samples were added to columns containing TiO_2 beads for 1 hour at room temperature with rotation. Unbound peptides were removed by centrifugation and washing with binding solution, wash 1 solution (65% ACN, 5% TFA) and wash 2 solution (65% ACN, 1% TFA) respectively. Phosphopeptides were eluted using an elution solution

(300 mM ammonium hydroxide, 5% (v/v) ACN). Following elution, samples were acidified to approximately 1% TFA using a 10% TFA stock, and desalted using Poros R3 beads (section 2.10).

For manual phosphopeptide enrichment using magnetic beads tryptic digest samples were incubated with 1 mg magnetic microspheres (Ti-IMAC or TiO_2 individually or at 25%:75% Ti-IMAC:TiO_2 ratio) for 20 minutes under agitation. Microspheres were resolved by magnet and washed with binding solution, followed by wash buffer 1 (80% MeCN, 1% TFA; 3 x 2 minutes). Phosphopeptides were eluted by incubation in an elution buffer (1% NH_4OH; 3 x 15 minutes under agitation), and acidified to approximately 1% TFA using a 10% TFA stock, and desalted using Poros R3 beads (section 2.10).

Automated phosphopeptide enrichments were performed using a KingFisher Flex (Thermo Scientific) magnetic particle-processing robot. The phosphopeptide enrichment program was developed by Tape et al., and downloaded for use (identifier 'Automated_Phosphopeptide_Enrichment.msz)', (Tape et al. 2014). Deep-well 96-well plates (Thermo Scientific) were loaded with the appropriate solution and assigned to each of the eight carousel positions (table 2.3). For the magnetic microsphere plate, pre washed beads were added at a Ti-IMAC/TiO_2 ratio of 75%:25% (v/v). All experiments were performed using the protocol detailed in table 2.3, with two 45 minute cycles (eluted phosphpeptides were removed from the elution plate and fresh elution solution added for each cycle). Eluates were immediately acidified to approximately 1% TFA using a 10% TFA stock, and desalted using Poros R3 beads (section 2.10).

Table 2.3. Automated phosphopeptide enrichment using KingFisher Flex (Tape et al. 2014).

Carousel position	Plate input	Time (minutes; total 45)	Volume (µL)
1	96-well tip heads (Thermo Scientific)	1	NA
2	Magnetic microspheres (1 mg per well in binding solution)	3	500
3	Binding solution (80% MeCN, 5% TFA, + 1 M glycolic acid)	5	500
4	Sample (tryptic digest in binding solution)	20	200
5	Binding solution (80% MeCN, 5% TFA, 1M glycolic acid)	2	500
6	Wash buffer 1 (80% MeCN, 1% TFA)	2	500
7	Wash buffer 2 (10% MeCN, 0.2% TFA)	2	500
8	Elution buffer (1% NH_4OH)	10	200

2.10 Peptide desalting

Tryptic peptide samples prepared by in-gel trypsin digestion or phosphoenrichment were desalted by addition to Poros R3 beads (Applied Biosystems, Paisley, UK). Peptides were collected by elution from beads in 50% ACN/0.1% formic acid, and evaporated to completion by vacuum centrifugation. Peptides were stored dried at 4°C, and resuspended in 5% ACN/0.1% formic acid prior to mass spectrometry analysis.

2.11 Mass spectrometry analysis

2.11.1 Orbitrap Elite- proteomic analysis

Samples were analysed by liquid chromatography (LC) tandem mass spectrometry (LC-MS/MS) using an UltiMate 3000 Rapid Separation LC (RSLC, Dionex Corporation, Sunnyvale, CA) coupled to an Orbitrap Elite (Thermo Fisher Scientific) mass spectrometer. Peptide mixtures were separated using a 250 mm x 75 µm i.d. 1.7 µM BEH C18, analytical column (Waters) with the LC gradient from 92% A (0.1% FA in water) and 8% B (0.1% FA in acetonitrile) to 33% B, in 104 minutes at 300 nL min^{-1}. Peptides were selected for fragmentation automatically by data dependant analysis.

2.11.2 Orbitrap Elite- phosphoproteomic analysis

Digested samples were analysed by LC-MS/MS using an UltiMate 3000 Rapid Separation LC (RSLC, Dionex) coupled to an Orbitrap Elite (Thermo Fisher Scientific) mass spectrometer. Peptide mixtures were separated using a 250 mm x 75 µm i.d. 1.7 µM BEH C18, analytical column (Waters) with the LC gradient from 95% A (0.1% FA in water) and 5% B (0.1% FA in acetonitrile) to 33% B, in 164 minutes at 300 nL min^{-1}. Peptides were selected for fragmentation automatically by data dependant analysis, and fragmented with multistage activation enabled.

2.11.3 Q Exactive

Digested samples were analysed by LC-MS/MS using an UltiMate 3000 Rapid Separation LC (RSLC, Dionex Corporation) coupled to a Q Exactive HF (Thermo Fisher Scientific) mass spectrometer. Peptide mixtures were separated using a 75 mm x 250 µm i.d. 1.7 µM CSH C18, analytical column (Waters) with the LC gradient from 95% A (0.1% FA in water) and 5% B (0.1% FA in acetonitrile) to 7% B at 1 minute, 18% B at 58 minutes, 27% B in 72 minutes and 60% B at 74 minutes at 300 nL min^{-1}. Peptides were selected for fragmentation automatically by data dependant analysis.

2.12 Mass spectrometry data processing

RAW data files were submitted to the Mascot server using Mascot Daemon (Matrix Science, London, UK) and database searching performed using an in house Mascot server. Peak lists were searched against a human database in FASTA format. For searches, carbamidomethylation of cysteine (+57.02 Da) was set as a fixed modification, and oxidation of methionine (-64.00 Da; +16.00 Da) as a variable modification. For phosphopeptide enriched samples, serine, threonine and

tyrosine phosphorylation were included as variable modifications. Only tryptic peptides with a maximum of one missed cleavage were considered. Monoisotopic precursor mass values were used, and peptides with a charge of 2+, 3+, 4+ were considered. Mass tolerances for precursor ions was 5 ppm, and for fragment ions, 0.5 Da (for data collected using the Orbitrap Elite) or 20 milli mass units (for data collected using the Q Exactive).

2.12.1 Spectral count analysis

Data obtained from mascot searches were validated and visualised using Scaffold (Proteome Software) (Searle 2010). A peptide threshold of 90%, a protein threshold of 99% and two peptides minimum were used for protein identification. Individual phosphopeptide identifications (based on one unique, validated peptide) were accepted if they could be established with at least 95% probability at the peptide level and at least 80% probability at the protein level. For quantification using spectral counting for proteomic data, the total number of spectral counts assigned to each protein was normalised to the total number of peptide identifications in the corresponding analysis. Where applicable, the normalised spectral count values were averaged for each identified protein across multiple repeats. For quantification using spectral counting for phosphoproteomic data (chapter 4), raw spectral count was used.

2.12.2 Ion intensity analysis

Ion intensity analysis was performed from RAW files using Progenesis QI (version 2.0, Non-linear dynamics, Newcastle-upon-Tyne, UK). For processing, automatic detection of alignment reference was used, and alignment was >70% in all cases (Ng et al. 2017).

2.12.2.1 Protein analysis

Relative quantification was performed using protein grouping with non-conflicting unique peptides for protein analysis. Proteomic data were exported as protein measurements. To account for differences in protein loading, raw abundance values were normalised to the summed raw abundance value in each condition. Only proteins identified with at least unique two peptides were considered. For each identified protein, Log_2 fold change values for each biological replicate were calculated using normalised raw values and the average taken.

2.12.2.2 Peptide analysis

Relative quantification was performed using all peptides for peptide analysis, and data were exported as peptide measurements. Data were filtered using the following criteria: only 2+, 3+, 4+ ions included, ions identified with a mascot score >28. For any replicate peptides (duplicate m/z values) those with the highest mascot score and/or mass error nearest to zero were selected. For peptides which fit these criteria, raw abundance values were normalised to the total raw abundance value in each condition, to account for differences in protein loading. For each identified

peptide, Log_2 fold change values for each biological replicate were calculated using normalised raw values and the average taken. To account for peptides in which the peptide abundance value was zero, a small addition (1×10^{-10}) was made to each value, and the average fold change was calculated using these values.

2.12.3 Protein-protein interaction network analysis

Protein-protein interaction network analysis was performed using Cytoscape (version 3.2.1)(Cline et al. 2007). Proteins were mapped onto a human interaction network composed of physical protein-protein interactions reported in the Protein Interaction Network Analysis (PINA) database (October 2012), the ECM database MatrixDB (April 2012) (Launay et al. 2014) and the literature-curated integrin adhesome (Zaidel-Bar et al. 2007;Zaidel-Bar and Geiger 2010) as previously described (Byron et al. 2015;Humphries et al. 2009)

2.12.4 Gene ontology analyses

Gene ontology (GO) enrichment analyses were performed using the Database for Annotation, Visualisation and Integrated Discovery (DAVID; version 6.7) (Huang et al. 2008;Huang et al. 2009) using GO categories: Kyoto encyclopedia of genes and genomes (KEGG) pathway, biological process, cellular compartment and molecular function. The background dataset used for analyses was the Homo sapiens genome.

2.12.5 Kinase prediction analysis

Identified phosphopeptides from phosphoproteomic datasets were analysed using the Group-based Prediction algorithm with the interaction filter (iGPS; version 1.09), (Song et al. 2012). To minimize false positives, the high threshold false positive rate was applied.

2.13 Fluorescence recovery after photobleaching

HUVECs were transfected with YFP tagged sSH2 DNA construct using the nucleofector device with HUVEC nucleofector kit according to manufacturer's instructions (3 µg plasmid DNA; program A-034; Lonza). Experiments were performed approximately 24 hours after transfection. Before imaging, HUVECs were trypsinised and plated on fibronectin coated glass bottom plates (14 mm diameter; MatTek) for 2 hours in SFM. For experiments involving VEGF treatment, plates were imaged before and after VEGF treatment which was added at a final concentration of 25 ng/mL and imaging begun 5 minutes after addition. For experiments involving Src inhibitor treatment, 10 µM Src inhibitor or an equivalent volume of DMSO was added to the medium at least 1 hour prior to imaging. Prepared cells were placed in the microscope chamber at 37°C. Images were collected using a 3i spinning disk inverted confocal microscope with a 60×/1.40 oil Plan-Apochromat objective, Evolve EMCCD camera (Photometrics, AZ, USA), and motorized XYZ stage (ASI). Samples were excited using 488 nm diode lasers via GFP filter cubes. Three images were taken before

photobleaching, and five IACs were bleached per cell with the 488 nm laser. Slidebook software was used to capture images every 10 seconds for a period of 4 minutes after photobleaching. Corrected recovery fluorescence intensities were normalized to intensity before bleaching. For determination of recovery half-time (t1/2), the normalized recovery data were fitted to the single exponential equation $F(t) = MF \times (1 - e\tau t)$ and the t1/2 was calculated by $t1/2 = \ln 0.5/-\tau$.

2.14 siRNA transfection

siRNA protein knockdown was performed using ON-TARGET plus smartpool siRNAs (Dharmacon, Thermo Fisher Scientific). Non-targeting siRNA was used as a negative control. Briefly, transfection of HUVECs was performed using GENEfector (VennNova, Florida, USA), using two rounds of transfection, according to manufacturer's instructions. HUVECs were cultured in 6-well plates or cell culture plates of 55 cm^2 for 24 hours. HUVECs were then washed in Optimem (Invitrogen), and left in Optimem for approximately 30 minutes. A siRNA:liposome mixture was prepared and added to cells (3 µl siRNA per well of a 6-well plate or 15 µl siRNA per 55 cm^2 dish, from a 20 µM siRNA stock). HUVECs were incubated for 3-5 hours in siRNA solution. Media was changed to EGM2, and left for 24 hours. HUVECs were then split at a ratio of 1:3 (section 2.2), and the GENEfector transfection protocol repeated 24 hours later. After further 24-48 hour incubation, experiments were performed (cell spreading assays).

2.15 Scratch wound migration assays

Scratch wound cell migration assays were performed using the IncuCyte Zoom Live Cell Imaging System (Essen BioScience, Michigan, USA). HUVECs were plated at a density of 90,000 cells per well (unless otherwise stated) in SFM in an IncuCyte ImageLock 96-well microtiter plate (Essen BioScience) and left for 3-4 hours (unless otherwise stated). The WoundMaker (Essen BioScience) was used to create scratch wounds in all wells of the 96-well plate simultaneously, according to manufacturer's instructions. Wells were washed to remove cell debris, and experimental solutions added to wells as required. Experimental solutions included SFM/VEGF at the stated concentration; Src, FAK, MEK and/or PKC inhibitors (section 2.1); integrin blocking antibodies (table 2.1). Wound closure was captured using the IncuCyte Zoom System, with images captured every hour for a minimum of 16 hours, using a 10x objective. Cell migration was analysed using the integrated cell migration analysis module (Essen BioScience) which analyses phase contrast cell migration images. Data are displayed as relative wound density (%). This readout measures the spatial cell density in the wound area relative to the spatial cell density outside of the wound area at each time point. The value is set to 0% at time zero, and 100% when the cell density inside the wound is the same as the cell density outside the initial wound.

Chapter 3: Proteomic analysis of HUVEC integrin adhesion complex composition

3.1 Overview

The aim of this study was to perform a global analysis of VEGF-adhesion crosstalk in ECs. The initial challenge was to characterise the adhesive properties of HUVECs, and establish a workflow to enrich and detect by mass spectrometry, adhesion complex proteins from ECs. Successful enrichment and identification of adhesion complex proteins has previously been performed on 2D substrates using a variety of adherent cells, including fibroblasts, melanoma and leukaemia cells (Horton et al. 2015). However, there are only limited studies that have performed a global analysis of EC adhesion complex composition (Atkinson et al. 2017). In this chapter, a series of optimisation steps were performed to establish a robust method for the enrichment of adhesion complexes from HUVECs, and used to define the protein composition of the HUVEC adhesion complex.

3.2 Adhesive properties of HUVECs

HUVECs were selected for proteomic analysis of EC adhesion complexes as they are a readily available source of ECs, are well characterised and are considered to reproduce many features of ECs in vivo (Park et al. 2006). To identify an adhesive substrate on which cells could be plated, the HUVEC integrin cell surface expression repertoire and ECM adhesive activity were assessed. The ECM components fibronectin, collagen and laminin, which interact with ECs in the resting and angiogenic state (Kumar et al. 2012), were chosen for analysis.

To identify which integrins were expressed on HUVECs, flow cytometry was used with a range of subunit-specific anti-integrin monoclonal antibodies (figure 3.1a). The results demonstrated cell surface expression of the α2, α3, α5, α6, αV, αVβ3, αVβ5 and β1 integrin subunits. These data suggest that α2β1, α3β1 and α6β1 (collagen- and laminin-binding) and α5β1, αVβ5, αVβ3 (fibronectin-binding) heterodimers are expressed in HUVECs, and suggest the fibronectin-binding integrin α5β1 displays the highest level of expression. Spreading and adhesion complex formation by HUVECs on these ligands was assessed by immunofluorescence microscopy using the adhesion complex markers vinculin and paxillin, together with phalloidin to detect F-actin. HUVECs adopted a flattened and spread morphology, and formed adhesion complexes when plated on collagen-I (10 μg/mL) and fibronectin (10 μg/mL) for 1 and 2 hours (figure 3.1b). Adhesion complexes were observed as punctate structures at the ends of actin filaments. In contrast, when plated on laminin, HUVECs did not appear to form adhesion complexes, and adopted an elongated morphology. For proteomic analysis of IACs enriched by affinity isolation of ventral membrane preparations, a non-integrin binding control is required to identify proteins which are isolated but are not specific to integrin-mediated adhesion complexes (Jones et al. 2015). When HUVECs were plated on the non-

integrin binding ligands poly-lysine, apotransferrin and concanavalin A for 1 and/or 2 hours (figure3.1b), they remained round, and did not form vinculin- or paxillin-positive adhesion complexes.

Taken together, these results demonstrate that adhesion complexes form, and may be enriched from HUVECs plated on fibronectin and collagen, although not on laminin, and that poly-lysine, apotransferrin and concanavalin A may be suitable negative control ligands for such an approach.

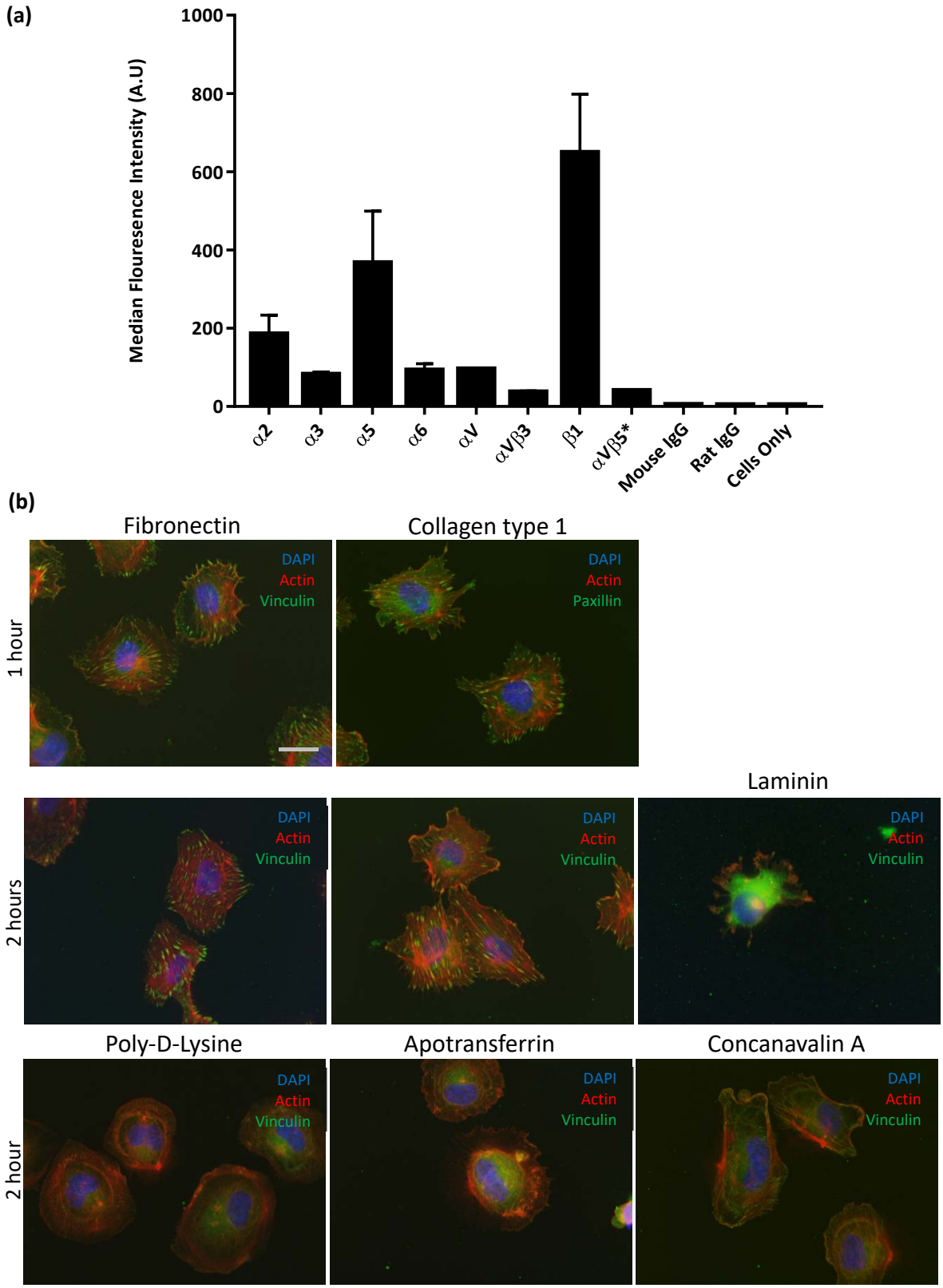

Figure 3.1. Adhesive characteristics of HUVECs. (a) Flow cytometry cell surface expression analysis of integrin subunits. HUVECs were incubated with mouse anti-human (α2, α3, α5, αV, αVβ3, β1 and αVβ5) or rat anti-human (α6) primary integrin antibodies, followed by fluorescently labelled secondary antibodies. Species specific IgG antibodies were used as controls. Data are presented as median of median fluorescence intensity, error bars indicate range. n=2 except for αVβ5* where n=1, A.U= Arbitrary Units. (b) Immunofluorescence microscopy of adhesion complex markers. HUVECs were plated on the indicated ligand coated coverslips for 1 or 2 hours, fixed and stained with Texas Red conjugated phalloidin (red), DAPI (blue) and the adhesion complex marker vinculin or paxillin (green), scale bar= 20 µm.

3.3 Establishment of a HUVEC adhesion complex enrichment protocol

To determine conditions to enrich IAC proteins from HUVECs, a previously developed protocol was employed (Jones et al. 2015), and a series of optimisation steps performed. Initial optimisation of the protocol focused on multiple stages, with analysis by SDS-PAGE in combination with Coomassie Blue staining and western blotting. Analysis by these methods can be used as a semi-quantitative method of protein quantification. In addition, as common protein quantification methods are incompatible with the buffers used in this protocol, Coomassie Blue staining was used as alternative semi-quantitative approach by comparing the lane intensity for each sample run on the same SDS-PAGE gel (section 2.7). The aim of these initial analyses was to ensure adhesion complexes were enriched with sufficient purity and yield, and that the method was reliable and reproducible, before moving to mass spectrometry analysis.

As a starting point, a protocol developed by the Humphries laboratory was performed (figure 3.2), (Jones et al. 2015). Briefly, HUVECs were plated on integrin binding ligands to allow adhesion complex formation, or non-integrin binding control ligands, cross-linked using DTBP to stabilise adhesion complexes, and cell bodies removed using a combination of detergent-based cell lysis and tap water wash. Remaining ligand-bound complexes were then collected for analysis. For initial optimisation, a previously developed protocol (figure 3.2) (Jones et al. 2015) was followed using HUVECs plated on collagen-I, fibronectin and poly-lysine (figure 3.3). Two 55 cm^2 cell culture plates were used per condition, with HUVECs plated at equal densities per plate. Samples were analysed, together with a HUVEC TCL sample, by SDS-PAGE and western blotting. Quantification by SDS-PAGE with Coomassie Blue staining (lane intensities are shown at the bottom of each lane for comparison) revealed differences in abundance of protein enriched in each condition, which need to be taken into account when comparing western blot band intensities from these samples. In addition, Coomassie Blue staining revealed differences in protein banding pattern between cells adhered to different ligands and the TCL sample (figure 3.3a). These data suggest that different ECM ligands can recruit specific sets of proteins to induced HUVEC adhesion complexes, and that these proteins differ from those recruited to non-integrin ligands or that are detected in HUVEC TCL samples. In addition, these specific sets of proteins can be isolated using this affinity-enrichment approach. Encouragingly, fewer bands were present in the enriched samples compared to the TCL, again suggesting specific protein enrichment had taken place (figure 3.3a). Western blotting for marker adhesion complex proteins (talin, vinculin, FAK and paxillin) confirmed enrichment in the fibronectin and collagen-I conditions, with minimal recruitment to the poly-lysine control (figure 3.3b). These differences were not due to differences in total protein composition of samples, as determined by Coomassie Blue staining (figure 3.3a). Furthermore, BAK was not detected; a

mitochondrial protein not associated with adhesion complexes and therefore not expected to be enriched with adhesion complex proteins.

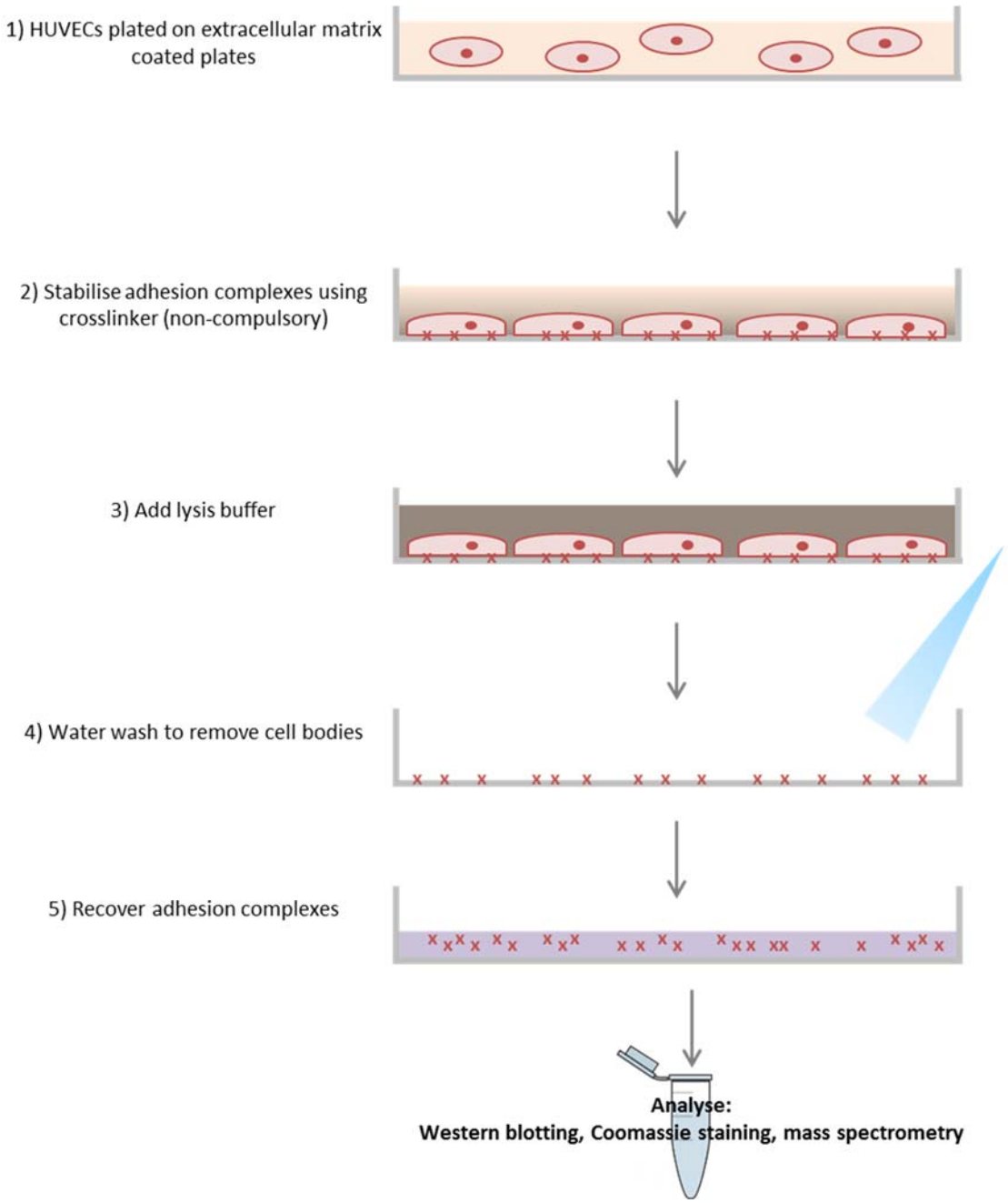

Figure 3.2. Schematic of the standard workflow used to isolate and analyse integrin adhesion complex proteins. The schematic shows the protocol used to enrich for adhesion complexes. Briefly cells are plated on an extracellular matrix ligand coated plate (1) and cross-linked if necessary (2). After plating/crosslinking a lysis buffer (3) is added to cell culture plates and cell bodies are removed using shear wash (4). Finally, remaining IAC proteins are collected by scraping in a recovery buffer, ready for analysis (5), (Jones et al. 2015).

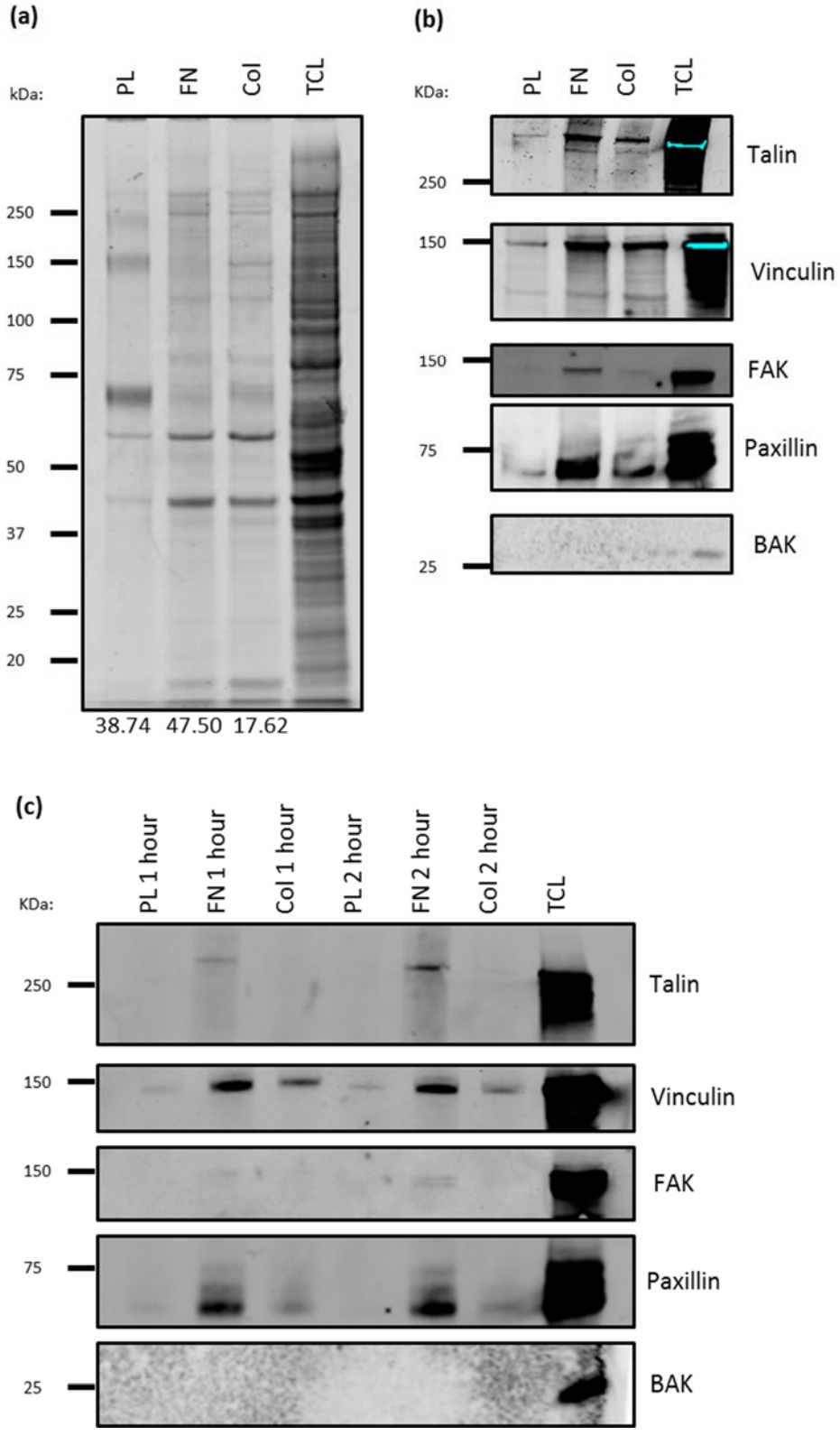

Figure 3.3. Optimisation of adhesion complex enrichment protocol: ligand and plating time. HUVECs were plated for 2 hours (or 1 hour where stated) on fibronectin (FN), collagen-I (Col) or poly-lysine (PL) coated plates, cross-linked using DTBP (6 mM for 5 minutes), and the remaining ligand bound complexes collected for analysis. (a) SDS-PAGE with Coomassie Blue staining was performed for total protein analysis, quantification of Coomassie Blue stained SDS-PAGE lanes (pixel intensity) is shown at bottom of each lane. Molecular weight values (kDa) are displayed to the left of the gel. (b,c) Western blot analysis to for positive and negative markers of adhesion complexes (positive: talin, vinculin, FAK and paxillin; negative: BAK). Quantification of Coomassie Blue stained SDS-PAGE lanes (pixel intensity) is shown at the bottom of each lane. Molecular weight values (kDa) are displayed to the left of each blot. TCL: total cell lysate.

These initial data confirm that adhesion complex proteins can be enriched from HUVECs plated on fibronectin and collagen-I compared to the non-integrin ligand poly-lysine. In addition to poly-lysine, apotransferrin, which has been used as a control in previous adhesion complex isolation studies (Horton et al. 2015;Robertson et al. 2015) and concanavalin A were assessed as alternative control substrates. However, many cells detached during the crosslinking and washing steps after spreading of cells on these ligands, resulting in minimal quantities of protein that could be isolated (data not shown). Therefore, poly-lysine was chosen as the control substrate for future studies.

The optimal time allowed for HUVECs to adhere and spread on ECM ligands was also investigated. Adhesion complex enrichment after two hours plating compared to one hour resulted in increased amounts of the adhesion complex proteins talin and FAK, as measured by western blotting (figure 3.3c). This optimisation experiment suggests that a longer plating time may increase the levels of adhesion complex protein that can be isolated using this protocol; however, keeping the plating time below 2-3 hours is desirable as after this point cells may start to produce and assemble their own ECM (Hayman and Ruoslahti 1979), which the cells will then use to aid adhesion complex formation, overriding the control ligand (Jones et al. 2015). A plating time of two hours was therefore selected for future experiments.

SDS-PAGE with Coomassie Blue staining and western blot analysis of talin, vinculin, FAK and paxillin indicated that increased levels of both total protein and specific adhesion complex components were present in samples from isolated IACs from cells plated on fibronectin when compared to collagen-I (figure 3.3). This apparent increase may reflect the higher expression of the fibronectin-binding integrin α5β1 compared to other integrins (figure 3.1a), which may result in an increase in the number, size and/or stability of adhesion complexes formed on fibronectin. Overall, fibronectin appeared to be the optimal substrate for enrichment of adhesion complexes from HUVECs, and was therefore used as the integrin-binding ligand for all future studies.

Previous experience within the Humphries laboratory has shown that optimal crosslinking conditions can differ when enriching adhesion complexes from different cell types. For example, the time and/or concentration of crosslinking may vary, or crosslinking may not be required at all (Jones et al. 2015). Therefore, to determine if crosslinking was required to enrich adhesion complex proteins from HUVECs, the protocol in figure 3.2 was performed in the presence and absence of crosslinker. For cells plated on poly-lysine, similar amounts of total protein and low levels of adhesion complex proteins (FAK, paxillin, ILK, filamin-A) were isolated in the presence or absence of crosslinker, with similar banding patterns. For fibronectin, similar protein levels were isolated using both conditions, although the banding patterns with and without crosslinking were different, suggesting differential protein isolation (figure 3.4a). As shown in previous experiments (figure 3.3),

FAK and paxillin were enriched when performing the protocol in the presence of crosslinker. In addition, western blots for the adhesion complex components ILK and filamin-A were performed; both proteins were detected with use of crosslinker. For this experiment, further negative control western blots for BAK and transferrin receptor were performed. Minimal levels of these negative control proteins were detected, generating further confidence in the use of this protocol for HUVECs. In contrast however, for the non-crosslinked samples, adhesion complex components (FAK, paxillin, ILK and filamin-A) and negative control proteins (BAK and transferrin receptor) were not detected, or detected at very low levels (figure 3.4b). These data suggest that for HUVECs, the adhesion complex enrichment protocol has a strong dependence on the crosslinking stage.

As crosslinking is required, the optimal conditions were investigated by comparison of adhesion complex isolations using a range of crosslinking concentrations and treatment times. Concentrations of 3, 6 and 12 mM DTBP for 5 minutes, as well as 6 mM for 5 and 10 minutes were investigated and compared. Increased DTBP concentration and incubation time appeared to increase total protein isolated from cells spread on fibronectin, although decreased total protein isolated from poly-lysine-plated cells (figure 3.5a). However, on both ligands, the levels of adhesion complex proteins increased with increasing DTBP concentration and time (figure 3.5b). Although in all cases adhesion complex proteins were enriched in the fibronectin condition over poly-lysine, the aim of optimising this protocol was to isolate adhesion complex proteins at a high yield from the fibronectin sample compared to the poly-lysine control. Therefore, the ratio of the abundance of adhesion proteins seen in the two conditions (ie poly-lysine/fibronectin) should be as low as possible, whilst containing similar total protein levels. This ratio was calculated using intensity values of normalised vinculin and paxillin western blot bands (normalised to their corresponding Coomassie Blue intensity values; figure 3.5c), for five replicate experiments. Although variability was highlighted between these different analyses, 6 mM DTBP for 5 minutes showed a consistently low ratio of the four conditions. The 5 minute, 6 mM DTBP crosslinking condition was therefore selected as optimal, and was used for all subsequent experiments.

To visualise the fibronectin-induced HUVEC adhesion structures that remain bound to the plate following the cell body removal stage of the protocol, and hence the structures that are collected for analysis, the isolation protocol was adapted for imaging. For this, the optimised protocol was performed up until the cell body removal stage (figure 3.2), and vinculin immunostaining performed on remaining IACs (figure 3.6). Importantly, the structures remaining were morphologically similar to that seen in whole cells (figure 3.1b), confirming that the punctate adhesion complex structures were being isolated. Actin staining indicated that a small amount of actin remained in some cells (figure 3.6); however, in most cases actin was completely removed (data not shown). DAPI staining confirmed complete removal of nuclei (data not shown). Together these data support western blot

data, confirming that adhesion complex proteins, representative of adhesion complexes, were enriched using the optimised protocol.

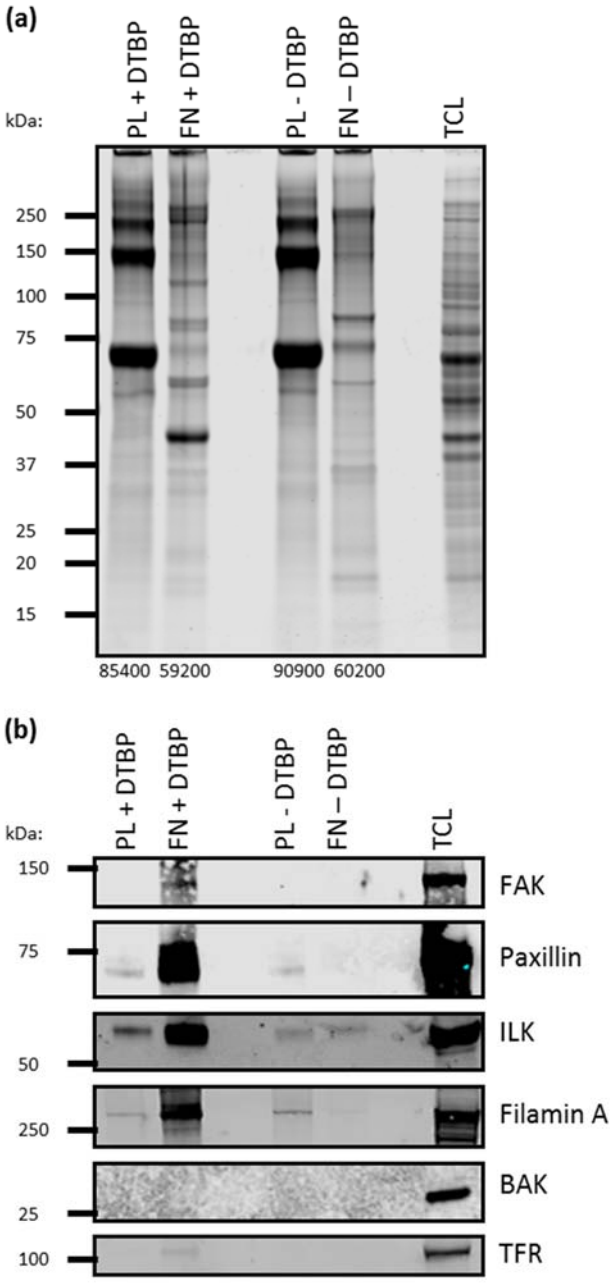

Figure 3.4. Optimisation of adhesion complex enrichment protocol: crosslinking requirement. HUVECs were plated for 2 hours on fibronectin (FN) or poly-lysine (PL) coated plates, treated with SFM (-DTBP) or cross-linked using DTBP (+DTBP) for 5 minutes, and cell bodies removed using a combination of cell lysis and tap water wash. The remaining ligand bound complexes were then collected for analysis. (a) SDS-PAGE with Coomassie Blue staining was performed for total protein analysis, quantification of Coomassie Blue stained SDS-PAGE lanes (pixel intensity) is shown at bottom of each lane. Molecular weight values (kDa) are displayed to the left of the gel. (b) Western blot analysis of positive and negative markers of adhesion complexes (positive: FAK, paxillin ,ILK and filamin-A; negative: BAK and TFR). Molecular weight values (kDa) are displayed to the left of each blot. TCL: total cell lysate.

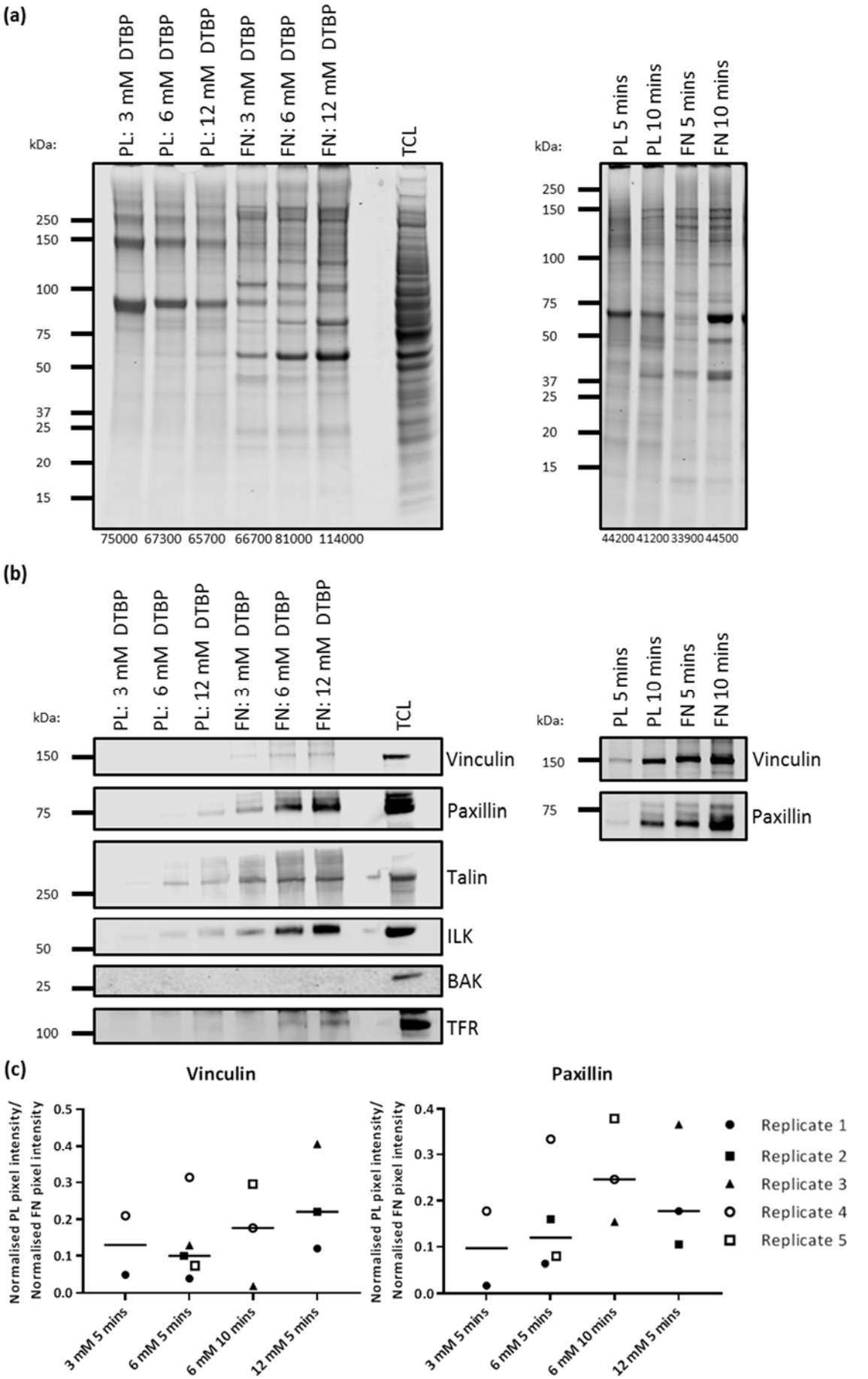

Figure 3.5. Optimisation of adhesion complex enrichment protocol: crosslinking concentration and time (see next page for legend).

Figure 3.5. Optimisation of adhesion complex enrichment protocol: crosslinking concentration and time (see previous page for figure). HUVECs were plated for 2 hours on fibronectin (FN) or poly-lysine (PL) coated plates, cross-linked using DTBP under the conditions detailed (3, 6 and 12 mM DTBP for 5 minutes, as well as 6 mM for 5 and 10 minutes), and cell bodies removed using a combination of cell lysis and tap water wash. The remaining ligand bound complexes were collected for analysis. (a) SDS-PAGE with Coomassie Blue staining was performed for total protein analysis, quantification of Coomassie Blue stained SDS-PAGE lanes (pixel intensity) is shown at bottom of each lane. Molecular weight values (kDa) are displayed to the left of the gel. (b) Western blot analysis of positive and negative markers of adhesion complexes (positive: vinculin, paxillin, talin, ILK; negative: BAK and TFR). Molecular weight values (kDa) are displayed to the left of each blot. (c,d) Ratio (PL/FN) of normalised (c) vinculin and (d) paxillin western blot bands. For (c) and (d) FN and PL vinculin and paxillin bands were normalised against the integrated density of the Coomassie Blue stained lane for the corresponding sample. Results are representative of 5 individual experiments, with 2-4 experiments performed per condition. TCL: total cell lysate.

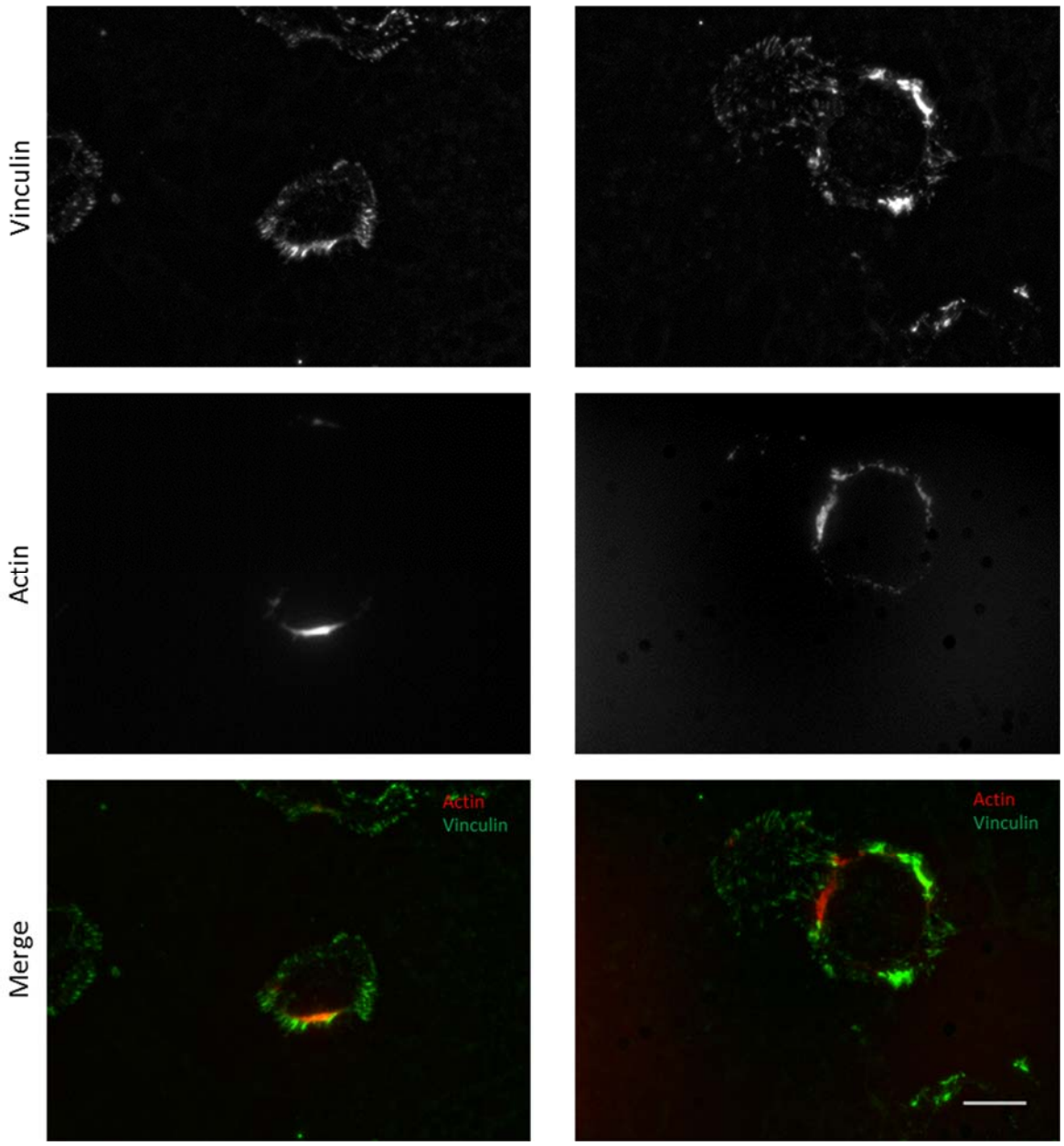

Figure 3.6. Immunofluorescence microscopy of isolated adhesion complexes. HUVECs were plated for 2 hours on fibronectin coated plates, cross-linked using DTBP (6 mM, 5 minutes), and cell bodies removed using a combination of cell lysis and tap water wash. The remaining ligand bound complexes were then processed for immunofluorescence staining. Adhesion complexes were visualised by immunofluorescent staining with vinculin, and actin visualised using Texas Red-conjugated phalloidin, scale bar= 20 µm. Two representative cells are displayed from a single experiment.

3.4 Proteomic analysis of HUVEC IACs

3.4.1 Optimisation of mass spectrometry analysis of HUVEC enriched adhesion complexes: comparison of different loading amounts

For proteomic quantitation strategies, it is important to achieve equal protein loading between samples to be quantified (Liu et al. 2009). Consequently, for the adhesion complex enrichment protocol, it is important that similar total protein amounts should be isolated in samples from fibronectin and poly-lysine conditions, to ensure any non-specific proteins are sufficiently accounted for when performing proteomic analysis. When using an equal number of cell culture plates per experiment, as performed in figure 3.2a, less protein was isolated on poly-lysine compared to fibronectin. Alternatively, when using the optimal conditions (6 mM DTBP, 5 minutes) using 33-50% more poly-lysine plates compared to fibronectin (performed in experiments displayed in figure 3.3 & 3.4), similar protein amounts between the two samples, or more in the poly-lysine conditions. This difference in plates was employed in all subsequent experiments.

To determine the protein quantity of enriched adhesion complexes required for mass spectrometry analysis, different sample quantities (for both poly-lysine and fibronectin) were analysed by mass spectrometry (table 3.1). For both fibronectin and poly-lysine conditions, two samples were prepared and analysed by mass spectrometry; sample 1 (S1, fibronectin and poly-lysine samples) was approximately five-fold less concentrated than sample 2 (S2, fibronectin and poly-lysine samples), when considering the number of prepared plates and dilution factor prior to mass spectrometry analysis (table 3.1). For analysis of these data following mass spectrometry, a subtractive approach was employed using the poly-lysine negative control, to identify specific fibronectin-induced adhesion complex associated proteins. Proteins were considered enriched to fibronectin if their normalised spectral counts were ≥two-fold higher in fibronectin compared to the corresponding poly-lysine sample. Using these criteria, a total of 265 (S1) proteins and 259 (S2) were deemed specific to fibronectin-induced integrin complexes, with 159 (44%) overlap (figure 3.7). The coverage of consensus adhesome, meta adhesome and LCA proteins was consistent with comparisons of other proteomic adhesion complex composition datasets (Horton et al. 2015), (figure 3.7). Although the number of identified spectra was higher for sample 2 (table 3.1), spectral counts, which can be used as a measure of relative protein abundance (Liu et al. 2004), for consensus adhesome proteins between the two samples were similar (figure 3.7b). These data indicate that mass spectrometry analysis of HUVEC adhesion complex samples isolated from two plates was sufficient for detection of significant numbers of well-characterised adhesome components as defined by the consensus adhesome.

Table 3.1. Mass spectrometry analysis of enriched adhesion complexes from HUVECs: comparison of different loading amounts. HUVECs were plated for 2 hours on fibronectin (FN) or poly-lysine (PL) coated plates (using the indicated amount of starting plates), cross-linked using DTBP (6 mM for 5 minutes), and the remaining ligand bound complexes collected, and prepared for mass spectrometry analysis using the indicated dilution factor. For sample 1 and sample 2, both a FN and PL sample were prepared for analysis. A peptide threshold of 90%, a protein threshold of 99% and 2 peptides minimum were used for protein identification. The total number of spectral counts assigned to each protein was then normalised to the total number of peptide identifications in the corresponding analysis. The number of spectra, proteins and proteins identified enriched ≥2-fold to FN over PL are indicated.

	Sample 1 (S1)		Sample 2 (S2)	
	FN	PL	FN	PL
Starting plates (10 cm)	4	6	2	3
Dilution prior to MS	1:10	1:10	No dilution	No dilution
Spectra identified	21904	22872	27610	28316
Proteins identified	437	261	466	302
Proteins identified enriched ≥2-fold to FN over PL	265		259	

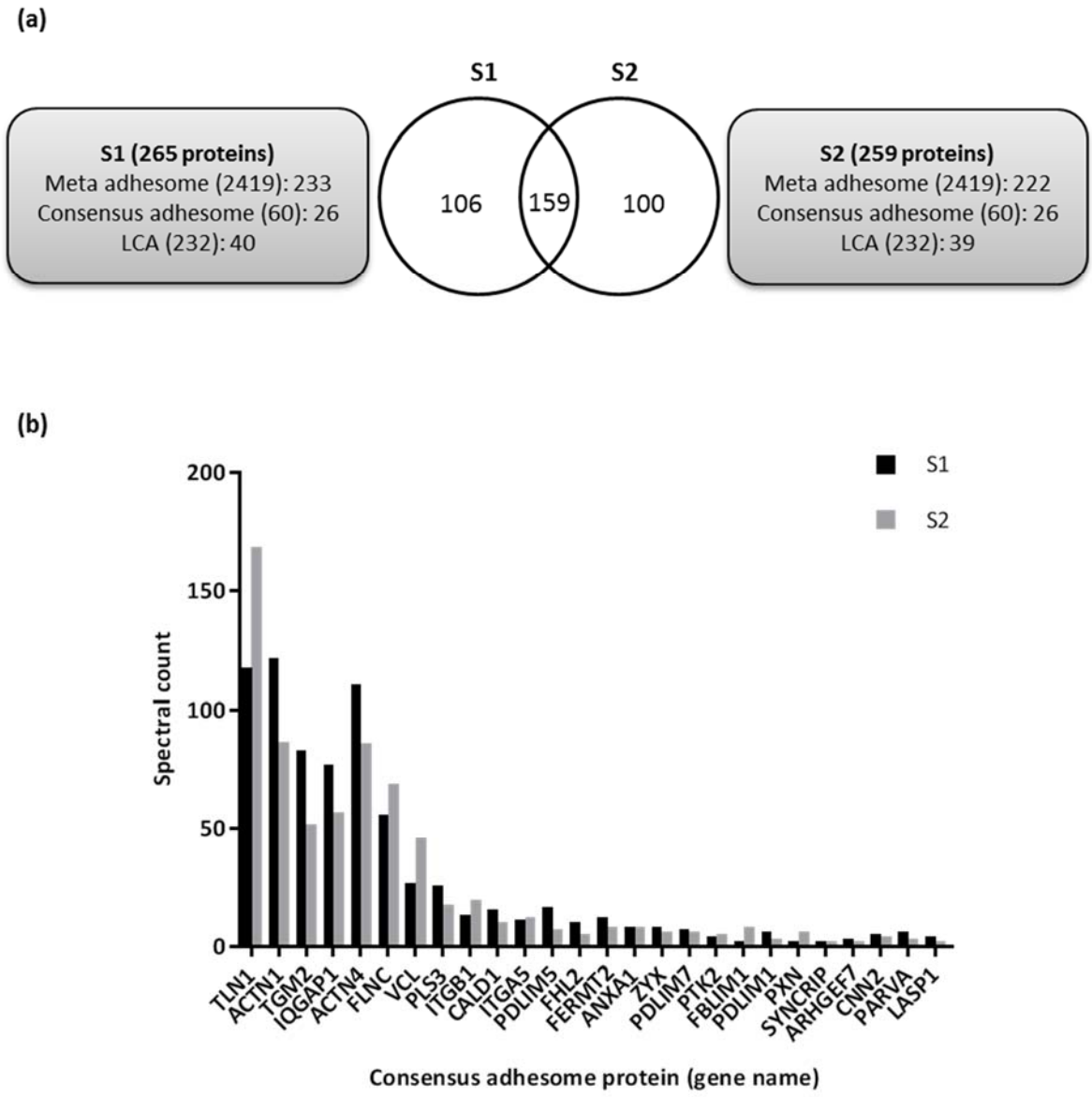

Figure 3.7. Mass spectrometry analysis of enriched adhesion complexes from HUVECs: comparison of different loading amounts. Details of sample 1 (S1) and sample 2 (S2) preparation are shown in table 3.1. (a) Venn diagram showing overlap of proteins identified in S1 and S2 by LC-MS/MS. Boxes highlight the number of meta, consensus and literature-curated adhesome proteins identified in S1 and S2. (b) Spectral counts for all consensus adhesome proteins identified (≥2-fold enriched in fibronectin compared to poly-lysine control), for S1 and S2 are displayed. n = 1 adhesion complex enrichments from HUVECs in each dataset. LCA: literature-curated adhesome.

Mass spectrometry analysis of enriched HUVEC adhesion complexes: overview

The previous sections determined optimal conditions for HUVEC adhesion complex enrichment and analysis by mass spectrometry (figure 3.8). Therefore, mass spectrometry analysis was used to address the initial aims of this project, i.e. to define the molecular composition of EC adhesion complexes. Adhesion complexes were enriched from HUVECs plated on fibronectin, and on poly-lysine as a control substrate. For each condition, three biological replicates were prepared and

analysed by mass spectrometry. Data analysis was then performed to generate a list of all proteins enriched to fibronectin-mediated integrin complexes in HUVECs.

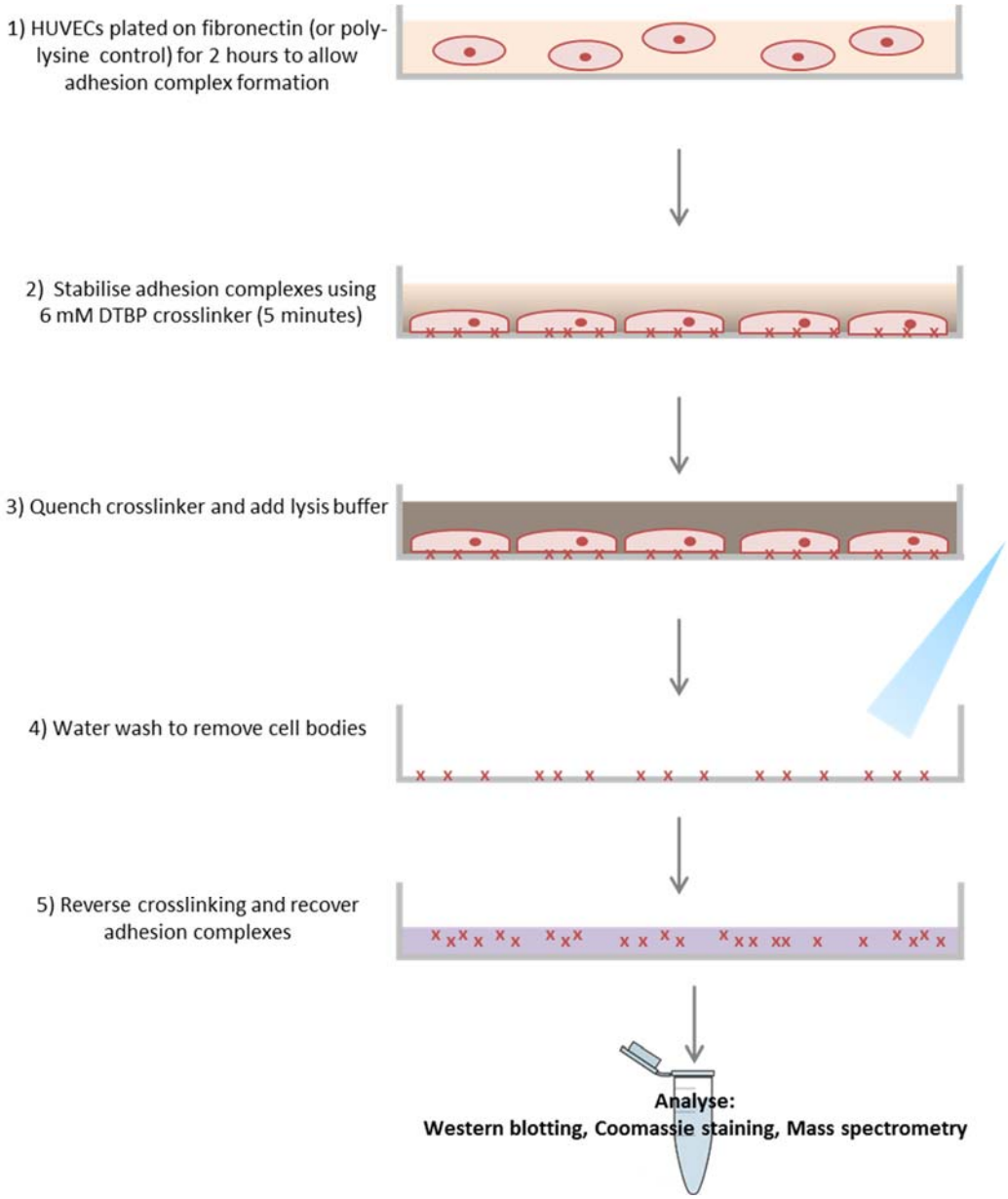

Figure 3.8. Schematic of the optimised workflow used to enrich and analyse HUVEC fibronectin-induced adhesion complex proteins. The schematic shows the optimised protocol used to enrich for adhesion complexes. During this project, steps 1 and 2 were optimised for adhesion complex enrichment from HUVECs, as well as the number of plates required for mass spectrometry analysis. The final optimised conditions are as follows. HUVECs are plated for 2 hours on fibronectin or poly-lysine coated plates (1) and cross-linked using 6 mM DTBP for 5 minutes (2). After this time, crosslinker is quenched by addition of Tris-HCL (pH 8, final concentration of 20 mM, [3]). Lysis buffer (50 mM Tris-HCl pH 7.6, 150 mM NaCl, 5 mM EDTA, 0.5% SDS, 1% Triton X-100, 1% Deoxycholate) is added to cell culture plates and cell bodies are removed using shear wash (4). Finally, remaining adhesion complex proteins are collected by scraping in recovery solution (125 mM Tris-HCl, pH 6.8, 1% SDS, 150 mM DTT) for analysis by western blotting, Coomassie Blue staining and/or mass spectrometry (5). Two (fibronectin) and three (poly-lysine) 55 cm^2 cell culture plates are required to identify sufficient numbers of adhesion complex proteins by mass spectrometry. For the mass spectrometry analysis, a peptide threshold of 90%, a protein threshold of 99% and 2 peptides minimum were used for protein identification. The total number of spectral counts assigned to each protein was then normalised to the total number of peptide identifications in the corresponding analysis.

Under the selected criteria for the fibronectin sample (peptide threshold of 90%, a protein threshold of 99% and two peptides minimum used for protein identification), a total of 632 proteins were detected. Proteins identified with low confidence were removed by employing a minimum spectral count cut-off. Proteins were filtered in two ways: a minimum of two spectral counts over the three replicates and a more conservative approach employing a minimum average of 2 spectral counts (6 spectral counts over three replicates). These proteins were further filtered to determine proteins that were specifically enriched to fibronectin-mediated integrin complexes in HUVECs. The average normalised spectral count for identified proteins was then calculated, and those exhibiting at least a two-fold enrichment to fibronectin condition compared to poly-lysine were selected. Under the same criteria (peptide threshold of 90%, a protein threshold of 99% and two peptides minimum used for protein identification), 103 proteins were identified in the poly-lysine sample. The first approach (minimum of two spectral counts over the three replicates) resulted in 566 proteins, whereas for the latter more conservative approach, 297 proteins were deemed enriched to fibronectin-induced integrin complexes (supplementary table 3.1b; appendix). It was decided to proceed with the more stringent cut-off criteria (minimum average of two spectral counts) to provide confidence that the final dataset generated is a true representation of the HUVEC adhesion complex protein composition.

3.4.2 Analysis of proteomic data: comparison of fibronectin-mediated HUVEC IAC proteins to previously reported adhesome datasets

To examine whether this dataset was representative of the HUVEC adhesion complex, and hence contained predominantly adhesion complex associated proteins, a range of analyses were performed. In this context, proteins used as positive markers of adhesion complexes for western blotting that were enriched to fibronectin (vinculin, talin, FAK, ILK, paxillin and filamin-A; figure 3.2, 3.3 and 3.4) were also determined to be enriched by mass spectrometry analysis compared to poly-lysine (supplementary table 3.1b; appendix).

Functional enrichment analysis was performed using DAVID gene ontology (GO), to gain an unbiased insight into the categories of proteins in the HUVEC dataset. GO uses a vocabulary of terms to describe and group genes based on their characteristics (Huang et al. 2008;Huang et al. 2009a), giving an overall view of groups of proteins within a sample. DAVID can also be used to perform KEGG pathway GO analysis, which maps gene products onto known functional network datasets. When KEGG pathway analyses were performed, five terms were significantly enriched (figure 3.9a), all of which have been previously identified in proteomic adhesion complex datasets (Robertson 2014;Paul 2014). Importantly, the most significant (Bonferroni corrected P-value <0.01) KEGG pathway term was that of focal adhesion. The 15 most significantly enriched (Bonferroni corrected P-value $<3 \times 10^{-4}$) gene ontology terms identified in the 'cellular compartment' and

'biological process' categories were adhesion-related terms. These included focal adhesion, cell adhesion, actin cytoskeleton and cell-substrate junction (figure 3.9b and 3.9c). Overall, these GO analyses indicate that adhesion components had been enriched from HUVECs using the workflow optimised in this thesis, with minimal contamination from other cellular compartments. The dataset is therefore likely to be a good representation of the HUVEC adhesion complex.

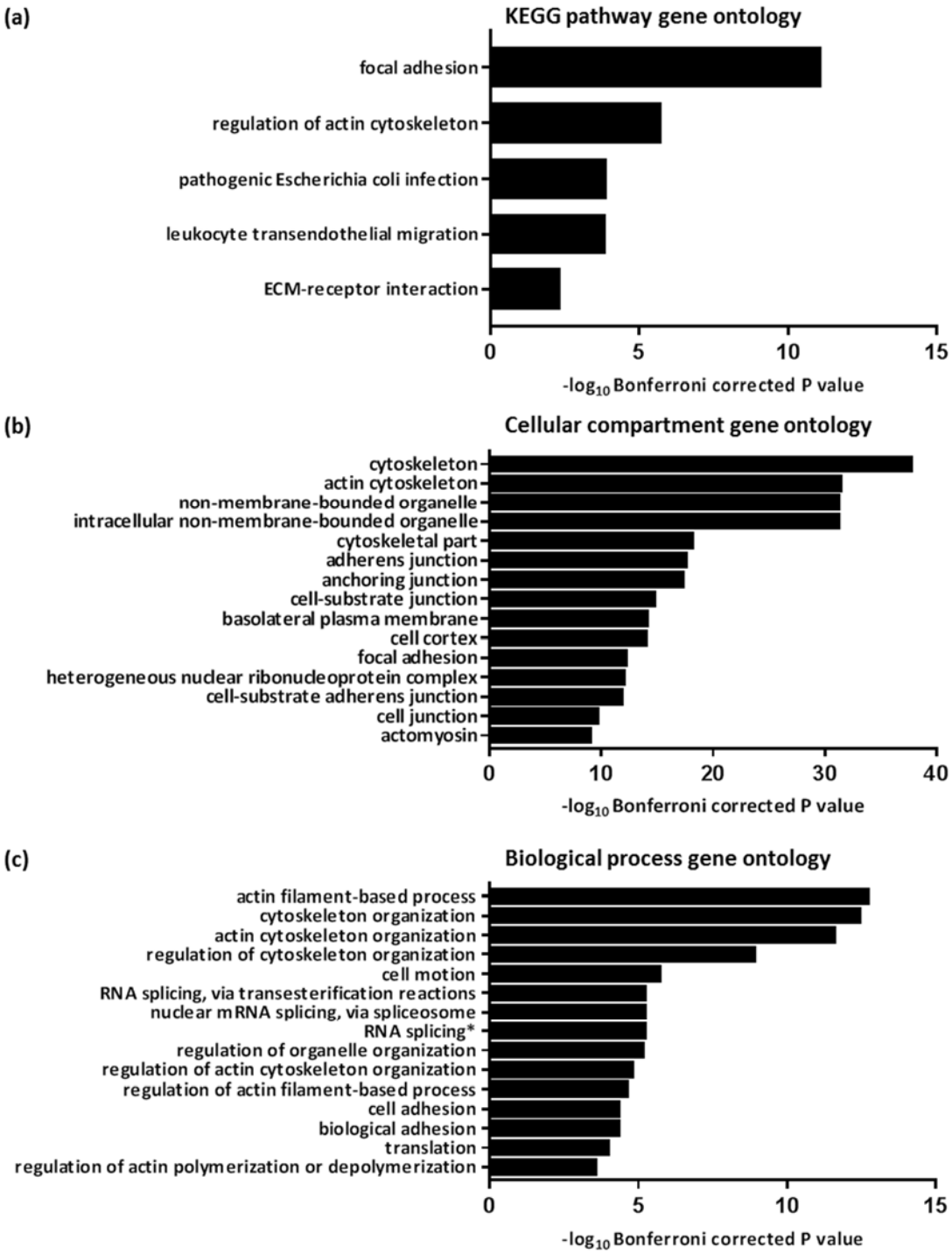

Figure 3.9. Gene ontology analysis of HUVEC fibronectin-induced adhesion complex proteins identified by mass spectrometry. All 297 proteins determined adhesion complex specific (enriched ≥two-fold in fibronectin over poly-lysine) from HUVECs were submitted for DAVID Gene Ontology analysis. The -$\log_{10}$ corrected P-values for all GO terms are plotted. (a) KEGG pathway terms (Bonferroni corrected P-value <0.01), 45% of the 297 proteins were assigned to KEGG pathways (b) Cellular compartment terms (15 highest ranking terms, Bonferroni corrected P <1 x 10^{-9}), 91% of the 297 proteins were assigned to a cellular compartment term (c) Biological process terms (15 highest ranking terms, Bonferroni corrected P-value <3 x 10^{-4}), 85% of the 297 proteins were assigned to a cellular compartment term. *RNA splicing, via transesterification reactions with bulged adenosine as nucleophile. KEGG: Kyoto encyclopedia of genes and genomes.

The 297 fibronectin-mediated proteins identified were displayed as a protein-protein interaction network (figure 3.10). Out of the 297 input proteins, 273 from were mapped onto the network. Each node represents an identified protein, each of which was labelled according its gene name and coloured to represent meta adhesome dataset occurrence. Square nodes differentiated consensus adhesome proteins, and nodes were organised to show meta, consensus, literature-curated and previously unidentified adhesome proteins (figure 3.10, supplementary table 3.1b; appendix). Connecting lines or edges represent reported protein-protein interactions. In addition, the overlap of protein numbers identified in this dataset with the meta, consensus and literature-curated adhesomes were represented as Venn diagrams (figure 3.11a and 3.11b). Of the 297 proteins, 85% were present in the meta adhesome, and have therefore been identified as enriched to fibronectin in proteomic datasets from FN-mediated adhesion complexes before (figure 3.10 & 3.11a), (Horton et al. 2015). From the LCA (section 1.3), 37 out of 237 proteins were identified (figure 3.10) (Winograd-Katz et al. 2014), and from the consensus adhesome 34 of 60 proteins were identified (figure 3.10 & 3.11b), (Horton et al. 2015). These analyses confirm that a high proportion of proteins identified in the HUVEC adhesion complex dataset are previously reported adhesion complex-associated proteins. However, 15% of identified proteins have not been associated with adhesion complexes previously (white nodes, figure 3.10), and may warrant further investigation. These may represent uncharacterised or endothelial-specific adhesion complex components.

As described in section 1.3 of this thesis, the consensus adhesome dataset consists of 60 proteins (figure 1.4). These are proteins identified in at least five of seven meta adhesome datasets. Of these 60, 34 were identified in the HUVEC adhesion complex dataset (figure 3.10 and 3.11), and were displayed as an overlay onto the consensus adhesome network (figure 3.12), (Horton et al. 2015). Proteins present in the consensus adhesome that are not present in this HUVEC dataset include integrin subunits αV and β3, which are nearly always present in fibronectin-mediated adhesion complex proteomic datasets (figure 3.11 and 3.12). This result was surprising as αVβ3 is a fibronectin-binding integrin that has been previously shown to be expressed in HUVECs (figure 3.1)(Stupack and Cheresh 2002). Immunofluorescence microscopy confirmed that β1 integrin, and not αVβ3 integrin, was present in adhesion complexes mediated by fibronectin (figure 3.13), confirming the results of the mass spectrometry dataset. In addition, vitronectin-mediated adhesion complexes (HUVECs plated on vitronectin coated plates for two hours), were stained as a positive control for αVβ3, and was the predominant integrin present, when compared to β1 (figure 3.13). These data suggest that this HUVEC dataset specifically represents a fibronectin-induced integrin α5β1-mediated adhesion complex.

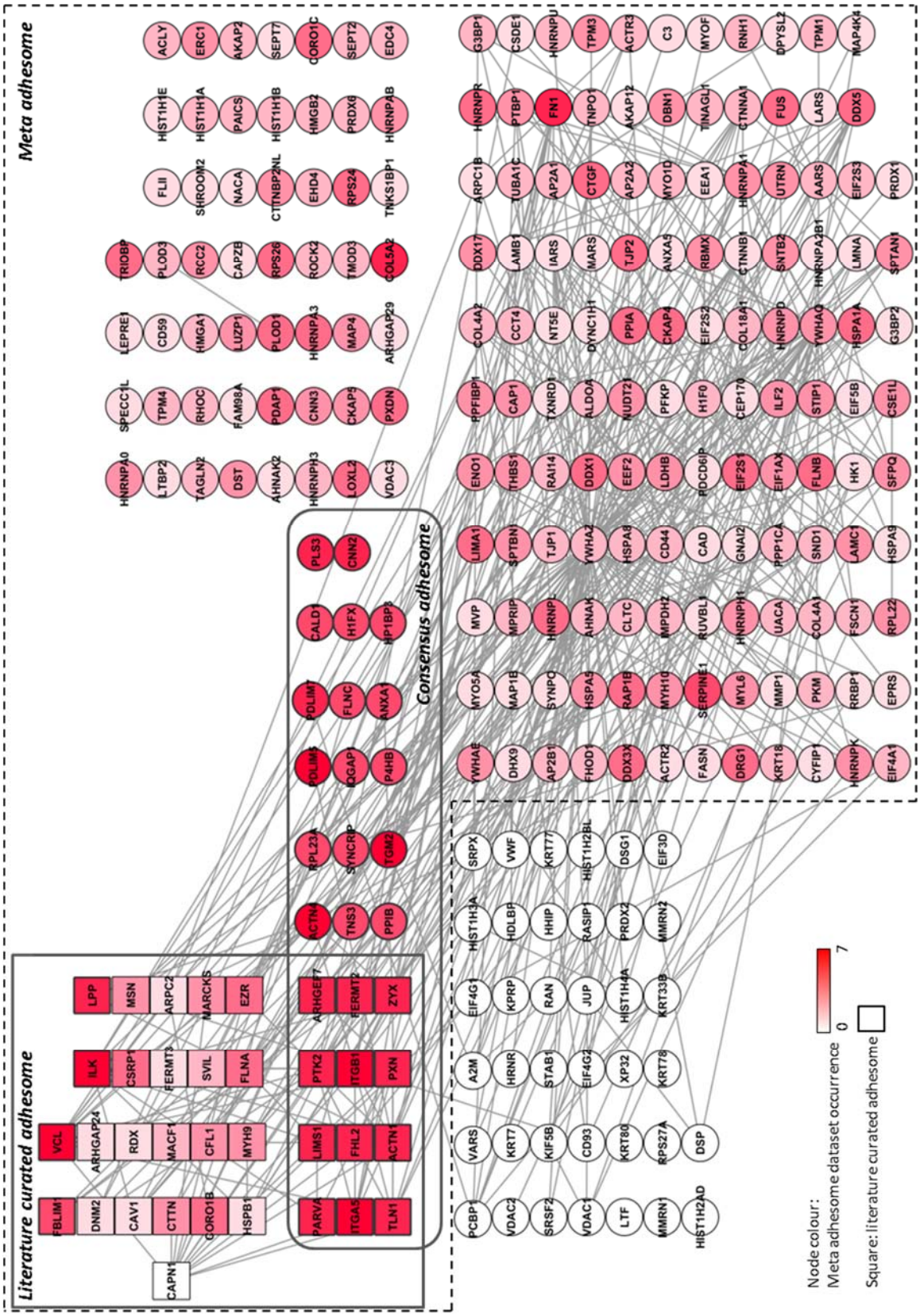

Figure 3.10. Network analysis of the HUVEC fibronectin-induced integrin adhesion complex adhesome. Proteins identified as specific to fibronectin-induced adhesion complexes in HUVECs (proteins ≥2-fold enriched in fibronectin vs poly-lysine and identified and with ≥2 mean spectral counts) were mapped onto a known human protein-protein interaction network. In total, out of 297 proteins (see supplementary table 3.1b; appendix), 273 were mapped onto the network. The network comprises 449 interactions (grey lines; edges) between the 273 proteins (circles/squares; nodes), which are labelled with gene names for clarity. Proteins are shaded according to occurrence in meta adhesome datasets, and arranged according to occurrence in meta, consensus and literature-curated adhesome datasets.

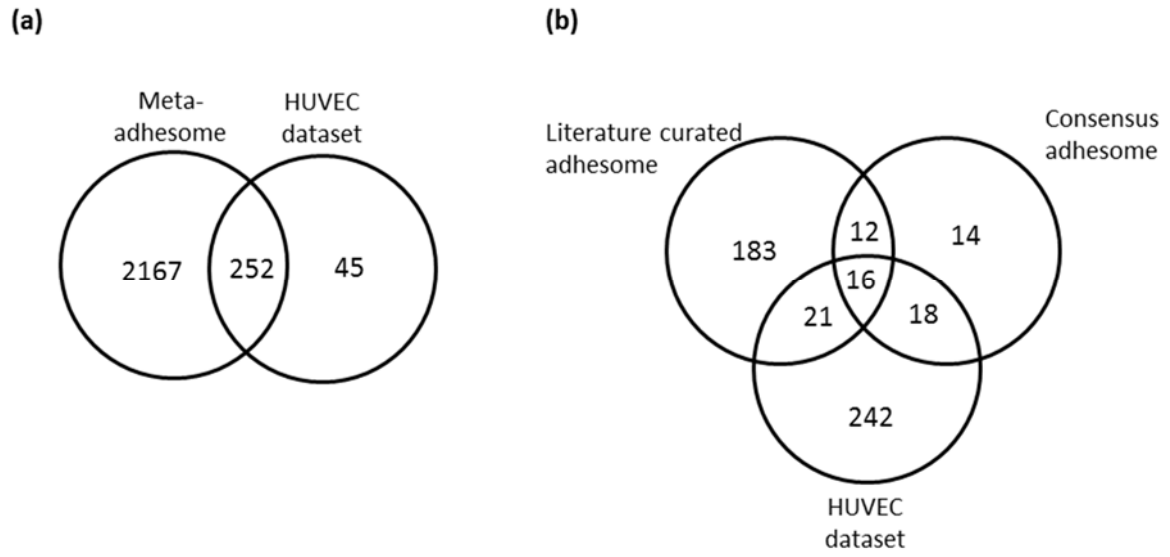

Figure 3.11. The HUVEC fibronectin-induced integrin adhesion complex adhesome: comparison with previously reported fibronectin-mediated adhesion complex mass spectrometry derived datasets. (a) Venn diagram showing overlap of proteins identified in the HUVEC adhesome dataset (enriched ≥2-fold in fibronectin sample compared to the poly-lysine control) and the meta adhesome. (b) Venn diagram showing overlap of proteins identified in the HUVEC adhesome dataset (enriched ≥2-fold in fibronectin sample compared to the poly-lysine control), the consensus and literature-curated adhesome.

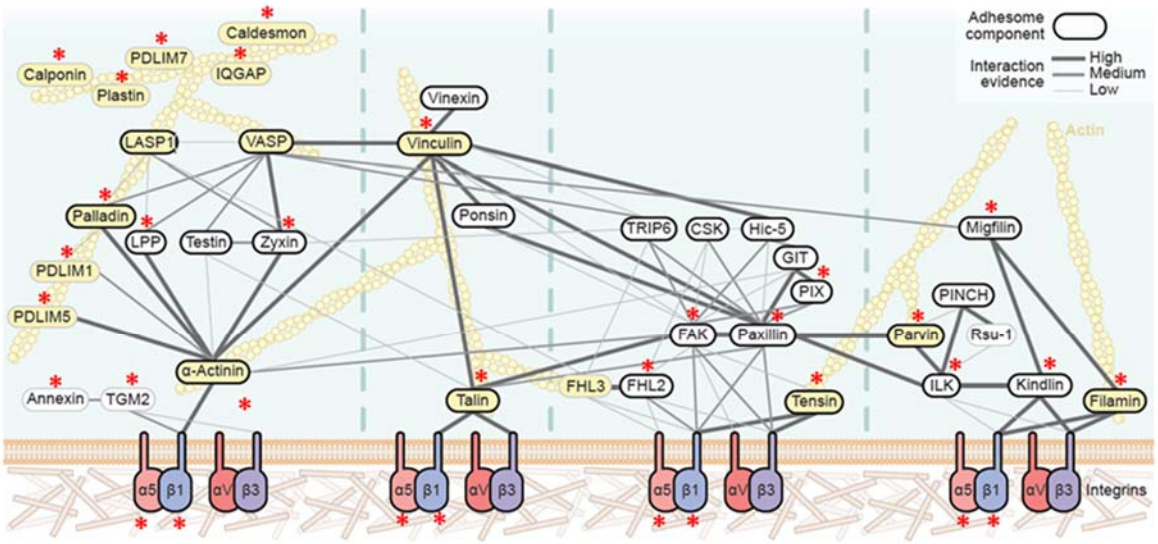

Additional consensus adhesome proteins present (not linked to the above network) in the HUVEC dataset:

SYNCRIP*
PPIB*
RPL23A*
P4HB*
H1FX*
HP1BP3*

Consensus adhesome proteins not in the HUVEC dataset:

BRIX1
CSK
DDX18
DDX27
DIMT1
DNAJB1
FAU
FEN1
FHL3
GIT2
ITGB3
ITGAV
LASP1
LIMD1
MRTO4
PALLD
POLDIP3
RSU1
SIPA1
SORBS1
SORBS3
TES
TGFB1I1
TRIP6
VASP

Figure 3.12. HUVEC fibronectin-induced adhesion complex proteins identified by mass spectrometry mapped onto the consensus adhesome protein network. Proteins determined specific to fibronectin-mediated integrin mediated adhesion complexes in HUVECs (proteins ≥2-fold enriched in the fibronectin compared to poly-lysine and with ≥2 mean spectral count) were mapped onto the consensus adhesome network, proteins detected in the HUVEC dataset are indicated with a red asterisks (*). In total, 34 consensus adhesome proteins were identified. Proteins in the consensus adhesome that are not identified in the HUVEC dataset are shown below the network in italics. Proteins coloured yellow are actin binding proteins. Figure adapted from Horton et al. 2015. HUVEC dataset: n = 3 adhesion complex enrichments from HUVECs.

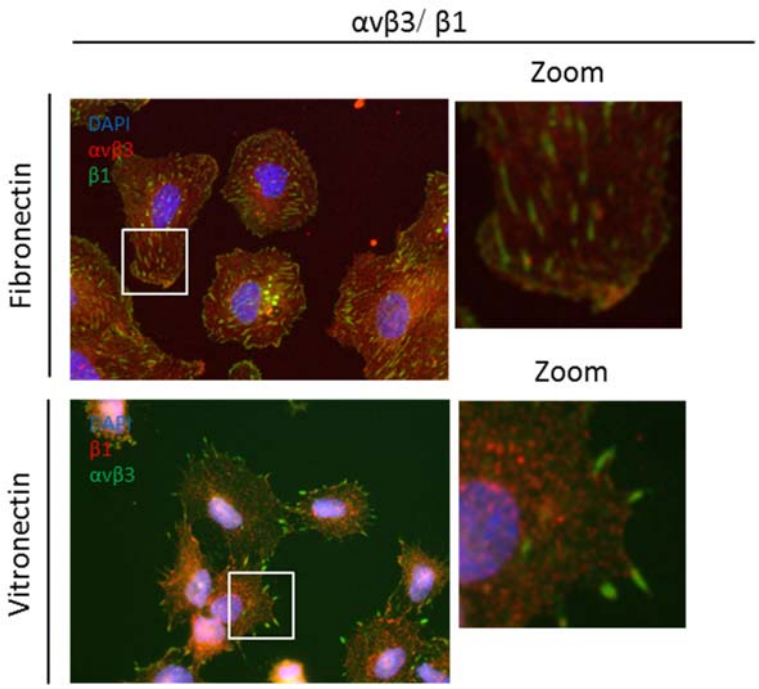

Figure 3.13. Immunofluorescence microscopy of aVβ3 integrin and β1 integrin in HUVECs. HUVECs were plated on fibronectin or vitronectin coated coverslips for 2 hours, fixed and stained with DAPI (blue), aVβ3 integrin and β1 integrin. White boxes indicate zoomed cell area. Scale bar= 20 µm.

Of the 297 HUVEC IAC proteins identified, the number present in at least x meta adhesome datasets (total number of proteins identified in the number of datasets [1-7] specified) decreased exponentially as the stringency in dataset number increased (figure 3.14a). In the meta adhesome, 1359 proteins were identified in only one dataset and considered low-abundance, context-specific adhesome components, or those difficult to detect by mass spectrometry. Of these meta adhesome proteins, 71 were identified in the HUVEC dataset and provide further validation of these as meta adhesome proteins, by increasing confidence that these 71 proteins may be true adhesion complex components (figure 3.14b). Proteins included in the consensus adhesome are those displayed in at least five out of seven meta adhesome datasets. To examine further how previous datasets compare to the HUVEC dataset, individual analyses were performed. Previously, comparative analysis of meta adhesome datasets identified variations in composition dependent on cell type, negative control and isolation method (Horton et al. 2015). The 297-protein dataset generated in this study is in the lower range when compared to other IAC proteomes, which ranged from 314 to 1023 proteins, with a mean value of 602 (Horton et al. 2015). However, the number of proteins present in each dataset is dependent on the cut-off criteria used for peptide and protein probabilities, spectral count cut-off and use of negative control. This HUVEC study has used stringent cut-off values; in particular the average spectral count cut-off of a minimum average of two spectral counts is higher than that used by some other studies. For example, for the K562 dataset (402 identified proteins), a less stringent cut-off employing a minimum of two unique

peptides over three replicates was employed, and considered specific if enriched ≥two-fold over the VCAM-1 control (Humphries et al. 2009). Seven HUVEC IAC proteins had been identified in all seven meta adhesome datasets, out of a total of 10 that were found in all seven meta adhesome datasets. The three unidentified proteins from this list of 10 were αV integrin, LIM and SH3 protein 1 (LASP1) and vasodilator-stimulated phosphoprotein (VASP), these proteins may warrant further investigation.

When the Jaccard index was used as a measure of dataset similarity, the HUVEC dataset was found to be most similar to the HFF dataset with 17.7% similarity (figure 3.14c), with an overlap of 92 proteins (figure 3.14d). In addition, when considering all 36 comparisons, the Jaccard index is fifth highest between HUVEC and HFF, suggesting a high level of similarity (figure 3.10c). Notably, the HFF dataset was prepared by a similar, although not identical method to the HUVEC dataset (figure 3.14e). The negative control ligand poly-lysine was used for each of these datasets, supporting previous data suggesting that datasets which use the same negative control and experimental condition are more similar (Horton 2015). However, heterogeneity in IAC composition is likely to be dependent on a number of combined factors (Horton 2015). Overall, these results show a good comparison to previous adhesion complex composition data from different cell types.

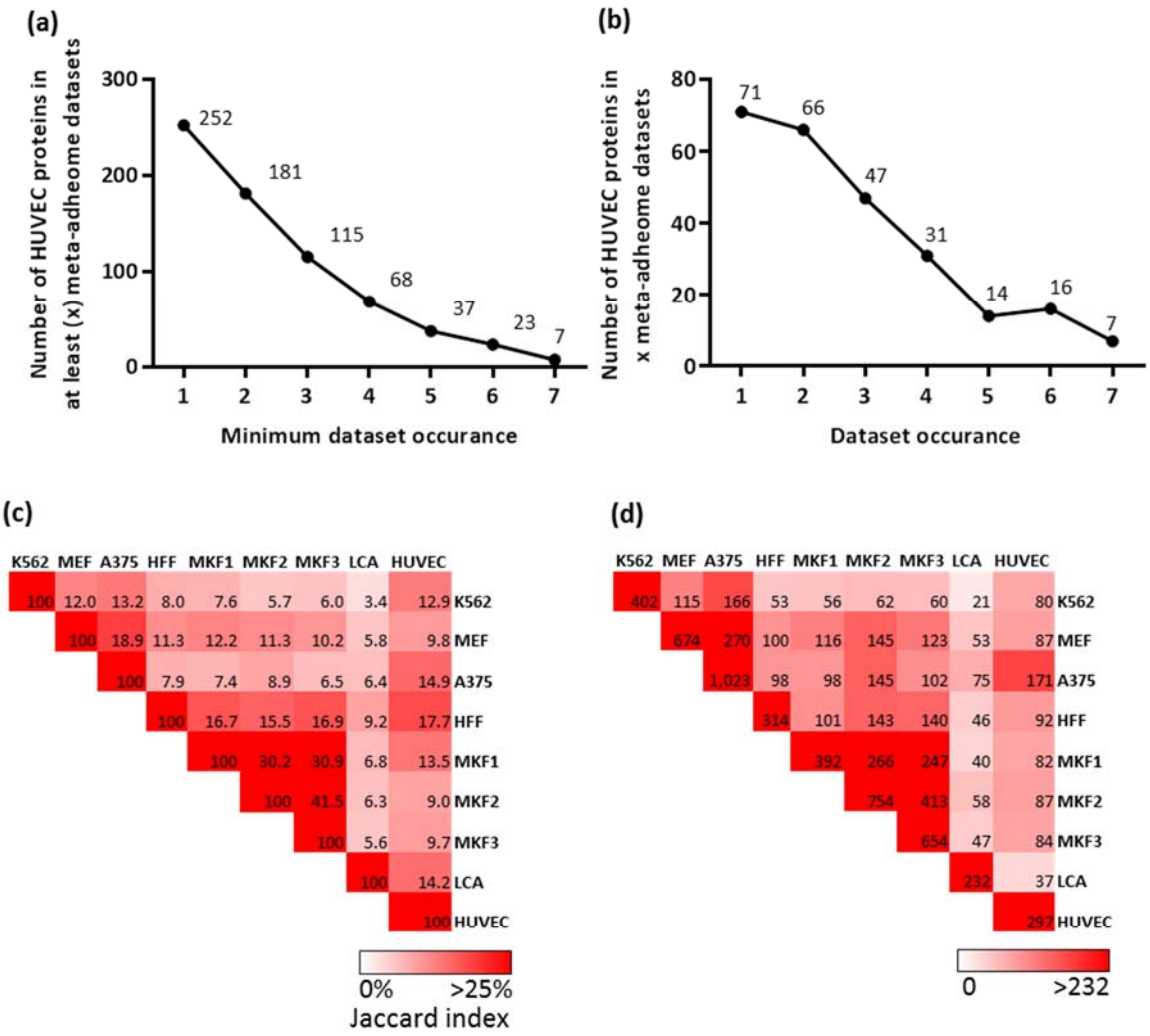

(e)

Dataset	Control	Isolation Approach	Time point	Lysis method	Crosslinker(s)	Publication
K562	VCAM-1	Bead	30 min	Detergent, sonication	DTBP (3 mM; 30 min)	Humphries, Byron et al. (2009)
MEF	Transferrin	2D substrate	2 hr	Detergent, sonication	DTBP (3 mM; 30 min)	Horton et al. (2015)
A375	Transferrin	2D substrate	2 hr	Detergent, hydrodynamic force	DTBP (3 mM; 30 min)	Robertson et al. (2015)
HFF	PL	2D substrate	2 hr	Detergent, sonication	DTBP (6 mM; 3 min)	Ng et al. (2014)
MKF1	PL	2D substrate	45 min	Detergent, hydrodynamic force	DSP, DPDPB (0.5 mM, 0.05 mM; 5 min)	Schiller et al. (2011)
MKF2	PL	2D substrate	45 min	Detergent, hydrodynamic force	DSP, DPDPB (0.5 mM, 0.05 mM; 5 min)	Schiller, Hermann et al. (2013)
MKF3	PL	2D substrate	90 min	Detergent, hydrodynamic force	DSP, DPDPB (0.5 mM, 0.05 mM; 5 min)	Schiller, Hermann et al. (2013)
LCA	-	-	-	-	-	Winograd-Katz et al. (2014)
HUVEC	PL	2D substrate	2 h	Detergent, hydrodynamic force	DTBP (6 mM; 5 min)	This study

Figure 3.14. Comparison of HUVEC fibronectin-induced adhesion complex proteins to meta adhesome datasets. (a-b) Number of integrin adhesion complex HUVEC proteins in the meta adhesome dataset: data expressed as a line graph showing (a) the cumulative proportion of meta adhesome proteins in at least x proteomic datasets, where x is the minimum dataset occurrence category and (b) the number of HUVEC IAC proteins in x number of datasets. The number of proteins identified (y value) are indicated for each data point. (c) Similarity comparison of the HUVEC IAC dataset, the seven proteomic datasets and the literature-curated adhesome, as measured by Jaccard index. (d) Numbers of proteins which overlap in each dataset. (e) Table indicating methodology by which each dataset was generated. K562, human chronic myelogenous leukaemia cells (Humphries et al. 2009); MEF, mouse embryonic fibroblast cells (Horton et al. 2015); A375, human malignant melanoma cells (Robertson et al. 2015); HFF, human foreskin fibroblast cells (Ng et al. 2014); MKF1, mouse kidney fibroblast cells (Schiller et al. 2011); MKF2 and MKF3, mouse kidney fibroblast cells (Schiller and Fässler 2013), LCA (Winograd-Katz et al. 2014).

3.5 HUVEC integrin adhesion complex dataset validation

Of particular interest are proteins that have not been observed or are rarely seen in previously reported fibronectin-mediated adhesion complex datasets (Horton et al. 2015), and those that are nearly always present, but not seen in this dataset. Of the 297 proteins identified, 45 have not been seen in previously reported fibronectin-mediated adhesion complex datasets: these may be proteins specific to EC adhesion complexes, or possibly co-purifying contaminants.

Validation of typically underappreciated adhesome proteins identified in this dataset, ARHGAP24 and MARCKS was performed using immunofluorescence staining. These proteins localise to the cell membrane and their staining localises close to paxillin-positive adhesion complexes, confirming the proteins would be expected to be isolated with IACs (figure 3.15). Validation of ARHGAP24 and MARCKS which were identified confirmed co-localisation of these previously underappreciated adhesion complex-associated proteins with the HUVEC adhesion complex. As confidence has been generated in the methodology used, and in the dataset used to identify the composition of fibronectin-mediated integrin complexes in HUVECs, the dataset can therefore be investigated in greater detail.

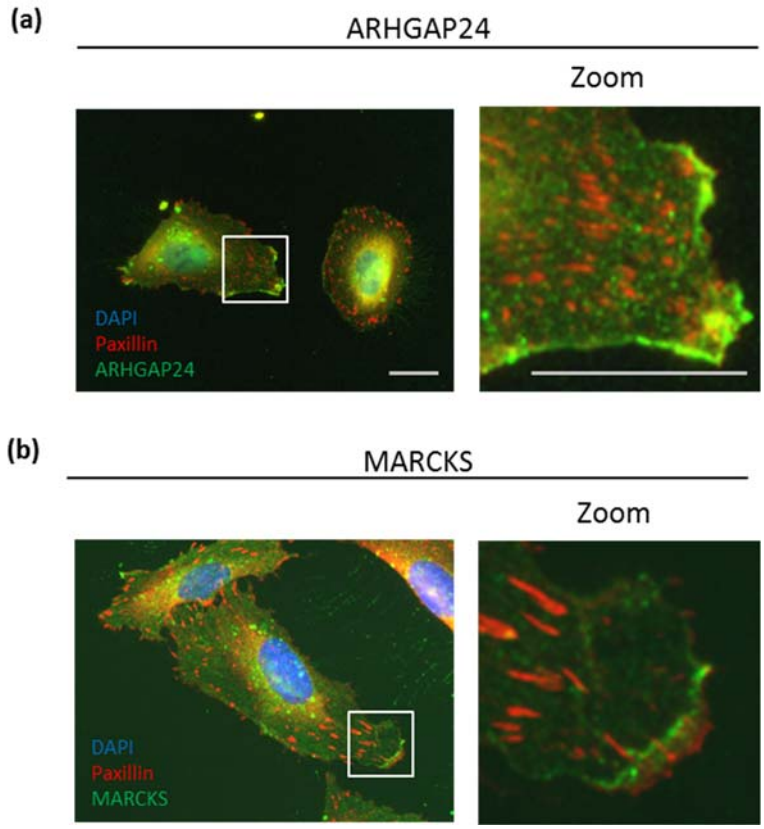

Figure 3.15. Validation of HUVEC adhesion complex proteins identified by mass spectrometry. HUVECs were plated on fibronectin-coated coverslips for 2 hours, fixed and stained with DAPI (blue), paxillin, and (a) ARHGAP24 or (b) MARCKS. White boxes indicate zoomed cell area. Scale bar= 20 µm.

3.6 Chapter 3 summary

The main aim of this chapter was to develop a workflow for the enrichment of IACs from ECs. First, the adhesive characteristics of HUVECs plated on both integrin-binding ligands and non-integrin binding control ligands were assessed. Immunocytochemical analysis suggested that HUVECs form adhesion complex like structures when plated on fibronectin and collagen, although not on laminin (possibly due to low expression of laminin binding integrins as determined by flow cytometry) and non-integrin binding ligands (poly-lysine, apotransferrin and concanavalin A). For establishment of the adhesion complex isolation workflow in HUVECs, assessment was made of the optimal conditions for HUVEC IAC enrichment at multiple stages of the workflow. This included choice of integrin binding and non-integrin binding control ligand, ligand plating time, and crosslinking conditions. During optimisation, adhesion complexes were nearly always isolated in sufficient quantity, with variability observed in total protein and adhesion complex protein levels isolated under different conditions, demonstrating that the enrichment protocol is reproducible, and works well under most conditions. In the final optimised workflow (figure 3.8), HUVECs were plated on fibronectin for two hours to allow IAC formation, or poly-lysine as a negative control, followed by crosslinking to stabilise IACs (6 mM DTBP; 5 minutes), cell body removal, and collection of remaining IACs.

Preliminary mass spectrometry analysis of enriched adhesion complexes confirmed that relatively low starting quantities (in comparison to similar analyses using different cell types; less than two 55 cm^2 cell culture plates worth) could be used to detect adhesion complex proteins from HUVECs. In addition, increasing this starting amount did not increase the total protein numbers identified, or the number previously identified adhesome proteins. However, around 100 proteins in these samples were uniquely identified, suggesting variability in the isolation process, or alternatively, that all proteins in a single sample cannot be identified by mass spectrometry. Either way, biological replicates are essential to ensure coverage of as many isolated IAC proteins as possible.

Subsequent mass spectrometry analyses, using three biological replicates of enriched IACs, defined, for the first time, the HUVEC IAC composition, a network of 297 proteins (enriched ≥two-fold over the poly-lysine negative control). The proteins identified in this dataset are largely representative of adhesion complex proteins, shown by gene ontology analysis and high similarity to previously reported IAC datasets, which indicated that this dataset contained a high proportion of adhesion related proteins.

Immunofluorescence staining was used to confirm presence of underappreciated adhesion proteins in HUVEC adhesion complexes, which were identified in the HUVEC IAC proteomic dataset.

A total of 45 previously unidentified adhesion proteins were detected in this HUVEC IAC dataset. Although some of these proteins may be co-purifying contaminants, many likely represent endothelial-specific adhesion complex proteins and are therefore relevant in the context of this study. Immunofluorescence staining confirmed that ARHGAP24 and MARCKS, which were identified in the proteomic dataset, localises close to paxillin-positive adhesion complexes. In addition, proteins that are nearly always present, but not seen in this dataset were highlighted for further investigation. Most notably, αV integrin, LASP1 and VASP are proteins seen in all seven meta adhesome datasets, but not identified in this study. VASP and αV were identified at a very low spectral count, below the limit to be included in this study. It may by that these proteins are present but at unexpectedly low levels. Alternatively, the signal in the mass spectrometer could be supressed by high levels of other proteins, causing the signal to be lost. However, further immunocytochemical investigation of αV and β3 integrin subunits, which were not identified in the HUVEC dataset, provided confidence that these proteins are not present in HUVEC fibronectin-induced adhesion complexes, suggesting these proteins were not detected due to very low presence. These validation analyses provided confidence that the spectral count cut-off values gave a correct representation of the HUVEC IAC and that the IAC optimised isolation workflow, from cell culture to data analysis, can be used to isolate and determine the composition of the HUVEC adhesion complex. Consequently, the dataset of 297 proteins identified is likely to be a true representation of the HUVEC adhesion complex, and the data and analysis can be used as a resource for future studies.

Chapter 4: Combined proteomic and phosphoproteomic analysis of VEGF-induced changes in HUVEC integrin adhesion complex composition

4.1 Overview

A workflow to enrich HUVEC IAC proteins has been established and used to produce a dataset of 297 proteins that defines the HUVEC adhesion complex protein composition. The next aim of this study was to use and further optimise this workflow to perform a global, unbiased analysis of changes in both protein composition and phosphorylation within HUVEC adhesion complexes upon VEGF treatment. To do this, a VEGF treatment step was to be introduced, and a workflow for phosphoproteomic analysis of HUVECs adhesion complex proteins developed. A number of steps were performed to determine the optimal conditions for both VEGF treatment and phosphoproteomic analysis. The final optimised conditions were then used to produce three mass spectrometry based datasets: VEGF-treated HUVEC IAC samples by (1) proteomic analysis and (2) phosphoproteomic analysis and (3) VEGF-treated TCL samples by phosphoproteomic analysis. These datasets were analysed quantitatively to determine how protein and protein phosphorylation changes occur globally in HUVEC IACs upon VEGF treatment.

4.2 Optimisation of the HUVEC response to VEGF treatment

As the overall aim of this study was to investigate the mechanisms of VEGF-adhesion crosstalk in ECs, the VEGF treatment conditions required to produce an optimal signalling response were investigated, in combination with the optimised HUVEC adhesion complex enrichment workflow (figure 3.8). As both proteomic and phosphoproteomic analysis of isolated adhesion complexes with and without VEGF treatment was to be performed, the activation of signalling proteins known to be phosphorylated in response to VEGF were used as a measure of activity. VEGF stimulation is known to phosphorylate ERK rapidly (Koch et al. 2011) and so, initially, ERK was used as a marker of VEGF signalling. First, the requirement for serum-starvation of HUVECs before plating on fibronectin was tested, to create a maximal VEGF response following the two-hour plating period performed in the adhesion complex enrichment protocol (figure 3.8). ERK phosphorylation response to VEGF stimulation with and without serum starvation, and with two hours and 16 hours of serum starving was investigated. Serum starving overnight resulted in a maximal fold change in ERK phosphorylation levels following VEGF treatment (figure 4.1), this condition was therefore used for all future experiments. VEGF treatment time was then investigated, and in addition to ERK phosphorylation, the phosphorylation response of adhesion complex protein sites previously reported to be phosphorylated in response to VEGF were assessed (FAK-Y397, paxillin-Y118 and Src-Y416) (Abedi and Zachary 1997;Abu-Ghazaleh et al. 2001;Eliceiri et al. 1999), as these are of greater relevance to the aims of this study. Following two hours of plating on fibronectin, VEGF treatment was performed between 5 - 12.5 minutes. TCLs were collected and analysed; for FAK-

Y397 and paxillin-Y118, 7.5 minutes VEGF treatment showed an optimal response, whereas for ERK phosphorylation, 10 minutes treatment gave an optimal response (figure 4.2). A similar VEGF-stimulated time course was then replicated, although testing isolated adhesion complex proteins following VEGF treatment. Total tyrosine phosphorylation and paxillin-Y118 changes were assessed, and these demonstrated a peak at 7.5 minutes, whereas changes in Src-Y416 peaked at 15 minutes (figure 4.3). The final VEGF treatment optimisation experiment confirmed that a concentration of 25 ng/mL (7.5 minutes), which has been used in all previous VEGF treatment experiments, was appropriate to induce paxillin and total tyrosine phosphorylation in adhesion complexes (figure 4.4), and was therefore used for future experiments. Together, these data demonstrate that HUVECs exhibit a robust response to VEGF treatment that, in the context of the optimised adhesion complex isolation workflow, appears to be optimal in activating phosphorylation of adhesion complex proteins at 25 ng/mL, for 7.5 minutes. These treatment conditions were therefore used for all future experiments involving VEGF treatment.

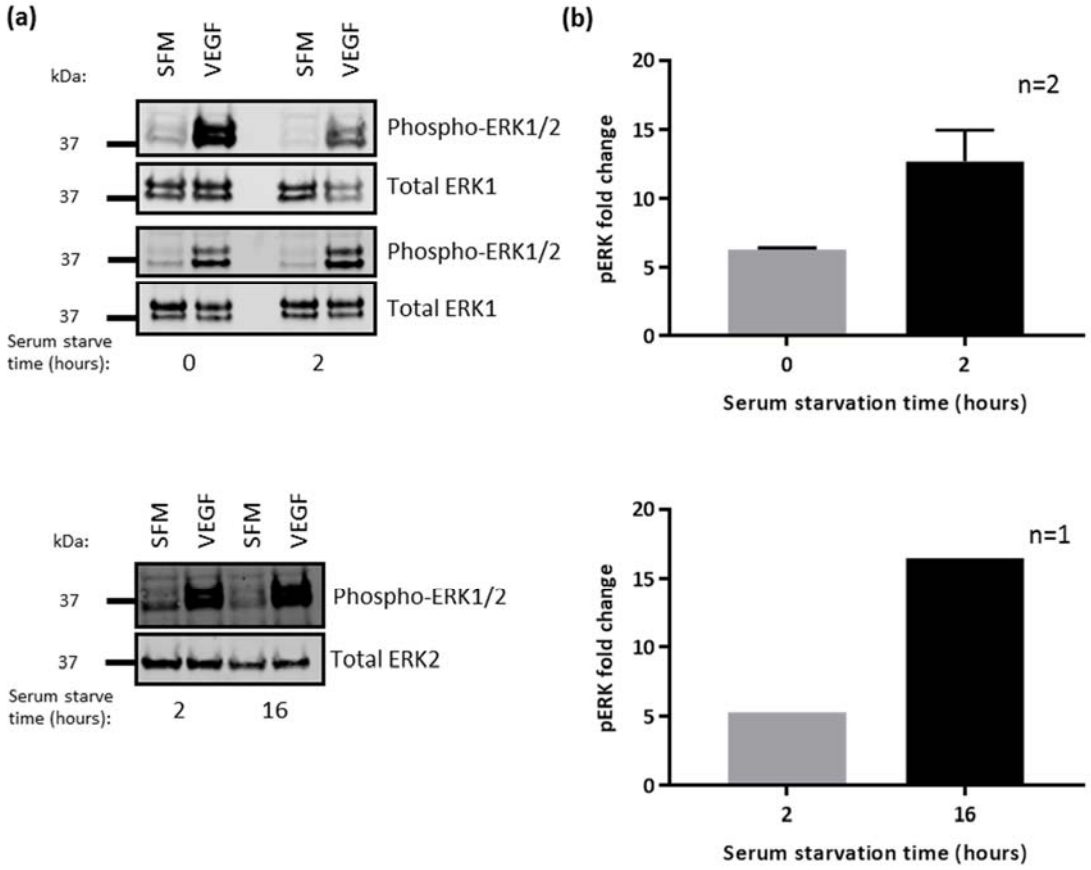

Figure 4.1. Optimisation of VEGF treatment: serum starvation. HUVECs were serum starved for the indicated time, plated for 2 hours on fibronectin coated plates, treated with SFM or VEGF (25 ng/mL, 7 or 10 minutes) and total cell lysates collected for analysis. (a) Western blot analysis of total ERK1 or ERK2 and phospho-ERK1/2. Molecular weight values (kDa) are displayed to the left of each blot. (b) Phospho-ERK fold change: phospho-ERK band intensity values were normalised to total ERK band intensity values and fold change calculated [VEGF/SFM]. n=1 or 2, for the latter, data are displayed as mean with SD.

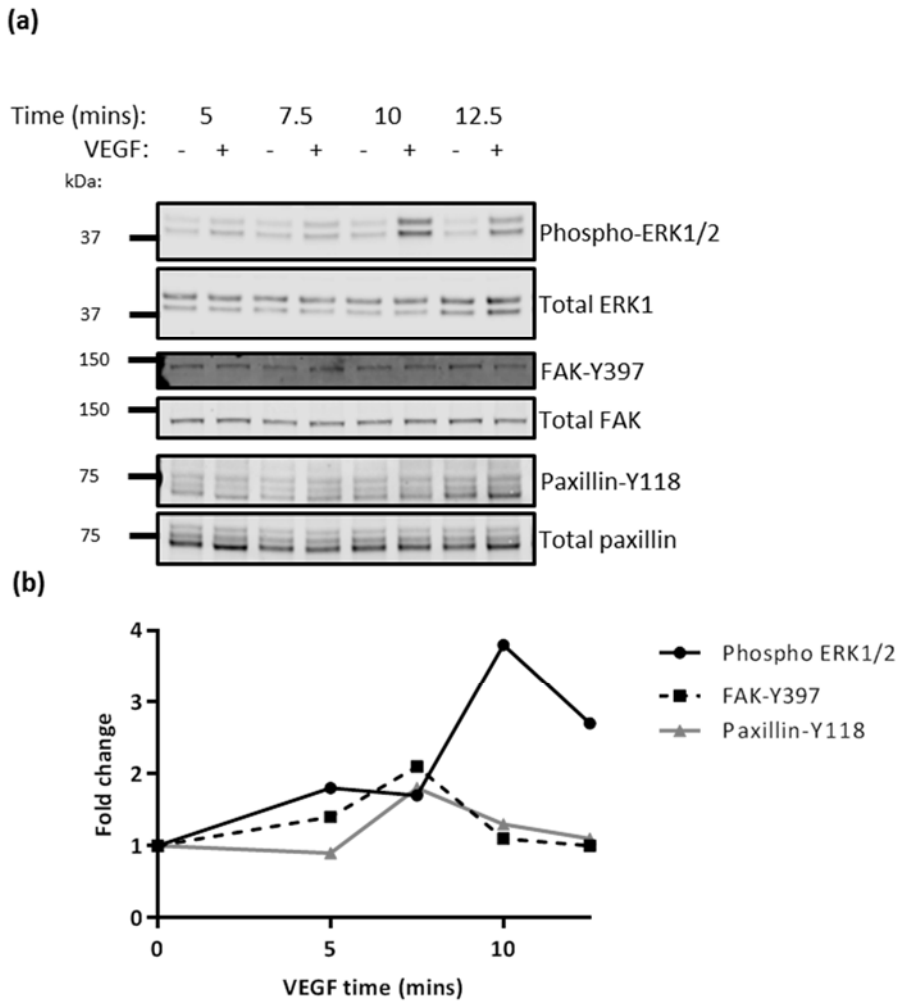

Figure 4.2. Optimisation of VEGF treatment time using VEGF treated HUVEC total cell lysate samples. HUVECs were serum starved overnight, plated for 2 hours on fibronectin coated plates, treated with SFM or VEGF (25 ng/mL) for the indicated time and total cell lysates collected for analysis. (a) Western blot analysis of total ERK1, FAK and paxillin and phospho-ERK1/2, FAK-Y397 and paxillin-Y118 phosphoprotein levels. Molecular weight values (kDa) are displayed to the left of each blot. (b) Phosphorylation fold change: phosphoprotein (ERK1/2, FAK-Y397 and paxillin-Y118) band intensity values were normalised to their corresponding total protein band intensity values. Normalised intensity values were used to calculate fold change [VEGF/SFM], n=1.

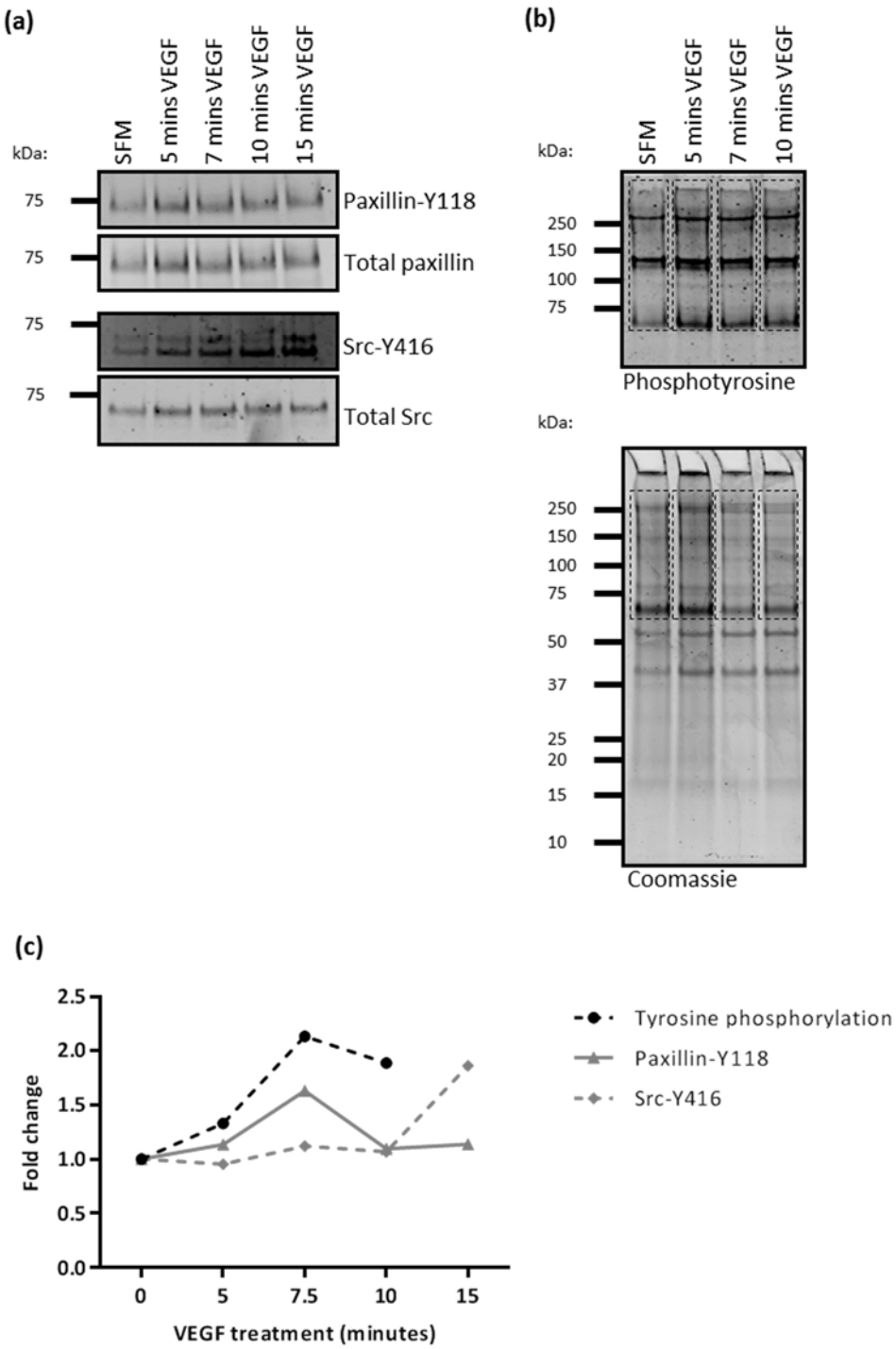

Figure 4.3. Optimisation of VEGF treatment time using VEGF treated integrin adhesion complex samples. HUVECs were serum starved overnight, plated for 2 hours on fibronectin coated plates, treated with SFM or VEGF (25 ng/mL) for the indicated time, and adhesion complexes isolated using the workflow previously optimised (figure 3.8). (a) Western blot analysis of total FAK and Src, and FAK-Y397 and Src-Y416 phosphoprotein levels. Molecular weight values (kDa) are displayed to the left of each blot. (b) Western blot analysis of total phosphotyrosine and SDS-PAGE with Coomassie Blue staining for total protein analysis. Molecular weight values (kDa) are displayed to the left of each gel/blot. (c) Phosphorylation fold change: phosphoprotein (paxillin-Y118 and Src-Y416) band intensity values were normalised to their corresponding total protein band intensity values, and phosphotyrosine intensity values were normalised to Coomassie Blue stained intensity values (regions quantified indicated by dashed boxes). Normalised intensity values were used to calculate fold change [VEGF/SFM], n=1.

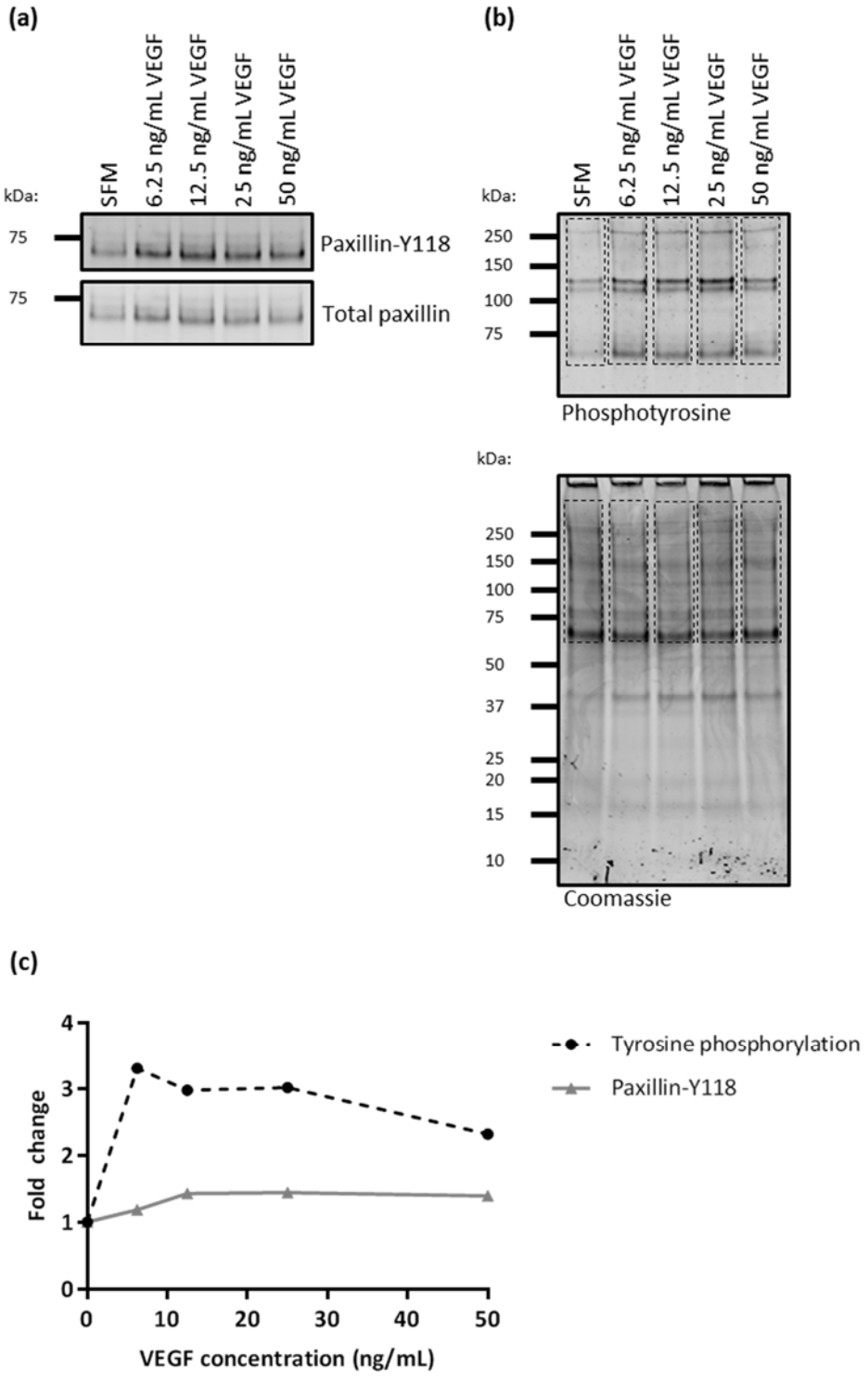

Figure 4.4. Optimisation of VEGF treatment concentration using VEGF treated integrin adhesion complex samples. HUVECs were serum starved overnight, plated for 2 hours on fibronectin coated plates, treated with SFM or VEGF at the indicated concentration for 7.5 minutes and adhesion complexes isolated using the workflow previously optimised (figure 3.8). (a) Western blot analysis of total paxillin and paxillin-Y118. Molecular weight values (kDa) are displayed to the left of each blot. (b) Western blot analysis of total phosphotyrosine and SDS-PAGE with Coomassie Blue staining for total protein analysis. Molecular weight values (kDa) are displayed to the left of each gel/blot. (c) Phosphorylation fold change: paxillin-Y118 band intensity values were normalised to their corresponding total protein intensity band values, and phosphotyrosine intensity values were normalised to Coomassie Blue stained intensity values (regions quantified are indicated by dashed boxes). Normalised intensity values were used to calculate fold change [VEGF/SFM], n=1.

4.3 Optimisation of the phosphoproteomic workflow

One of the aims of this study was to perform a global analysis of the phosphorylation events that are regulated by VEGF signalling, in relation to adhesion complexes and adhesion signalling. A global analysis of adhesion phosphorylation events has been performed previously (Schiller et al. 2011;Robertson et al. 2015), and demonstrated that, when performing phosphopeptide analysis from TCL samples, very few adhesion-related proteins could be identified. However, a high proportion of phosphoproteins can be identified from adhesion complex samples, indicating that phosphoproteomic analysis of enriched IAC samples enables a more detailed coverage of adhesion complex phosphorylation events (Robertson et al. 2015). Ideally, combined proteomic and phosphoproteomic analysis of isolated IAC samples and lysate samples extracted from whole cells would be performed to provide an overview of signalling that is taking place. Adhesion complex data would provide details of signalling occurring directly at the adhesion complex, whereas lysate data would highlight adhesion-associated signalling events, which may take place away from the adhesion complex itself.

An in-solution phosphopeptide enrichment protocol has previously been developed in the laboratory (Robertson et al. 2017;Robertson et al. 2015) and successfully applied to enriched adhesion complex samples. This protocol used TiO_2 chromatography for phosphopeptide enrichment. An alternative method often used for phosphopeptide enrichment uses IMAC. Previous reports suggest that different levels of phosphopeptide coverage are observed using IMAC and TiO_2, and hence there is no consensus on the optimal method (Mann 2009). For this reason, in this study, a comparison of the two phosphoenrichment methods was performed to determine the optimal conditions for HUVEC phosphopeptide enrichment.

4.3.1 Optimisation of phosphoenrichment protocol: total cell lysate samples

Three bead types for phosphopeptide enrichment were investigated; TopTip TiO_2 (Glygen) beads, which have been used in the laboratory previously to enrich phosphopeptides from IACs (Robertson et al. 2015;Robertson et al. 2017), magnetic TiO_2 beads (MagReSyn) and magnetic Ti-IMAC beads (MagReSyn). As the amount of starting material required for phosphopeptide enrichment is usually high (often in the mg range) (Solari et al. 2015), a HUVEC TCL sample was used to test the different strategies, as high protein amounts can be easily collected. Enrichments for each approach were performed, all using 500 µg starting protein, and each sample analysed in duplicate on the Orbitrap Elite mass spectrometer. It has been reported that increasing LC separation time during LC-MS/MS improves the detection of low abundance phosphopeptides, which are often not detected due to preferential selection of more abundant co-eluting peptides for fragmentation by the mass spectrometer (Han et al. 2010;Montoya et al. 2011). Therefore, each sample was analysed using

both a one hour and three hour LC gradient to test whether increasing LC gradient would improve the number of phosphopeptides detected.

The proportion of phosphopeptides to total peptides was 72% for TopTip TiO_2 beads, and for magnetic TiO_2 and Ti-IMAC, 52% and 55% respectively, suggesting successful phosphopeptide enrichment (figure 4.5). When comparing the one hour and three hour samples, a 1.2–1.4-fold increase in phosphopeptides and phosphoproteins was observed for the TiO_2 and Ti-IMAC approaches (figure 4.6). However, only a 1.1-fold increase in phosphopeptides and phosphoproteins identified was observed when increasing run time from one to three hours for the TopTip samples (figure 4.6). These data demonstrate that LC run time is an important parameter to be controlled, at least when using the magnetic bead approaches. As the three hour LC gradient resulted in an increase in identifications, these data were used for further analysis and a three hour LC gradient used for subsequent runs on the Orbitrap Elite.

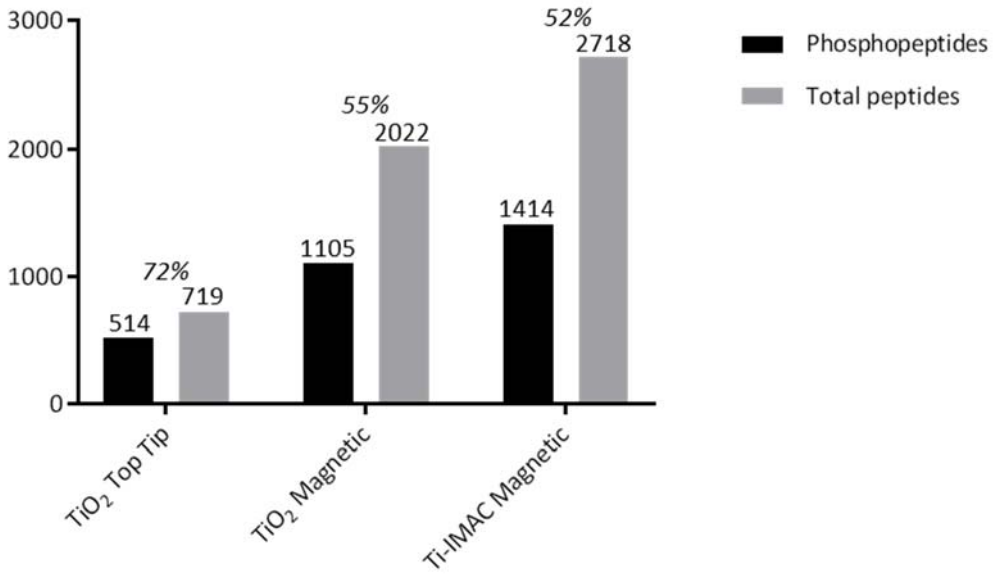

Figure 4.5. Detection of peptides and phosphopeptides from HUVEC total cell lysate samples following 1 hour and 3 hour LC gradient LC-MS/MS run on the Orbitrap Elite mass spectrometer. HUVECs were plated for 2 hours on fibronectin coated plates, after which total cell lysates (500 µg) were collected. Samples were proteolytically digested and enriched for phosphopeptides using Ti-IMAC magnetic, TiO_2 magnetic or TiO_2 TopTip beads. Samples were analysed in duplicate using both a 1 hour and 3 hour LC gradient by LC-MS/MS using an Orbitrap Elite mass spectrometer. Numbers of phosphopeptides and total peptides are indicated above each bar and the percentage enrichment (non-phosphorylated peptides/ phosphorylated peptides identified) are represented in italics. Numbers are displayed as peptides identified in combined 1 hour and 3 hour LC gradient, from two technical replicates.

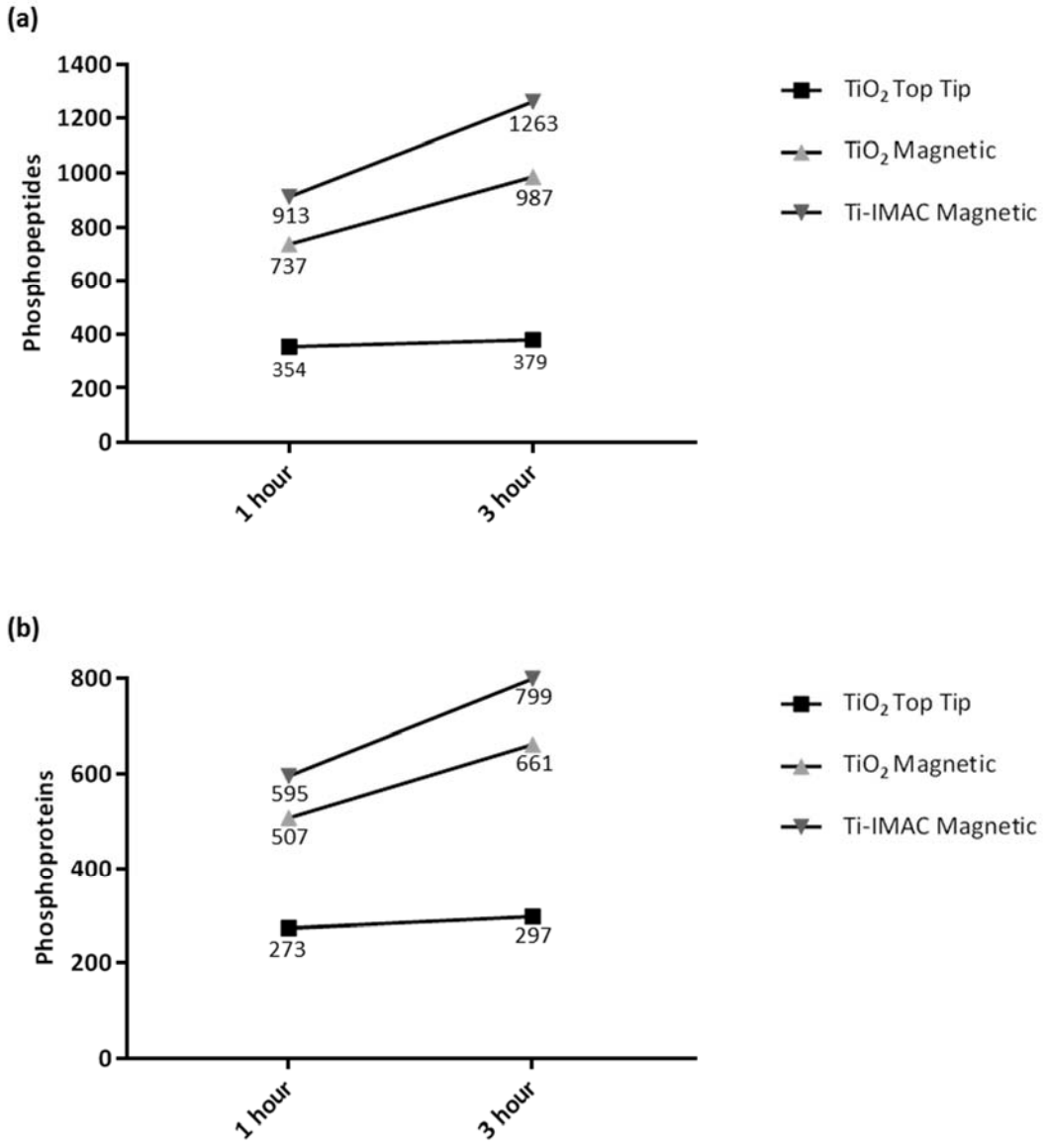

Figure 4.6. Detection of phosphopeptides and phosphoproteins from HUVEC total cell lysate samples following 1 hour and 3 hour gradient LC-MS/MS run using an Orbitrap Elite mass spectrometer. HUVECs were plated for 2 hours on fibronectin coated plates, after which total cell lysates (500 µg) were collected. Samples were proteolytically digested and enriched for phosphopeptides using Ti-IMAC magnetic, TiO_2 magnetic or TiO_2 TopTip beads. Samples were analysed in duplicate using both a 1 hour and 3 hour LC gradient by LC-MS/MS using an Orbitrap Elite mass spectrometer. Comparisons were made by comparing the number of (a) phosphopeptides and (b) phosphoproteins from each sample. Numbers are displayed as peptides identified from two technical replicates.

Analysis performed so far (figure 4.5 & 4.6) has indicated that use of magnetic MagReSyn beads give improved results over the TopTip TiO_2. For TopTip TiO_2 beads, 379 phosphopeptides, and 297 phosphoproteins were enriched. This increased using the magnetic beads, with 987 and 1263 phosphopeptides and 661 and 799 phosphoproteins, for the TiO_2 and Ti-IMAC approaches, respectively (figure 4.6 & 4.7). The majority of phosphopeptides identified (97%) were obtained

using the magnetic TiO_2 and Ti-MAC beads approaches (figure 4.7a). Between the two magnetic bead approaches, a 32% and 43% overlap in phosphopeptides and phosphoproteins was identified, respectively. This overlap was relatively low, and demonstrated that different sets of phosphopeptides may be enriched using the two approaches. To gain a better coverage, the two methods could be used as complementary approaches. TiO_2 and Ti-MAC have been used in combination previously, and determined to be optimal using 25% TiO_2 and 75% Ti-MAC, with a total of 1 mg beads per sample (Tape et al. 2014). This combination approach was therefore used in future studies.

4.3.2 Optimisation of phosphoenrichment protocol: HUVEC adhesion complex samples

As the phosphoenrichment protocol was proven to work with a HUVEC TCL sample, the protocol was applied to enriched HUVEC adhesion complex samples. Before phosphoproteomic analyses of enriched adhesion complexes, a small proportion of all samples were subject to Coomassie Blue staining and western blotting to confirm successful adhesion complex isolation. As a starting point, 10 plates (approximately 50 µg of protein) of adhesion complexes were prepared, the phosphoenrichment protocol applied using the recommended ratio of 25% TiO_2 and 75% Ti-IMAC beads, and samples run on the Orbitrap Elite mass spectrometer using a LC 3 hour gradient. A total of 265 phosphoproteins and 485 phosphopeptides were identified (75% of the total peptides identified), indicating that the phosphopeptide enrichment method worked well for isolated HUVEC IAC samples (figure 4.8). This protein number is comparable to the 297 of proteins shown to be specific to HUVEC adhesion complexes in chapter 3. However, it is worth noting that no negative control was used in this instance, which if used may reduce this number further. Of the 265 phosphoproteins, 54 meta, four consensus and 12 literature-curated adhesome proteins, corresponding to 20%, 1.5% and 4.5% of the total dataset respectively, were identified. However, these numbers and proportions were much lower than that identified in the HUVEC IAC dataset generated in chapter 3 (figure 3.10 & 3.11). To aid identification of phosphopeptides a number of optimisation steps were performed.

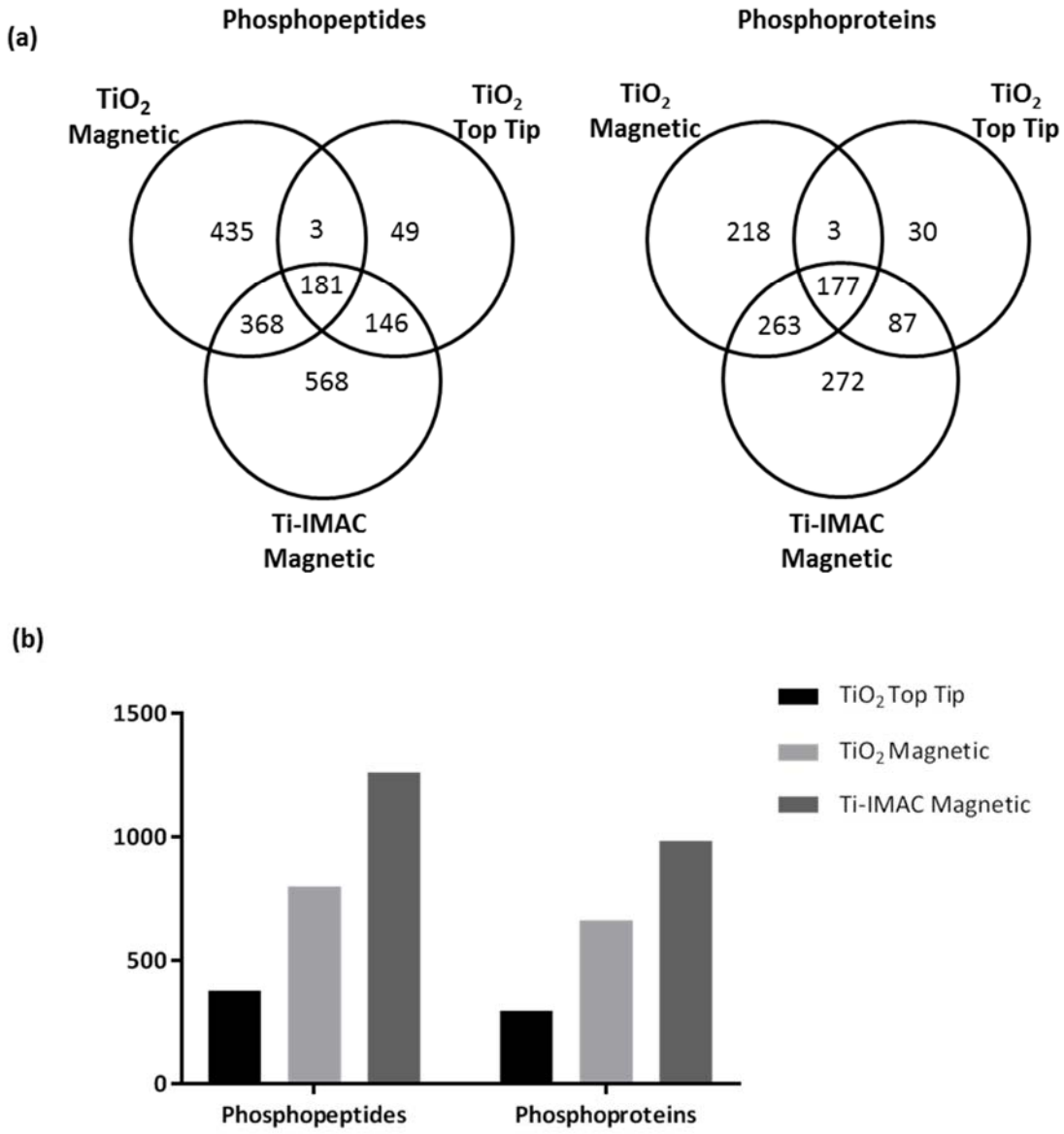

Figure 4.7. Detection of phosphopeptides and phosphoproteins from HUVEC total cell lysate samples using Ti-IMAC magnetic, TiO_2 magnetic and TiO_2 TopTip beads. HUVECs were plated for 2 hours on fibronectin coated plates, after which total cell lysates (500 µg) were collected. Samples were proteolytically digested and enriched for phosphopeptides using Ti-IMAC magnetic, TiO_2 magnetic or TiO_2 TopTip beads. Samples were analysed in duplicate using a 3 hour LC gradient by LC-MS/MS using an Orbitrap Elite mass spectrometer. Comparisons were made by comparing the number of phosphopeptides and phosphoproteins identified using each bead method represented as (a) Venn diagrams to determine the number of phosphopeptides and phosphoproteins exclusive to each bead method and (b) Bar charts to represent overall numbers of phosphopeptides and phosphoproteins. Numbers are displayed as phosphopeptides or phosphopeptides identified in two technical replicates.

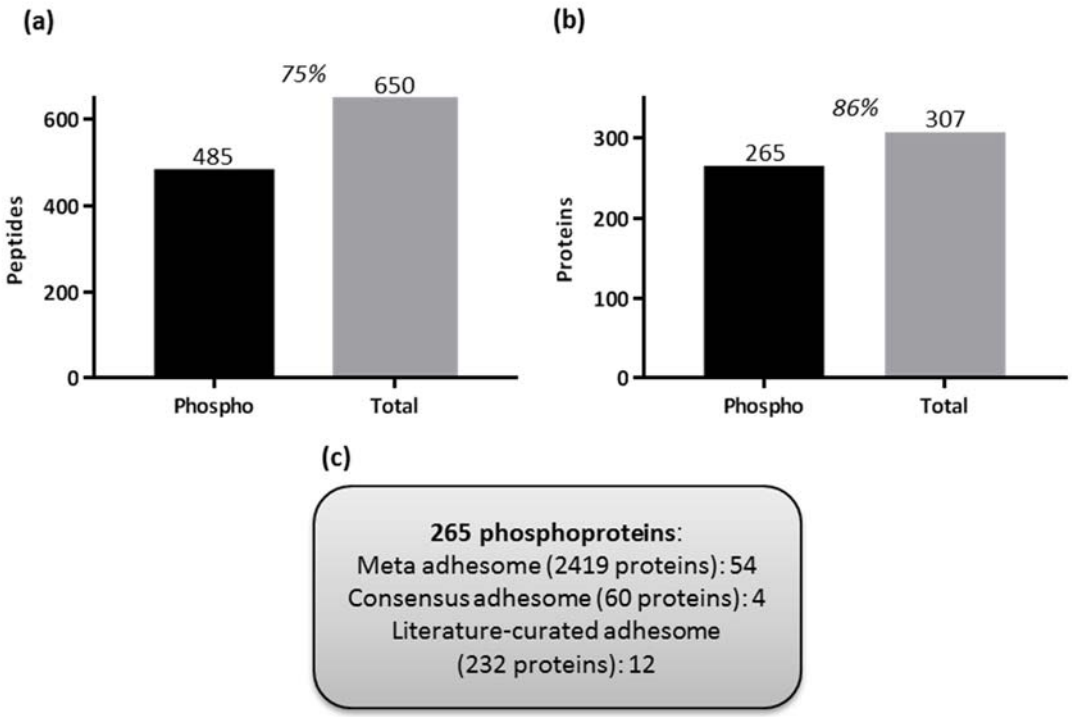

Figure 4.8. Detection of phosphopeptides and phosphoproteins enriched from HUVEC isolated integrin adhesion complex samples: 10 plates of sample. HUVECs were plated for 2 hours on fibronectin coated plates, cross-linked using DTBP (6 mM for 5 minutes), cell bodies removed using a combination of cell lysis and tap water wash, and the remaining ligand bound complexes collected for analysis (10 plates or approximately 50 µg protein). Samples were proteolytically digested and enriched for phosphopeptides using 75% Ti-IMAC magnetic and 25% TiO_2 magnetic beads. Samples were analysed in duplicate using a 3 hour LC gradient by LC-MS/MS using an Orbitrap Elite mass spectrometer. Comparisons were made by comparing the number of (a) phosphopeptides and total peptides and (b) phosphoproteins and total proteins identified. Numbers are displayed as peptides or proteins identified from two technical replicates. Numbers of phosphopeptides or total peptides are indicated above each bar and the percentage enrichment are represented in italics. (c) Numbers of meta adhesome, consensus adhesome and literature-curated adhesome proteins in this HUVEC IAC phosphoproteomic dataset are shown.

Phosphoproteomic analysis is often performed with much larger starting amounts of protein than used for IAC samples (milligrams rather than micrograms) (Solari et al. 2015). To determine whether increasing the starting protein amount increased the number of unique phosphopeptides, phosphoproteins and adhesome dataset proteins that could be identified, a scale-up experiment was performed. Due to limitations in the amount of adhesion complex material that could be prepared in one day, 15 plates of HUVEC adhesion complexes were prepared on three separate days using the optimised protocol, and a proportion taken for SDS-PAGE and western blotting to confirm successful IAC isolation. The remaining sample was then combined to produce a single sample containing 45 plates of enriched HUVEC adhesion complex sample. This sample was then split unequally into two for processing, resulting in a 10- and 35- plate sample. Phosphoenrichment was performed on these samples side-by-side, and enriched samples run in duplicate on the Orbitrap Elite mass spectrometer using a 3 hour LC gradient. A total of 464 phosphopeptides and 250 phosphoproteins were identified in the 10 plate sample, increasing to 949 and 471 respectively for the 35 plate sample (figure 4.9a & b). Of the 471 proteins identified in the 35 plate sample, 267 meta, 23 consensus and 53 literature-curated adhesome proteins were identified, corresponding to 57%, 4.9% and 3.2% of the total dataset respectively. This was a large increase compared to the 10 plate sample from which 59 meta, seven consensus and 15 literature-curated adhesome proteins were identified (figure 4.9c). Interestingly, of the 214 extra phosphoproteins identified when increasing from the 10 to 35 plate sample, 208 were meta adhesome proteins. This indicates that almost all additional phosphopeptides identified when scaling up protein amount from 10 to 35 plates were from previously identified adhesion complex proteins. Encouragingly, the coverage of adhesome dataset proteins identified in the 35 plate sample was similar to that identified in the HUVEC IAC dataset generated in chapter 3 (figure 3.10 & 3.11). Overall, scale-up of starting protein material by 3.5-fold prior to phosphoproteomic analysis increased the number of phosphoproteins and phosphopeptides identified, and improved the number of identified IAC proteins.

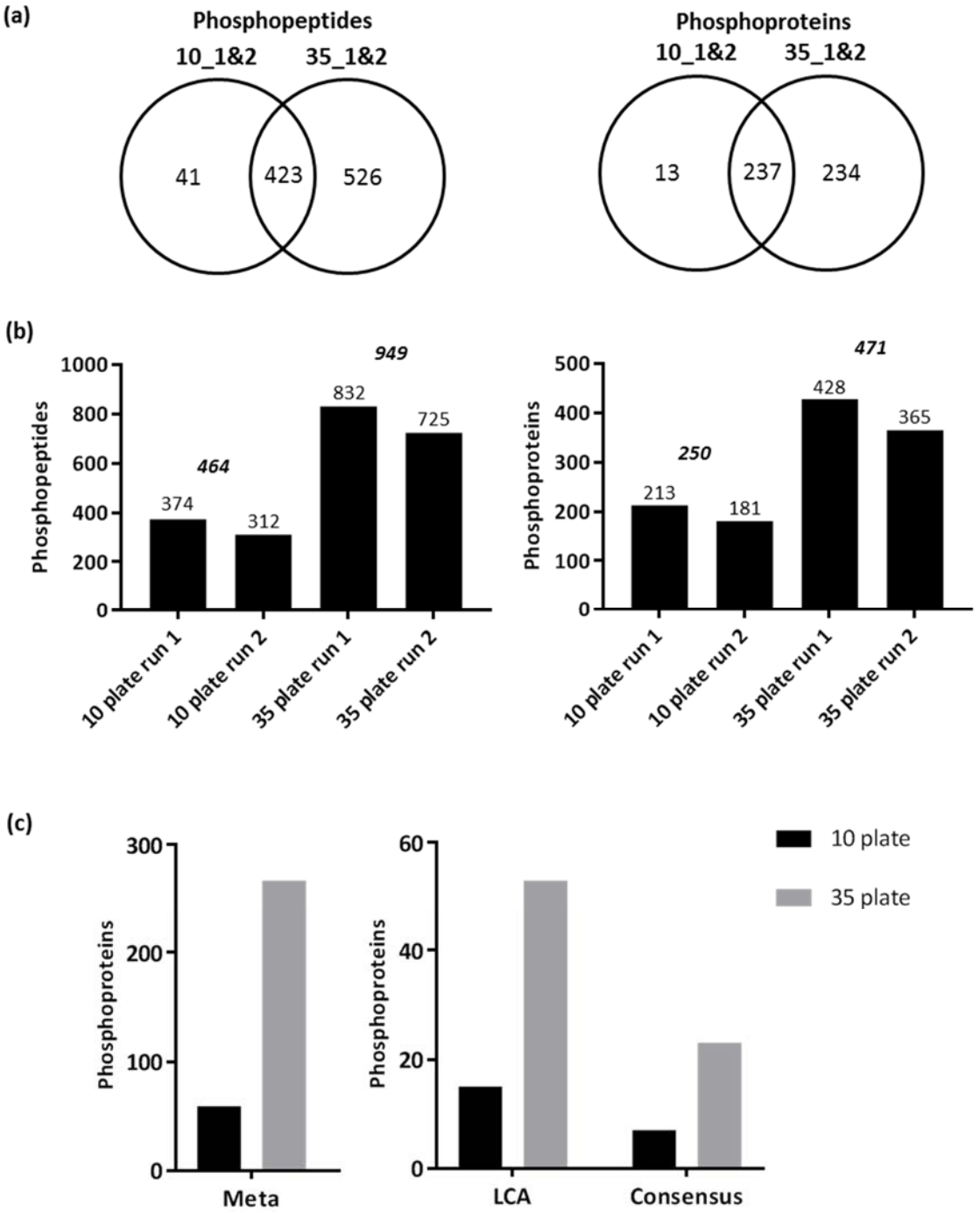

Figure 4.9. Detection of phosphopeptides and phosphoproteins from enriched from HUVEC isolated integrin adhesion complex samples: 10 vs 35 plates of sample. HUVECs were plated for 2 hours on fibronectin coated plates, cross-linked using DTBP (6 mM for 5 minutes), cell bodies removed using a combination of cell lysis and tap water wash, and the remaining ligand bound complexes collected for analysis (10 plates, [approx. 50 µg protein] or 35 plates [approx. 175 µg protein]). Samples were proteolytically digested and enriched for phosphopeptides using 75% Ti-IMAC magnetic and 25% TiO_2 magnetic beads. Samples were analysed in duplicate using a 3 hour LC gradient by LC-MS/MS using an Orbitrap Elite mass spectrometer. Comparisons were made by comparing the number of phosphopeptides identified in the 10- and 35- plate sample represented as (a) Venn diagrams to determine the overlap of phosphopeptides between each sample, numbers of peptides are displayed as the average of two technical replicates. (b) Bar charts to represent overall numbers of phosphopeptides identified in each of the individual runs, numbers of phosphopeptides or phosphoproteins are indicated above each bar and the number of total unique phosphopeptides and phosphoproteins identified when including overlap in duplicate samples are represented in italics. (c) Numbers of meta adhesome, consensus adhesome and literature-curated adhesome proteins in the 10- and 35- plate HUVEC IAC phosphoproteomic datasets are shown.

4.3.3 Optimisation of phosphoenrichment protocol: automated phosphopeptide enrichment

Phosphopeptide enrichment strategies used in this project to this point have been manually applied rather than using automation. In future experiments, the application of multiple replicates and biological conditions will increase the number of samples that will need to be enriched for phosphopeptides at once. In addition, due to the requirement of phosphopeptide quantification between biological conditions, it is important that sample-to-sample preparation is uniform for all samples within an experiment, to improve quantification accuracy. For these reasons, the phosphopeptide enrichment method developed was adapted, and performed using the KingFisher Flex purification system. This approach has been shown to be much quicker and highly reproducible, when compared to the manual approach (Tape et al. 2014). Initial application was tested using 1 mg of HUVEC TCL sample. Following enrichment, this sample was run using a 3 hour LC gradient on the Orbitrap Elite mass spectrometer. In addition, due to its recent acquisition, samples were also run on a Q Exactive Hybrid Quadrupole-Orbitrap Mass Spectrometer using a 60 minute LC gradient. The Q Exactive mass spectrometer is reported to have faster scan rate and higher resolution, leading to increased numbers of peptide and protein groups identified form samples compared to that of other mass spectrometers (Sun et al. 2013;Kelstrup et al. 2012;Scheltema et al. 2014). Therefore, each sample was analysed using both mass spectrometers to test whether using the Q Exactive would improve the number of phosphopeptides detected.

The automated phosphopeptide enrichment method resulted in 72% phosphopeptide purity, indicating that enrichment was successful using this approach. The Orbitrap Elite mass spectrometer identified 1234 phosphopeptides and 805 phosphoproteins, whereas the Q Exactive identified 2061 and 1199 respectively, indicating that the latter may perform better, at least for identification of phosphopeptides in a complex TCL sample (figure 4.10).

Surprisingly in the TCL sample enriched using the automated method, 417 meta, 20 consensus and 61 literature-curated adhesome proteins were identified by Q Exactive analysis and 343, 18 and 46, respectively, for the Orbitrap Elite analysis data (figure 4.11). The number of meta adhesome proteins identified in this analysis, even when using the Orbitrap Elite data for direct comparison purposes, was increased when compared to that previously identified in the 35 plate adhesion complex experiment displayed in figure 4.9 (figure 4.11). In addition, a range of well characterised adhesion protein sites were identified (Src-Y416, Paxillin-Y118, FAK-Y576) that are known to be upregulated in response to integrin-mediated adhesion (Robertson et al. 2015). These data suggest that phosphoproteomic analysis of HUVEC TCL samples may provide sufficient sample coverage to be used to study adhesion complex phosphorylation events. TCL phosphoproteomic data following VEGF treatment, along with adhesion complex phosphoproteomic data with VEGF treatment may

be used in combination to gain a better understanding of changes occurring during VEGF-adhesion crosstalk. These combined analyses will give a view of changes occurring both close and distal to adhesion complex following VEGF treatment. For this reason, phosphoproteomic analysis of both adhesion complex and TCL samples following VEGF treatment was performed.

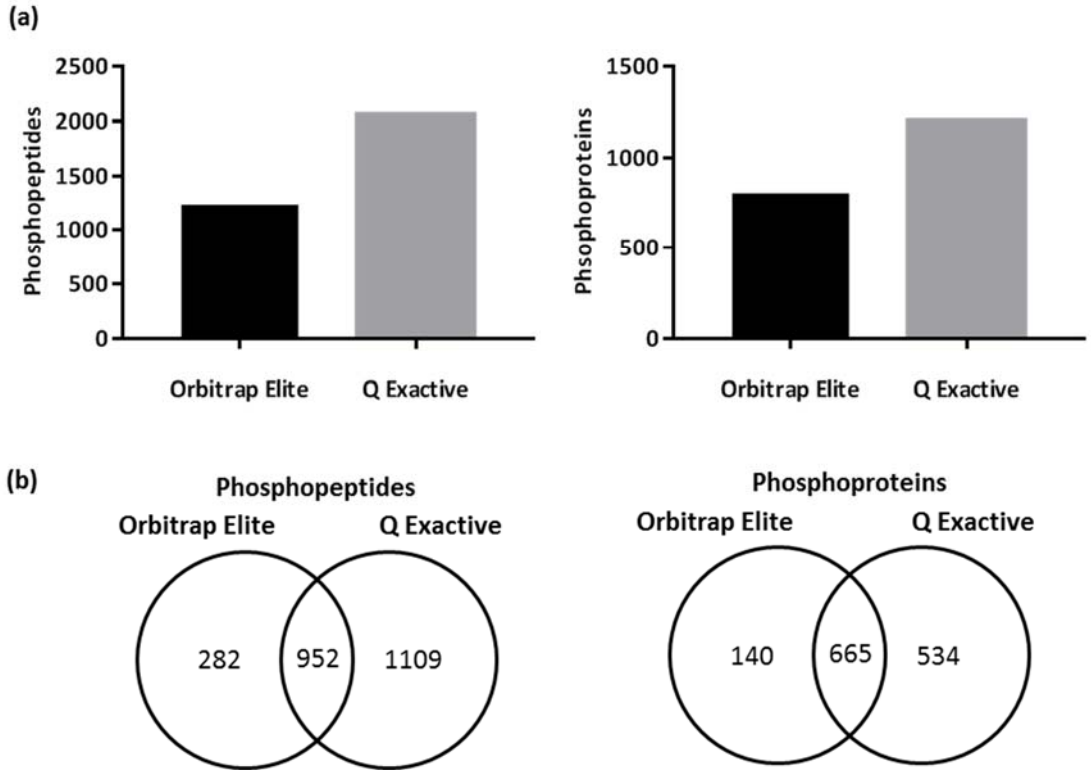

Figure 4.10. Detection of phosphopeptides and phosphoproteins enriched from HUVEC total cell lysate samples using the automated phosphoenrichment method, and analysed by Orbitrap Elite and Q Exactive mass spectrometers. HUVECs were plated for 2 hours on fibronectin coated plates, after which total cell lysates (1 mg) were collected. Samples were proteolytically digested and enriched for phosphopeptides using 75% Ti-IMAC magnetic and 25% TiO_2 magnetic beads using the KingFisher Flex automated protocol. Samples were analysed in duplicate by LC-MS/MS using Orbitrap Elite (3 hour LC gradient) and Q Exactive (60 minute LC gradient) mass spectrometers. Comparisons were made by comparing the number of (a) phosphopeptides and phosphoproteins identified using each mass spectrometer. (b) Venn diagrams displaying the overlap of phosphopeptides between each sample. Numbers are displayed as phosphopeptides or phosphopeptides identified in two technical replicates.

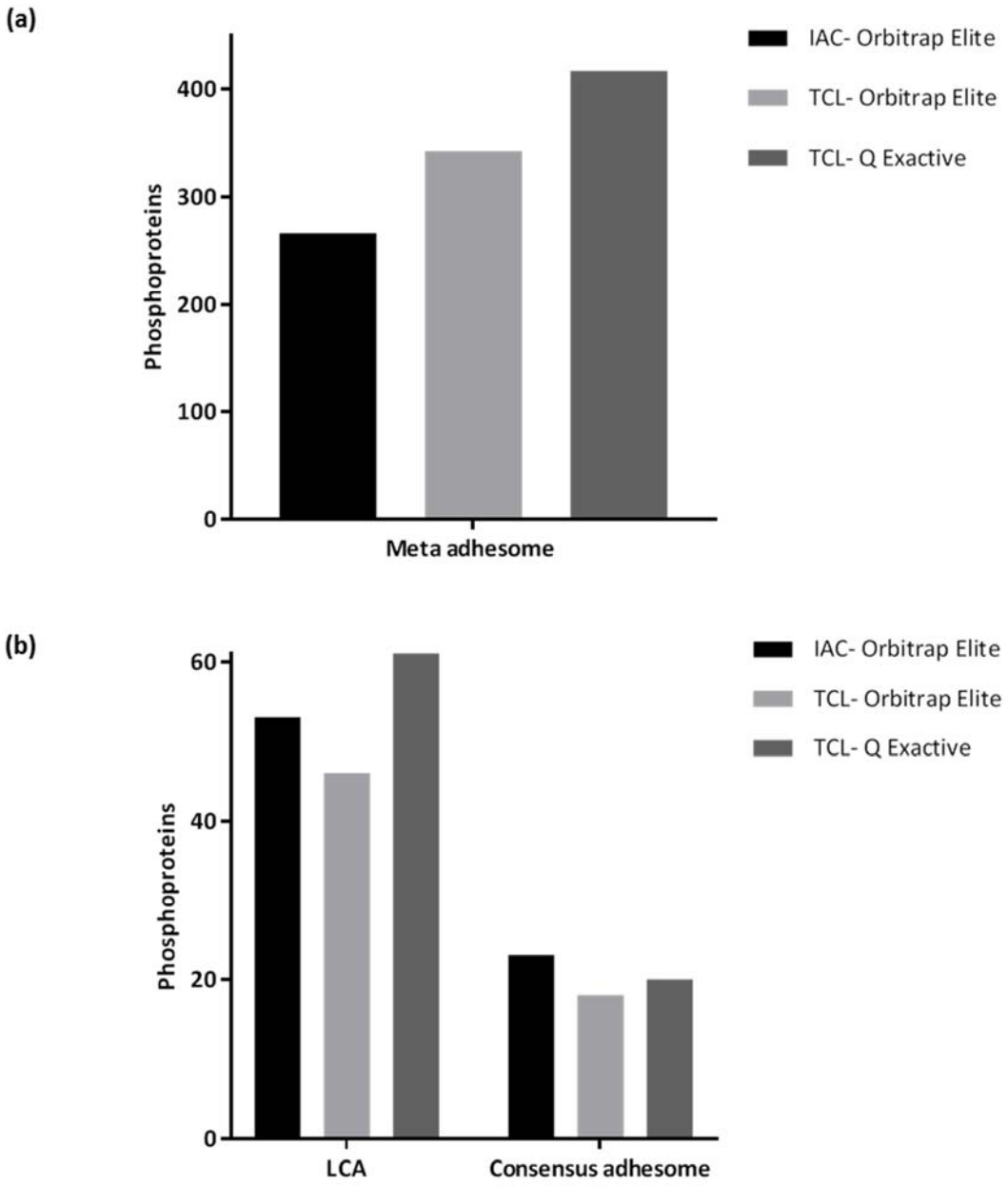

Figure 4.11. Detection of adhesome phosphoproteins from HUVEC total cell lysate and isolated integrin adhesion complex samples. HUVECs were plated for 2 hours on fibronectin coated plates, after which total cell lysates (1 mg) were collected or adhesion complexes isolated by cross-linking with DTBP (6 mM for 5 minutes), cell bodies removed using a combination of cell lysis and tap water wash, and collection of remaining ligand bound complexes for analysis. Samples were proteolytically digested and enriched for phosphopeptides using 75% Ti-IMAC magnetic and 25% TiO_2 magnetic beads using the KingFisher Flex automated protocol. Total cell lysate samples were analysed using a LC-MS/MS using Orbitrap Elite (3 hour LC gradient) and Q Exactive (60 minute LC gradient) mass spectrometers, and adhesion complex sample analysed using the Orbitrap Elite (3 hour LC gradient). Comparisons were made by comparing the number of numbers of (a) meta adhesome, (b) consensus adhesome and literature-curated adhesome proteins identified in each analysed sample.

As had been performed before using the manual phosphopeptide enrichment protocol, a scale up experiment was carried out to test how increasing starting IAC protein amount when using the automated phosphoenrichment method affected the number of phosphopeptides identified. Again, one sample of 45 plates of adhesion complexes were prepared over 3 separate days, pooled, and split into two samples (one 10- and 35- plate sample). For comparison purposes, these samples were run on the Orbitrap Elite using a 1 hour and 3 hour LC gradient and the Q Exactive using a 60 and 90 minute gradient. In all cases, the 35 plate sample gave a large increase in the number of phosphopeptides and phosphoproteins identified when compared to the 10 plate sample (figure 4.12), consistent with previous results using the manual phosphoenrichment method (figure 4.9). In most cases, increasing LC gradient time (when comparing data from the same mass spectrometer) gives an improvement in the numbers of phosphopeptides and phosphoproteins identified (figure 4.12). Surprisingly, for the 35 plate sample, the Orbitrap Elite (3 hour LC gradient) outperformed the Q Exactive (90 minute LC gradient), with 575 and 500 phosphopeptides identified, respectively. However, for the 10 plate sample, only a small difference was seen in the numbers of phosphopeptides and phosphoproteins when comparing the different mass spectrometers. In addition, the number of meta, consensus and literature-curated adhesome components identified was optimal when using the Orbitrap Elite, 3 hour LC run (figure 4.12c).

These data suggest that performance of different mass spectrometers and LC gradient times is dependent on the type and/or amount of sample present. This supports data which suggests the Q Exactive performs better on highly complex samples, such as TCLs (Scheltema et al. 2014). Overall, for isolated IAC analysis, from the conditions tested, using a 35 plate adhesion complex sample run on the Orbitrap Elite mass spectrometer on a 3 hour LC gradient appears to be optimal, resulting in the highest number of phosphoproteins, phosphopeptides and IAC proteins identified when compared to other conditions.

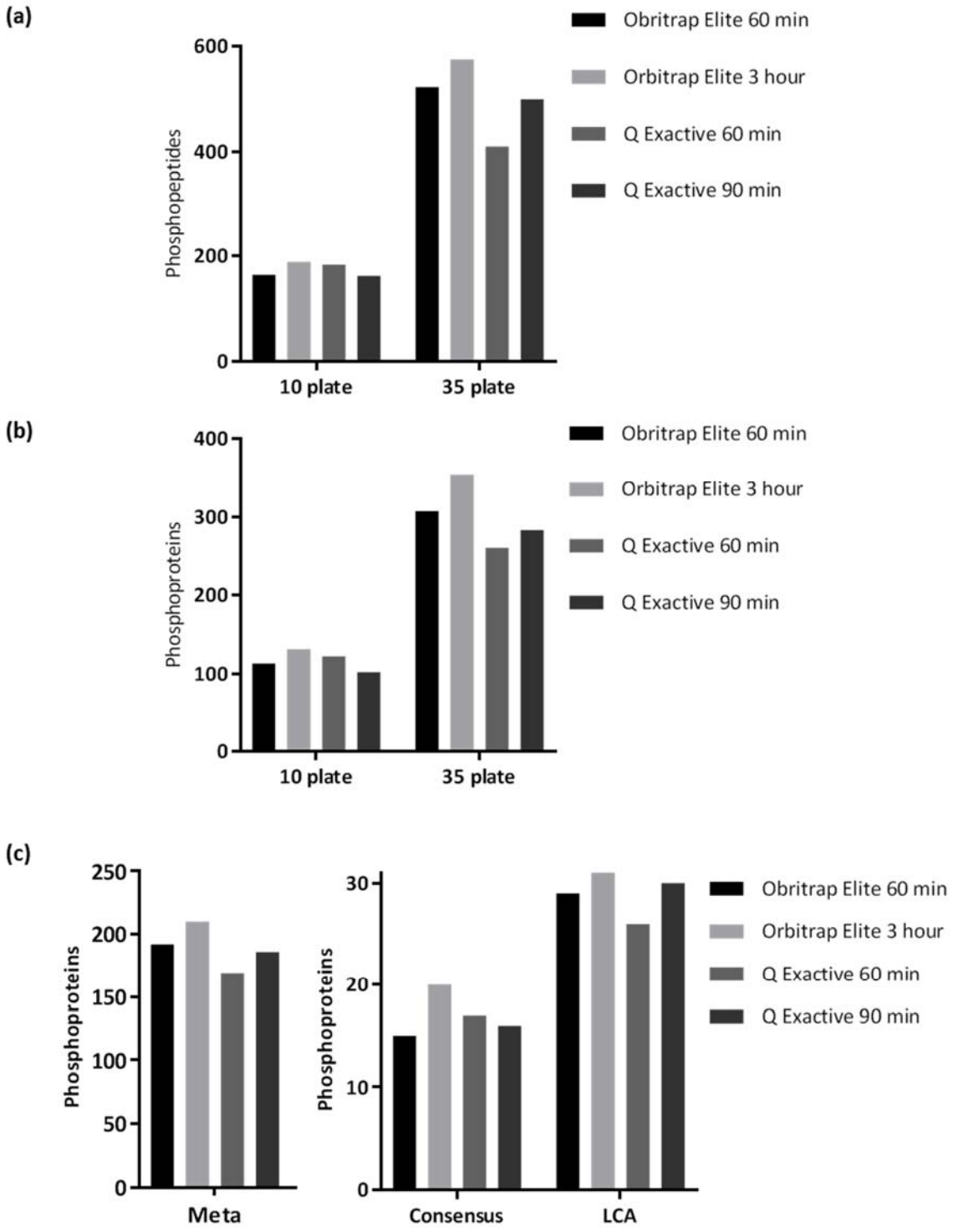

Figure 4.12. Detection of phosphopeptides and phosphoproteins from HUVEC isolated integrin adhesion complex samples analysed by LC-MS/MS on Orbitrap Elite (1 and 3 hour LC gradient) and Q Exactive (60 and 90 minute LC gradient) mass spectrometers. HUVECs were plated for 2 hours on fibronectin coated plates, cross-linked using DTBP (6 mM for 5 minutes), cell bodies removed using a combination of cell lysis and tap water wash, and the remaining ligand bound complexes collected for analysis (10 plates [approx. 50 µg protein] or 35 plates [approx.175 µg protein]). Samples were proteolytically digested and enriched for phosphopeptides using 75% Ti-IMAC magnetic and 25% TiO_2 magnetic beads using the KingFisher Flex automated protocol. Samples were analysed by LC-MS/MS using Orbitrap Elite (1 or 3 hour LC gradient) and Q Exactive (60 or 90 minute LC gradient) mass spectrometers. (a-b) Comparison of the number of phosphopeptides and phosphoproteins identified by each run. (c) Number of meta adhesome, consensus adhesome and literature-curated adhesome proteins identified in each analysed sample.

4.3.4 Preliminary phosphoproteomic analysis following VEGF treatment

To test the ability to perform the full optimised phosphoenrichment protocol, and subsequent mass spectrometry analysis of phosphopeptides, an initial small-scale, preliminary experiment was performed including a VEGF treatment step (25 ng/mL, 7.5 minutes) prior to lysis (for TCL samples) or crosslinking and IAC isolation. Both isolated IAC and TCL samples were tested, as it had been determined that both methods may be useful to study adhesion complex phosphorylation events in HUVECs (section 4.3.1-4.3.3). The optimised VEGF treatment protocol was performed (section 4.2), and cells either lysed (generating 1.5 mg protein per condition), or adhesion complexes enriched (15 plates per condition). The optimised, automated phosphoenrichment protocol was then performed. Both lysate and adhesion complex samples were run on the Q Exactive mass spectrometer (90 minute LC gradient), and adhesion complex samples also run on the Orbitrap Elite (3 hour LC gradient) mass spectrometer for comparison purposes.

4.3.4.1 Adhesion complex samples following VEGF treatment- Orbitrap Elite vs Q Exactive

Similar numbers of phosphopeptides and phosphoproteins were identified for the VEGF-treated samples when comparing the two mass spectrometers (figure 4.13 & table 4.1). However, the Q Exactive identified more phosphopeptides and phosphoproteins than the Orbitrap Elite for the SFM-treated samples (table 4.1 & figure 4.13). Q Exactive analysis also gave different percentage identifications (%ID) for the SFM- and VEGF-treated samples (12% vs 8.4%), which may explain the differences in numbers identified (table 4.1). In addition, the ratio of phosphopeptides:total number of spectra for the corresponding sample was calculated; this analysis corresponds to the spectral counting normalisation method used for phosphoproteomic analysis when comparing two samples directly for quantification purposes. Similar values were obtained for the SFM and VEGF samples using the Orbitrap Elite analysis, whereas values have greater difference when using the Q Exactive (table 4.1). As final experiments including VEGF treatment require quantification to be performed, it was important that the %IDs and normalised values were similar between samples, as differences may lead the errors in quantification. For this reason, and the fact that the Orbitrap Elite outperformed the Q Exactive in optimisation experiments involving IAC samples (figure 4.12), the Orbitrap Elite was chosen as the preferred mass spectrometer for final experiments.

Table 4.1. Phosphoproteomic analysis of isolated IAC samples from HUVECs analysed with Orbitrap Elite and Q Exactive mass spectrometers. The total number of unique phosphoproteins, phosphopeptides, spectra, phosphopeptides/spectra and % identifications are displayed, as validated by Scaffold. Samples were analysed in duplicate on the Q Exactive mass spectrometer using a 90 minute LC gradient, and a single run was performed on the Orbitrap Elite mass spectrometer using a 3 hour LC gradient.

	Instrument	Phospho-proteins	Total unique phospho-peptides	Spectra	Phosphopeptides/ spectra	IDs (%)
IAC SFM_1	Q Exactive	271	443	7345	0.060	13
IAC SFM_2	Q Exactive	255	409	7548	0.054	11
IAC VEGF_1	Q Exactive	160	258	6261	0.041	8.5
IAC VEGF_2	Q Exactive	180	293	6914	0.042	8.3
IAC SFM	Orbitrap Elite	185	291	13437	0.022	4.4
IAC VEGF	Orbitrap Elite	148	229	11109	0.021	4.3

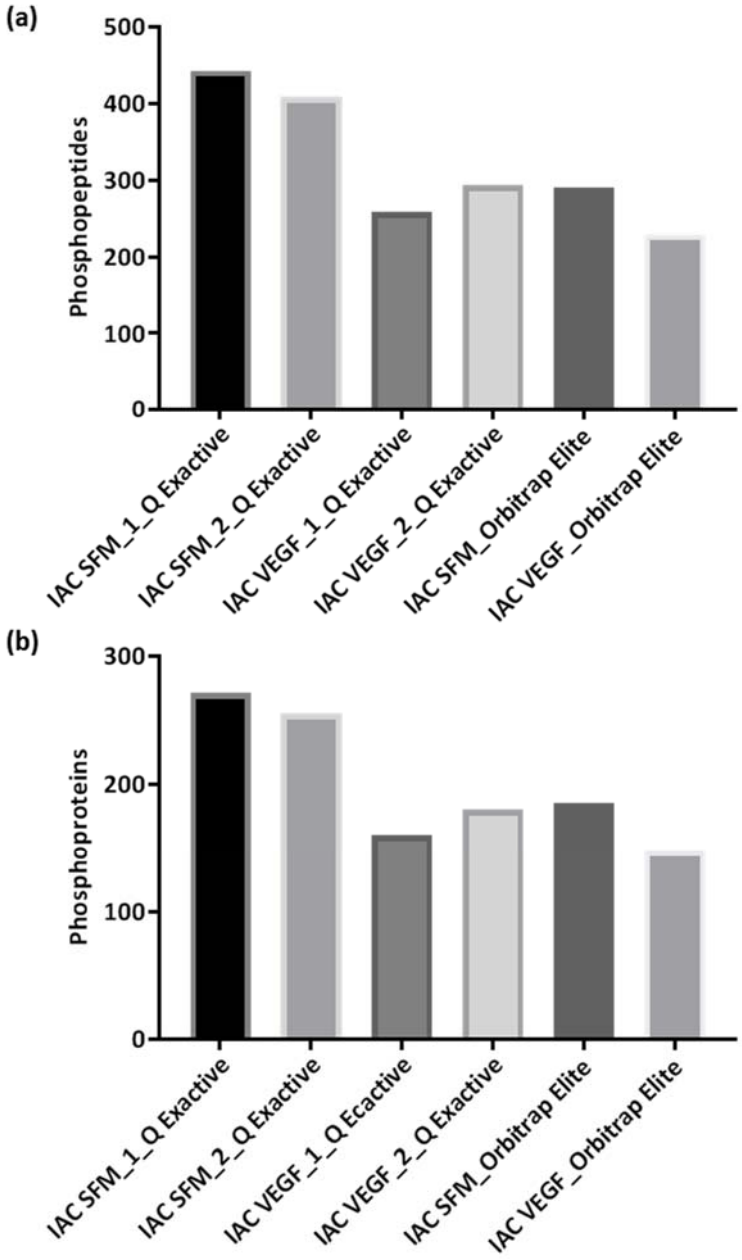

Figure 4.13. Detection of phosphopeptides and phosphoproteins from HUVEC isolated integrin adhesion complex samples following SFM or VEGF treatment analysed by LC-MS/MS on Orbitrap Elite (3 hour LC gradient) and Q Exactive (90 minute LC gradient) mass spectrometers. HUVECs were plated for 2 hours on fibronectin coated plates, treated with SFM or VEGF (25 ng/mL, 7.5 minutes) after which cross-linking was performed using DTBP (6 mM for 5 minutes), cell bodies removed using a combination of cell lysis and tap water wash, and the remaining ligand bound complexes collected for analysis (15 plates per sample). Samples were proteolytically digested and enriched for phosphopeptides using 75% Ti-IMAC magnetic and 25% TiO_2 magnetic beads using the KingFisher Flex automated protocol. Samples were analysed by LC-MS/MS using Orbitrap Elite (3 hour LC gradient) and Q Exactive (90 minute LC gradient) mass spectrometers. Comparison of the number of phosphopeptides (a) and phosphoproteins (b) identified by each run.

4.3.4.2 Total cell lysate samples following VEGF treatment

SFM- and VEGF-treated TCL samples (1.5 mg) were analysed in duplicate using a 90 minute LC gradient on the Q Exactive mass spectrometer. The numbers of phosphopeptides and phosphoproteins identified were similar when comparing the SFM- and VEGF-treated samples (figure 4.14). In addition, similar numbers of %IDs (45 - 46%) and total spectra (17823 - 18671) were identified between the duplicate SFM and VEGF samples. Therefore, analysis of these data suggests that comparisons can be made between SFM- and VEGF-treated samples. In addition, as seen before when using TCL samples for phosphoenrichment, much higher numbers of phosphopeptides and phosphoproteins were identified from the meta adhesome, consensus adhesome and LCA compared to the adhesion complex samples (figure 4.15).

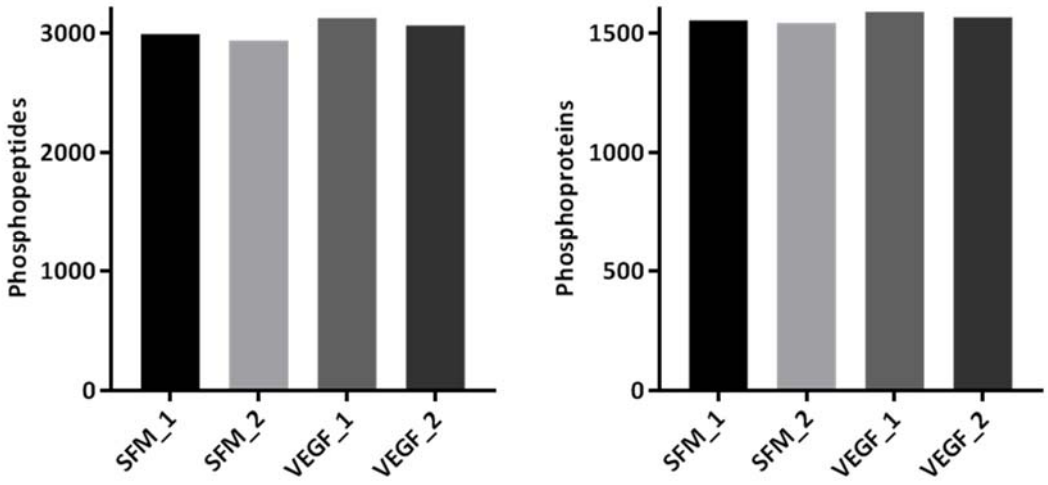

Figure 4.14. Detection of phosphopeptides and phosphoproteins from HUVEC total cell lysate samples following SFM or VEGF treatment. HUVECs were plated for 2 hours on fibronectin coated plates, treated with SFM or VEGF (25 ng/mL, 7.5 minutes) after which total cell lysates (1.5 mg per sample) were collected. Samples were proteolytically digested and enriched for phosphopeptides using 75% Ti-IMAC magnetic and 25% TiO_2 magnetic beads using the KingFisher Flex automated protocol. Samples were analysed in duplicate using a 3 hour LC gradient by LC-MS/MS using a Q Exactive mass spectrometer. Comparison of the number of phosphopeptides and phosphoproteins identified by each run is displayed.

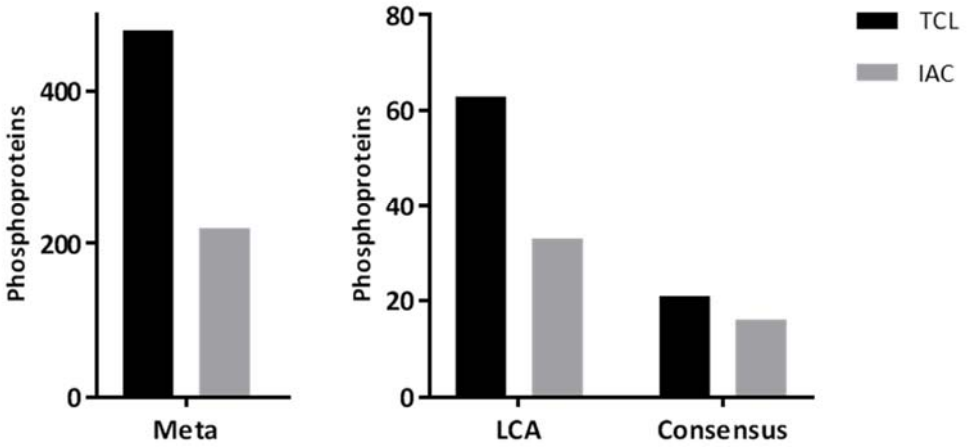

Figure 4.15. Number of meta adhesome, consensus adhesome and literature-curated adhesome proteins identified by phosphoproteomic analysis of VEGF-treated total cell lysate (TCL) and isolated integrin adhesion complex (IAC) samples. HUVECs were plated for 2 hours on fibronectin coated plates, treated with SFM or VEGF (25 ng/mL, 7.5 minutes), after which total cell lysates (1.5 mg) were collected or adhesion complexes isolated by cross-linking with DTBP (6 mM for 5 minutes), cell bodies removed using a combination of cell lysis and tap water wash, and collection of remaining ligand bound complexes for analysis (15 plates; approx. 75 µg protein). Samples were proteolytically digested and enriched for phosphopeptides using 75% Ti-IMAC magnetic and 25% TiO_2 magnetic beads using the KingFisher Flex automated protocol. Samples were analysed in duplicate using a Q Exactive (90 minute LC gradient) mass spectrometer. Comparisons were made by comparing the number of numbers of meta adhesome, consensus adhesome and literature-curated adhesome (LCA) proteins identified in each analysed sample. Number displayed are representative of combined SFM and VEGF treated samples in duplicate (4 runs combined).

4.4 Combined proteomic and phosphoproteomic analysis of HUVEC integrin adhesion complexes following VEGF stimulation

Analyses of the HUVEC IAC dataset generated in chapter 3 demonstrated that the adhesion complex isolation protocol permitted the enrichment and identification of IAC proteins that were representative of the HUVEC adhesion complex. To identify changes in protein composition of adhesion complexes in response to VEGF, a VEGF (25 ng/mL; 7.5 minutes) or SFM control (7.5 minutes) treatment of HUVECs was performed under the optimised conditions (section 4.2). Under these conditions, TCL samples (4 replicates) were generated and adhesion complexes isolated (4 replicates; figure 4.16). Phosphoproteomic analysis using methods optimised in this chapter were applied to both VEGF-treated TCL and isolated IAC samples (figure 4.16). In addition, to investigate total protein abundance changes, and the relationship between phosphorylated and associated total protein levels at adhesion sites, proteomic analysis (in addition to phosphoproteomic analysis) of isolated HUVEC IACs upon VEGF treatment was required. Coomassie Blue staining was used to estimate the yield of adhesion complex protein amount isolated, and the amount of sample prepared for analysis was adjusted to ensure equal protein amounts for SFM and VEGF samples within replicates were taken forward for phosphoproteomic analysis.

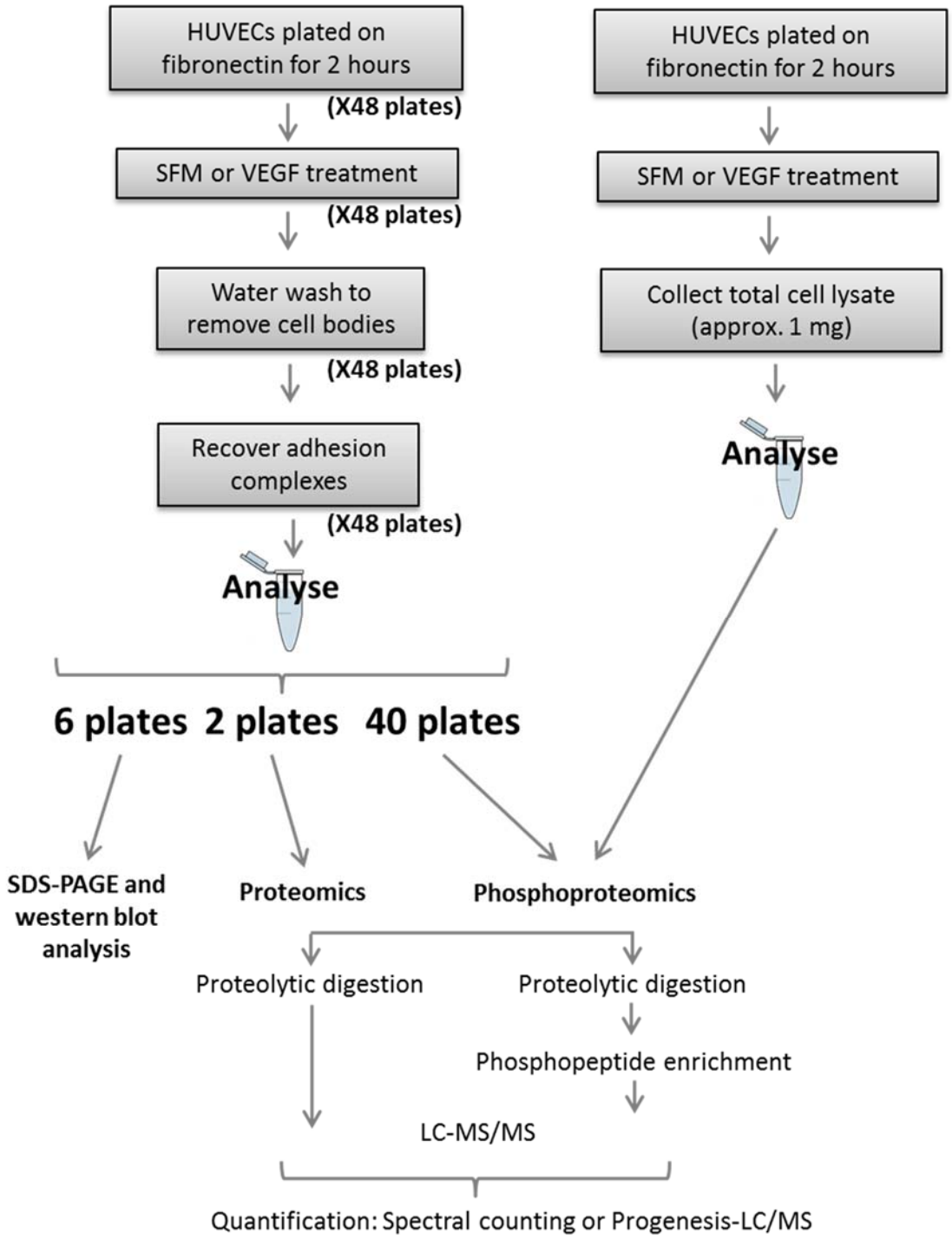

Figure 4.16. Schematic of the optimised workflow used to prepare and analyse VEGF treated HUVEC isolated integrin adhesion complexes and total cell lysate samples. HUVECs were plated for 2 hours on fibronectin coated plates, and the treated with SFM (7.5 minutes) or VEGF (25 ng/mL, 7.5 minutes). Following treatment, total cell lysates (approximately 1 mg per condition) were collected or adhesion complexes isolated by cross-linking with DTBP (6 mM for 5 minutes), cell bodies removed using a combination of cell lysis and tap water wash, and collection of remaining ligand bound complexes for analysis. For adhesion complex isolation, 48 plates were prepared per condition for each replicate, with a total of 4 replicates, leading to a total preparation of 384 plates. Coomassie Blue staining with SDS-PAGE and western blot analysis was used to confirm successful adhesion complex isolation in all samples (6 plates per sample). For proteomic analysis, samples were proteolytically digested by in-gel trypsin digestion (2 plates per IAC sample), and analysed by LC-MS/MS using an Orbitrap Elite mass spectrometer (2 hour LC gradient). Samples for phosphoproteomic analysis (40 plates per adhesion complex sample, 1 mg per lysate sample) were proteolytically digested and enriched for phosphopeptides using 75% Ti-IMAC magnetic: 25% TiO_2 magnetic beads and analysed by LC-MS/MS using an Orbitrap Elite mass spectrometer (3 hour LC gradient).

4.4.1 Proteomic analysis of adhesion complexes isolated from HUVECs following VEGF treatment

As detailed in figure 4.16, from the 48 plates of isolated adhesion complex sample per condition, two plates worth of sample was taken for proteomic processing by in-gel trypsin digestion and mass spectrometry analysis using an Orbitrap Elite mass spectrometer (2 hour LC gradient). A total of 855 proteins were identified using the selected criteria (section 2.12). The calculated fold change of all proteins are presented (figure 4.17), and a complete protein list and associated statistical analyses are displayed in supplementary table 4.1 (appendix).

In total, 507 meta adhesome proteins (figure 4.18a, table 4.2b), 50 LCA proteins (figure 4.18b, table 4.2b) and 40 consensus adhesome proteins (figure 4.18c, table 4.2b) were identified in this VEGF-treated HUVEC IAC proteomic dataset (Geiger and Zaidel-Bar, 2012; Horton et al., 2016). The percentage of meta, consensus and literature-curated adhesome proteins in the HUVEC IAC dataset generated in chapter 3 (table 4.2a) and this VEGF-treated dataset (table 4.2b) were displayed. In addition, the percentage of proteins in the HUVEC IAC dataset generated in chapter 3 and this VEGF-treated dataset present in each of the meta, consensus and literature-curated adhesome datasets were displayed. These results indicate a higher abundance of adhesome dataset proteins in the VEGF-treated dataset, although with a lower overall adhesome protein proportion. This coverage was of a similar scale to that of the HUVEC IAC dataset generated in chapter 3 and of other mass spectrometry IAC datasets, which display a range, and is dependent on the conditions in which IACs were observed (Horton et al. 2015)(chapter 3, section 3.4.3). Overall this dataset appears to be representative of the HUVEC adhesion complex validating its use for further analysis and studies.

Surprisingly, the majority of proteins identified (847, 99%; figure 4.17), including all proteins identified from the consensus adhesome (figure 4.18), changed in abundance by less than two-fold upon VEGF treatment. In total, only eight proteins changed in abundance by at least two-fold (5 decreased, 3 increased; figure 4.17, table 4.3). None of these changing proteins were consensus adhesome or LCA proteins (figure 4.18b & c), and only three were meta adhesome proteins (figure 4.18a). Furthermore, only two of the proteins that changed greater than two-fold upon VEGF treatment were statistically significant (p-value ≤0.05; table 4.3). These analyses decrease confidence that these proteins were altered in abundance following VEGF treatment and suggest that HUVEC IAC protein composition is largely unaffected by VEGF treatment.

As comparison of this protein data with phosphoproteomic peptide data is to be performed, peptide analysis of this proteomic data was also performed (supplementary table 4.2; appendix). In the IAC proteomic dataset, a total of 6153 peptides were identified under the selected criteria (section 2.12.2.2) of which 251 (4.1%) changed greater than two-fold upon VEGF treatment. Of

these 76 (1.2% of the total identified peptides) were significant changes (p-value ≤0.05, supplementary table 4.2; appendix). These analyses confirm that in in addition to the minimal changes observed in protein level in IACs upon VEGF treatment, individual peptide levels remain largely stable.

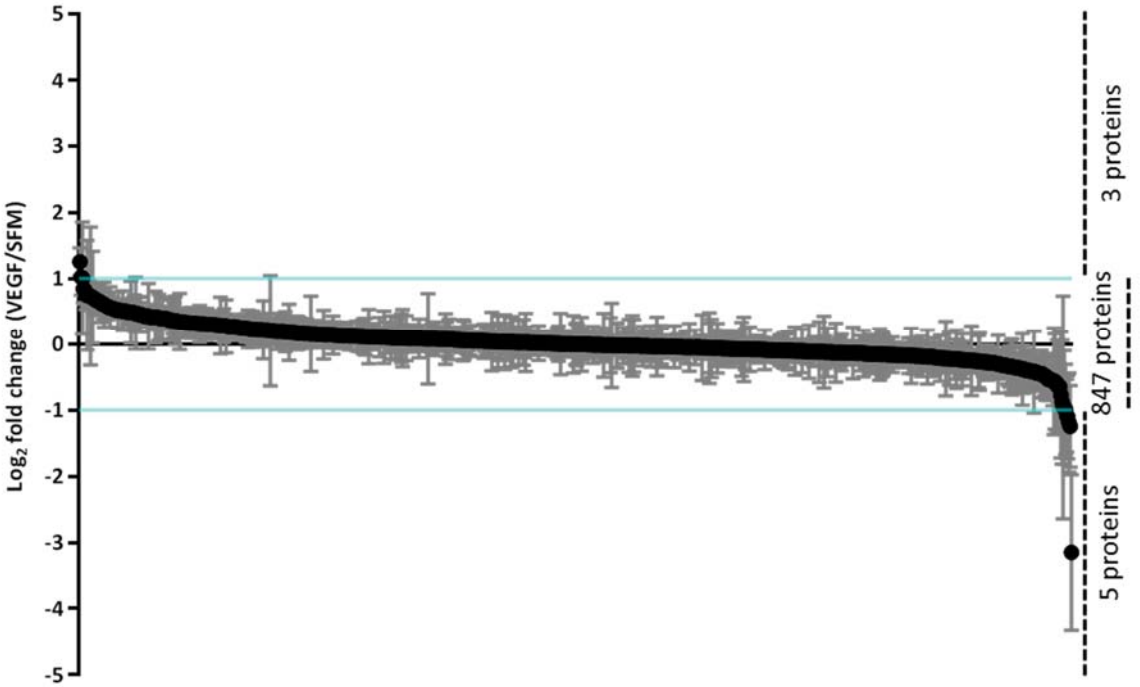

Figure 4.17. Quantification of mass spectrometry-based proteomic analysis of isolated integrin adhesion complex samples from HUVECs treated with SFM or VEGF. Isolated IACs were prepared as described in figure 4.16, subjected to MS-based proteomic analysis and quantified using Progenesis QI. A total of 855 proteins were identified and quantified with least two unique peptides per protein. Ratios of normalised ion intensity values $\log_2$ fold change (VEGF/SFM) were calculated for each protein in each replicate experiment. Graph shows mean ± SEM, n = 4. Blue lines represent a 2-fold change. The numbers of proteins within this 2-fold change is also indicated.

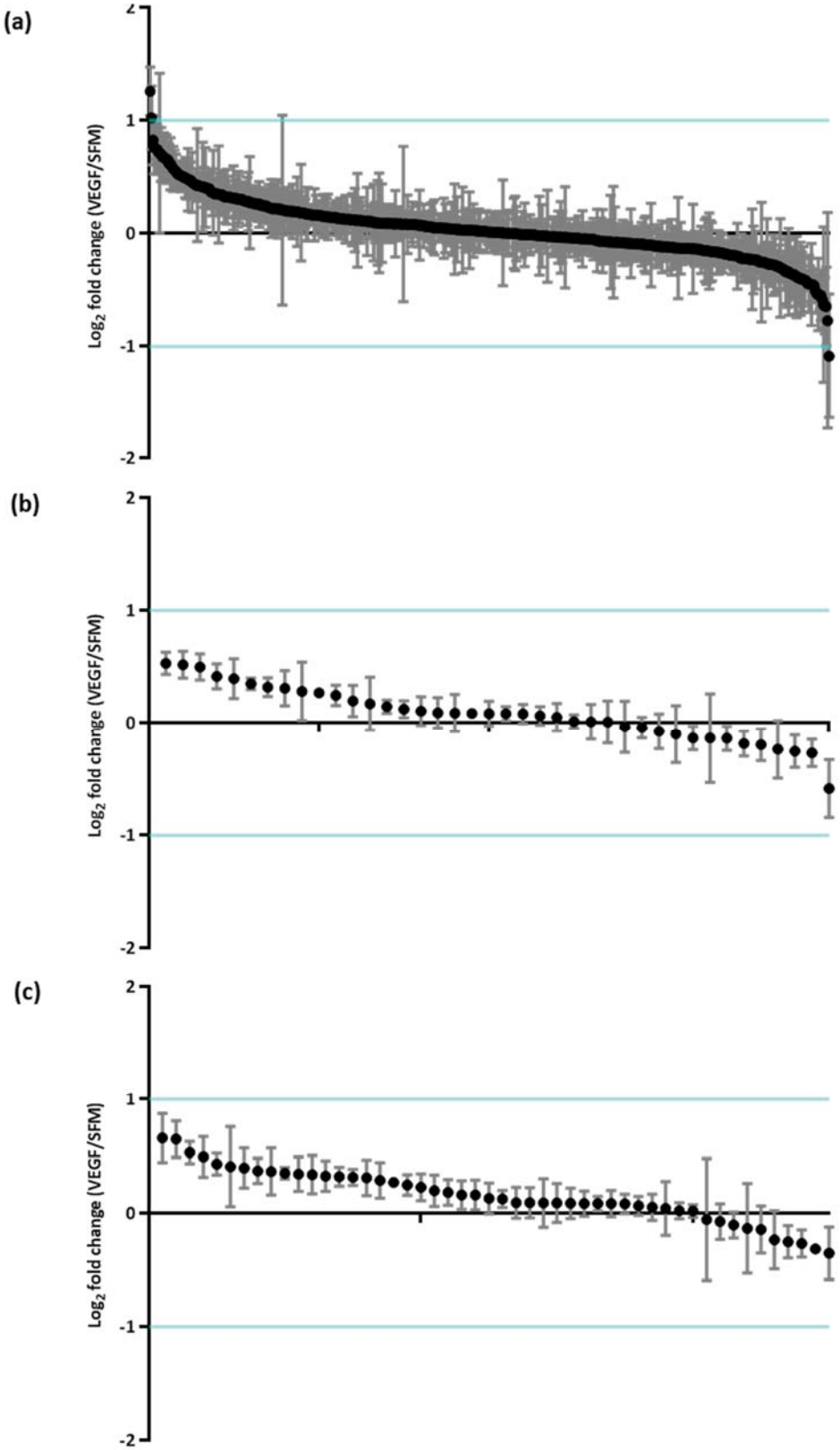

Figure 4.18. Quantification of adhesome dataset proteins identified from mass spectrometry-based proteomic analysis of isolated integrin adhesion complex samples from HUVECs treated with SFM or VEGF. Isolated IACs were prepared as described in figure 4.16, subjected to MS-based proteomic analysis and quantified using Progenesis QI. A total of 855 proteins were identified and quantified with least 2 unique peptides per protein. Ratios of normalised intensity values Log_2 fold change (VEGF/SFM) were calculated for each protein in each replicate experiment. Graph shows mean ± SEM, n = 4. Blue lines represent a 2-fold change. (a) meta adhesome proteins identified, (b) consensus adhesome proteins identified, (c) literature-curated adhesome proteins identified.

Table 4.2. Number of proteins and/or phosphopeptides belonging to adhesome datasets (meta, consensus and literature-curated) identified in mass spectrometry based proteomic datasets.
(a) Isolated IAC proteomic dataset generated in chapter 3, (b) VEGF treated isolated integrin adhesion complex (IAC) proteomic dataset (section 4.4.2), (c) VEGF treated isolated IAC phosphoproteomic dataset (section 4.4.3), (d) VEGF treated total cell lysate phosphoproteomic dataset (section 4.4.4). LCA: literature-curated adhesome.

(a) Proteomic IAC dataset

	Number of proteins (total 297)	% of HUVEC dataset	% of adhesome dataset
Meta	252	84.8	10.4
Consensus	37	12.5	61.7
LCA	34	11.4	14.7

(b) Proteomic VEGF IAC dataset

	Number of proteins (total 855)	% of HUVEC dataset	% of adhesome dataset
Meta	507	59.3	21.0
Consensus	40	4.7	66.7
LCA	50	5.8	21.6

(c) Phosphoproteomic VEGF IAC dataset

	Number of phosphopeptides (total 211)	% of HUVEC Dataset	Number of proteins (total 124)	% of dataset	% of adhesome dataset
Meta	161	76.3	83	66.9	3.4
Consensus	13	6.2	8	6.5	13.3
LCA	35	16.6	20	16.1	8.6

(d) Phosphoproteomic VEGF total cell lysate dataset

	Number of phosphopeptides (total 4811)	% of HUVEC dataset	Number of proteins (total 1240)	% of dataset	% of adhesome dataset
Meta	2038	42.4	379	26.7	15.7
Consensus	74	1.5	14	1.0	23.3
LCA	252	5.2	51	3.6	22.0

Table 4.3. Proteins identified by mass spectrometry-based proteomic analysis of integrin adhesion complexes isolated from HUVECs treated with SFM or VEGF with ≥two-fold change in abundance.

	Log_2 fold change (VEGF/SFM)					**Present in adhesome dataset (Yes/No)**			
Gene name	**R1**	**R2**	**R3**	**R4**	**Mean**	**Meta**	**Consensus**	**LCA**	**P-value**
MYH10	0.73	0.41	1.32	1.64	1.02	Y	N	N	0.0018
TNKS1BP1	1.66	0.66	1.32	1.39	1.26	Y	N	N	0.0084
KRT4	0.22	-3.77	-5.27	-3.77	-3.15	N	N	N	0.0900
QSOX1	-2.17	-1.06	0.66	-1.84	-1.10	N	N	N	0.1091
CLEC14A	-0.71	-1.52	0.53	-3.06	-1.19	N	N	N	0.1518
HMGB3	-0.38	-0.02	-2.43	-1.53	-1.09	Y	N	N	0.1481
S100A8	-1.21	-0.44	-0.33	-3.00	-1.25	N	N	N	0.2503
SMC1A	3.54	0.08	0.51	-0.11	1.01	N	N	N	0.5534

Isolated IAC samples were prepared as described in figure 4.16, subjected to MS-based proteomic analysis and quantification using Progenesis QI. Four biological replicates (R1, R2, R3 and R4) of complexes isolated from HUVECs treated with SFM or VEGF were prepared for proteomic analysis. Log_2 fold change values for each of the four biological replicates were calculated between SFM and VEGF conditions using normalised raw values. Proteins with a fold change greater than two are displayed. P-values were calculated from normalised abundance values between SFM and VEGF conditions using the Holm-Sidak method for multiple comparisons, with each protein analysed individually, without assuming a consistent standard deviation. Meta, consensus and literature-curated adhesome dataset presence is indicated for each protein. LCA: literature-curated adhesome.

4.4.2 Phosphoproteomic analysis of adhesion complexes isolated from HUVECs following VEGF treatment

As detailed in figure 4.16, from the 48 plates of isolated adhesion complex sample per condition, 40 plates worth of sample was taken for phosphoproteomic processing by proteolytic digestion and phosphopeptide enrichment. Although four replicates were prepared, due to loss of sample; only three replicates were taken forward for phosphoproteomic processing. Enrichment of phosphopeptides was performed using the KingFisher Flex automated protocol employing 75% Ti-IMAC magnetic and 25% TiO_2 magnetic beads, and samples analysed with an Orbitrap Elite mass spectrometer (3 hour LC gradient).

For quantification, both ion intensity analyses using Progenesis QI and spectral counting were employed. Both of these methods have benefits and drawback as a method of label-free quantification, and for their use in different data analysis methods that are to be used in this study. In addition, using in combination increases confidence in the data analysis and interpretation.

4.4.2.1 Spectral counting analyses

Under the selected criteria (peptide threshold of 95%, a protein threshold of 80% and 1 peptide minimum were used for protein identification), a total of 389 unique phosphopeptides were identified, from 206 proteins (supplementary table 4.3a-c; appendix). Each individual sample contained between 53 – 72% phosphopeptides, indicating successful phosphopeptide enrichment (table 4.4). Encouragingly, for each condition within each replicate, the %ID values were similar, although differences were observed in the total number of IDs per sample (table 4.4). Spectral count quantification data are displayed in supplementary table 4.3b (appendix). Quantification by spectral counting uses discrete data points, and low spectral count numbers can be unreliable for quantification. This analysis identified phosphopeptides with very low spectral count numbers, as displayed in supplementary table 4.3a-c (appendix). In addition, only four unique phosphopeptides (1% of total) were tyrosine phosphorylated, which is lower than would be expected for an enriched adhesion complex protein dataset of this type (~5-7% would be expected), (Robertson et al. 2015;Paul 2014;Robertson 2014). For this HUVEC dataset, although quantification by spectral count analysis may provide useful information to take forward, due to the low spectral count numbers and proportion of tyrosine phosphorylated residues in this dataset, interpretation should be completed with care.

Table 4.4. Mass spectrometry-based phosphoproteomic analysis of IACs isolated from HUVECs treated with SFM or VEGF. The total number of unique peptides, phosphopeptides, phosphoproteins, spectra identifications and spectra are displayed, as validated by Scaffold.

	SFM			VEGF		
	R1	R2	R3	R1	R2	R3
Total unique peptides	115	195	202	125	267	103
Total unique phosphopeptides	61	128	126	84	192	66
% phosphopeptides	53	66	62	67	72	64
Phosphoproteins	45	99	95	63	136	50
IDs	112	246	238	162	411	125
Spectra	5947	7298	8263	7509	10015	4073
% ID	3.4	4.8	4.4	3	5.3	4.6

4.4.2.2 Quantification by ion intensity measurement

As performed for proteomic analysis, ion intensity analysis was performed from RAW files using Progenesis QI. A total of 211 different peptides from 124 proteins were identified using the selected criteria (section 2.12). In total, 161 phosphopeptides belonged to meta adhesome proteins (76% of dataset, table 4.2c), 35 phosphopeptides belonged to LCA proteins (17% of dataset, table 4.2c) and 13 peptides belonged to consensus adhesome proteins (6.2% of dataset, table 4.2c) (Geiger and Zaidel-Bar 2012;Horton et al. 2015). For the meta, literature-curated and consensus adhesome, these phosphopeptides were assigned to eight, 20 and eight proteins respectively. The number of proteins was lower than in other IAC datasets generated during this project; however, the proportion of adhesome components was high in relation to other datasets (table 4.2), indicating that the phosphopeptides identified can be assumed to be true adhesome components.

Overall, 38 (18%) phosphopeptides changed in abundance greater than two-fold upon VEGF treatment (21 increased and 17 decreased; figure 4.19, table 4.5). This included 29 meta, four consensus and four literature-curated adhesome proteins (table 4.5). Of these changes upon VEGF treatment, six were statistically significant ($p<0.05$), all of which were increases (table 4.5). These analyses suggest that the abundance of a proportion of phosphopeptides identified in HUVEC IACs may be altered upon VEGF treatment, although further analyses need to be done to confirm this.

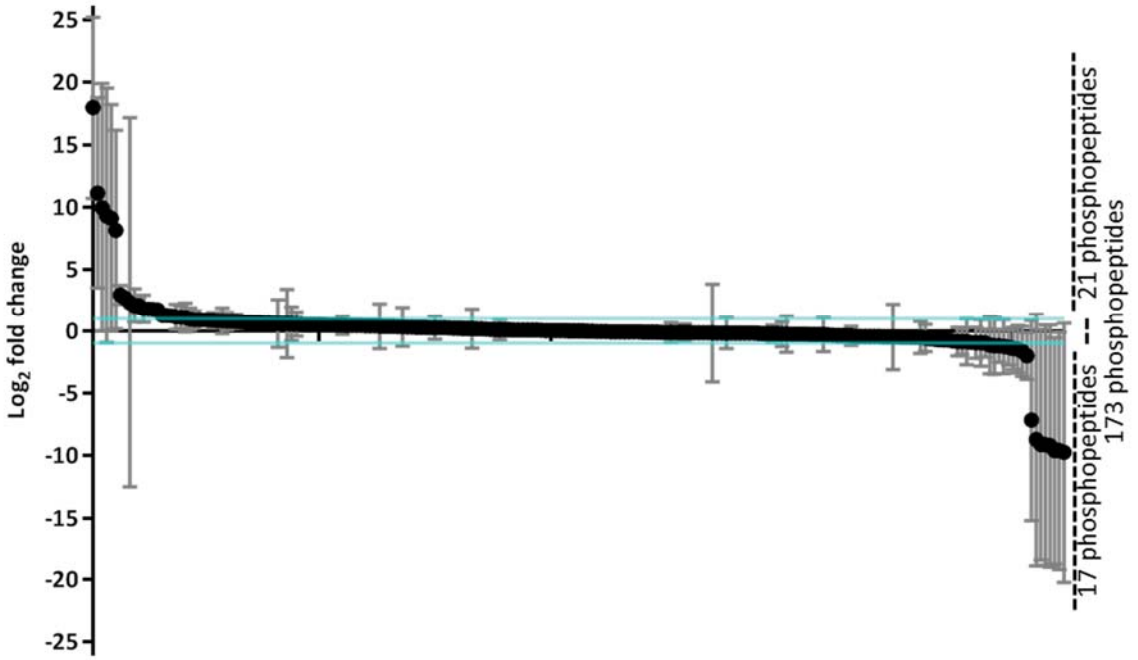

Figure 4.19. Quantification of mass spectrometry-based phosphoproteomic analysis of isolated integrin adhesion complex samples from HUVECs treated with SFM or VEGF. Isolated IACs were prepared as described in figure 4.16, subjected to MS-based phosphoproteomic analysis and quantification using Progenesis QI. A total of 211 phosphopeptides were identified and quantified. Ratios of normalised intensity values $\log_2$ fold change (VEGF/SFM) were calculated for each phosphopeptide identified in each replicate experiment. Graph shows mean ± SEM, n = 3. Blue lines represent a 2-fold change. The numbers of phosphopeptides within this 2-fold change are also indicated.

Table 4.5. Phosphopeptides identified by mass spectrometry-based phosphoproteomic analysis of integrin adhesion complexes isolated from HUVECs treated with SFM or VEGF with ≥two-fold change in abundance.

Gene name	Peptide sequence	Modification(s)	Log_2 fold change (VEGF/SFM)				Present in adhesome dataset (Yes/No)			P-value
			R1	R2	R3	Mean	Meta	Consensus	LCA	
FLNC	LGSFGSITR	[3] Phospho (ST)	1.19	1.26	1.23	1.23	Y	Y	N	0.0063
AHNAK	FGTFGGLGSK	[3] Phospho (ST)	26.35	2.18	4.87	11.13	Y	N	N	0.2977
AHNAK	ISAPNVDFNLEGPK	[2] Phospho (ST)	0.00	1.72	-23.27	-7.18	Y	N	N	0.5754
YTHDC1	GISPIVFDR	[3] Phospho (ST)	-0.24	0.88	-5.61	-1.66	N	N	N	0.6807
PARVA	SPTPKSPPSR	[6] Phospho (ST)	29.88	0.00	0.00	9.96	Y	Y	Y	0.3739
SPTBN1	RPPSPEPSTK	[4] Phospho (ST)	-0.23	24.14	0.56	8.15	Y	N	N	0.9304
SPTBN1	RPPSPEPSTK	[4] Phospho (ST)	1.32	29.63	-3.07	9.29	Y	N	N	0.4304
KRT5	ISISTSGGSFR	[4] Phospho (ST)	0.01	0.51	-4.83	-1.44	Y	N	N	0.4943
AHNAK	ASLGSLEGEAEAEASSPK	[5] Phospho (ST)	0.60	0.34	-28.73	-9.26	Y	N	N	0.6719
AHNAK	FKAEAPLPSPK	[9] Phospho (ST)	2.78	0.85	1.60	1.75	Y	N	N	0.0108
TJP2	KVQVAALQASPPLDQDDR	[10] Phospho (ST)	2.75	1.26	-0.63	1.13	Y	N	N	0.2009
USP6NL	IEVLPVDTGAGGYSGNSGSPK	[19] Phospho (ST)	-0.52	0.23	-5.77	-2.02	Y	N	N	0.4820
ARHGAP22	TSSLDGAAVAVLSR	[3] Phospho (ST)	-25.26	25.68	6.45	2.29	Y	N	N	0.3727
CCNYL1	SFSADNFIGIQR	[3] Phospho (ST)	1.61	1.75	0.44	1.27	N	N	N	0.0105
PPP1R12A	TGSYGALAEITASK	[3] Phospho (ST)	0.00	0.97	-28.53	-9.19	Y	N	N	0.6731
KRT13	MIGFPSSAGSVSPR	[12] Phospho (ST)	0.00	0.00	27.31	9.10	N	N	N	0.3739
MAP4	DGVLTLANNVTPAK	[11] Phospho (ST)	-1.26	0.17	-27.81	-9.63	Y	N	N	0.4705
CTNNA1	TPEELDDSDFETEDFDVR	[1] Phospho (ST)	0.00	3.48	-0.17	1.10	Y	N	N	0.4508
C15orf52	SPPTQVAISSDSAR	[1] Phospho (ST)	0.20	0.01	-4.18	-1.33	N	N	N	0.5686
LUZP1	TQSSLTVSEVLTR	[3] Phospho (ST)	0.82	0.40	-30.62	-9.80	Y	N	N	0.8816
JUP	ALMGSPQLVAAVVR	[5] Phospho (ST)	1.69	1.06	-29.01	-8.75	N	N	N	0.6606
KRI1	AFVEDSEDEDGAGEGGSSLLQK	[6] Phospho (ST)	1.16	0.65	-5.59	-1.26	N	N	N	0.9837
AHNAK	ISMQDVDLSLGSPK	[12] Phospho (ST)	2.51	3.63	1.85	2.66	Y	N	N	0.0850
AHNAK	ISMQDVDLSLGSPK	[12] Phospho (ST)	4.48	2.16	2.16	2.93	Y	N	N	0.0136
PHLDB1	LSTAITLLPLEEGR	[2] Phospho (ST)	24.73	3.48	25.74	17.98	Y	N	N	0.1477
G3BP1	YQDEVFGGFVTEPQEESEEEVEEPEER	[17] Phospho (ST)	4.66	1.49	0.06	2.07	Y	N	N	0.4239
VIM	ISLPLPNFSSLNLR	[10] Phospho (ST)	1.55	1.94	0.29	1.26	Y	N	Y	0.0775
CDK11B	DLLSDLQDISDSER	[12] Phospho (ST)	2.99	2.84	-0.44	1.80	N	N	N	0.3365
KANK1	SYSAGNASQLEQLSR	[3] Phospho (ST)	0.37	-0.18	-3.86	-1.22	Y	N	N	0.6460
AHNAK	LPSGSGAASPTGSAVDIR	[5] Phospho (ST)	1.35	1.54	2.26	1.72	Y	N	N	0.0191
AHNAK	EFSGPSTPTGTLEFEGGEVSLEGGK	[11] Phospho (ST)	2.33	1.69	1.32	1.78	Y	N	N	0.0528
ZAK	VSQSALNPHQSPDFK	[11] Phospho (ST)	-0.42	0.22	-28.73	-9.64	N	N	N	0.6279
KRT1	SGGGFSSGSAGIINYQR	[9] Phospho (ST)	1.48	0.64	-5.74	-1.21	Y	N	N	0.4537
AHNAK	LPSGSGAASPTGSAVDIR	[3] Phospho (ST) [9] Phospho (ST)	2.83	2.51	0.79	2.04	Y	N	N	0.0328
KCTD12	SPSGGAAGPLLTPSQSLDGSR	[3] Phospho (ST)	0.02	0.18	-27.66	-9.15	N	N	N	0.6949
ITGA5	LLESSLSSSEGEEPVEYK	[7] Phospho (ST)	0.42	0.48	-5.32	-1.47	Y	Y	Y	0.7544
ITGA5	LLESSLSSSEGEEPVEYK	[8] Phospho (ST)	0.08	0.14	3.19	1.14	Y	Y	Y	0.3721
HNRNPU	LQAALDDEEAGGRPAMEPGNGSLDLGG DSAGR	[22] Phospho (ST)	1.29	1.04	-5.79	-1.15	Y	N	N	0.7093

Details: Isolated IACs were prepared as described in figure 4.16, subjected to MS-based phosphoproteomic analysis and quantification using Progenesis QI. Three biological replicates (R1, R2, R3) of complexes isolated from HUVECs treated with SFM or VEGF were prepared for proteomic analysis. The identified peptide sequence is displayed. Modified peptide residue is indicated in the modification column; the [#] number represents the modified peptide from the N terminus of the identified peptide, Phospho (ST) represents a serine or threonine modification. Log_2 fold change values for each of the three biological replicates were calculated between SFM and VEGF conditions using normalised raw values. Proteins with a fold change greater than two are displayed. P-values were calculated from normalised abundance values between SFM and VEGF conditions, with each protein analysed individually, without assuming a consistent standard deviation. Meta, consensus and literature-curated adhesome dataset presence is indicated for each protein. LCA: literature-curated adhesome.

4.4.3 Phosphoproteomic analysis of HUVEC total cell lysate samples following VEGF treatment

As detailed in figure 4.16, in addition to isolated IACs following VEGF treatment, HUVEC TCL samples were also prepared for phosphoproteomic processing. Four replicates were prepared, and were taken forward for processing by proteolytic digestion and phosphopeptide enrichment. Enrichment of phosphopeptides was performed using the KingFisher Flex automated protocol employing 75% Ti-IMAC magnetic and 25% TiO_2 magnetic beads, and samples analysed with an Orbitrap Elite mass spectrometer (3 hour LC gradient).

As performed previously, both ion intensity analyses using Progenesis QI and spectral counting were employed for quantification.

4.4.3.1 Spectral counting analyses

Under the selected criteria (peptide threshold of 95%, a protein threshold of 80% and 1 peptide minimum were used for protein identification), a total of 3174 unique phosphopeptides were identified, from 1568 proteins (supplementary table 4.5a-c; appendix). Each individual sample contained between 88 – 93% phosphopeptides, indicating successful phosphopeptide enrichment (table 4.6). For each condition within each replicate, the percentage ID values and total number of IDs per sample were similar (table 4.6). This analysis identified phosphopeptides with generally higher spectral counts than for the IAC data (supplementary table 4.5a-c; appendix) thereby increasing the reliability of quantification by spectral counting for this dataset. Spectral count quantification data are displayed in supplementary table 4.5 (appendix). Of note, ERK1/2 (MAPK1/3), which is activated in response to VEGF, had increased phosphorylation in all replicates with an overall 29-fold increase in MAPK1 and 5.6-fold increase in MAPK3 (supplementary table 4.5b; appendix). This indicates that VEGF signalling was active in all samples, and that spectral counting may be a valid method of quantification for this sample set. This analysis will be used for future reference and analysis purposes; however, ion intensity analysis was selected as the main method of quantification.

Table 4.6. Mass spectrometry-based phosphoproteomic analysis of HUVEC total cell lysate samples treated with SFM or VEGF. The total number of unique peptides, phosphopeptides, phosphoproteins, spectra identifications and spectra are displayed, as validated by Scaffold.

	SFM				VEGF			
	R1	**R2**	**R3**	**R4**	**R1**	**R2**	**R3**	**R4**
Total unique peptides	2117	2004	1889	2072	2286	2004	2083	1757
Total unique phosphopeptides	1933	1852	1735	1868	2130	1870	1916	1554
% phosphopeptides	91	92	92	90	93	93	92	88
Phosphoproteins	1156	1072	1066	1108	1242	1084	1136	962
IDs	6714	6282	5822	6436	7053	6442	6326	5432
Spectra	19290	18531	18693	18883	20020	19340	18783	17130
% ID	35	34	31	34	35	33	34	32

4.4.3.2 Quantification by ion intensity measurement

As performed for proteomic and phosphoproteomic analysis of isolated IACs, ion intensity analysis was performed from RAW files using Progenesis QI. A total of 3504 unique phosphopeptides were identified from the 4811 different peptide ions that could be used for quantification. These peptides were assigned to 1420 unique proteins, although not all phosphopeptides could be assigned to a protein. In total, 2038 phosphopeptides belonged to meta adhesome proteins (42% of dataset), 252 phosphopeptides belonged to LCA proteins (5.2% of dataset) and 74 peptides belonged to consensus adhesome proteins (1.5% of dataset) (Horton et al. 2015;Geiger and Zaidel-Bar 2012). For the meta, literature-curated and consensus adhesome, these phosphopeptides were assigned to 379, 51 and 14 proteins respectively. The percentage of meta, consensus and literature-curated adhesome proteins in the HUVEC IAC dataset are displayed in table 4.2d. As expected for a lysate sample, the number of proteins identified was increased compared to IAC datasets generated during this project (table 4.2), and the proportion of adhesome components identified was lower. However, there was an increase in the total number of adhesome proteins, and therefore coverage of adhesome datasets (table 4.2). Due to the high level of adhesome dataset proteins indented in this dataset, it can be filtered accordingly and used to investigate how the abundance of known adhesion complex proteins may be altered upon VEGF treatment in HUVECs.

From the 3504 phosphopeptides identified in this TCL sample, 1623 (34%) changed in abundance greater than two-fold upon VEGF treatment (862 decreased, 761 increased; figure 4.20, supplementary table 4.6 [appendix]). This included 675 meta, 21 consensus and 76 literature-curated adhesome phosphopeptides (table 4.2d, figure 4.21), equalling 683 adhesome phosphopeptides in total when taking into account overlap between datasets. Of the phosphopeptides that changed greater than two-fold, 38 were determined to be statistically significant, 29 of which increased (supplementary table 4.6; appendix). In addition, 20 out of these

38 belonged to meta and/or literature-curated adhesome proteins. As a further, more stringent data filter, phosphopeptides that increased or decreased in a minimum of three replicates were calculated (supplementary table 4.6; appendix). A total of 924 (516 increasing and 408 decreasing) phosphopeptides changed greater than two-fold (increase or decrease) in at least three out of four replicates (supplementary table 4.6; appendix).

Of the 4811 peptide ions identified, 1.2% (57) were tyrosine phosphorylated peptides, and 99% (4784) threonine or serine phosphorylated peptides. Of the 2038 phosphopeptides identified in the meta adhesome 1.3% (27) were tyrosine phosphorylated. This proportion increased to 4.4% (11 phosphopeptides) when considering the 252 LCA phosphopeptides, as would be expected as adhesion complexes have a relatively high level of tyrosine phosphorylation (Zamir et al. 1999;Robertson et al. 2015). Of the 57 tyrosine phosphorylated phosphopeptides, 21 (37%) changed greater than two-fold. Of these, 15 increased and six decreased, indicating that when compared to overall phosphorylation, which appears to decrease upon VEGF treatment (figure 4.19, 4.20), the proportion of tyrosine phosphorylation increases upon VEGF treatment (figure 4.22).

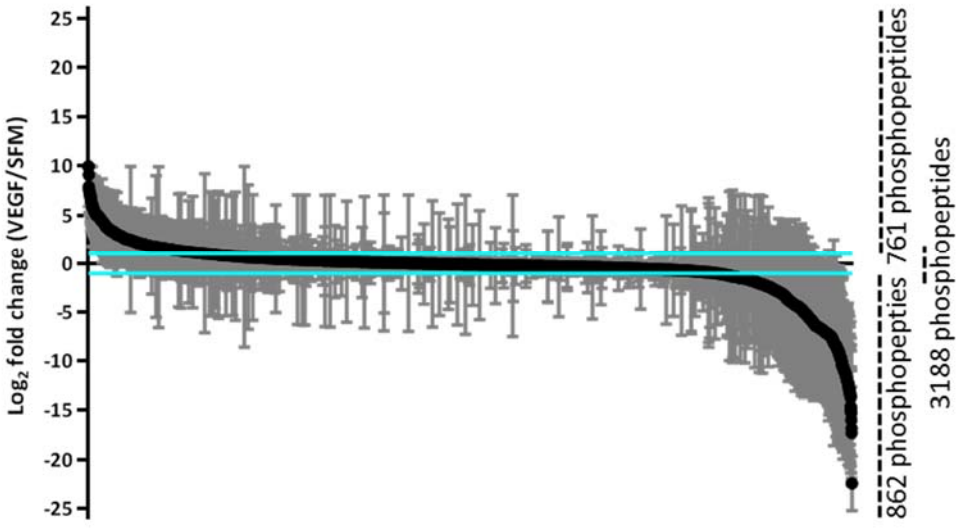

Figure 4.20. Quantification of mass spectrometry-based proteomic analysis of SFM or VEGF treated HUVEC total cell lysates. Total cell lysates were prepared as described in figure 4.16, subjected to MS-based phosphoproteomic analysis and quantification using Progenesis QI. A total of 4811 features were identified and quantified. Ratios of normalised intensity values log_2 fold change (VEGF/SFM) were calculated for each phosphopeptide in each replicate experiment. Graph shows mean ± SEM, n = 4. Blue lines represent a 2-fold change. The number of proteins within this 2-fold change is also indicated.

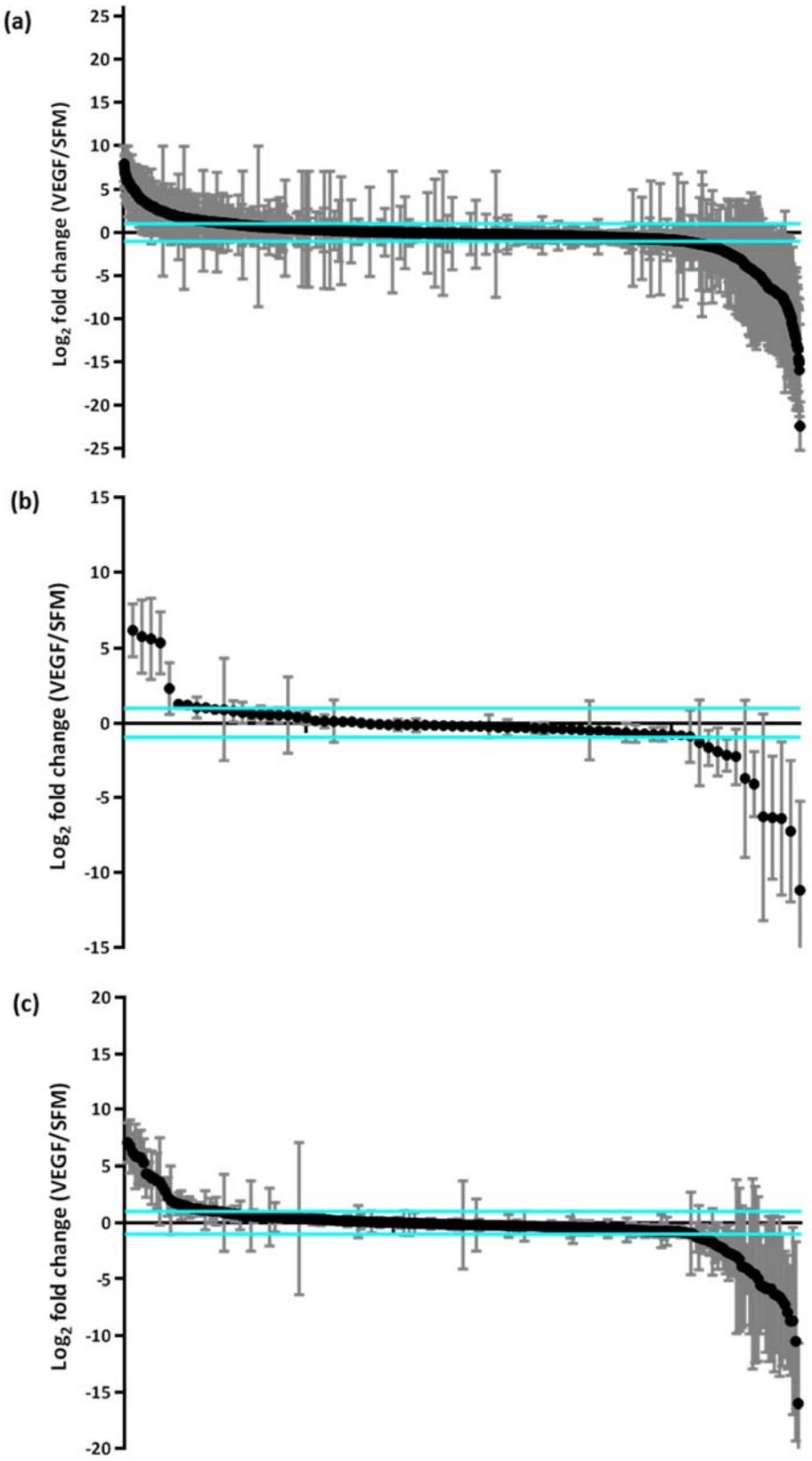

Figure 4.21. Quantification of adhesome dataset proteins from mass spectrometry-based proteomic analysis of SFM or VEGF treated HUVEC total cell lysates. Total cell lysates were prepared as described in figure 4.16, subjected to MS-based phosphoproteomic analysis and quantification using Progenesis QI. A total of 4811 features were identified and quantified. Ratios of normalised intensity values log_2 fold change (VEGF/SFM) were calculated for each phosphopeptide in each replicate experiment. Graph shows mean ± SEM, n = 4. Blue lines represent a 2-fold change. (a) meta adhesome proteins identified, (b) consensus adhesome proteins identified, (c) literature-curated proteins identified.

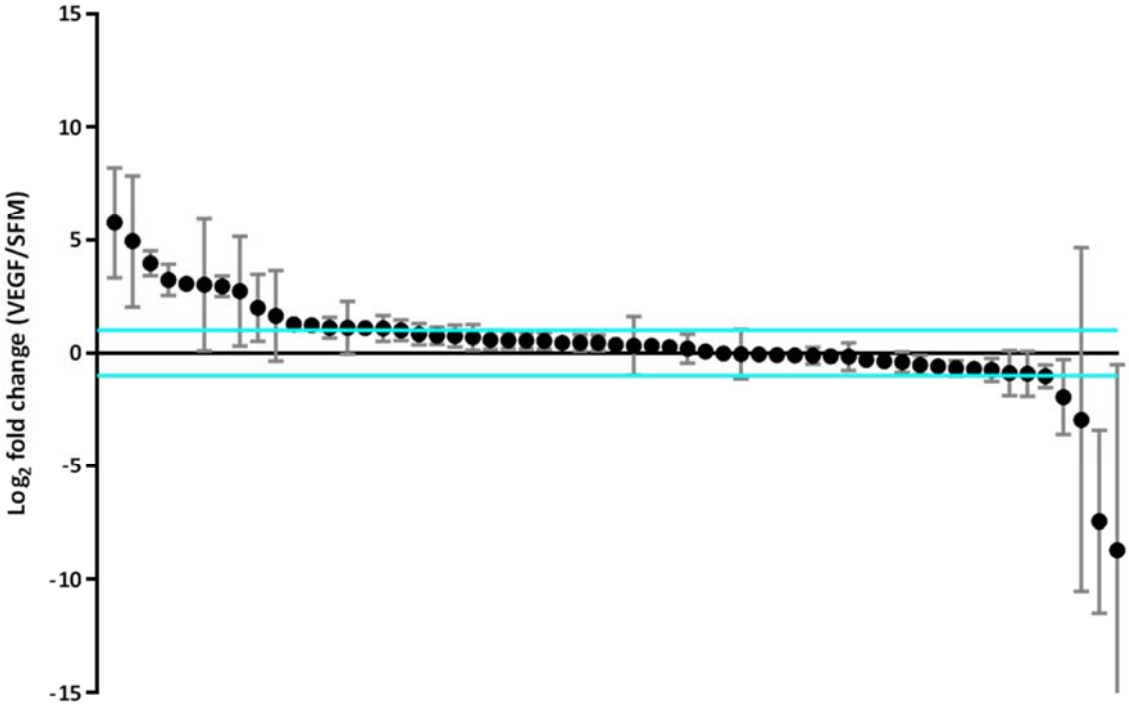

Figure 4.22. Quantification of identified tyrosine phosphorylated peptides from mass spectrometry-based proteomic analysis of SFM or VEGF treated HUVEC total cell lysates. Total cell lysates were prepared as described in figure 4.15, subjected to MS-based proteomic analysis and quantification using Progenesis LC-MS. A total of 4811 features were identified and quantified. Ratios of normalised intensity values log_2 (VEGF/SFM) were calculated for each phosphopeptide in each replicate experiment. Graph shows 57 identified phosphopeptide ions, mean ± SEM, n = 4. Blue lines represent proteins with ≤ two-fold change between conditions.

4.5 Chapter 4 summary

The main aim of this chapter was to perform a global, unbiased analysis of changes in both protein composition and phosphorylation within adhesion complexes upon VEGF treatment. First, optimal conditions for VEGF treatment of HUVECs were determined. Western blot analysis suggested that the optimal phosphorylation response, when considering both ERK as a marker of VEGF signalling and IAC proteins, occurred when HUVECs had been serum starved, and after 7.5 minutes of VEGF treatment. To study the phosphorylation status of proteins within EC adhesion complexes, a phosphoproteomic workflow was required. For establishment of the phosphoproteomic workflow, assessment was made of the optimal conditions to enrich IAC protein phosphopeptides from TCL and isolated IAC samples at multiple stages. This included starting sample amount, choice of phosphopeptide enrichment beads, use of an automated system, mass spectrometer and associated LC run time. One surprising observation was that when using HUVEC TCL for optimisation purposes, a high proportion of IAC proteins were detected. This chance observation meant that, in addition to phosphoproteomic analysis of IAC samples following VEGF treatment, TCL samples could be used to investigate VEGF-induced phosphorylation events in IACs. Following these

optimisation steps, three final proteomic datasets were produced. VEGF-treated HUVEC IAC samples by (1) proteomic analysis and (2) phosphoproteomic analysis and (3) VEGF-treated TCL samples by phosphoproteomic analysis.

For the three datasets generated, a combination of analyses was performed. For the isolated IAC proteomic dataset, quantification by ion intensity measurements suggested that HUVEC IAC protein composition is largely unaffected by VEGF treatment. For the phosphoproteomic datasets, both ion intensity and spectral counting were performed as a method of quantification. For the isolated IAC phosphoproteomic dataset, when compared to the proteomic dataset, a higher proportion of changes upon VEGF treatment were identified (18% phosphopeptide ions vs 1% proteins). For both isolated IAC datasets, a high proportion of previously identified adhesome dataset proteins were identified, confirming successful IAC isolation. For the TCL phosphoproteomic dataset, the number of previously identified adhesome proteins was increased in comparison to the IAC dataset. Of these adhesome proteins identified in the TCL dataset, a high proportion (33%) of phosphopeptides changed upon VEGF treatment. Overall phosphoproteomic analyses suggested that the abundance of a proportion of phosphopeptides identified in HUVEC IACs may be altered upon VEGF treatment. When combined with proteomic analysis, these results suggest that while adhesion complex composition remains largely unchanged during VEGF-adhesion crosstalk, changes and signalling events occur mainly through phosphorylation.

The datasets generated here hold a large amount of data, beyond the limit of discussion in this chapter. The next major challenge was to perform a comparative analysis of the three generated datasets, and use this analysis to identify potential proteins and signalling events that may contribute to VEGF-adhesion crosstalk. This data analysis would thereby highlight proteins of interest to follow up, and study in detail their involvement in EC VEGF-adhesion crosstalk.

Chapter 5: Detailed analysis and follow up of proteomic and phosphoproteomic VEGF-treated integrin adhesion complex and total cell lysate TCL datasets.

5.1 Overview

In chapter 4, using the established IAC isolation protocol combined with the proteomic and phosphoproteomic workflow optimised, three mass spectrometry based datasets were prepared: VEGF-treated HUVEC IAC samples by (1) proteomic analysis and (2) phosphoproteomic analysis and (3) VEGF-treated TCL samples by phosphoproteomic analysis. These datasets were analysed quantitatively to determine how protein and protein phosphorylation changes occur globally in HUVEC IACs upon VEGF treatment. In this chapter, a range of analyses of this data were performed to identify candidates from these datasets that may be involved in VEGF-adhesion crosstalk. First a range of protein-protein interaction networks were constructed, statistical analyses of the datasets employed, and detailed kinase prediction analysis performed. These combined analyses suggested a role for Src kinase activity in VEGF adhesion crosstalk, and led to selection of VASP, filamin-A, GIT1, paxillin, vinculin and ILK for follow-up analyses. To investigate the role of selected candidates in VEGF-induced cellular processes, western blotting was employed to investigate changes in VEGF signalling using phospho-ERK as a readout, and an assay was developed to investigate the role of these candidates on adhesion-specific, VEGF-induced HUVEC migration. In addition, live cell imaging analysis by FRAP was used to investigate VEGF-induced changes in phosphorylation within IACs. Overall, analysis of proteomic and phosphoproteomic datasets produced highlight many potential candidates that may be involved in VEGF signalling and VEGF-adhesion crosstalk, with further functional analyses suggesting a role for protein phosphorylation mediated by Src kinase.

5.2 Mass spectrometry dataset analysis: investigating VEGF-induced changes in adhesion complex proteins

To highlight potential candidates of VEGF-adhesion crosstalk, detailed analyses of the VEGF-treated datasets (proteomic and TCL/IAC phosphoproteomic) generated in chapter 4 were performed.

5.2.1 Protein-protein interaction network analysis

Initially, protein-protein interaction networks were constructed to visualise the proteins identified in each network and their reported interactions. The 855 proteins identified in the isolated IAC VEGF proteomic dataset (section 4.4.2) were displayed as a protein-protein interaction network (figure 5.1). Nodes representing detected proteins were coloured according to their VEGF-induced-fold change compared to controls, indicating that most proteins detected change less than two-fold. To allow visualisation of VEGF- and adhesion-related proteins in this network a number of filters were applied. Proteins identified in the consensus adhesome and LCA were displayed (figure 5.2); in this network, consensus adhesome-specific proteins formed their own cluster, suggesting that these adhesion associated proteins have more known interactions. In addition, although

VEGFR2 was not identified in this dataset, a network showing VEGFR2 1-hop and integrin 1-hop proteins was constructed. This resulted in a network of 42 proteins directly connected to integrins (30 proteins) or VEGFR2 (8 proteins) (figure 5.3). The network was first organised to indicate integrin and VEGFR2 1-hop proteins (figure 5.3a). Of the 42 proteins displayed in the network, all calculated fold changes were less than 1.6-fold. Only three proteins in this network changed significantly (p-value <0.05): these were filamin-A, filamin-B and myosin heavy chain 9; however, further work would need to be performed to confirm these observations. Alternatively, this network of 42 proteins was organised to show that β1-integrin was the most connected node in this network (figure 5.3b). β1-integrin was directly connected to 29/41 proteins in this network, reiterating previous observations (chapter 3) that under the conditions used in this study, IACs were predominantly β1-integrin mediated. Although other proteins in this dataset should not be disregarded, these filtered networks allow a more detailed view of the proteins, and their interactions within this isolated IAC dataset.

Phosphoproteins identified in both the phosphoproteomic isolated IAC and TCL datasets were also added to the isolated IAC proteomic network, to indicate coverage of the phosphoproteomic datasets (figure 5.4). Around a third of proteins (235 out of 689 proteins) identified in the isolated IAC proteomic dataset were identified in the IAC and/or TCL phosphoproteomic datasets. Of these 235 proteins (figure 5.4), the majority (227) were identified in the TCL phosphoproteomic dataset. Furthermore, of these 235 proteins, 61 were identified in the isolated IAC phosphoproteomic dataset, although only three of these proteins were uniquely identified in the IAC phosphoproteomic dataset. These data highlighted that, of the phosphoproteomic datasets, the TCL dataset provided the best coverage of adhesion complex proteins. However, of the 61 proteins identified in both, agreement in quantification data can provide much more confidence than in either dataset alone. Many adhesion complex proteins typically phosphorylated within adhesion complexes were identified, such as FAK (PTK2) and paxillin (PXN). However, only one integrin subunit (α5) was identified in the phosphoproteomic dataset (identified in both IAC and TCL), compared to five different subunits in the IAC proteomic data, most of which have been identified previously in IAC phosphoproteomic analysis (Robertson et al. 2015). These data highlight that although there is abundant phosphorylation coverage of identified IAC proteins in these combined datasets, there may be many proteins present in prepared samples that are unidentified by the phosphoproteomic methods employed.

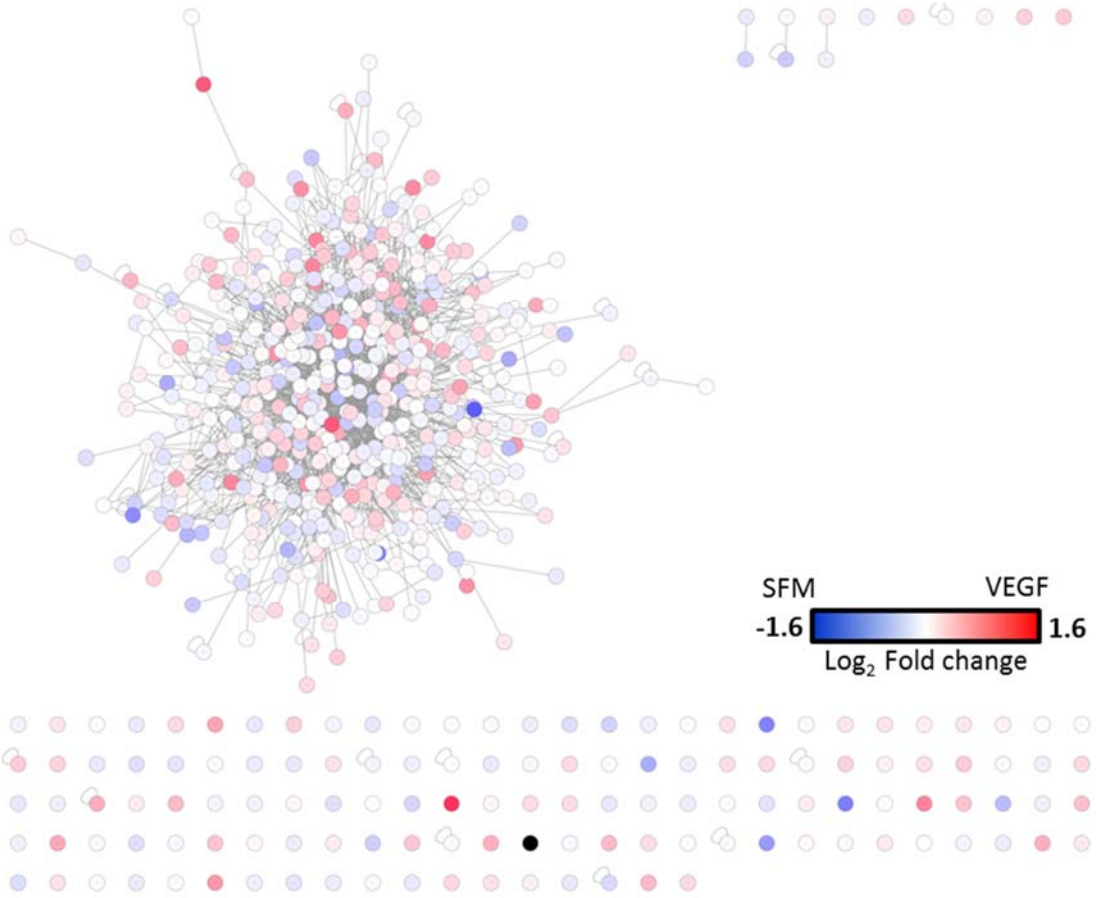

Figure 5.1. Network analysis of VEGF-induced changes in HUVEC adhesion complex protein composition, identified by mass spectrometry-based proteomic analysis of isolated HUVEC integrin adhesion complex samples. Proteins identified in the isolated IAC proteomic dataset were mapped onto a known human protein-protein interaction network. In total, out of 855 proteins, 689 were mapped onto the network and shaded according to their fold change (Log_2 VEGF/SFM), log_2 range -1.6 to 1.6 (3-fold change), black nodes have a fold change outside of the 3-fold colour range. The network comprises 1890 interactions (grey lines; edges) between the 689 proteins (circles; nodes).

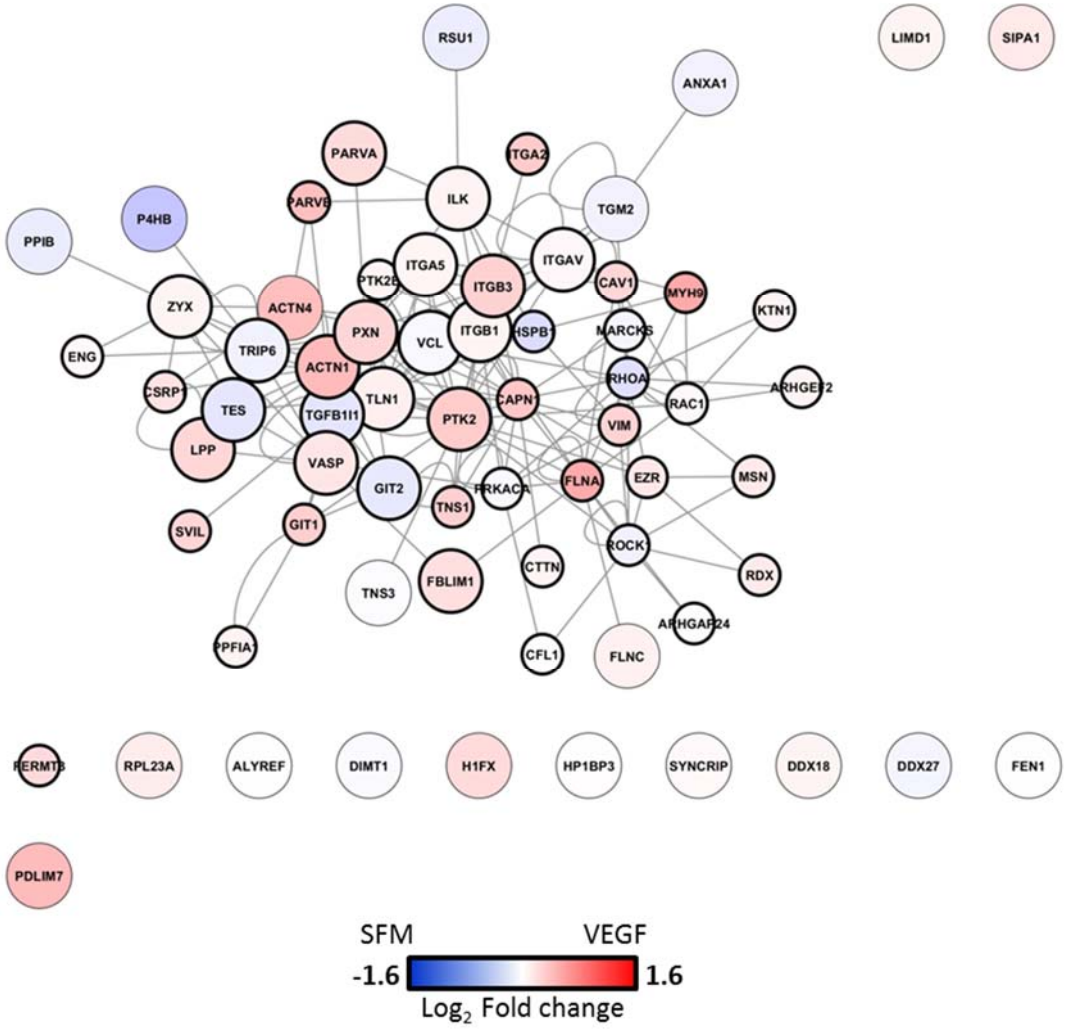

Figure 5.2. Network analysis of VEGF-induced changes in literature-curated adhesome and consensus adhesome proteins identified by mass spectrometry-based proteomic analysis of isolated HUVEC integrin adhesion complex samples. Proteins identified in the isolated IAC proteomic dataset were mapped onto a known human protein-protein interaction network. In total, out of 855 proteins, 689 were mapped onto the network (figure 5.1), 68 of which belonged to the literature-curated adhesome and/or consensus adhesome and are shown in this network. Nodes are shaded according to their fold change (Log_2 VEGF/SFM), log_2 range -1.6 to 1.6 (3-fold change). The network comprises 166 interactions (grey lines; edges) between the 68 proteins (circles; nodes). Consensus adhesome proteins are represented by larger nodes and literature-curated adhesome proteins are represented with black node border. Nodes are labelled with gene names for clarity.

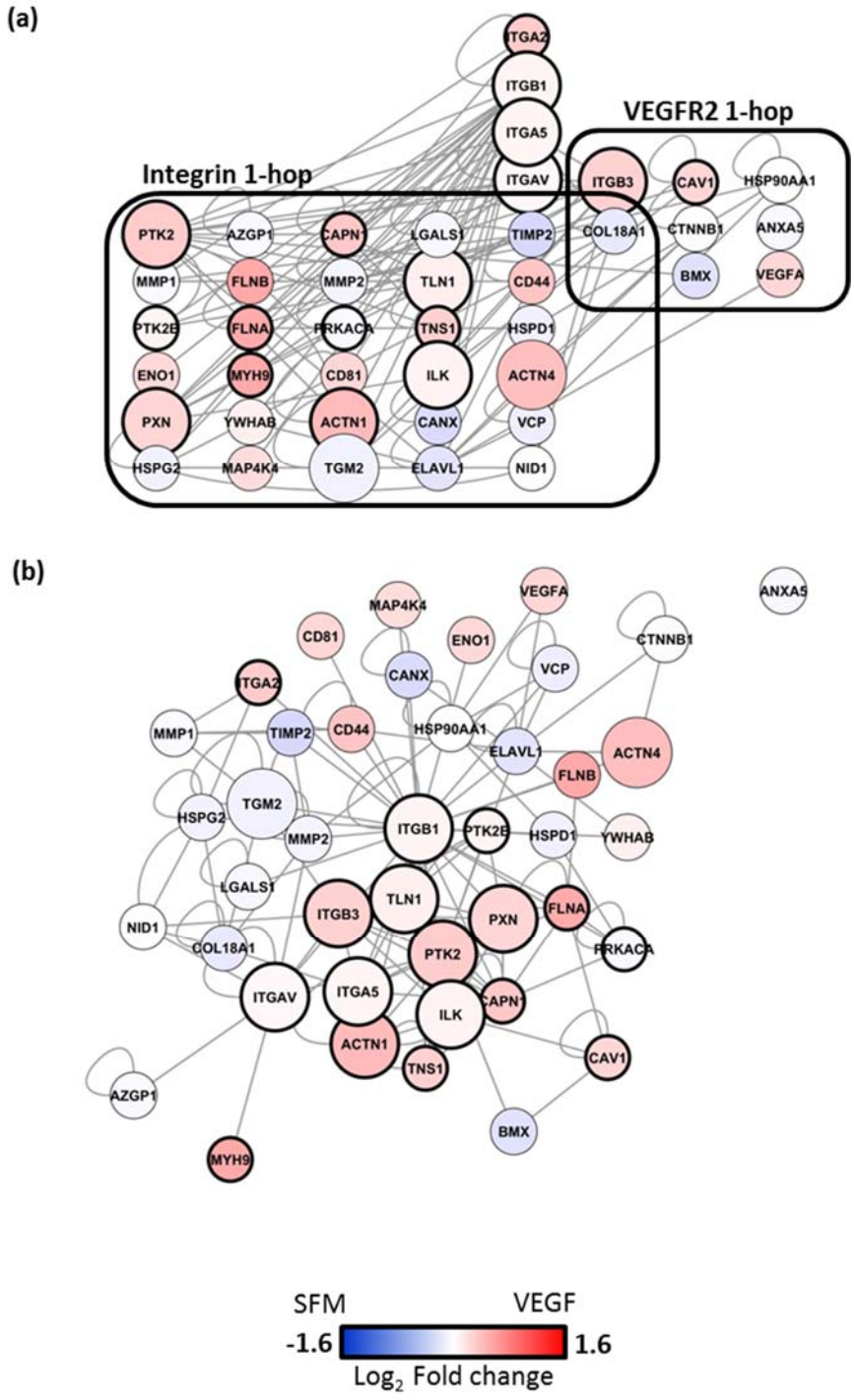

Figure 5.3. Network analysis of VEGF-induced changes in integrin 1-hop and VEGFR2 1-hop proteins identified by mass spectrometry-based proteomic analysis of isolated HUVEC integrin adhesion complex samples. Proteins identified in the isolated IAC proteomic dataset were mapped onto a known human protein-protein interaction network. In total, out of 855 proteins, 689 were mapped onto the network (figure 5.1), 42 of which were integrins, integrin 1-hop and/or VEGFR2 1-hop proteins. Nodes are shaded according to their fold change (Log_2 VEGF/SFM), log_2 range -1.6 to 1.6 (3-fold change). The network comprises 121 interactions (grey lines; edges) between the 42 proteins (circles; nodes). Consensus adhesome proteins are represented by larger nodes, literature-curated adhesome proteins are represented with black node border. Nodes are labelled with gene names for clarity. (a) Nodes are organised according to their 1-hop binding partners (b) Perfuse force directed layout applied.

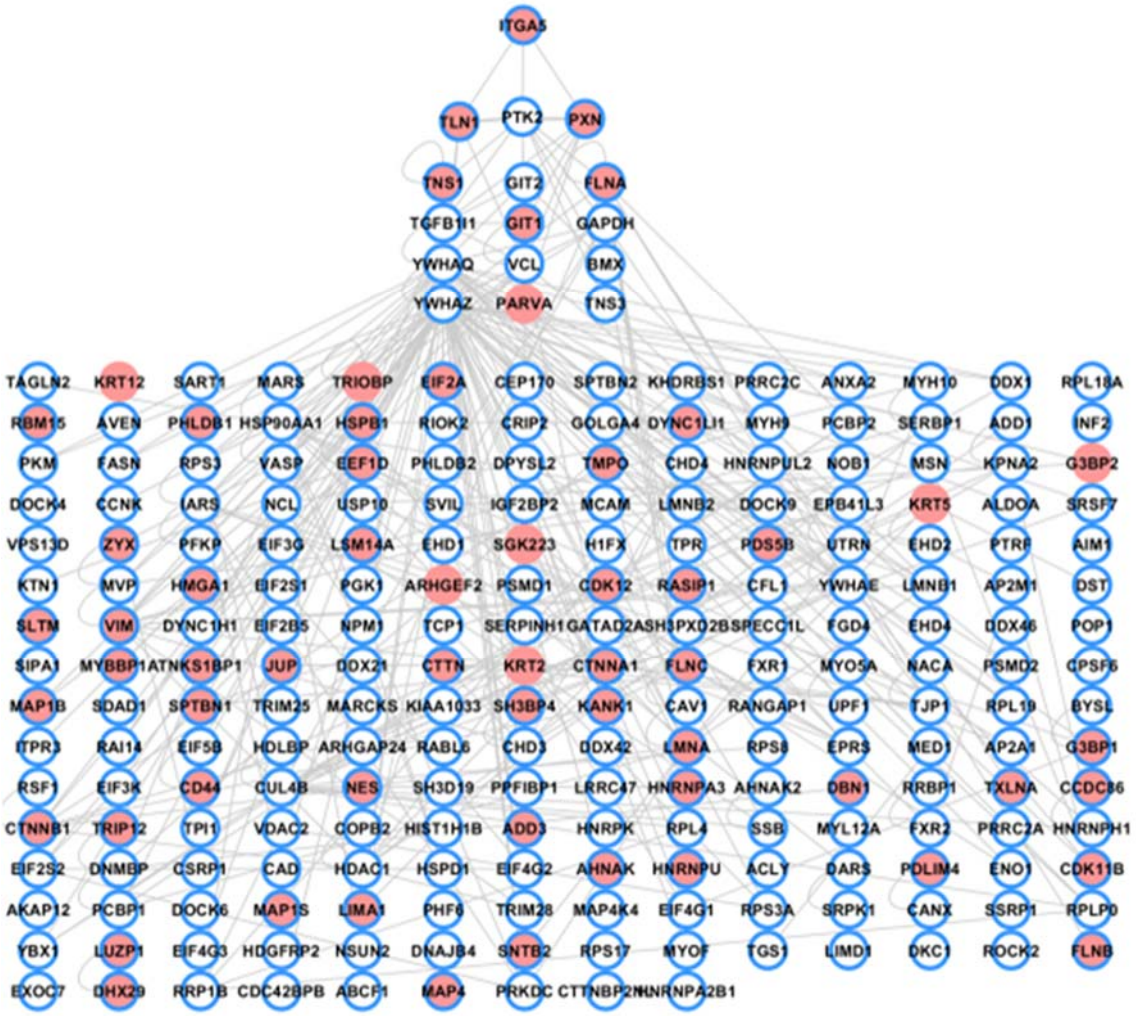

Figure 5.4. Network analysis of proteins identified by mass spectrometry-based proteomic and phosphoproteomic analysis of isolated HUVEC integrin adhesion complex (IAC) samples, and phosphoproteomic analysis of HUVEC total cell lysate (TCL) samples. The proteomic and phosphoproteomic (IAC and TCL) datasets were combined and mapped onto a known human protein-protein interaction network, and filtered to show all 235 phosphorylated proteins identified in the phosphoproteomic datasets that were also identified in the IAC proteomic dataset. The network comprises 335 interactions (grey lines; edges) between the 235 proteins (circles; nodes). Pink nodes represent phosphoproteins identified in the IAC phosphoproteomic dataset and a blue node border represents phosphoproteins identified in the TCL phosphoproteomic dataset. Nodes are arranged to show integrin-α5 1-hop, 2-hop and ≥3-hop proteins. Nodes are labelled with gene names for clarity.

Only 61/124 proteins identified in the isolated IAC phosphoproteomic dataset were also identified in the proteomic dataset, indicating that phosphoproteomic analysis of adhesion complexes samples, along with proteomic analysis can provide a more detailed coverage of adhesion complex protein composition, in agreement with Robertson et al. 2015. The combined isolated IAC proteomic and phosphoproteomic analysis resulted in a more comprehensive dataset of 918 proteins (data not shown), and provided increased confidence in the 61 protein identifications that overlap between the two datasets. To provide a view of these proteins, the 124 phosphoproteins identified in the IAC phosphoproteomic dataset were displayed as a network, highlighting proteins that were also identified in the IAC proteomic dataset (figure 5.5). This network had a higher proportion of unconnected nodes than previous networks generated possibly due to many interconnecting proteins not being identified in this IAC phosphoproteomic dataset.

Proteins and phosphoproteins identified in these datasets were also mapped onto the consensus adhesome (Horton et al. 2015) to provide an overview of the coverage. The structural connection between integrins and actin, as viewed in the consensus adhesome, can be broadly divided into four canonical signalling modules (Horton et al. 2015), and are separated accordingly in the consensus adhesome figure. The 40 consensus adhesome proteins identified in the proteomic dataset were mapped onto the consensus adhesome (figure 5.6). There was high coverage (>50%) of each of the four axes defined by the consensus adhesome (Horton et al. 2015;Horton et al. 2016a). A particularly high coverage of the axis including two sub-modules, connected through a kindlin–integrin-linked kinase (ILK) interaction was apparent. The 19 proteins identified in both the IAC and TCL phosphoproteomic dataset were also mapped onto the consensus adhesome (figure 5.7). Although there was less coverage of the overall consensus adhesome compared to the proteomic dataset (figure 5.6 & 5.7, 40 vs 19 proteins), there was increased coverage of the axis that contains FAK and paxillin (5 vs 6 proteins). This may be an indication of proteins in this node being highly phosphorylated.

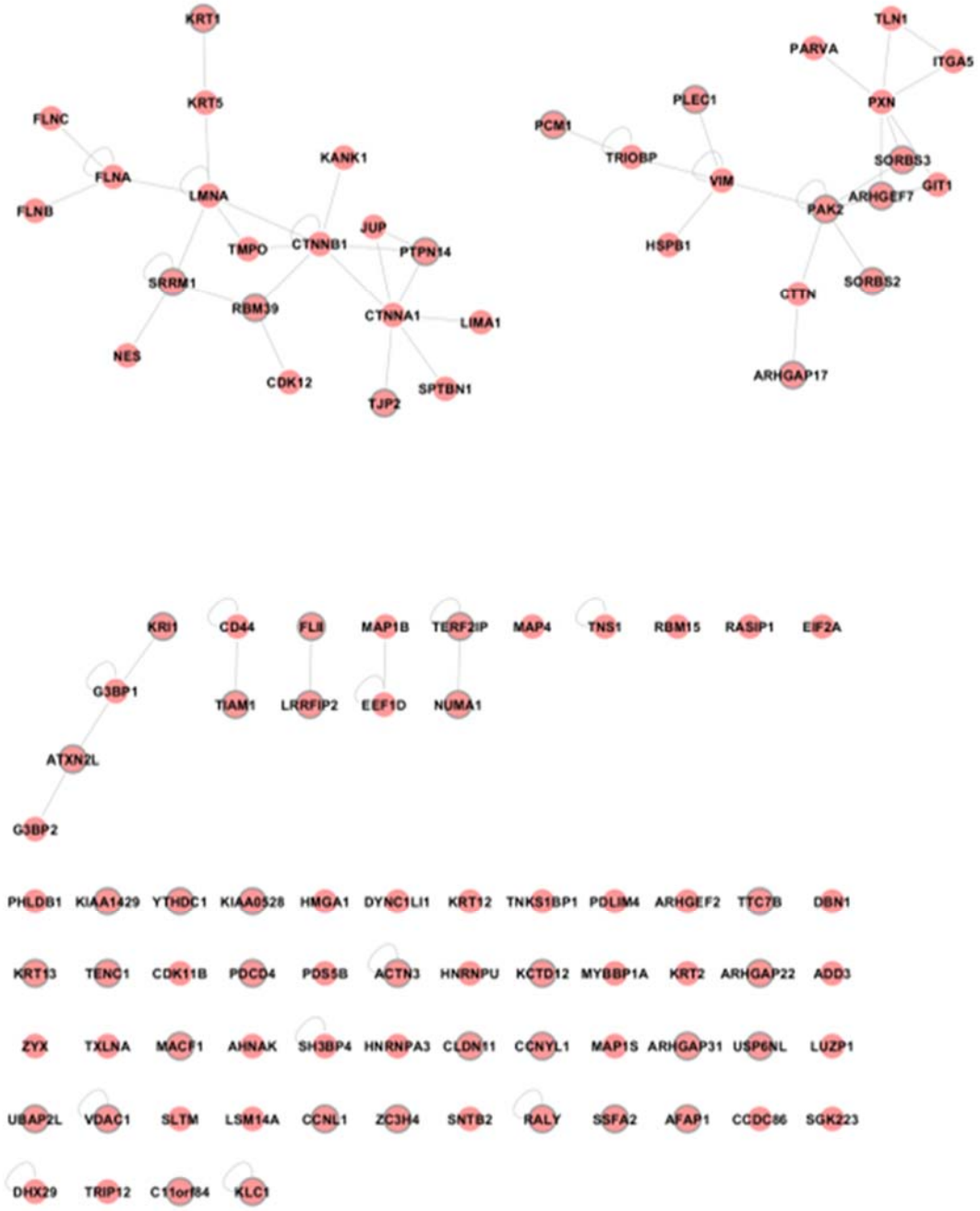

Figure 5.5. Network analysis of proteins identified by mass spectrometry-based phosphoproteomic analysis of isolated HUVEC integrin adhesion complex samples. Proteins identified in the phosphoproteomic integrin adhesion complex dataset were mapped onto a known human protein-protein interaction network. In total, out of 124 proteins, 104 were mapped onto the network. The network comprises 66 interactions (grey lines; edges) between the 104 proteins (circles; nodes). A thick, grey node border specifies proteins also identified in the IAC proteomic dataset. Perfuse force directed layout applied.

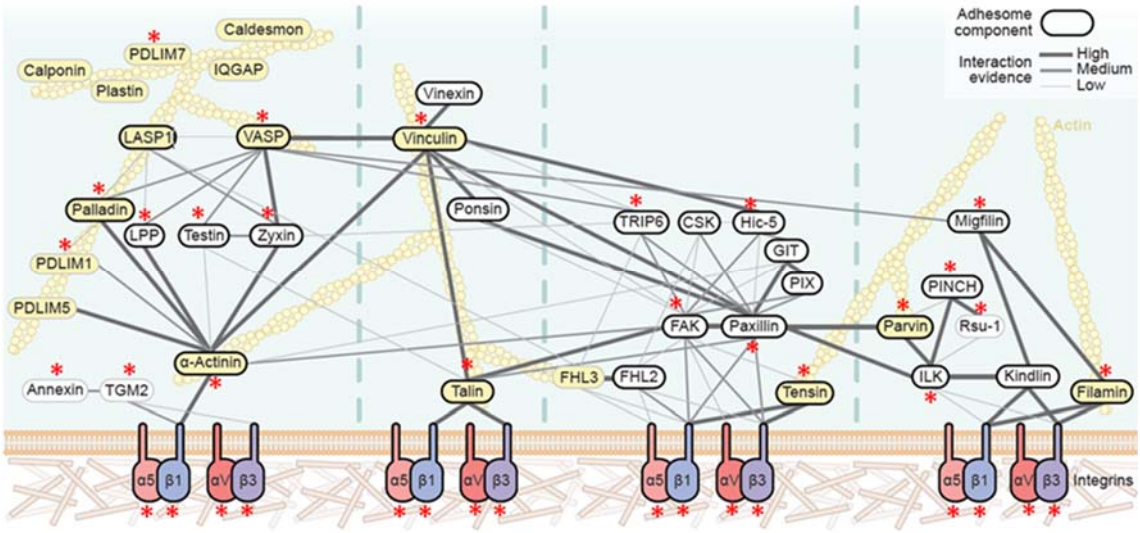

Figure 5.6. Proteins identified by mass spectrometry-based proteomic analysis of isolated HUVEC integrin adhesion complex samples mapped onto the consensus adhesome protein network. Proteins in the HUVEC isolated integrin adhesion complex proteomic dataset were mapped onto the consensus adhesome network, proteins detected are indicated with a red asterisks (*). In total, 34 consensus adhesome proteins were identified. Proteins coloured yellow are actin binding proteins. Figure adapted from Horton et al. 2015. Additional consensus adhesome proteins present and not linked to the above network: SYNCRIP, PPIB, RPL23A, P4HB, H1FX, HP1BP3, ALYREF, DDX18, DDX27, DIMT1, LIMD1, GIT2, SIPA1.

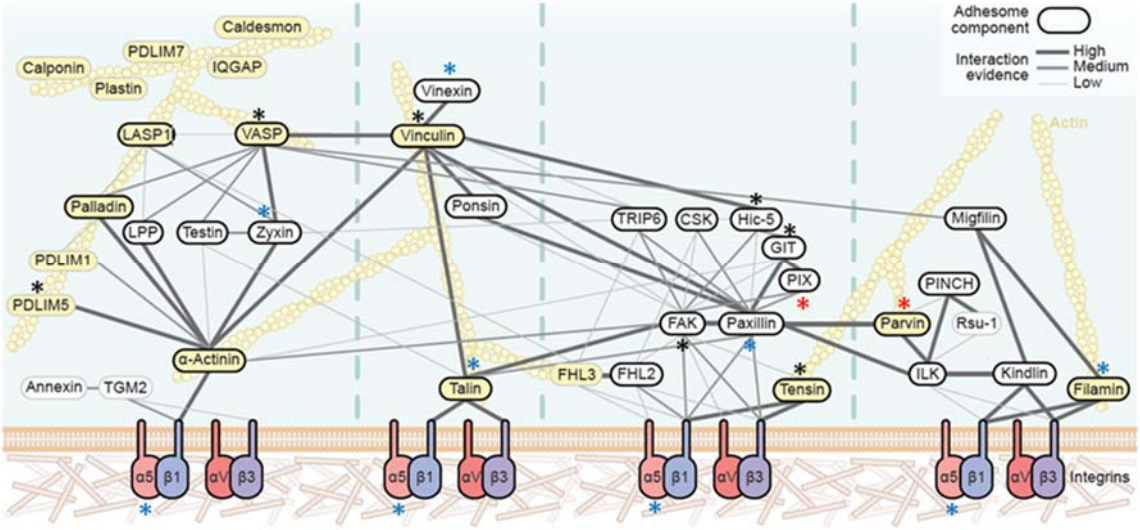

Figure 5.7. Phosphoproteins identified by mass spectrometry-based phosphoproteomic analysis of isolated HUVEC integrin adhesion complex (IAC) and total cell lysate (TCL) samples from HUVECs mapped onto the consensus adhesome protein network. Phosphoproteins in HUVEC isolated IAC and TCL phosphoproteomic datasets were mapped onto the consensus adhesome network. Proteins detected are indicated with an asterisk; red (*) in the IAC dataset only, black (*) in the TCL dataset and blue (*) if detected in both datasets. In total, 19 consensus adhesome proteins were identified. Proteins coloured yellow are actin binding proteins. Figure adapted from Horton et al. 2015. Additional consensus adhesome proteins identified in the TCL phosphoproteomic dataset and not linked to the above network: H1FX, LIMD1, GIT2, SIPA1.

5.2.2 Statistical analysis of phosphopeptide changes upon VEGF treatment

To identify specific phosphopeptides that displayed an increase or decrease in the phosphoproteomic datasets, volcano plots were used. First, each of the 855 proteins identified in the IAC proteomic data was displayed (figure 5.8a). For the IAC phosphoproteomic dataset, each phosphopeptide identified was displayed (figure 5.8b). Phosphopeptides with a fold change >2 and a low p-value (<0.1) may be of interest for further investigation (phosphopeptides from filamin, vimentin and AHNAK). In addition, all LCA and consensus adhesome phosphopeptides identified in the TCL phosphoproteomic dataset were displayed as a volcano plot (figure 5.8c), also highlighting phosphopeptides which may be of interest for further investigation. Comparison of these graphs highlighted that larger changes were observed in the phosphoproteomic data compared to that of the proteomic analysis. These overall analyses will be considered in the following sections when selecting candidates from these datasets to investigate further.

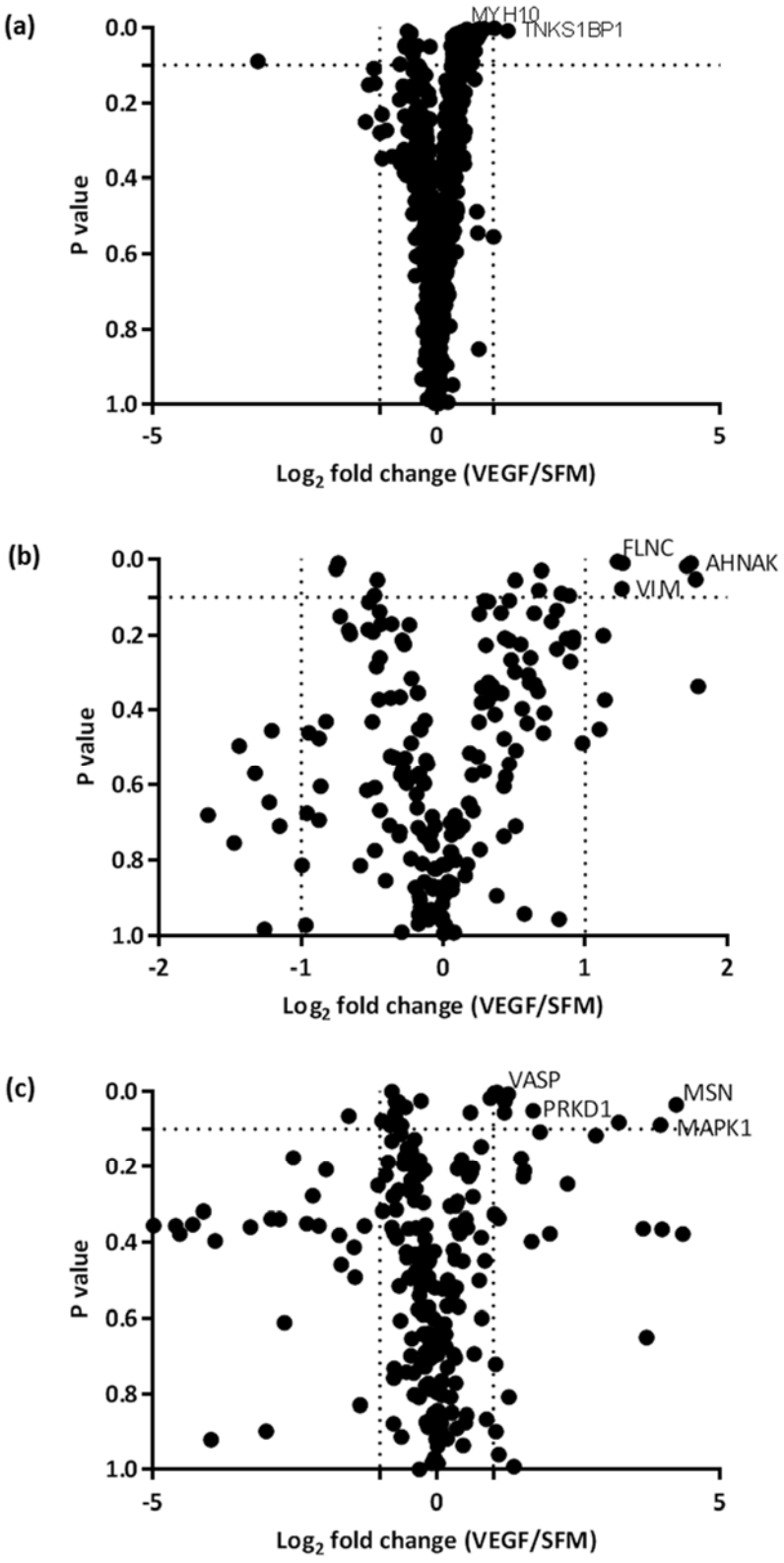

Figure 5.8. Proteins and phosphopeptides identified by mass spectrometry-based proteomic/phosphoproteomic analysis of isolated integrin adhesion complex samples or total cell lysate samples from HUVECs displayed as a volcano plot. (a) 855 proteins identified in the HUVEC isolated integrin adhesion complex proteomic dataset, (b) 211 phosphopeptides identified in the HUVEC isolated integrin adhesion complex phosphoproteomic dataset and (c) 252 literature-curated adhesome phosphopeptides identified in the HUVEC total cell lysate phosphoproteomic dataset. Horizontal dotted lines indicate a two-fold change and vertical dotted lines indicate a p-value of 0.1. Points with a p-value of <0.1, and >two-fold change are indicated by displaying gene name. For phosphoproteomic data, if a protein has multiple phosphopeptides within this range, only one is labelled.

5.2.3 Kinase predication analysis

One method of analysing phosphoproteomic data is to use a software package to interrogate all identified phosphorylation sites, and assign them as potential substrates for a particular protein kinase or group/family of protein kinases. To identify protein kinases that are potentially involved in VEGF adhesion crosstalk, the iGPS kinase prediction tool was used (Song et al. 2012), which specifically predicts in vivo site-specific kinase-substrate relations. The tool was used to analyse both the isolated IAC and TCL phosphoproteomic data generated in chapter 4.

5.2.3.1 Integrin adhesion complex phosphoproteomic data

Of the 389 unique phosphopeptides identified using spectral count analysis of the IAC phosphoproteomic dataset, 255 were identified in the SFM condition and 276 in the VEGF condition. These individual lists of phosphopeptides identified in the SFM or VEGF conditions (supplementary table 5.1a; appendix) were inputted into the iGPS tool and output data analysed (supplementary table 5.1b; appendix). Overall, 189 and 212 phosphopeptides were identified as potential substrates for a particular protein kinase or group/family of protein kinases, in the SFM and VEGF conditions respectively (supplementary file 5.1; appendix). A total of 42 protein kinases or group/family of protein kinases were identified, and the numbers of unique phosphopeptides predicted to be substrates of each kinase are shown in table 5.1 and figure 5.9. The $\log_2$ fold change (VEGF/SFM) of phosphopeptides predicted to be substrates of each identified kinase/group of kinases was displayed (table 5.1, figure 5.10). These results indicate that for a high proportion of kinases or kinase groups identified (19/42), the number of identified unique phosphorylation sites is increased in the VEGF sample.

In addition to adhesion-associated kinases such as FAK and Src, the prediction tool identified a large number of kinases that do not have well characterised roles in adhesion signalling. For example, many phosphorylation sites predicted to be substrates of serine/threonine kinases of the CMGC group (including the CDK, glycogen synthase kinase and mitogen-activated protein kinase families) were identified, and appeared to decrease upon VEGF treatment (figure 5.9 & 5.10). In addition, the AGC group of kinases was identified (including the AKT, protein kinase A, G and C families) with numbers of predicted phosphorylation sites increased upon VEGF treatment (figure 5.9 & 5.10). These analyses suggest that these kinases may play important roles in adhesion signalling, and VEGF-adhesion crosstalk. Accordingly, previous studies involving kinase prediction analyses on phosphoproteomic isolated IAC mass spectrometry datasets have identified kinases with roles in adhesion signalling, such as CDK1 (Robertson et al. 2015). However, in this study (Robertson et al. 2015), much higher numbers of starting phosphopeptides were identified from isolated IACs, whereas comparatively low numbers were identified in this HUVEC study. For example, where 15 and 28 sites were identified as FAK and Src substrates, respectively (Robertson et al. 2015), only

one of each was identified in this study (table 5.1, figure 5.9). Therefore, although these results may provide interesting information regarding the role of protein kinase families in VEGF-adhesion crosstalk, results should be interpreted with care.

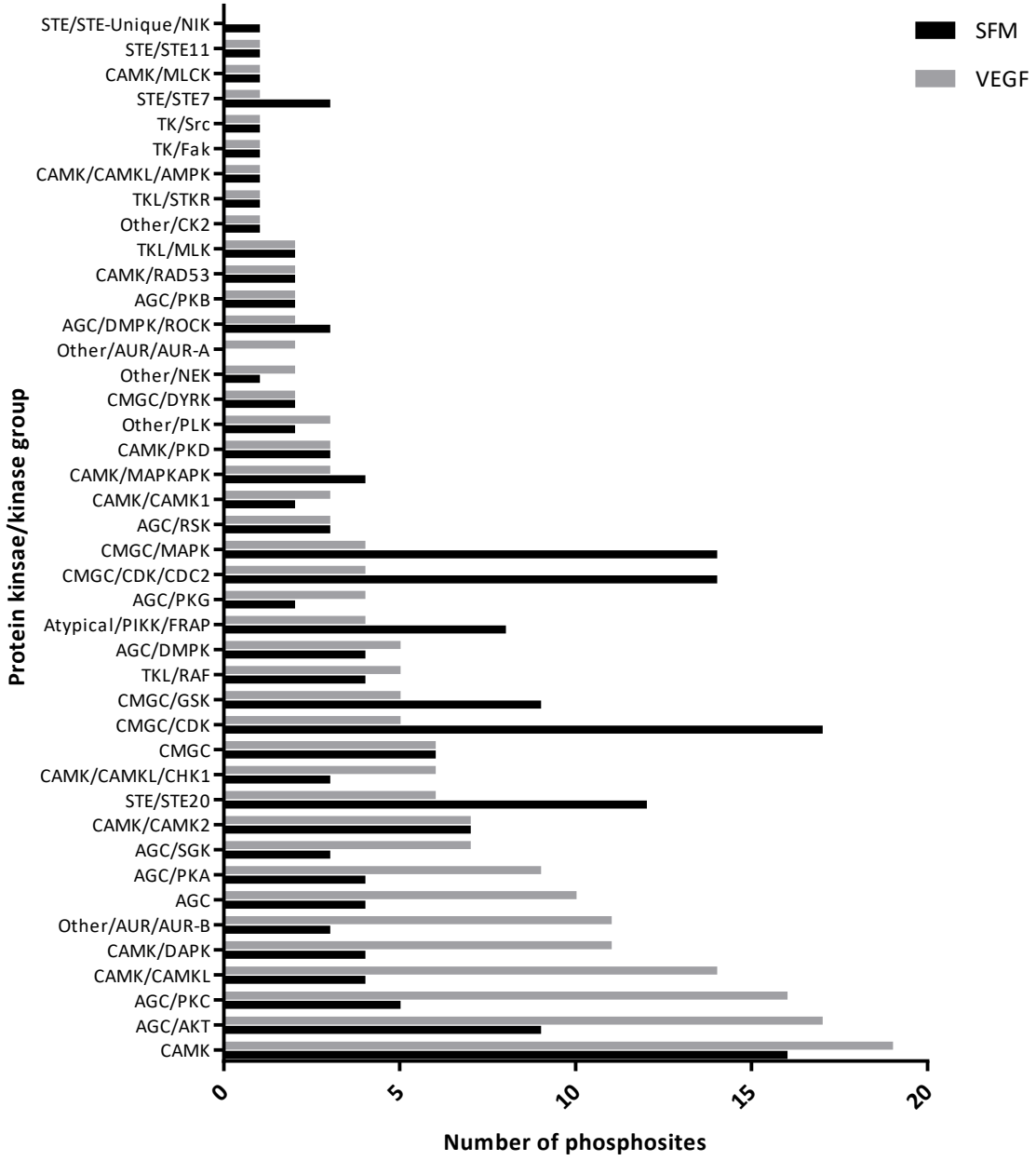

Figure 5.9. iGPS kinase prediction analysis of SFM and VEGF isolated HUVEC integrin adhesion complex phosphoproteomic datasets: numbers of phosphopeptides identified as predicted substrates for each protein kinase or group/family of protein kinase identified. All identified unique phosphopeptides from the integrin adhesion complex phosphoproteomic data sample, SFM (255 peptides) and VEGF (276 peptides) conditions were input into the iGPS tool. Graph displays all 42 protein kinases or group/family of protein kinases identified, and the number of unique phosphopeptides predicted to be phosphorylated by each in the SFM and VEGF datasets (data also shown in table 5.1). Original data, including assigned phosphosites are shown in supplementary file 5.1 (appendix).

Table 5.1. iGPS kinase prediction analysis of HUVEC SFM and VEGF isolated integrin adhesion complex phopshoproteomic datasets: protein kinases or group/family of protein kinases identified. All identified unique phosphopeptides for SFM (255) and VEGF (276) conditions were input into the iGPS tool. Table shows all 42 protein kinases or group/family of protein kinases identified, the number of unique phosphopeptides predicted to be phosphorylated by each in the SFM and VEGF datasets, and the log_2 fold change (VEGF/SFM) values. Original data, including assigned phosphosites are shown in supplementary file 5.1 (appendix).

Protein kinase or group/family of protein kinases	SFM	VEGF	Log_2 fold change (VEGF/SFM)
AGC	4	11	1.5
AGC/AKT	9	19	1.1
AGC/DMPK	4	7	0.8
AGC/DMPK/ROCK	3	5	0.7
AGC/PKA	4	5	0.3
AGC/PKB	2	3	0.6
AGC/PKC	5	9	0.8
AGC/PKG	2	5	1.3
AGC/RSK	3	3	0
AGC/SGK	3	4	0.4
Atypical/PIKK/FRAP	8	5	-0.7
CAMK	16	7	-1.2
CAMK/CAMK1	2	2	0
CAMK/CAMK2	7	4	-0.8
CAMK/CAMKL	4	16	2
CAMK/CAMKL/AMPK	1	1	0
CAMK/CAMKL/CHK1	3	14	2.2
CAMK/DAPK	4	6	0.6
CAMK/MAPKAPK	4	1	-2
CAMK/MLCK	1	2	1
CAMK/PKD	3	3	0
CAMK/RAD53	2	1	-1
CMGC	6	10	0.7
CMGC/CDK	17	6	-1.5
CMGC/CDK/CDC2	14	3	-2.2
CMGC/DYRK	2	2	0
CMGC/GSK	9	6	-0.6
CMGC/MAPK	14	11	-0.3
Other/AUR/AUR-A	0	1	0
Other/AUR/AUR-B	3	17	2.5
Other/CK2	1	4	2
Other/NEK	1	2	1
Other/PLK	2	2	0
STE/STE11	1	1	0
STE/STE20	12	4	-1.6
STE/STE7	3	1	-1.6
STE/STE-Unique/NIK	1	0	0
TK/Fak	1	3	1.6
TK/Src	1	1	0
TKL/MLK	2	2	0
TKL/RAF	4	2	1
TKL/STKR	1	1	0

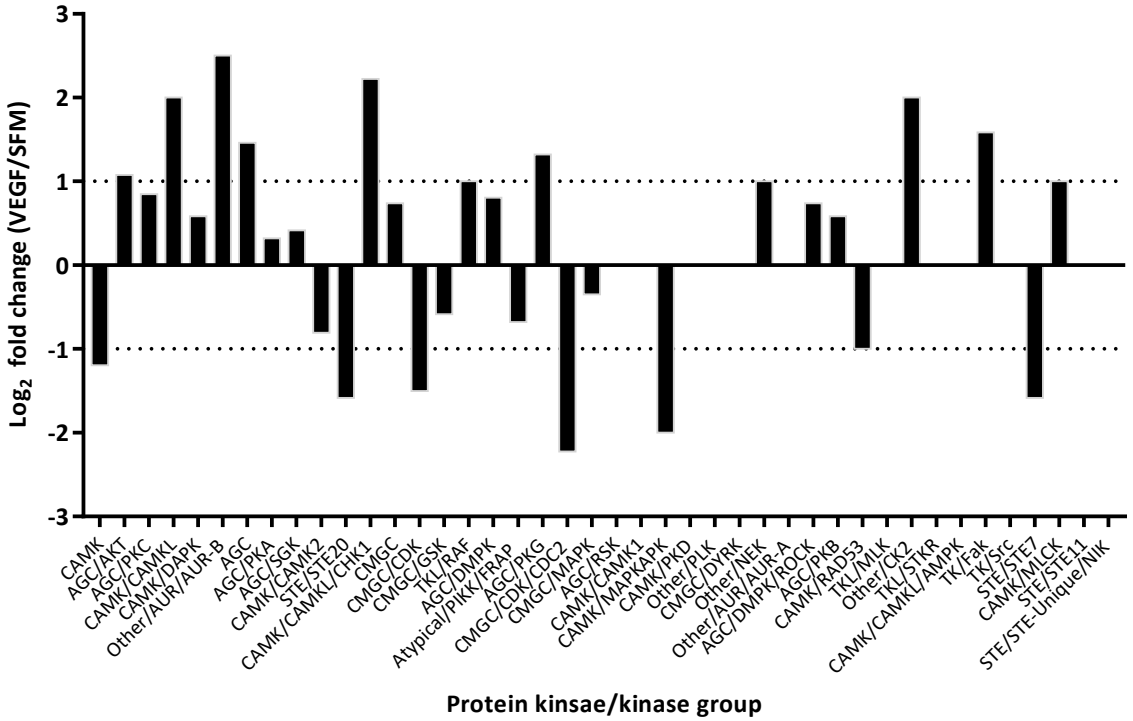

Figure 5.10. iGPS kinase prediction analysis of isolated HUVEC integrin adhesion complex phosphoproteomic data: VEGF-induced fold change of phosphopeptides identified as predicted substrates for protein kinases or group/family of protein kinases identified. All identified unique phosphopeptides from the integrin adhesion complex phosphoproteomic data sample, SFM (255 peptides) and VEGF (276 peptides) conditions were input into the iGPS tool. Graph displays the $\log_2$ fold change (VEGF/SFM) of phosphopeptides predicted to be substrates of the 42 protein kinases or group/family of protein kinases identified in this analysis (phosphopeptide numbers and fold change are also displayed in table 5.1 and figure 5.9). Dotted lines represent a 2-fold change. Original data, including assigned phosphosites are shown in supplementary file 5.1 (appendix).

5.2.3.2 Total cell lysate phosphoproteomic data

Kinase prediction analysis was also performed on the TCL phosphoproteomic samples. Two separate analyses were performed, using both the total dataset, and the dataset filtered for all phosphopeptides from previously identified adhesion components (meta adhesome, literature-curated adhesome and HUVEC dataset generated in chapter 3).

For the first analysis, phosphopeptides identified were filtered for previously detected adhesion components (meta adhesome, LCA and HUVEC dataset generated in chapter 3). In total, 2332 and 2368 unique phosphopeptides, for the SFM and VEGF samples respectively, were inputted into the iGPS tool. Overall, 645 and 763 phosphopeptides were identified as potential substrates for a particular protein kinase or group/family of protein kinases, in the SFM and VEGF conditions respectively (supplementary file 5.3; appendix). A total of 74 protein kinases or group/family of protein kinases were identified, and the numbers of unique phosphopeptides predicted to be

substrates of each kinase are shown in table 5.2 and figure 5.11. Compared to the iGPS analysis of the IAC phosphoproteomic data, much higher numbers of phosphopeptides were predicted to be substrates for protein kinases or group/family of protein kinases, meaning analysis of this data may provide more reliable results.

Again, the log_2 fold change (VEGF/SFM) of phosphopeptides predicted to be substrates of each identified kinase/group of kinases were calculated (table 5.2), and those that display a fold change above or below zero are displayed in figure 5.12. As was the case with the IAC data analysis, for the majority of kinases or kinase groups identified, the number of identified unique phosphosites increased in the VEGF sample. All 42 kinases or group/family of kinases identified in both the IAC and adhesome-filtered TCL datasets are displayed in table 5.3, with associated peptide numbers and fold changes. Many of the AGC group of kinases decreased in both datasets, and the CMGC groups increased in both datasets. These were the only kinases/kinase groups that changed consistently in both datasets, generating further confidence that these kinases do change their activity level within the adhesion complex and/or on adhesion complex proteins upon VEGF treatment.

Table 5.2. iGPS kinase prediction analysis of HUVEC SFM or VEGF, total cell lysate (adhesome filtered) phopshoproteomic datasets: protein kinases or group/family of protein kinases identified. All identified unique phosphopeptides, from proteins in the meta adhesome, literature-curated adhesome and HUVEC dataset generated in chapter 3, for SFM (2332) and VEGF (2368) conditions were input into the iGPS tool. Table shows all 74 protein kinases or group/family of protein kinases identified, the number of unique phosphopeptides predicted to be phosphorylated by each in the SFM and VEGF datasets, and the fold change and log_2 fold change (VEGF/SFM) values. Original data, including assigned phosphosites are shown in supplementary file 5.2 (appendix).

Protein kinase or group/family of protein kinases	SFM	VEGF	Log_2 fold change (VEGF/SFM)
AGC	17	20	0.2
AGC/AKT	39	52	0.4
AGC/DMPK	15	17	0.2
AGC/DMPK/ROCK	14	16	0.2
AGC/GRK	10	7	-0.5
AGC/PKA	16	17	0.1
AGC/PKB	3	6	1
AGC/PKC	17	13	-0.4
AGC/PKG	7	5	-0.5
AGC/RSK	16	16	0
AGC/SGK	8	8	0
Atypical/PDHK	2	6	1.6
Atypical/PIKK	3	4	0.4
Atypical/PIKK/ATM	8	12	0.6
Atypical/PIKK/ATR	0	1	0
Atypical/PIKK/DNAPK	1	1	0
Atypical/PIKK/FRAP	34	38	0.2
CAMK	71	75	0.1
CAMK/CAMK1	5	5	0
CAMK/CAMK2	22	22	0
CAMK/CAMKL	31	29	-0.1
CAMK/CAMKL/AMPK	1	1	0
CAMK/CAMKL/CHK1	12	13	0.1
CAMK/CAMKL/LKB	0	2	1
CAMK/DAPK	3	2	-0.6
CAMK/MAPKAPK	9	10	0.2
CAMK/MLCK	8	6	-0.4
CAMK/PHK	1	1	0
CAMK/PKD	22	18	-0.3
CAMK/RAD53	9	8	-0.2
CK1	25	27	0.1
CMGC	47	53	0.2
CMGC/CDK	170	162	-0.1
CMGC/CDK/CDC2	114	113	0
CMGC/DYRK	43	39	-0.1
CMGC/GSK	113	108	-0.1
CMGC/MAPK	99	96	0
Other/AUR	0	1	0
Other/AUR/AUR-A	2	2	0
Other/AUR/AUR-B	7	6	-0.2
Other/CK2	73	73	0
Other/IKK	25	32	0.4
Other/NEK	7	7	0
Other/PEK	1	3	1.6
Other/PLK	41	45	0.1
Other/Wnk	0	1	0
STE/STE11	10	6	-0.7
STE/STE20	27	29	0.1
STE/STE7	7	9	0.4
STE/STE-Unique/COT	1	1	0
STE/STE-Unique/NIK	14	12	-0.2
TK/Abl	4	1	-2
TK/Axl	1	1	0
TK/Csk	1	0	0
TK/EGFR	4	8	1
TK/Eph	4	4	0
TK/Fak	6	5	-0.3
TK/Fer/Fer	3	4	0.4
TK/Fer/Fes	2	1	-1
TK/InsR	1	2	1
TK/JakA	1	1	0
TK/Met	2	2	0
TK/PDGFR	3	6	1
TK/Ret	1	1	0
TK/Src	6	10	0.7
TK/Syk	4	4	0
TK/Tec	3	3	0
TK/Tie	1	1	0
TK/Trk	1	1	0
TK/VEGFR	0	2	1
TKL/IRAK	0	2	1
TKL/MLK	13	12	-0.1
TKL/RAF	24	22	-0.1
TKL/STKR	25	21	-0.3

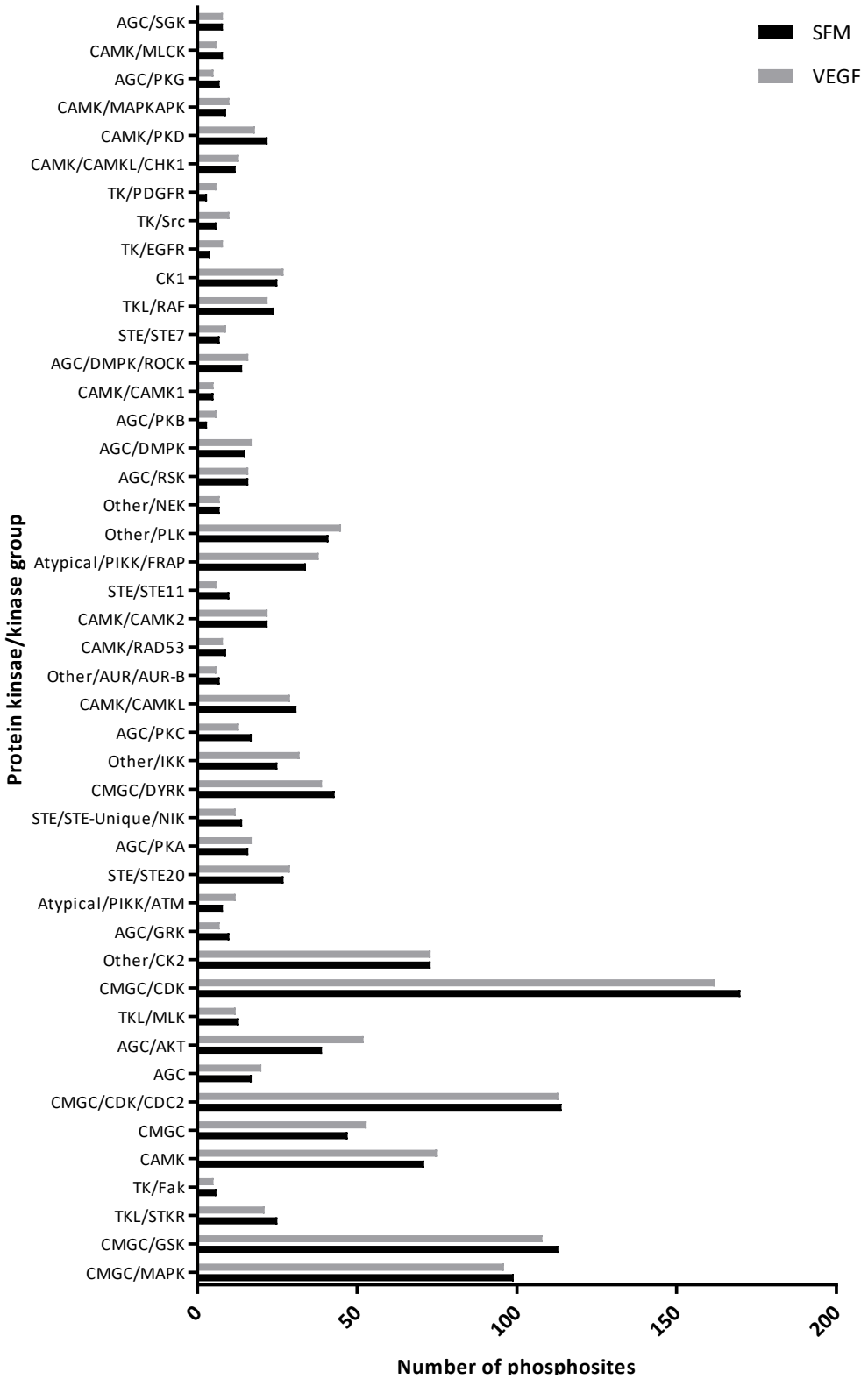

Figure 5.11. iGPS kinase prediction analysis of HUVEC SFM and VEGF treated, total cell lysate (adhesome filtered) phosphoproteomic datasets: numbers of phosphopeptides identified as predicted substrates for each protein kinase or group/family of protein kinase identified. All identified unique phosphopeptides identified in total cell lysate phosphoproteomic datasets from proteins in the meta adhesome, literature-curated adhesome and HUVEC dataset generated in chapter 3, for SFM (2332 peptides) and VEGF (2368 peptides) conditions were input into the iGPS tool. Graph displays protein kinases or group/family of protein kinases identified (kinases with <5 phosphopeptides assigned in both SFM and VEGF conditions were eliminated), and the number of unique phosphopeptides predicted to be phosphorylated by each in the SFM and VEGF datasets (data also shown in table 5.2). Original data, including assigned phosphosites are shown in supplementary file 5.2 (appendix).

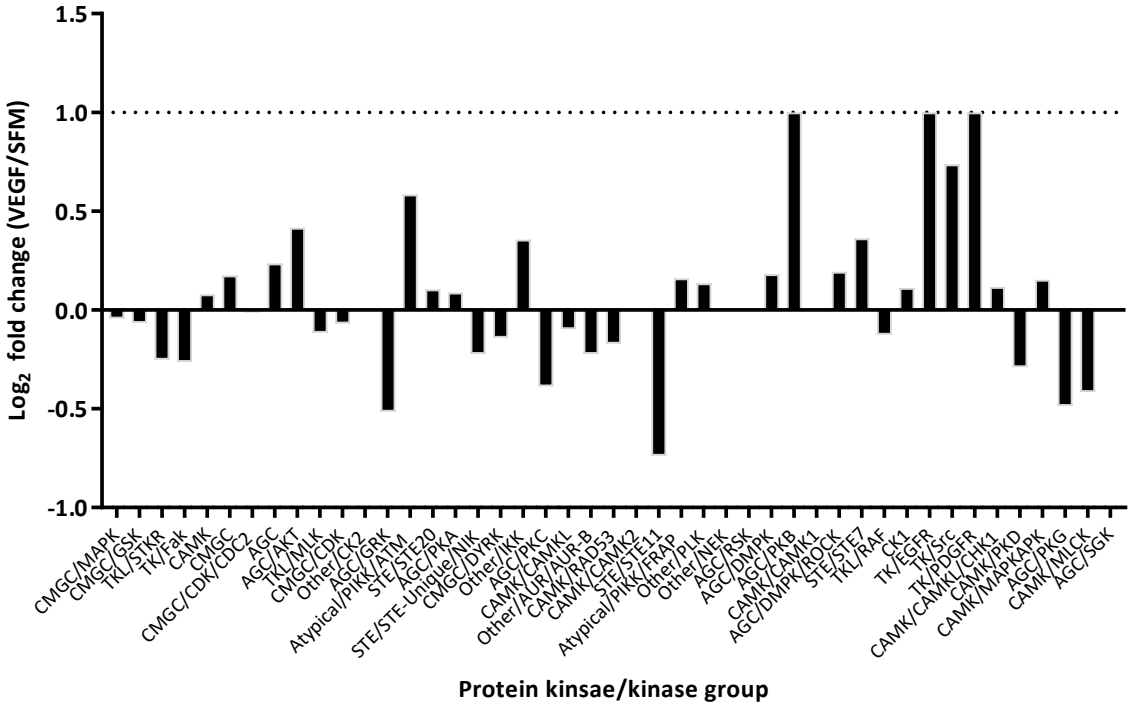

Figure 5.12. iGPS kinase prediction analysis of HUVEC total cell lysate (adhesome filtered) phosphoproteomic data: VEGF-induced fold change of phosphopeptides identified as predicted substrates for protein kinases or group/family of protein kinases identified. All identified unique phosphopeptides identified in total cell lysate phosphoproteomic datasets, from proteins in the meta adhesome, literature-curated adhesome and HUVEC dataset generated in chapter 3, for SFM (2332 peptides) and VEGF (2368 peptides) conditions were input into the iGPS tool. Graph displays the $\log_2$ fold change (VEGF/SFM) of phosphopeptides predicted to be substrates of the protein kinases or group/family of protein kinases identified in this analysis (kinases with <5 phosphopeptides assigned in both SFM and VEGF conditions were eliminated to increase accuracy, phosphopeptide numbers and fold change values for all kinases are also displayed in table 5.2 and figure 5.11). Dotted lines represent a 2-fold change. Original data, including assigned phosphosites are shown in supplementary table 5.2 (appendix).

Table 5.3. iGPS kinase prediction analysis of HUVEC SFM or VEGF, phopshoproteomic datasets: protein kinases or group/family of protein kinases identified. All identified unique phosphopeptides for SFM and VEGF conditions from (a) Isolated integrin adhesion complex dataset, (b) total cell lysate adhesome filtered dataset and (c) total cell lysate dataset were input into the iGPS tool. Table shows all protein kinases or group/family of protein kinases identified, the number of unique phosphopeptides predicted to be phosphorylated by each in the SFM and VEGF datasets, and the fold change and log_2 fold change values, cells are shaded according to their fold change (red increased in VEGF, blue increased in SFM).

	(a)				(b)				(c)			
Protein kinase or group/family of protein kinases	SFM	VEGF	Fold change (VEGF/SFM)	Log_2 FC (VEGF/SFM)	SFM	VEGF	Fold change (VEGF/SFM)	Log_2 FC (VEGF/SFM)	SFM	VEGF	Fold change (VEGF/SFM)	Log_2 FC (VEGF/SFM)
AGC	4	11	2.8	1.5	17	20	1.2	0.2	62	90	1.45	0.54
AGC/AKT	9	19	2.1	1.1	39	52	1.3	0.4	156	200	1.28	0.36
AGC/DMPK	4	7	1.8	0.8	15	17	1.1	0.2	33	42	1.27	0.35
AGC/DMPK/ROCK	3	5	1.7	0.7	14	16	1.1	0.2	28	38	1.36	0.44
AGC/PKA	4	5	1.3	0.3	16	17	1.1	0.1	45	57	1.27	0.34
AGC/PKB	2	3	1.5	0.6	3	6	2.0	1.0	18	24	1.33	0.42
AGC/PKC	5	9	1.8	0.8	17	13	0.8	-0.4	61	71	1.16	0.22
AGC/PKG	2	5	2.5	1.3	7	5	0.7	-0.5	21	25	1.19	0.25
AGC/RSK	3	3	1.0	0.0	16	16	1.0	0.0	70	88	1.26	0.33
AGC/SGK	3	4	1.3	0.4	8	8	1.0	0.0	39	52	1.33	0.42
Atypical/PIKK/FRAP	8	5	0.6	-0.7	34	38	1.1	0.2	217	214	0.99	-0.02
CAMK	16	7	0.4	-1.2	71	75	1.1	0.1	131	151	1.15	0.20
CAMK/CAMK1	2	2	1.0	0.0	5	5	1.0	0.0	24	28	1.17	0.22
CAMK/CAMK2	7	4	0.6	-0.8	22	22	1.0	0.0	54	64	1.19	0.25
CAMK/CAMKL	4	16	4.0	2.0	31	29	0.9	-0.1	71	88	1.24	0.31
CAMK/CAMKL/AMPK	1	1	1.0	0.0	1	1	1.0	0.0	18	21	1.17	0.22
CAMK/CAMKL/CHK1	3	14	4.7	2.2	12	13	1.1	0.1	42	52	1.24	0.31
CAMK/DAPK	4	6	1.5	0.6	3	2	0.7	-0.6	13	13	1.00	0.00
CAMK/MAPKAPK	4	1	0.3	-2.0	9	10	1.1	0.2	50	56	1.12	0.16
CAMK/MLCK	1	2	2.0	1.0	8	6	0.8	-0.4	23	29	1.26	0.33
CAMK/PKD	3	3	1.0	0.0	22	18	0.8	-0.3	44	50	1.14	0.18
CAMK/RAD53	2	1	0.5	-1.0	9	8	0.9	-0.2	20	18	0.90	-0.15
CMGC	6	10	1.7	0.7	47	53	1.1	0.2	270	278	1.03	0.04
CMGC/CDK	17	6	0.4	-1.5	170	162	1.0	-0.1	362	350	0.97	-0.05
CMGC/CDK/CDC2	14	3	0.2	-2.2	114	113	1.0	0.0	320	325	1.02	0.02
CMGC/DYRK	2	2	1.0	0.0	43	39	0.9	-0.1	111	105	0.95	-0.08
CMGC/GSK	9	6	0.7	-0.6	113	108	1.0	-0.1	267	256	0.96	-0.06
CMGC/MAPK	14	11	0.8	-0.3	99	96	1.0	0.0	317	317	1.00	0.00
Other/AUR/AUR-A	0	1	0.0	0.0	2	2	1.0	0.0	9	9	1.00	0.00
Other/AUR/AUR-B	3	17	5.7	2.5	7	6	0.9	-0.2	12	11	0.92	-0.13
Other/CK2	1	4	4.0	2.0	73	73	1.0	0.0	220	233	1.06	0.08
Other/NEK	1	2	2.0	1.0	7	7	1.0	0.0	15	16	1.07	0.09
Other/PLK	2	2	1.0	0.0	41	45	1.1	0.1	96	99	1.03	0.04
STE/STE11	1	1	1.0	0.0	10	6	0.6	-0.7	22	19	0.86	-0.21
STE/STE20	12	4	0.3	-1.6	27	29	1.1	0.1	68	86	1.26	0.34
STE/STE7	3	1	0.3	-1.6	7	9	1.3	0.4	19	27	1.42	0.51
STE/STE-Unique/NIK	1	0	0.0	0.0	14	12	0.9	-0.2	27	31	1.15	0.20
TK/Fak	1	3	3.0	1.6	6	5	0.8	-0.3	14	15	1.07	0.10
TK/Src	1	1	1.0	0.0	6	10	1.7	0.7	22	37	1.68	0.75
TKL/MLK	2	2	1.0	0.0	13	12	0.9	-0.1	18	20	1.11	0.15
TKL/RAF	4	2	2.0	1.0	24	22	0.9	-0.1	39	37	0.95	-0.08
TKL/STKR	1	1	1.0	0.0	25	21	0.8	-0.3	80	76	0.95	-0.07

For the final analysis, all phosphopeptides identified in the TCL sample were subjected to kinase prediction analysis. A total of 4859 and 5024 unique phosphopeptides, for the SFM and VEGF samples respectively, were inputted into the iGPS tool. Overall, 1760 and 1862 phosphopeptides, in the SFM and VEGF conditions respectively, were identified as potential substrates for a particular protein kinase or group/family of protein kinases. These phosphosites were assigned to 76 protein kinases or group/family of protein kinases, and the numbers of unique phosphopeptides predicted to be substrates of each are shown in table 5.4 and figure 5.13. In addition, the log_2 fold change (VEGF/SFM) values of each identified kinase/group of kinases were calculated (table 5.4), and those that displayed a fold change above or below 1.2 are displayed in figure 5.14. This analysis resulted in 34 kinases or group/family of protein kinases, of which the majority increased upon VEGF treatment, although only three of these changes were above two-fold (figure 5.14).

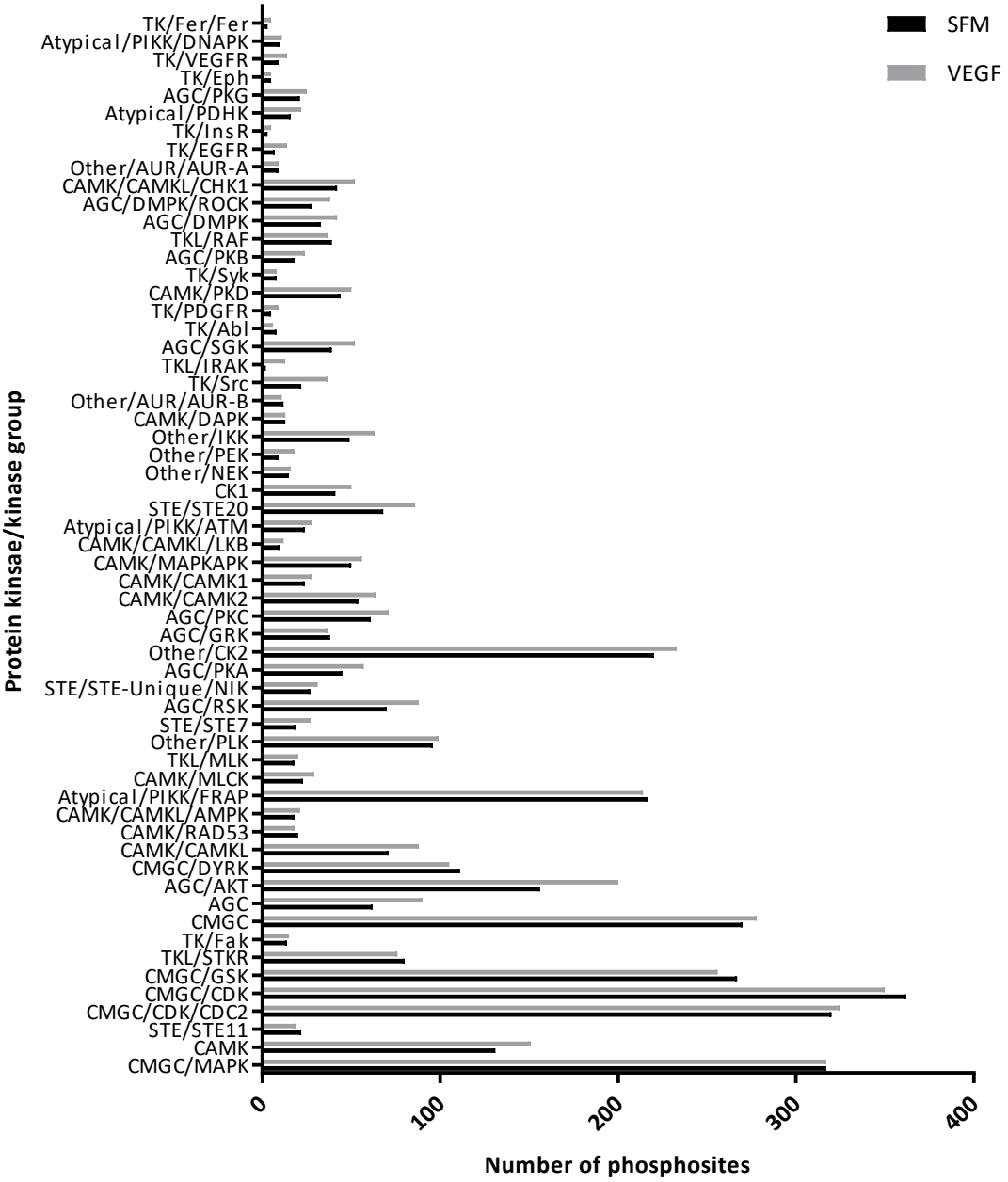

Figure 5.13. iGPS kinase prediction analysis of HUVEC SFM and VEGF, total cell lysate phosphoproteomic datasets: numbers of phosphopeptides identified as predicted substrates for each protein kinase or group/family of protein kinase identified. All identified unique phosphopeptides identified in total cell lysate phosphoproteomic datasets, from proteins in the SFM (4859 peptides) and VEGF (5024 peptides) conditions were input into the iGPS tool. Graph displays protein kinases or group/family of protein kinases identified (kinases with <5 phosphopeptides assigned in both SFM and VEGF conditions were eliminated) and numbers of phosphopeptides predicted to be phosphorylated by each in the SFM and VEGF datasets (data also shown in table 5.2). Original data, including assigned phosphosites are shown in supplementary table 5.3 (appendix).

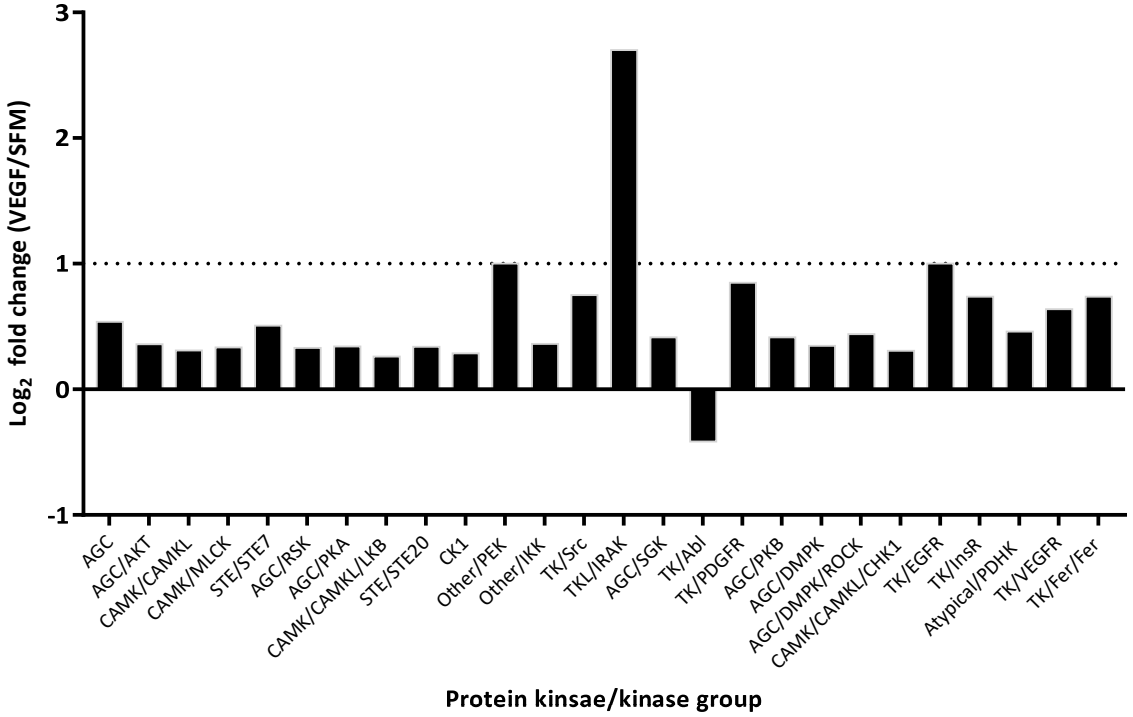

Figure 5.14. iGPS kinase prediction analysis of HUVEC total cell lysate phosphoproteomic data: VEGF-induced fold change of phosphopeptides identified as predicted substrates for protein kinases or group/family of protein kinases identified. All identified unique phosphopeptides, identified in total cell lysate phosphoproteomic datasets for SFM (4859 peptides) and VEGF (5024 peptides) conditions were input into the iGPS tool. Graph displays the log_2 fold change (VEGF/SFM) of phosphopeptides predicted to be substrates of the protein kinases or group/family of protein kinases identified in this analysis (kinases with <5 phosphopeptides assigned in both SFM and VEGF conditions and that increase change <1.2-fold were eliminated, phosphopeptide numbers and fold change values for all kinases are also displayed in table 5.4). Dotted lines represent a 2-fold change. Original data, including assigned phosphosites are shown in supplementary file 5.3 (appendix).

Table 5.4. iGPS kinase prediction analysis of HUVEC SFM or VEGF, total cell lysate phopshoproteomic datasets: protein kinases or group/family of protein kinases identified. All identified unique phosphopeptides for SFM (4859) and VEGF (5024) conditions were input into the iGPS tool. Table shows all protein kinases or group/family of protein kinases identified, the number of unique phosphopeptides predicted to be phosphorylated by each in the SFM and VEGF datasets, and the log_2 fold change (VEGF/SFM) values. Original data, including assigned phosphorylation sites are shown in supplementary file 5.3 (appendix).

Protein kinase or group/family of protein kinases	SFM	VEGF	Log_2 fold change
AGC	62	90	0.5
AGC/AKT	156	200	0.4
AGC/DMPK	33	42	0.3
AGC/DMPK/ROCK	28	38	0.4
AGC/GRK	38	37	0
AGC/PKA	45	57	0.3
AGC/PKB	18	24	0.4
AGC/PKC	61	71	0.2
AGC/PKG	21	25	0.3
AGC/RSK	70	88	0.3
AGC/SGK	39	52	0.4
Atypical/PDHK	16	22	0.5
Atypical/PIKK	4	4	0
Atypical/PIKK/ATM	24	28	0.2
Atypical/PIKK/ATR	0	1	0
Atypical/PIKK/DNAPK	10	11	0.1
Atypical/PIKK/FRAP	217	214	0
CAMK	131	151	0.2
CAMK/CAMK1	24	28	0.2
CAMK/CAMK2	54	64	0.2
CAMK/CAMKL	71	88	0.3
CAMK/CAMKL/AMPK	18	21	0.2
CAMK/CAMKL/CHK1	42	52	0.3
CAMK/CAMKL/LKB	10	12	0.3
CAMK/DAPK	13	13	0
CAMK/MAPKAPK	50	56	0.2
CAMK/MLCK	23	29	0.3
CAMK/PHK	1	3	1.6
CAMK/PKD	44	50	0.2
CAMK/RAD53	20	18	-0.2
CK1	41	50	0.3
CMGC	270	278	0
CMGC/CDK	362	350	0
CMGC/CDK/CDC2	320	325	0
CMGC/DYRK	111	105	-0.1
CMGC/GSK	267	256	-0.1
CMGC/MAPK	317	317	0
Other/AUR	0	1	0
Other/AUR/AUR-A	9	9	0
Other/AUR/AUR-B	12	11	-0.1
Other/CK2	220	233	0.1
Other/IKK	49	63	0.4
Other/NEK	15	16	0.1
Other/PEK	9	18	1
Other/PLK	96	99	0
Other/Wnk	2	4	1
STE/STE11	22	19	-0.2
STE/STE20	68	86	0.3
STE/STE7	19	27	0.5
STE/STE-Unique/COT	1	4	2
STE/STE-Unique/NIK	27	31	0.2
TK/Abl	8	6	-0.4
TK/Axl	1	1	0
TK/EGFR	7	14	1
TK/Eph	5	5	0
TK/Fak	14	15	0.1
TK/Fer/Fer	3	5	0.7
TK/Fer/Fes	3	4	0.4
TK/FGFR	0	1	0
TK/InsR	3	5	0.7
TK/JakA	2	4	1
TK/JakA	2	0	1
TK/Met	2	2	0
TK/PDGFR	5	9	0.8
TK/Ret	1	1	0
TK/Ret	1	0	0
TK/Src	22	37	0.8
TK/Syk	8	8	0
TK/Tec	3	4	0.4
TK/Tie	1	2	1
TK/Trk	1	1	0
TK/VEGFR	9	14	0.6
TKL/IRAK	2	13	2.7
TKL/MLK	18	20	0.2
TKL/RAF	39	37	-0.1
TKL/STKR	80	76	-0.1

Detailed examination of the three datasets analysed by iGPS were performed, which involved examination of proteins and peptide residues that were predicted to be phosphorylated, in addition to quantification data for these residues. For TCL analysis, growth factor receptor kinase substrates were increased (figure 5.15). These kinases included PDGFR, EGFR, InsR and VEGFR2. The specific phosphopeptides predicted to be phosphorylated by these kinases are shown in table 5.5. These analyses provide further evidence that growth factor signalling is occurring in these cells upon VEGF treatment.

The iGPS data analysis performed provides a great deal of data that can be analysed and used to identify protein candidates or protein kinases and kinase substrates that may be involved in VEGF-adhesion crosstalk. As already discussed, many phosphorylation sites predicted to be substrates of serine/threonine kinases of the CMGC group were identified, and appeared to decrease upon VEGF treatment, and the AGC group of kinases was identified with a number of predicted phosphorylation sites increasing upon VEGF treatment (table 5.3). These kinases and kinase substrates may warrant further investigation.

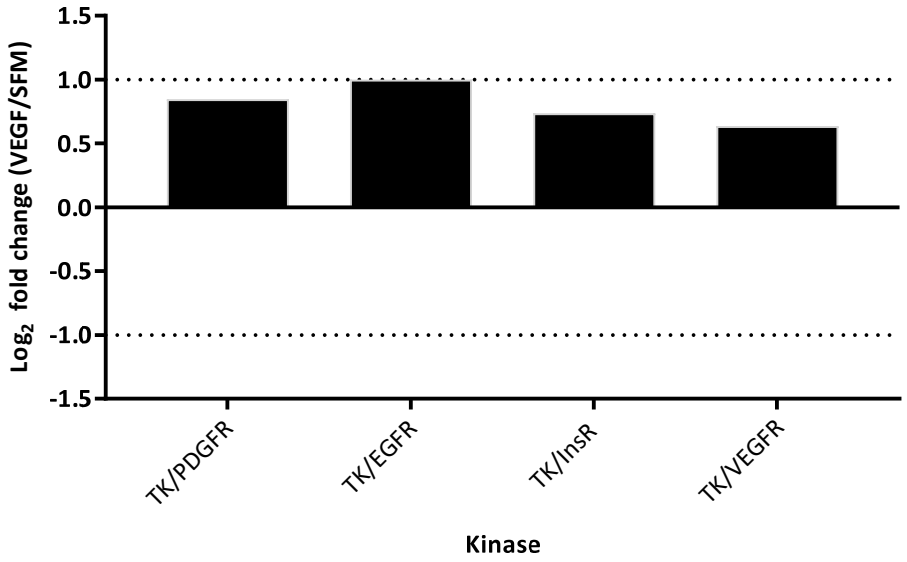

Figure 5.15. iGPS kinase prediction analysis of HUVEC total cell lysate phosphoproteomic datasets: VEGF-induced fold change of phosphopeptides identified as predicted substrates for growth factor protein kinases. All identified unique phosphopeptides, identified in total cell lysate phosphoproteomic datasets for SFM (4859 peptides) and VEGF (5024 peptides) conditions were input into the iGPS tool. Graph displays the $\log_2$ fold change (VEGF/SFM) of phosphopeptides predicted to be substrates of the growth factor protein kinases PDGFR, EGFR, InsR and VEGFR2 identified in this analysis (growth factor kinases with <5 phosphopeptides assigned in both SFM and VEGF conditions were eliminated to increase accuracy, phosphopeptide numbers and fold change values for all kinases are also displayed in table 5.4). Original data, including assigned phosphosites are shown in supplementary file 5.3 (appendix).

Table 5.5. Phosphopeptides identified as substrates for growth factor receptor kinases in iGPS analysis of total cell lysate phosphoproteomic data. All identified unique phosphopeptides for SFM (4859) and VEGF (5024) conditions were input into the iGPS tool. Table shows 66 phosphopeptides (24 SFM unique phosphopeptides and 42 VEGF unique phosphopeptides) which were identified as substrates for PDGFR, EGFR, InsR and VEGFR2 kinases. Table indicates the input phosphopeptide in PhosPep format, residue number and amino acid (Y/S/T) predicted to be phosphorylated by the listed kinase and peptide gene name. Rows are colour coordinated blue or pink for peptides in the SFM and VEGF conditions respectively.

Sample	Phosphopeptide	Residue	Y/S/T	GN	Kinase
SFM	SDSRSEpSPEPGpYVVTSSGLLLPVLLPR	1469	Y	ALS2	TK/EGFR
SFM	HGpSGADSDpYENTQSGDPLLGLEGK	598	Y	GIT1	TK/EGFR
SFM	VQIPVSRPDPEPVpSDNEEDSpYDEEIHD	132	Y	TJP1	TK/EGFR
SFM	VQIPVSRPDPEPVpSDNEEDSpYDEEIHD	132	Y	TJP1	TK/EGFR
SFM	HGSGADSDpYENTQSGDPLLGLEGK	598	Y	GIT1	TK/EGFR
SFM	THAVSVSEpTDDYAEIIDEEDTpYTMPSTR	429	Y	FAK	TK/EGFR
SFM	SDpSRSESPEPGpYVVTSSGLLLPVLLPR	1469	Y	ALS2	TK/EGFR
VEGF	pSDSRSESPEPGpYVVTSSGLLLPVLLPR	1469	Y	ALS2	TK/EGFR
VEGF	VQIPVSRPDPEPVpSDNEEDSpYDEEIHD	132	Y	TJP1	TK/EGFR
VEGF	VQIPVSRPDPEPVpSDNEEDSpYDEEIHD	132	Y	TJP1	TK/EGFR
VEGF	HGpSGADSDpYENTQSGDPLLGLEGK	598	Y	GIT1	TK/EGFR
VEGF	HGSGADSDpYENpTQSGDPLLGLEGK	598	Y	GIT1	TK/EGFR
VEGF	SDSRSEpSPEPGpYVVTSSGLLLPVLLPR	1469	Y	ALS2	TK/EGFR
VEGF	SESVVpYADIR	263	Y	MPZL1	TK/EGFR
VEGF	HGSGADpSDpYENTQSGDPLLGLEGK	598	Y	GIT1	TK/EGFR
VEGF	THAVSVSETDDpYAEIIDEEDTpYTMPSTR	419	Y	FAK	TK/EGFR
VEGF	THAVSVSETDDpYAEIIDEEDTpYTMPSTR	429	Y	FAK	TK/EGFR
VEGF	LDpSSEMDHSENEDpYTMSSPLPGKK	1187	Y	PDS5B	TK/EGFR
VEGF	HGSGADSDpYENTQpSGDPLLGLEGK	598	Y	GIT1	TK/EGFR
VEGF	HGSGADSDpYENTQSGDPLLGLEGK	598	Y	GIT1	TK/EGFR
VEGF	LDSSEMDHpSENEDpYTMSSPLPGK	1187	Y	PDS5B	TK/EGFR
SFM	SDSRSEpSPEPGpYVVTSSGLLLPVLLPR	1469	Y	ALS2	TK/InsR
SFM	THAVSVSEpTDDYAEIIDEEDTpYTMPSTR	429	Y	FAK	TK/InsR
SFM	SDpSRSESPEPGpYVVTSSGLLLPVLLPR	1469	Y	ALS2	TK/InsR
VEGF	pSDSRSESPEPGpYVVTSSGLLLPVLLPR	1469	Y	ALS2	TK/InsR
VEGF	SSSSSGVPpYSPAIPNKR	249	Y	EXOC7	TK/InsR
VEGF	SDSRSEpSPEPGpYVVTSSGLLLPVLLPR	1469	Y	ALS2	TK/InsR
VEGF	THAVSVSETDDpYAEIIDEEDTpYTMPSTR	419	Y	FAK	TK/InsR
VEGF	THAVSVSETDDpYAEIIDEEDTpYTMPSTR	429	Y	FAK	TK/InsR
SFM	IGEGTpYGVVYK	15	Y	CDK3	TK/PDGFR
SFM	HGpSGADSDpYENTQSGDPLLGLEGK	598	Y	GIT1	TK/PDGFR
SFM	YVDSEGHLpYTVPIR	14	Y	CAV1	TK/PDGFR
SFM	IGEGpTpYGVVYK	15	Y	CDK3	TK/PDGFR
SFM	HGSGADSDpYENTQSGDPLLGLEGK	598	Y	GIT1	TK/PDGFR
VEGF	IGEGpTpYGVVYK	15	Y	CDK3	TK/PDGFR
VEGF	HGpSGADSDpYENTQSGDPLLGLEGK	598	Y	GIT1	TK/PDGFR
VEGF	HGSGADSDpYENpTQSGDPLLGLEGK	598	Y	GIT1	TK/PDGFR
VEGF	IGEGTpYGVVYK	15	Y	CDK3	TK/PDGFR
VEGF	HGSGADpSDpYENTQSGDPLLGLEGK	598	Y	GIT1	TK/PDGFR
VEGF	THAVSVSETDDpYAEIIDEEDTpYTMPSTR	419	Y	FAK	TK/PDGFR
VEGF	THAVSVSETDDpYAEIIDEEDTpYTMPSTR	419	Y	FAK	TK/PDGFR
VEGF	HGSGADSDpYENTQpSGDPLLGLEGK	598	Y	GIT1	TK/PDGFR
VEGF	HGSGADSDpYENTQSGDPLLGLEGK	598	Y	GIT1	TK/PDGFR
SFM	VVLGDGVQLPPGDpYSTTPGGTLFSTpTPGGTR	34	Y	EIF4EBP1	TK/VEGFR
SFM	ADVQLFMDDDSpYpSHHSGLEYADPEK	19	Y	CAV2	TK/VEGFR
SFM	ADVQLFMDDDSpYSHHpSGLEYADPEK	19	Y	CAV2	TK/VEGFR
SFM	ADVQLFMDDDpSpYSHHpSGLEYADPEK	19	Y	CAV2	TK/VEGFR
SFM	ADVQLFMDDDSpYpSHHpSGLEYADPEK	19	Y	CAV2	TK/VEGFR
SFM	ADVQLFMDDDpSpYpSHHSGLEYADPEK	19	Y	CAV2	TK/VEGFR
SFM	ADVQLFMDDDpSpYSHHSGLEYADPEK	19	Y	CAV2	TK/VEGFR
SFM	FHpYDNTAGISQYLQNSK	1214	Y	KDR	TK/VEGFR
SFM	FHpYDNTAGISQYLQNSK	1214	Y	KDR	TK/VEGFR
VEGF	ADVQLFMDDDSpYSHHpSGLEYADPEK	19	Y	CAV2	TK/VEGFR
VEGF	ADVQLFMDDDSpYSHHSGLEYADPEK	19	Y	CAV2	TK/VEGFR
VEGF	ADVQLFMDDDpSpYSHHpSGLEYADPEK	19	Y	CAV2	TK/VEGFR
VEGF	ADVQLFMDDDSpYpSHHpSGLEYADPEK	19	Y	CAV2	TK/VEGFR
VEGF	VVLGDGVQLPPGDpYSTTPGGTLFSTpTPGGTR	34	Y	EIF4EBP1	TK/VEGFR
VEGF	ADVQLFMDDDpSpYpSHHSGLEYADPEK	19	Y	CAV2	TK/VEGFR
VEGF	THAVSVSETDDpYAEIIDEEDTpYTMPSTR	419	Y	FAK	TK/VEGFR
VEGF	THAVSVSETDDpYAEIIDEEDTpYTMPSTR	419	Y	FAK	TK/VEGFR
VEGF	LDpSSEMDHSENEDpYTMSSPLPGKK	1187	Y	PDS5B	TK/VEGFR
VEGF	FHpYDNTAGISQYLQNSK	1214	Y	KDR	TK/VEGFR
VEGF	FHpYDNTAGISQYLQNSK	1214	Y	KDR	TK/VEGFR
VEGF	ADVQLFMDDDSpYSHHpSGLEpYADPEK	19	Y	CAV2	TK/VEGFR
VEGF	LDSSEMDHpSENEDpYTMSSPLPGK	1187	Y	PDS5B	TK/VEGFR
VEGF	ADVQLFMDDDpSpYSHHSGLEYADPEK	19	Y	CAV2	TK/VEGFR

Another of the protein kinases which was identified in all three samples (table 5.3), and stands out due its known links to adhesion and growth factor signalling is Src. Predicted Src phosphorylation sites increased in both the TCL adhesome-filtered and TCL analysis; those identified in the adhesome-filtered SFM and VEGF-treated samples are listed in table 5.6. Only low numbers were present in the isolated IAC sample to be able to detect an increase (table 5.1). Src is a protein kinase involved in a range of signalling pathways. For example, it has well known roles in integrin-mediated adhesion, and there is some evidence linking it with VEGF signalling and VEGF-induced angiogenesis (table 1.1). However, there are very limited studies that suggest a role of Src in VEGF-adhesion crosstalk (Wang et al. 2009). To increase confidence that Src kinase activity is increased in these samples, further data analysis was performed. The phosphopeptides predicted to be phosphorylated, along with their quantification data for both Progenesis QI ion intensity analysis and spectral counting are shown in table 5.7. Although not all identified phosphosites were increased, these data suggest a role for Src kinase in VEGF-adhesion crosstalk, and in particular paxillin, FAK and GIT1 as substrates.

Table 5.6. Phosphopeptides identified as substrates for Src kinase in iGPS analysis of total cell lysate adhesome filtered phosphoproteomic data. All identified unique phosphopeptides, from proteins in the master adhesome, literature-curated adhesome HUVEC dataset generated in chapter 3, for SFM (2332) and VEGF (2368) conditions were input into the iGPS tool. Table shows 16 phosphopeptides (6 SFM unique phosphopeptides and 9 VEGF unique phosphopeptides) which were identified as substrates for Src kinase. Table indicates the input phosphopeptide in PhosPep format, residue number and amino acid (Y/S/T) predicted to be phosphorylated by the listed kinase and peptide gene name. Rows are colour coordinated blue or pink for peptides in the SFM and VEGF conditions respectively.

Sample	Phosphopeptide	Residue	Y/S/T	GN	Kinase
SFM	THAVSVSEpTDDYAEIIDEEDTpYTMPSTR	429	Y	FAK	TK/Src
VEGF	THAVSVSETDDpYAEIIDEEDTpYTMPSTR	419	Y	FAK	TK/Src
SFM	HGpSGADSDpYENTQSGDPLLGLEGK	598	Y	GIT1	TK/Src
SFM	HGSGADSDpYENTQSGDPLLGLEGK	598	Y	GIT1	TK/Src
VEGF	HGpSGADSDpYENTQSGDPLLGLEGK	598	Y	GIT1	TK/Src
VEGF	HGSGADSDpYENpTQSGDPLLGLEGK	598	Y	GIT1	TK/Src
VEGF	HGSGADpSDpYENTQSGDPLLGLEGK	598	Y	GIT1	TK/Src
VEGF	HGSGADSDpYENTQpSGDPLLGLEGK	598	Y	GIT1	TK/Src
VEGF	HGSGADSDpYENTQSGDPLLGLEGK	598	Y	GIT1	TK/Src
SFM	VGEEEHVpYSFPNK	118	Y	PXN	TK/Src
VEGF	VGEEEHVpYSFPNK	118	Y	PXN	TK/Src
VEGF	FIHQQPQSSpSPVpYGSSAK	88	Y	PXN	TK/Src
SFM	TGDLGIPPNPEDRpSPSPEPIpYNSEGK	87	Y	SF1	TK/Src
VEGF	TGDLGIPPNPEDRpSPSPEPIpYNSEGK	87	Y	SF1	TK/Src
SFM	VQIPVSRPDPEPVpSDNEEDSpYDEEIHD	132	Y	TJP1	TK/Src
VEGF	VQIPVSRPDPEPVpSDNEEDSpYDEEIHD	132	Y	TJP1	TK/Src

Table 5.7. Proteins and phosphorylated residue identified as substrates for Src kinase in iGPS analysis of total cell lysate adhesome filtered phosphoproteomic data. All identified unique phosphopeptides, from proteins in the master adhesome, literature-curated adhesome HUVEC dataset generated in chapter 3, for SFM (2332) and VEGF (2368) conditions were input into the iGPS tool. Table shows 7 phosphosites which were identified as substrates for Src kinase. Table indicates gene names and phosphorylated residue, the number of unique phosphopeptides identified in the SFM and VEGF datasets and any quantification data available from Progenesis QI ion intensity and analysis and spectral counting (chapter 4).

	Number of unique phosphopeptides		Quantification	
Gene name/phosphorylated reside	SFM	VEGF	Progenesis QI	Spectral counting
FAK/Y397	1	0	Not identified	SFM: 0, VEGF: 1
FAK/Y407	0	2	1.45-fold increase	SFM: 0, VEGF: 1
GIT1/Y598	2	5	1.36-fold increase	SFM: 7, VEGF: 14
SF1/Y86	1	1	1.04-fold increase	SFM: 8, VEGF: 5
PXN/Y118	1	2	Not identified	SFM: 9, VEGF: 4
PXN/Y88	0	1	Not identified	SFM: 0, VEGF: 1
TJP1/Y132	1	1	Not identified	SFM: 2, VEGF: 0

5.3 Functional assay optimisation

Analysis of mass spectrometry datasets (section 5.2) was to be used to identify IAC protein candidates that are important in VEGF-induced signalling and associated downstream effects. However, to investigate the effects of these proteins, for example using protein inhibitor or knockdown studies, assays are required to investigate their effect on cell processes. ERK phosphorylation has been used as a readout of VEGF signalling, and been shown to increase significantly upon VEGF treatment of HUVECs (figure 4.1). Western blotting of ERK phosphorylation can be used to investigate how adhesion-associated components of interest affect canonical VEGF signalling pathways. In addition, VEGF-induced migration is a common assay used to investigate the effects of protein inhibition or knockdown. To do this in relation to adhesion signalling and the mass spectrometry datasets generated in this study, an assay was developed in which VEGF-induced migration could be studied in an IAC-dependent manner.

5.3.1 Optimisation of VEGF-induced HUVEC migration assays

To investigate VEGF-induced migration, a scratch wound migration assay was developed. A range of different conditions were tested to ensure optimal conditions were employed. For typical scratch wound assays, cells are plated overnight in complete (serum-containing) medium, prior to scratching, to generate a dense cell monolayer (Cory 2011;Lampugnani 1999). However, the aim of the migration assay in this study, in line with all previous VEGF experiments, was to see the effects in a fibronectin-induced IAC-dependent manner. Using a minimal spreading time would decrease the amount of ECM proteins that can be produced and deposited by cells themselves, and plating cells in serum-free medium would decrease deposition of ECM components from serum, keeping adhesion fibronectin-specific (Hayman and Ruoslahti 1979). In addition, the time that cells should remain in serum-free medium should be kept minimal to prevent cell death (Gorman et al. 1996). Therefore, to determine the optimal plating conditions for this assay, HUVECs were plated for 3 hours in serum-free medium or 16 hours in full EGM medium, on fibronectin coated 96-well plates. In addition, a poly-lysine control was included for both plating times. Scratches were then introduced, SFM or VEGF added, and images taken every hour for a minimum of 16 hours.

The first factor that was considered was optimal plating density for the 3 hour condition, to result in confluent layer of cells in which a scratch could be introduced. 90,000, 70,000 or 45,000 cells were plated per well, and SFM or VEGF added. VEGF-induced migration was optimal at the higher plating densities (70,000 and 90,000 cells per well, figure 5.16). As it is preferred that the density of the monolayer is high prior to scratching, 90,000 cells per well was chosen as the optimal confluency for a scratch that could be used to study VEGF-induced migration. The optimal VEGF concentration to induce migration was also investigated using the 3 hour plating time; migration was optimal at 6.25 ng/mL VEGF (figure 5.17a). Representative images of cells under this condition were displayed,

for visualisation of VEGF-induced cell migration (figure 5.18). For the 16 hour condition, a lower level of migration was observed, and although an increase in migration was apparent upon VEGF treatment (figure 5.17b), no significant differences were identified until 16 hours, when cells began to appear unhealthy. This optimisation experiment suggests that the three hour plating condition, the preferred method for the purpose of this assay, is suitable to detect VEGF-induced migration. When plated on poly-lysine, overall migration was reduced compared to the VEGF-treated conditions (figure 5.19). In addition, on poly-lysine for 3 hours there was no induction following VEGF treatment, whereas although reduced, a VEGF-induced increase in migration was apparent in the overnight poly-lysine condition. These optimisation experiments suggest that the VEGF-induced increase in migration for the 3 hour condition was dependent on fibronectin-induced adhesion. Therefore the 3 hour condition, using a VEGF concentration of 6.25 ng/mL was used to investigate the effects of VEGF induced migration in this study.

To investigate further the role of integrins in VEGF-induced migration, preliminary studies were performed to test the effect of two integrin blocking antibodies, anti-integrin β1 and anti-integrin α5. With β1 inhibition, migration decreased for both SFM and VEGF conditions; although a VEGF-induced increase was still apparent (figure 5.20a). Upon α5 integrin inhibition, the VEGF-induced increase in migration was lost, although overall migration showed little difference (figure 5.20b). However, it is important to note for these experiments that none of the changes were statistically significant and only a limited number of replicates were performed. These results suggest an important role for integrins in HUVEC migration, and in particular a dependence of α5 integrin in VEGF-induced migration, although due to the limited replicates performed here, further studies are required to confirm this observation.

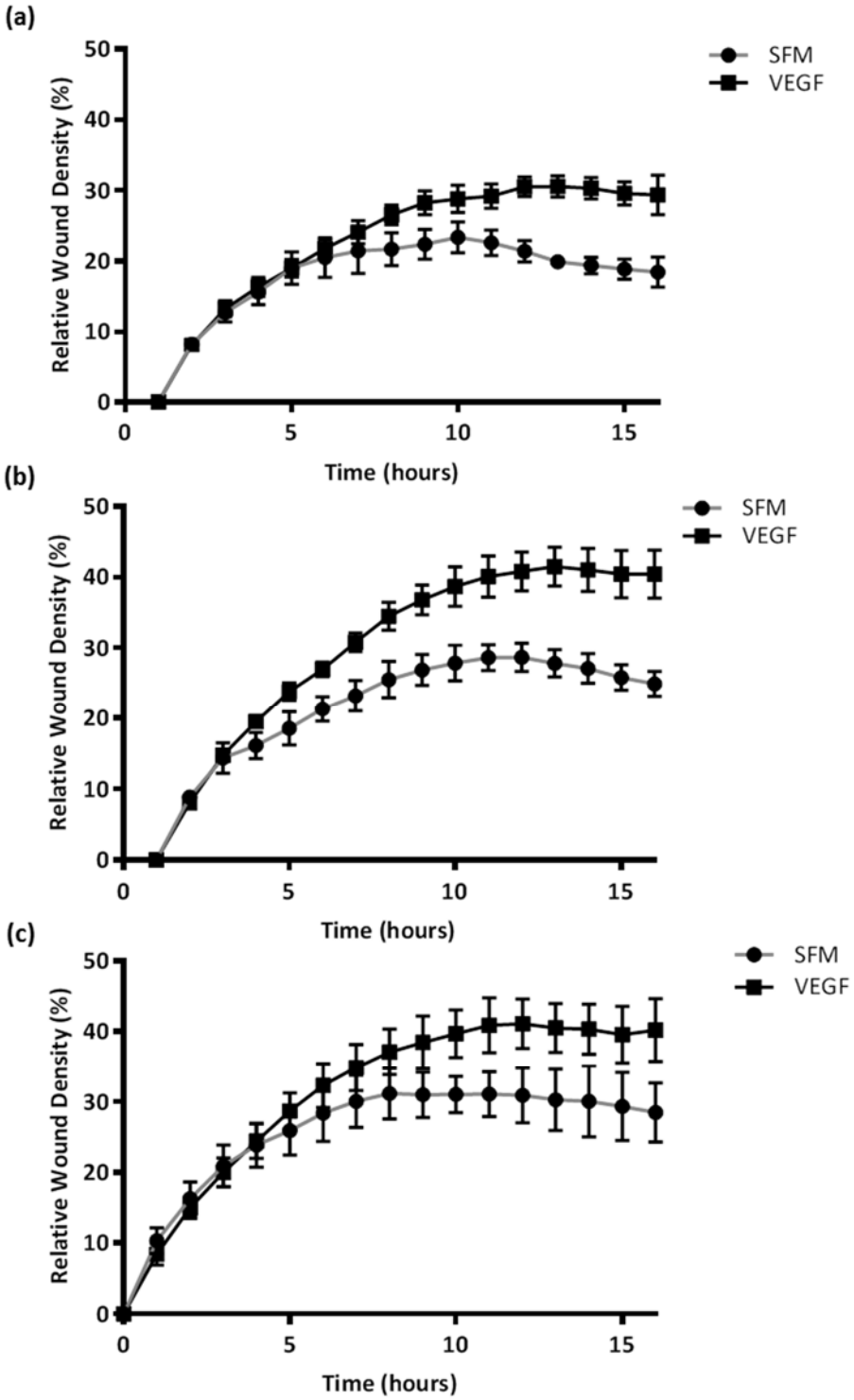

Figure 5.16. Measurement of scratch wound closure of HUVECs plated at different densities on fibronectin, and treated with SFM or VEGF. (a) 45,000, (b) 70,000 or (c) 90,000 HUVECs per well were plated for 3 hours in SFM on fibronectin coated 96-well plates. Scratches were then introduced, test solution (VEGF at 25 ng/mL or SFM) added and images taken every hour for 16 hours. Data is displayed as relative wound density (%) at each time point, ± SEM, n=3 wells per experiment.

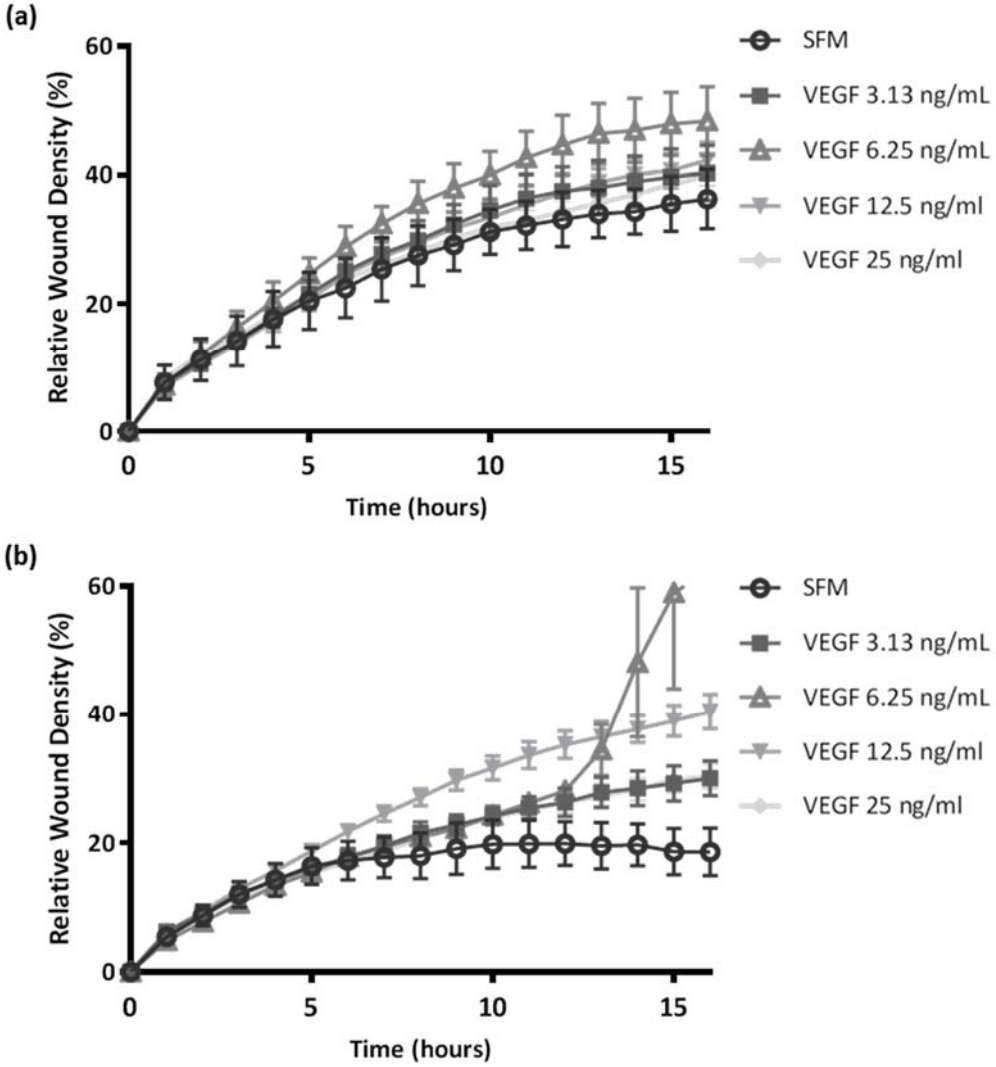

Figure 5.17. Measurement of scratch wound closure of HUVECs plated on fibronectin, and treated with SFM or a range of VEGF concentrations. HUVECs were plated for (a) 3 hours in SFM or (b) 16 hours in full EGM medium, on fibronectin coated 96-well plates. Scratches were then introduced, test solution (VEGF or SFM at a range of concentrations) added and images taken every hour for 16 hours. Data is displayed as relative wound density (%) at each time point, ± SEM, n=3-6 wells per experiment, 2 experiments showed the same trend. $p<0.05$ (two-way ANOVA, SFM vs VEGF conditions) only for 3 hour fibronectin plated condition SFM vs VEGF 6.25 ng/mL, from 8 hours onwards.

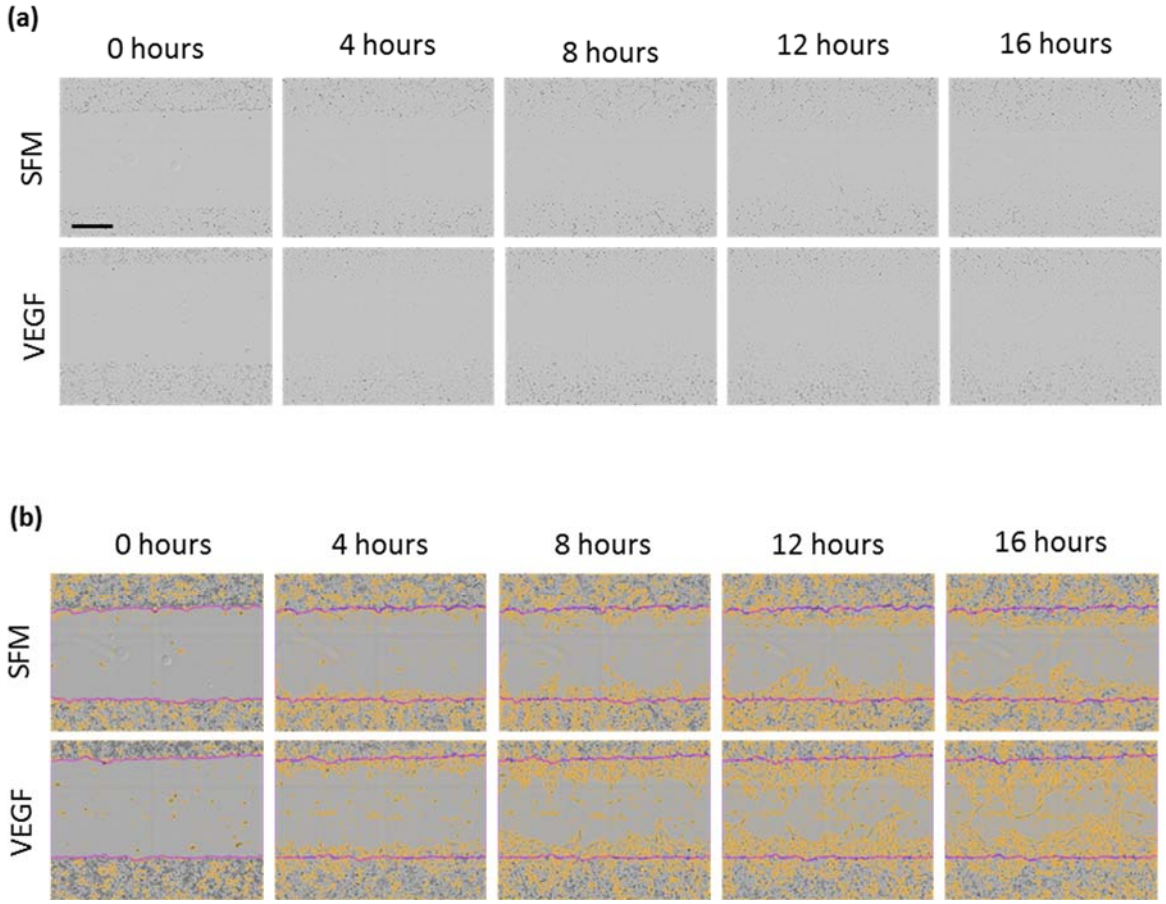

Figure 5.18. Representative images of scratch wound closure of HUVECs plated on fibronectin, and treated with SFM or VEGF. HUVECs were plated for 3 hours in SFM, on fibronectin coated 96-well plates. Scratches were then introduced, test solution (SFM or 6.25 ng/mL VEGF) added and images taken every hour for 16 hours. Representative images of one well per condition are shown at at 0, 4, 8, 12 and 16 hours. (a) original phase images, (b) Images from IncuCyte Scratch Wound Processing data analysis, initial scratch wound position is represented by purple lines, confluence mask areas are outlined in orange. Scale bar = 300 µm.

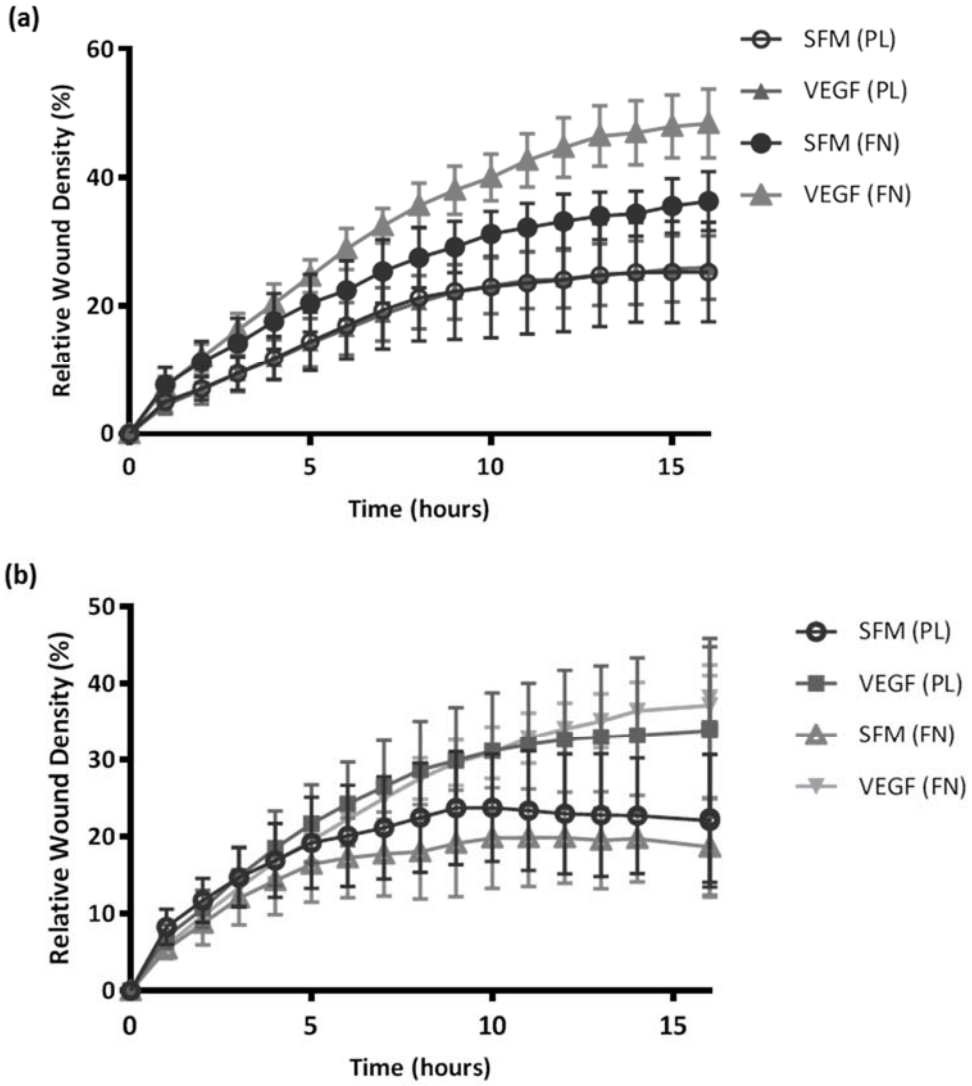

Figure 5.19. Measurement of scratch wound closure of HUVECs plated on fibronectin or poly-lysine treated with SFM or VEGF. HUVECs were plated for (a) 3 hours in SFM or (b) 16 hours in full EGM medium, on fibronectin (FN) or poly-lysine (PL) coated 96-well plates. Scratches were then introduced, test solution (SFM or 6.25 ng/mL VEGF) added and images taken every hour 16 hours. Data is displayed as relative wound density (%) at each time point, ± SEM, n=3-6 wells per experiment. (a) $p<0.05$ (two-way ANOVA) only for fibronectin plated condition SFM vs VEGF, from 8 hours onwards. (b) $p<0.05$ (two-way ANOVA) for fibronectin plated condition SFM vs VEGF from 10 hours onwards, and for poly-lysine plated condition SFM vs VEGF from 12 hours onwards.

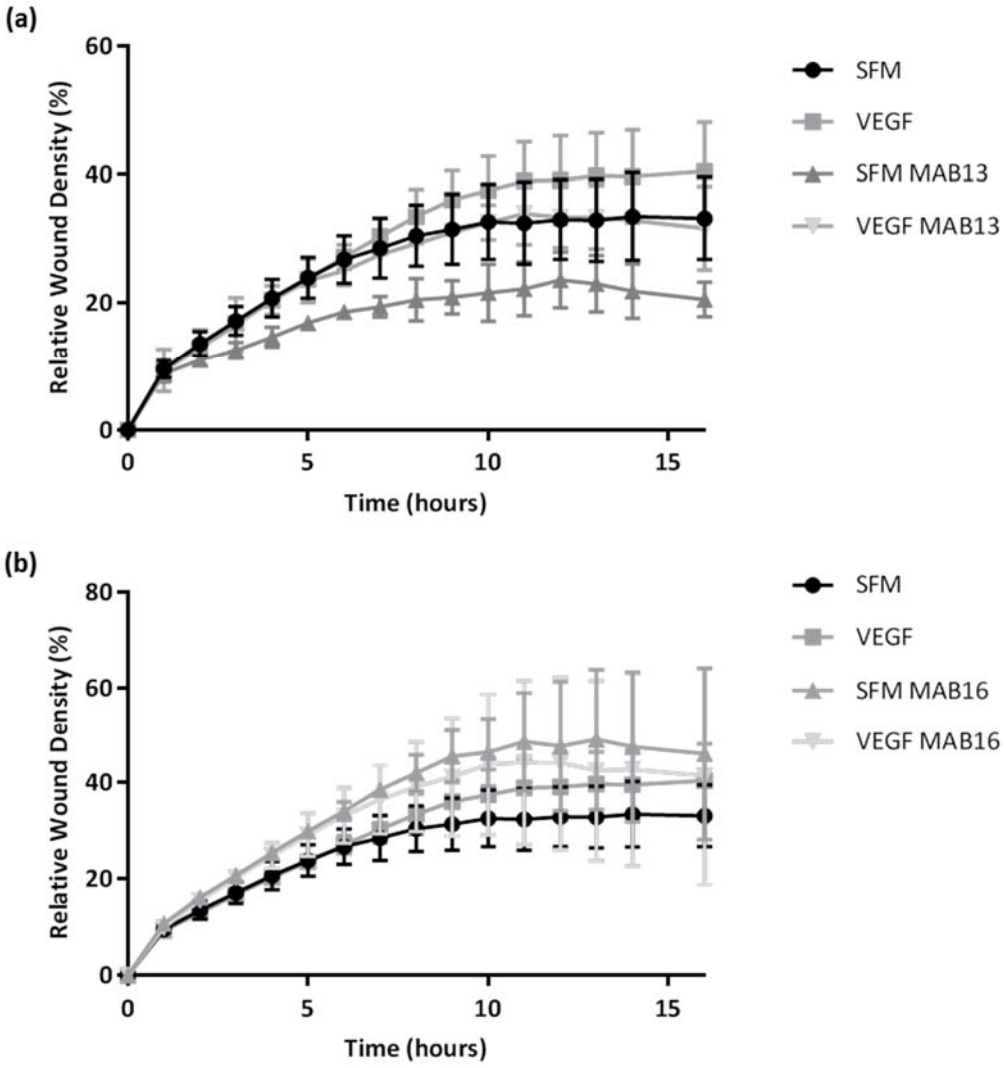

Figure 5.20. Measurement of scratch wound closure of HUVECs plated on fibronectin treated with SFM or VEGF and integrin blocking antibodies. HUVECs were plated for 3 hours in SFM on fibronectin coated to 96-well plates. Scratches were then introduced, test solution SFM or VEGF with (a) MAB13 (β1 blocking antibodies, 10 µg/mL) or (b) MAB16 (α5 blocking antibodies, 10 µg/mL). Images were taken every hour for 16 hours. Data is displayed as relative wound density (%) at each time point, ± SEM, n=2-6 wells per experiment, 1 or 2 experiments showed the same trend.

5.4 Investigation into the role of Src and FAK kinase in VEGF-adhesion crosstalk

As Src kinases have been identified as potential mediators of VEGF-adhesion crosstalk using kinase prediction analysis, their role was investigated further using a Src kinase inhibitor. Src function was disturbed using the small molecule Src kinase inhibitor saracatinib (AZD0530; Src [i]). In addition, as FAK is linked closely with Src kinase signalling, and has a well-studied role in VEGF-adhesion crosstalk (Brunton and Frame 2008), FAK inhibition using AZ13256675 (FAK [i]) was performed alongside Src inhibition experiments.

Initial experiments were performed to determine the concentration of Src and FAK inhibitor required to inhibit Src and FAK catalytic activity, respectively. HUVECs were plated on fibronectin-coated plates for 1 hour prior to addition of test solutions (dilutions of the inhibitors AZD0530 (Src [i]), AZ13256675 (FAK [i]) or an equivalent volume of DMSO) which were added for 1 hour, following which total cell lysates were collected for analysis. Untreated cells spread on fibronectin for two hours were used to detect maximal kinase activity. For Src kinase inhibition, activity was quantified by western blotting for the Src substrate paxillin-Y118, and the Src activation site Src-Y416 (figure 5.21a & b). Paxillin-Y118 and Src-Y416 were normalised against total paxillin and Src, respectively, in each condition. For both phosphorylation sites tested, inhibition was optimal at 10 μM, the highest concentration tested (figure 5.21c & d). FAK activity was quantified by western blotting lysates for the FAK autophosphorylation residue, FAK-Y397 (figure 5.22a). FAK-Y397 was normalised against total FAK (figure 5.22b). Again, inhibition was maximal at 10 μM, the highest concentration used.

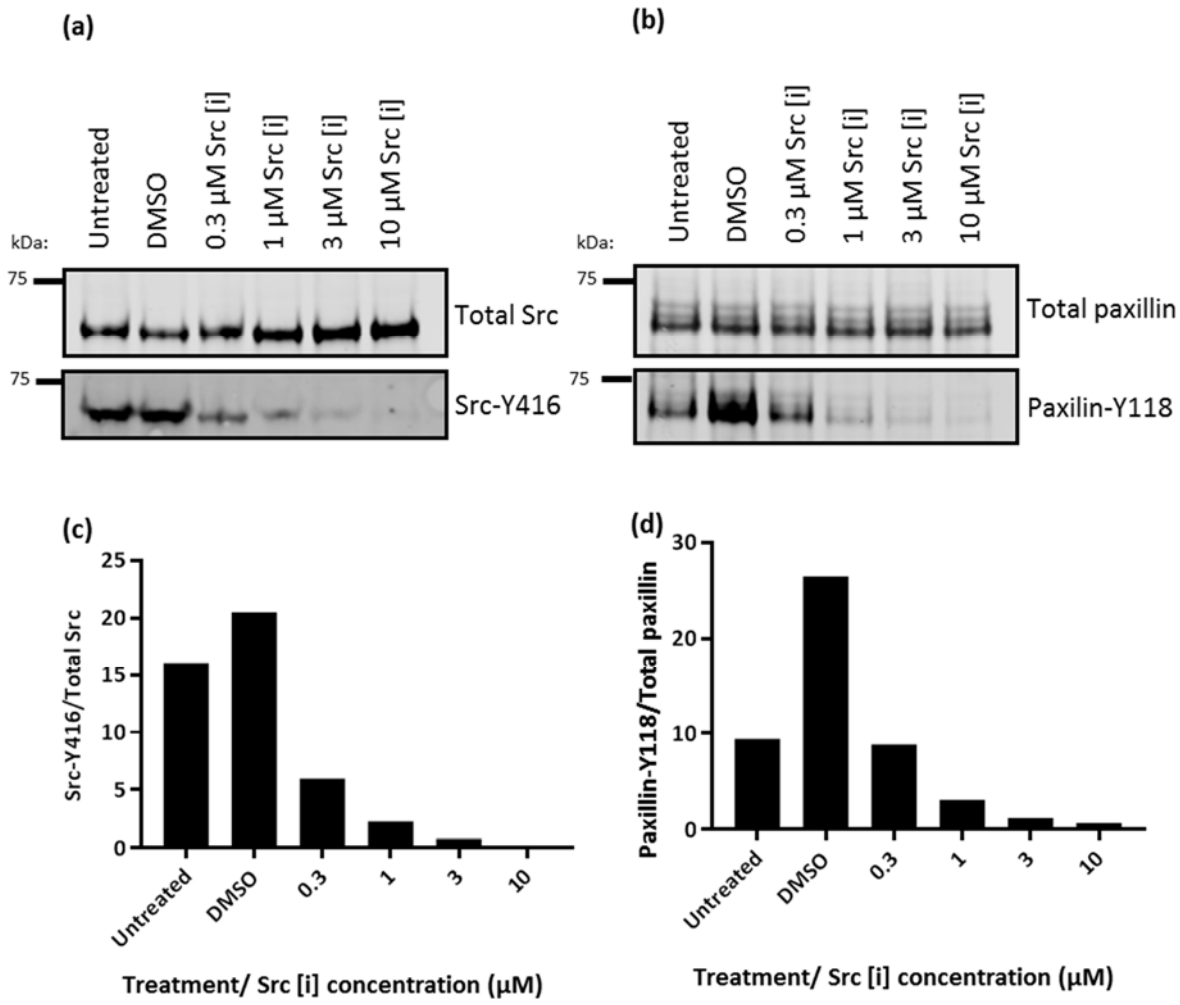

Figure 5.21. Inhibition of Src activity by inhibition in HUVECs. HUVECs were spread on fibronectin coated plates for 1 hour and treated with DMSO or Src inhibitor at a range of concentrations for 1 hour using half-log dilutions. Untreated cells spread on fibronectin for 2 hours were used as an additional control. Src-Y416 and paxillin-Y118 were used to asses Src catalytic activity. Western blotting of (a) Src-Y416 and (b) paxilin-Y118 phosphorylation sites in total cell lysate samples. Molecular weight values (kDa) are displayed to the left of each blot. (c,d) Quantification of western blot membranes; (c) Src-Y416 and (d) paxillin-Y118 phosphorylation were normalised to total Src or paxillin protein levels respectively, n = 1.

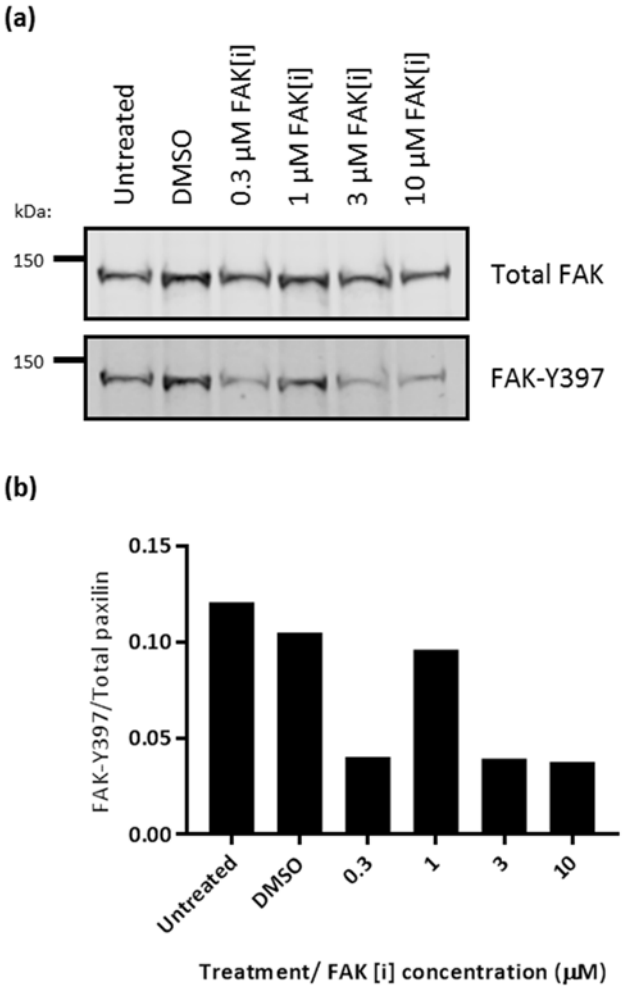

Figure 5.22. Inhibition of FAK activity by inhibition in HUVECs. HUVECs were spread on fibronectin coated plates for 1 hour and treated with DMSO or FAK inhibitor at a range of concentrations for 1 hour using half-log dilutions. Untreated cells spread on fibronectin for 2 hours were used as an additional control. FAK-Y397 was used to asses FAK catalytic activity. (a) Western blotting of FAK-Y397 in total cell lysates. Molecular weight values (kDa) are displayed to the left of each blot. (b) Quantification of western blot membranes; FAK-Y397 phosphorylation levels were normalised to total FAK protein levels, n = 1.

5.4.1 Role of Src and FAK kinase in VEGF signalling

Following determination that 10 µM Src [i] or FAK [i] can effectively inhibit Src and FAK activity, respectively, the effect of inhibition on VEGF signalling was examined. HUVECs plated on fibronectin-coated plates for one hour were treated with DMSO, 10 µM Src [i] or 10 µM FAK [i]. Untreated cells spread on fibronectin for two hours were used as an additional control. To be consistent with previous experiments involving VEGF treatment, following the two hour incubation time HUVECs were treated with SFM or VEGF (25 ng/mL) for 7.5 minutes. Total cell lysates were collected and assessed by western blotting. In all experiments, reduction of paxillin-Y118 was confirmed in the Src [i] samples, indicating inhibition (figure 5.23a). No significant difference was detected in VEGF-induced phospho-ERK fold change upon Src [i] and FAK [i] inhibition (figure 5.23b, c), suggesting that inhibition has no effect on VEGF signalling via the ERK pathway.

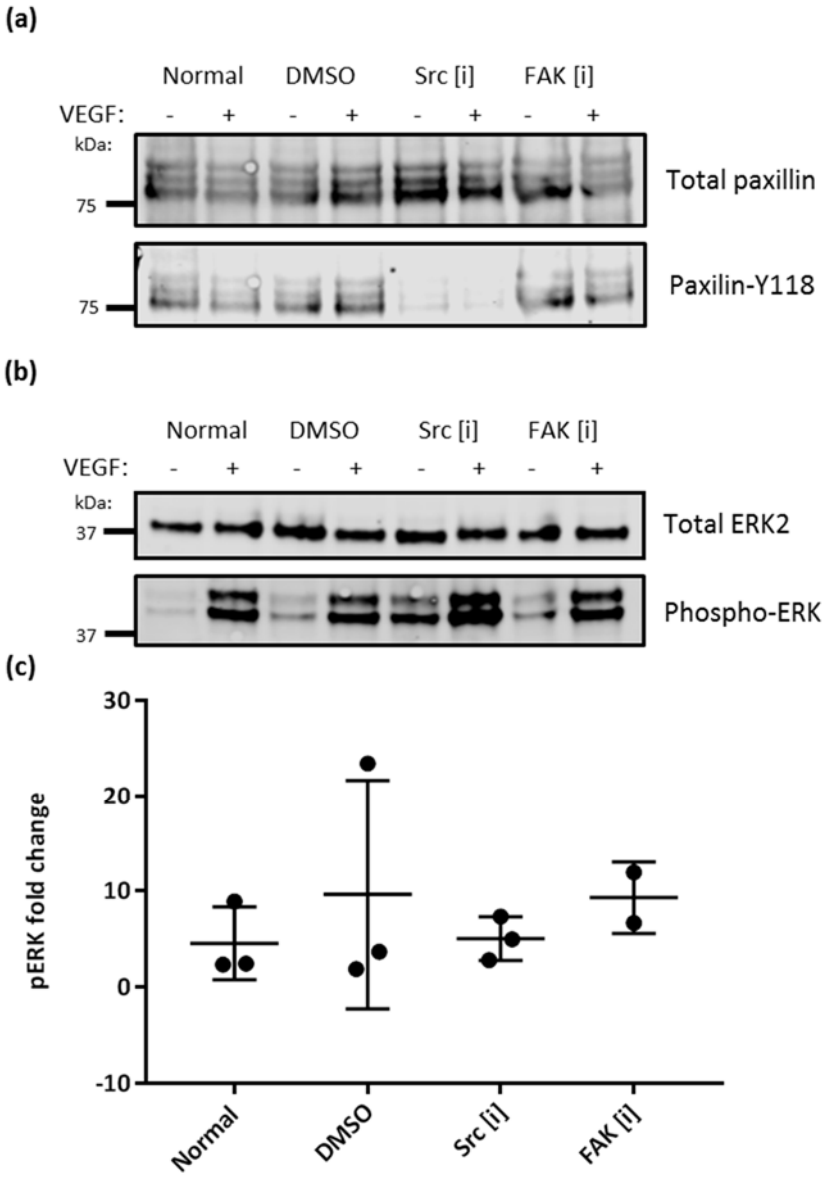

Figure 5.23. Effect of Src and FAK inhibition on VEGF signalling in HUVECs. HUVECs were spread on fibronectin coated plates for 1 hour and treated with DMSO, Src or FAK inhibitor at 10 μM for 1 hour. Untreated cells spread on fibronectin for 2 hours were used as an additional control. (a) Paxillin-Y118 was used to asses Src catalytic activity, representative western blot shown, data are representative of three experiments. Molecular weight values (kDa) are displayed to the left of each blot. (b) Western blot analysis of total ERK2 and phospho-ERK1/2, data are representative of three experiments. Molecular weight values (kDa) are displayed to the left of each blot. (c) Phospho-ERK fold change: phospho-ERK band intensity values were normalised to total ERK band intensity values and fold change calculated (VEGF/SFM), n=3 or 2, plotted as individual values, displaying mean and standard deviation.

5.4.2 Role of Src and FAK kinase in VEGF-induced HUVEC migration

Preliminary experiments were performed to investigate the effect of Src and FAK inhibition on VEGF-induced cell migration. The optimal conditions for VEGF-induced migration of HUVECs, as determined in section 5.3. were employed, with a Src and FAK treated condition, and DMSO control. Src inhibition reduced overall HUVEC migration (figure 5.24). However, Src [i] reduced VEGF-induced migration, supporting previous phosphoproteomic data from this study that suggested VEGF induces IAC phosphorylation, and kinase prediction analysis suggesting Src is important in these phosphorylation events. In contrast, FAK inhibition either increased or resulted in no change in overall HUVEC migration (figure 5.25). In addition, FAK [i] treatment reduced VEGF-induced migration. These results suggest a role of FAK in VEGF-induced migration and VEGF-adhesion crosstalk. Furthermore, the combined effect of Src and FAK inhibition further reduced overall migration, although there still appeared to be a small VEGF-induced effect (figure 5.26). These results suggest that by preventing functioning of both kinases, which form a signalling complex and have overlapping functions (Brunton and Frame 2008;Kim et al. 2009;Sulzmaier et al. 2014), has a greater effect than inhibiting those individually.

The role of two other kinases, MEK and PKC which have well known roles in VEGF signalling, were also investigated in relation to VEGF signalling. Preliminary experiments were performed, where inhibition of MEK and PKC both had effects of overall migration (figure 5.27 & 5.28), although these effects varied between experiments. Blocking the ERK pathway using MEK inhibitor (figure 5.27) prevented VEGF-induced migration, confirming a role for this pathway. PKC inhibition also reduced VEGF-induced migration. The effects of blocking these known VEGF signalling protein kinases (MEK and PKC) on VEGF-induced migration provide further confidence that the similar results shown by Src and FAK inhibition suggest an important role for these kinases in VEGF-induced migration.

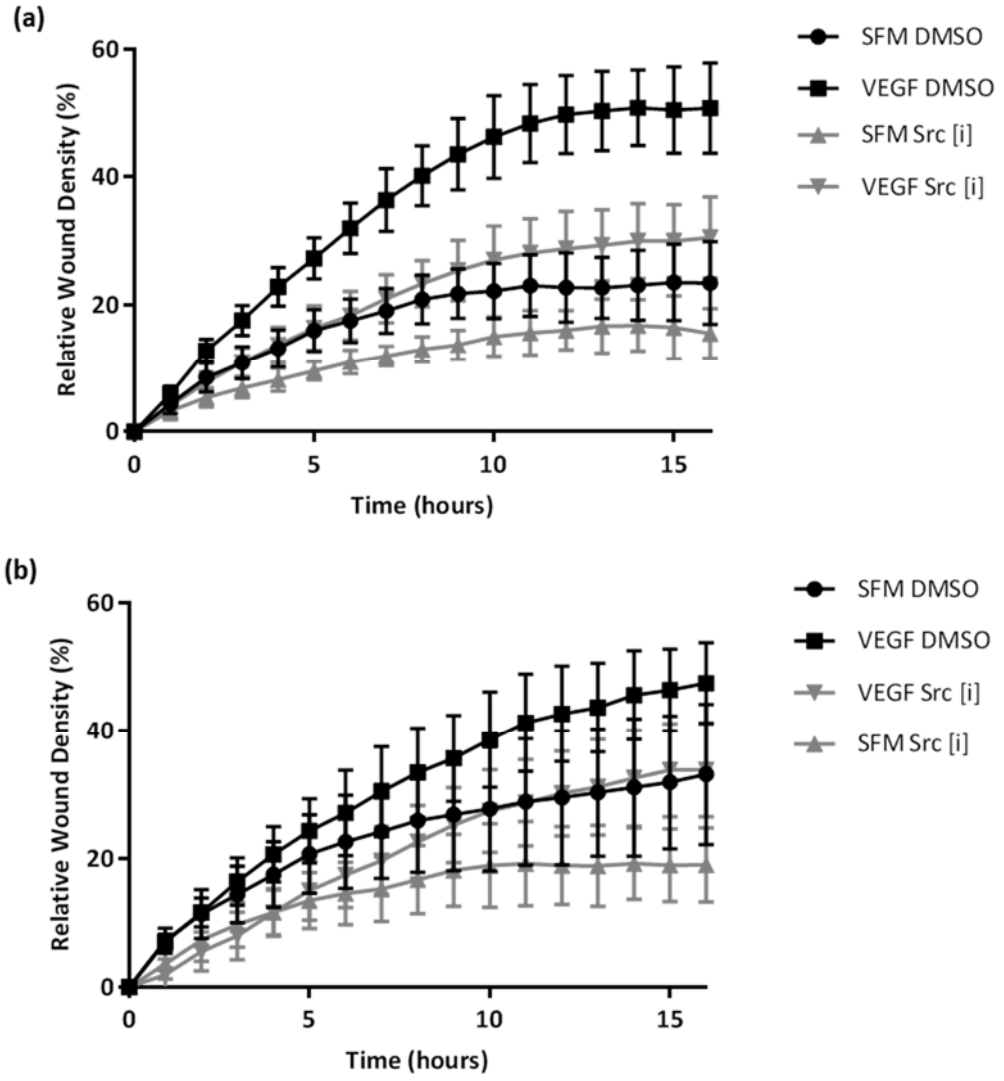

Figure 5.24. Measurement of scratch wound closure of HUVECs plated on fibronectin, and treated with SFM/VEGF and DMSO/Src inhibitor. HUVECs were plated for 3 hours in SFM, on fibronectin coated 96-well plates. Scratches were then introduced, test solution (VEGF or SFM with DMSO or Src [i]) added and images taken every hour for 16 hours. Data is displayed as relative wound density (%) at each time point, ± SEM, n=6 wells per experiment, 2 independent experiments shown. (a) $p<0.05$ (two-way ANOVA), comparing SFM DMSO vs VEGF DMSO conditions and SFM Src [i] vs VEGF Src [i]) from 11 hours onwards. (b) $p<0.05$ (two-way ANOVA), comparing SFM DMSO vs VEGF DMSO conditions from 3 hours onwards, and SFM Src [i] vs VEGF Src [i] from 5 hours onwards.

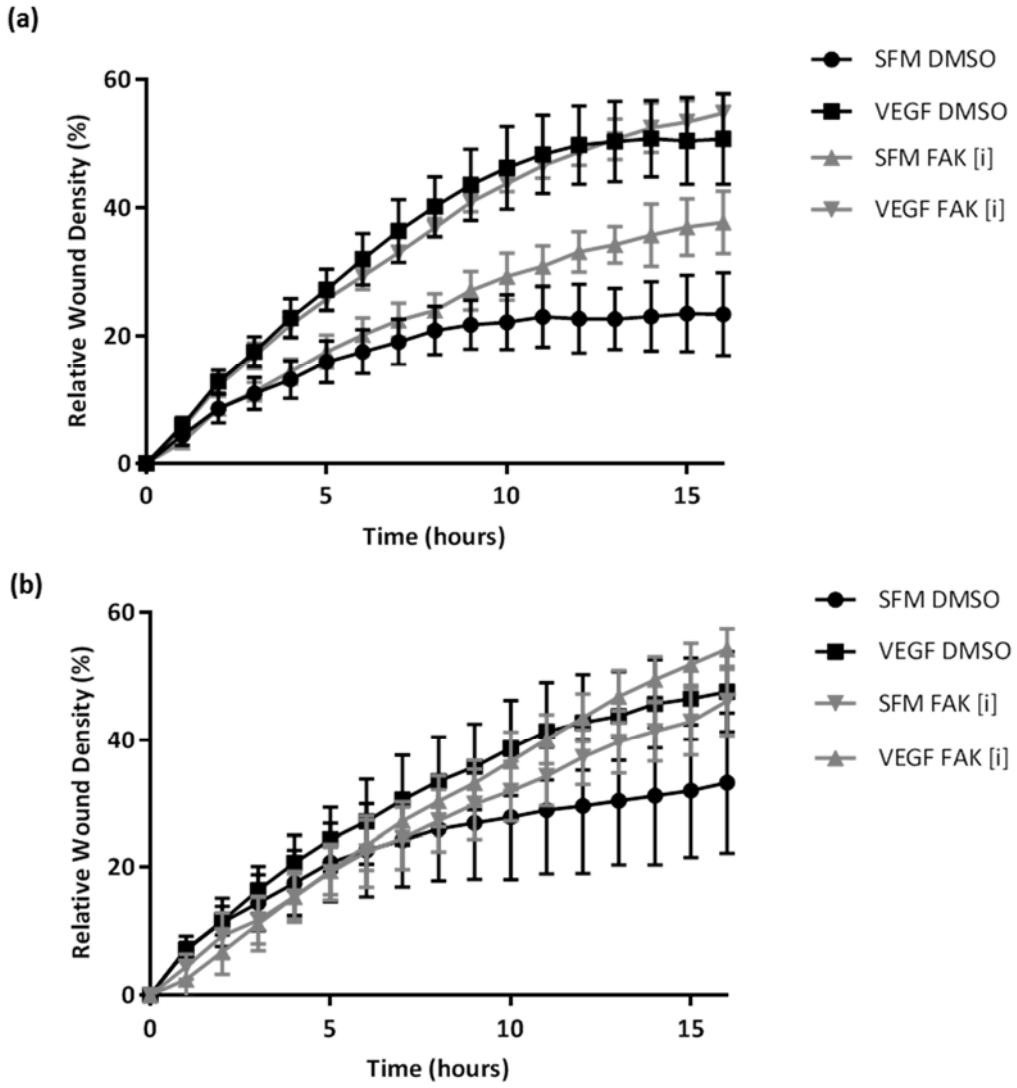

Figure 5.25. Measurement of scratch wound closure of HUVECs plated on fibronectin, and treated with SFM/VEGF and DMSO/FAK inhibitor. HUVECs were plated for 3 hours in SFM, on fibronectin coated 96-well plates. Scratches were then introduced, test solution (VEGF or SFM with DMSO or FAK [i]) added and images taken every hour for 16 hours. Data is displayed as relative wound density (%) at each time point, ± SEM, n=6 wells per experiment, 2 independent experiments shown. (a) $p<0.05$ (two-way ANOVA), comparing SFM DMSO vs VEGF DMSO conditions from 9 hours onwards and SFM FAK [i] vs VEGF FAK [i] from 11 hours onwards. (b) $p<0.05$ (two-way ANOVA), comparing SFM DMSO vs VEGF DMSO conditions from 3 hours onwards, and SFM FAK [i] vs VEGF FAK [i] from 4 hours onwards.

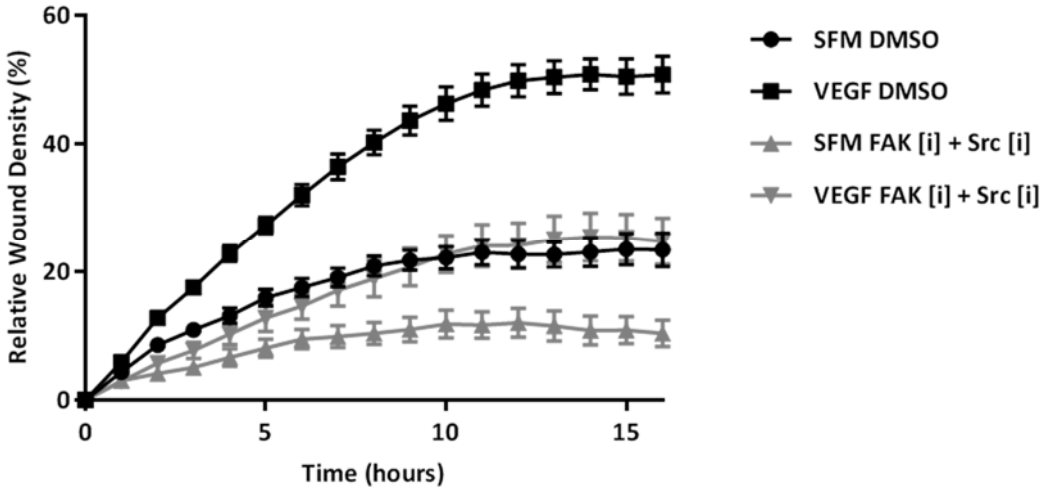

Figure 5.26. Measurement of scratch wound closure of HUVECs plated on fibronectin, and treated with SFM/VEGF and DMSO or combined FAK and Src inhibitors. HUVECs were plated for 3 hours in SFM, on fibronectin coated 96-well plates. Scratches were then introduced, test solution (VEGF or SFM with DMSO or combined Src + FAK [i]) added and images taken every hour for 16 hours. Data is displayed as relative wound density (%) at each time point, ± SEM, n= 5-6 wells per experiment, 1 individual experiment performed. $p<0.05$ (two-way ANOVA), comparing SFM DMSO vs VEGF DMSO conditions from 4 hours onwards and SFM Src + FAK [i] vs VEGF Src + FAK [i] from 8 hours onwards.

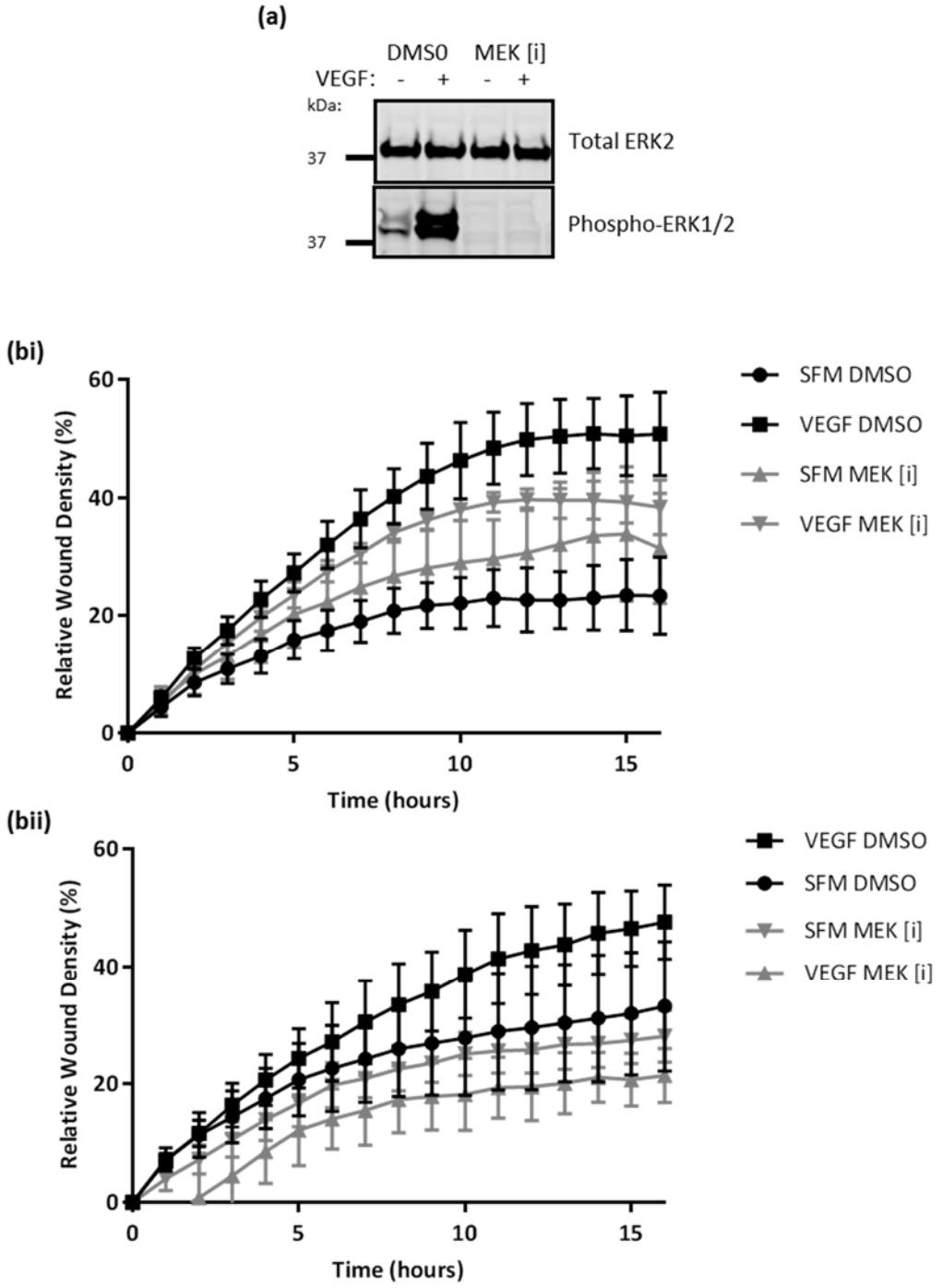

Figure 5.27. Inhibition of MEK activity in HUVECs and measurement of scratch wound closure of HUVECs plated on fibronectin, and treated with SFM/VEGF and DMSO/MEK inhibitor. (a) HUVECs were spread on fibronectin coated plates for 1 hour and treated with DMSO or MEK [i] at 1 µg/mL for 1 hour, data show western blot analysis of total ERK2 and phospho-ERK1/2. Molecular weight values (kDa) are displayed to the left of each blot. (b) Scratch wound migration assay: HUVECs were plated for 3 hours in SFM, on fibronectin coated 96-well plates. Scratches were then introduced, test solution (VEGF or SFM with DMSO or MEK [i]) added and images taken every hour for a minimum of 16 hours. Data is displayed as relative wound density (%) at each time point, ± SEM, n=5-6 wells per experiment, 2 independent experiments shown. (bi) $p<0.05$ (two-way ANOVA), comparing SFM DMSO vs VEGF DMSO conditions from 9 hours onwards and SFM MEK [i] vs VEGF MEK [i] from 11 hours onwards. (bii) $p<0.05$ (two-way ANOVA), comparing SFM DMSO vs VEGF DMSO conditions from 4 hours onwards.

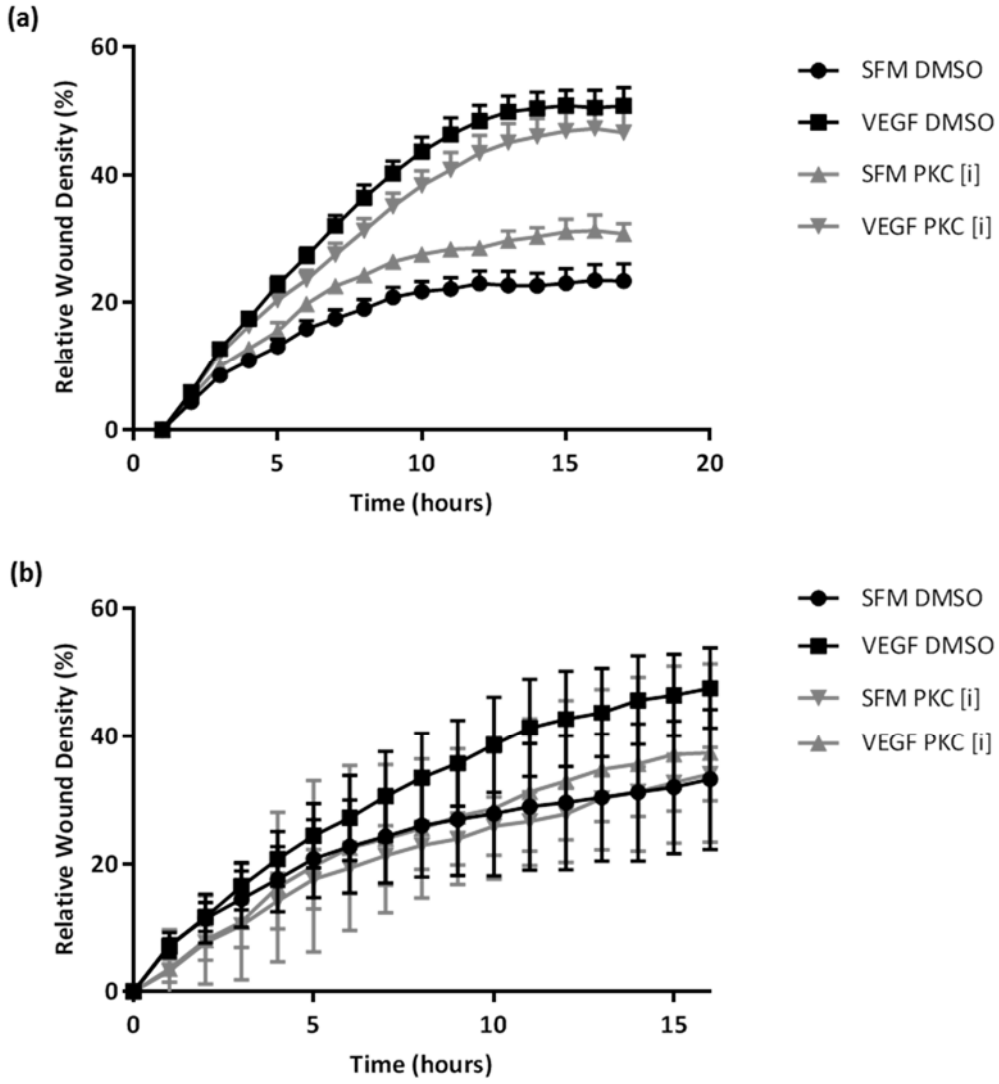

Figure 5.28. Measurement of scratch wound closure of HUVECs plated on fibronectin, and treated with SFM/VEGF and DMSO/PKC inhibitor. HUVECs were plated for 3 hours in SFM, on fibronectin coated 96-well plates. Scratches were then introduced, test solution (VEGF or SFM with DMSO or PKC [i]) added and images taken every hour for 16 hours. Data is displayed as relative wound density (%) at each time point, ± SEM, n=6 wells per experiment, 2 independent experiments shown. (a) $p<0.05$ (two-way ANOVA), comparing SFM DMSO vs VEGF DMSO conditions from 9 hours onwards and (b) $p<0.05$ (two-way ANOVA), comparing SFM DMSO vs VEGF DMSO conditions from 3 hours onwards and SFM MEK [i] vs VEGF MEK [i] from 7 hours onwards.

5.5 Selection of proteins for follow-up analysis

From the three mass spectrometry-based datasets generated in chapter 4, many analyses have been performed (chapter 4 and this chapter). From the combination of quantitative, statistical, protein-protein interaction network analyses and kinase prediction analyses, a range of identified consensus adhesome proteins were selected for further analysis. These were VASP, filamin-A, GIT1, paxillin, vinculin and ILK. The rationale for selecting each of these proteins is detailed below.

5.5.1 VASP

VASP stands out in statistical analysis of phosphopeptide changes (figure 5.8c), as there are two different phosphosites (S322 & S325) that increased consistently (3/4 replicates) in in the TCL phosphoproteomic Progenesis QI analysis. Both of these peptides increased by >2.3-fold, with a p-value below 0.1. In the proteomic IAC dataset VASP increased by 1.15-fold, with a p-value of 0.44, suggesting the overall protein level doesn't change upon VEGF treatment. In addition, VASP is a highly connected node in the consensus adhesome, suggesting that this is an important node in the network (figure 5.6 & 5.7).

5.5.2 Filamin

In the isolated IAC phosphoproteomic analysis, 5/6 filamin phosphopeptides identified increased according to Progenesis QI analysis (2 FLNA, 2 FLNB, 1 FLNC, figure 5.8b). In contrast, 12/13 filamin phosphopeptides identified in the TCL sample decreased. Of the filamin peptides detected, Filamin-A-S1081 stood out as consistently increased in the isolated IAC sample, and was not identified in the TCL sample. In addition, filamin was one of the only proteins identified in the phosphoproteomic datasets belonging to the final consensus adhesome axis containing two sub-modules that are connected through the kindlin–integrin-linked kinase (ILK) interaction (figure 5.7).

5.5.3 GIT1

One of the stand-out phosphorylation sites predicted to be phosphorylated by Src with VEGF treatment was GIT1-Y598 (table 5.6 & 5.7). In addition, there is a small amount of evidence suggesting a role for GIT1 in VEGF-induced cellular processes (table 1.1). Of the 16 GIT1 phosphopeptides identified in the TCL analysis, nine decreased and seven increased. One of these peptides included GIT1-Y598, which was identified and increased in both Progenesis QI and spectral count data (table 5.7) in 3/4 replicates. GIT1 was also identified in the IAC proteomic dataset and increased 1.3-fold upon VEGF treatment (p-value 0.13). These data suggest a role for GIT1, and in particular GIT1-Y598 in VEGF- adhesion crosstalk.

5.5.4 Paxillin

Paxillin is a central consensus adhesome protein with established roles in VEGF signalling (table 1.1). Two paxillin phosphorylation sites (Y118, Y88) identified in TCL phosphoproteomic data were predicted to be phosphorylated by Src kinase. A decrease in Y118 was observed in the spectral

count analysis upon VEGF treatment, although this site was not identified by Progenesis QI analysis. Paxillin increased by 1.25-fold (p-value 0.24) in the IAC proteomic dataset upon VEGF treatment. Due to these observed changes, its predicted association with Src kinase, and its previously determined importance in both VEGF signalling and integrin mediated adhesion, paxillin was selected as a candidate of interest for future study.

5.5.5 Vinculin

A small and insignificant change was detected in vinculin levels upon VEGF treatment in the IAC proteomic dataset. Seven different vinculin phosphopeptides were identified in the TCL phosphoproteomic dataset, four of which demonstrated a decrease in 3/4 replicates upon VEGF treatment (S345, S434, S721, T604). These changes suggest a potential role for vinculin in VEGF adhesion crosstalk. The role of vinculin in the HUVEC IAC adhesome network is also of interest due to its position as key connecting node in the consensus adhesome and in protein-protein interaction networks generated in this study (figure 5.2-5.4 & 5.7).

5.5.6 ILK

ILK was identified in the IAC proteomic dataset, with no identified change upon VEGF treatment. ILK was not identified in either phosphoproteomic dataset. As no changes were identified, and as a key connecting in the consensus adhesome and protein interaction networks generated with the IAC proteomic dataset from this study (figure 5.2 & 5.3), ILK was selected as a protein of interest. In addition, investigating this protein with no identified change, or no known role in VEGF signalling (in comparison to other candidates) will provide additional information.

5.5.7 siRNA knockdown of selected candidates

To investigate the role of VASP, filamin-A, GIT1, paxillin, vinculin and ILK these proteins were silenced in HUVECs using siRNA-mediated knockdown. siRNA treatment resulted in over 80% knockdown for all candidates. Initial experiments using silenced HUVECs investigated the effects on VEGF-induced ERK phosphorylation. In all cases, VEGF treatment following candidate knockdown induced ERK phosphorylation (figure 5.29). The phsopho-ERK fold change was slightly reduced in all samples (figure 5.29b). However only one replicate was performed here and variability in the phospho-ERK fold has been observed previously (e.g. figure 5.23). Therefore, further experiments need to be performed to confirm these observations. However, when HUVECs were plated on poly-lysine, VEGF treatment still induced an increase in ERK phosphorylation (figure 5.30), suggesting the response is not adhesion specific. It would therefore be interesting to test the effects of knockdown of these candidates using an adhesion-dependent assay.

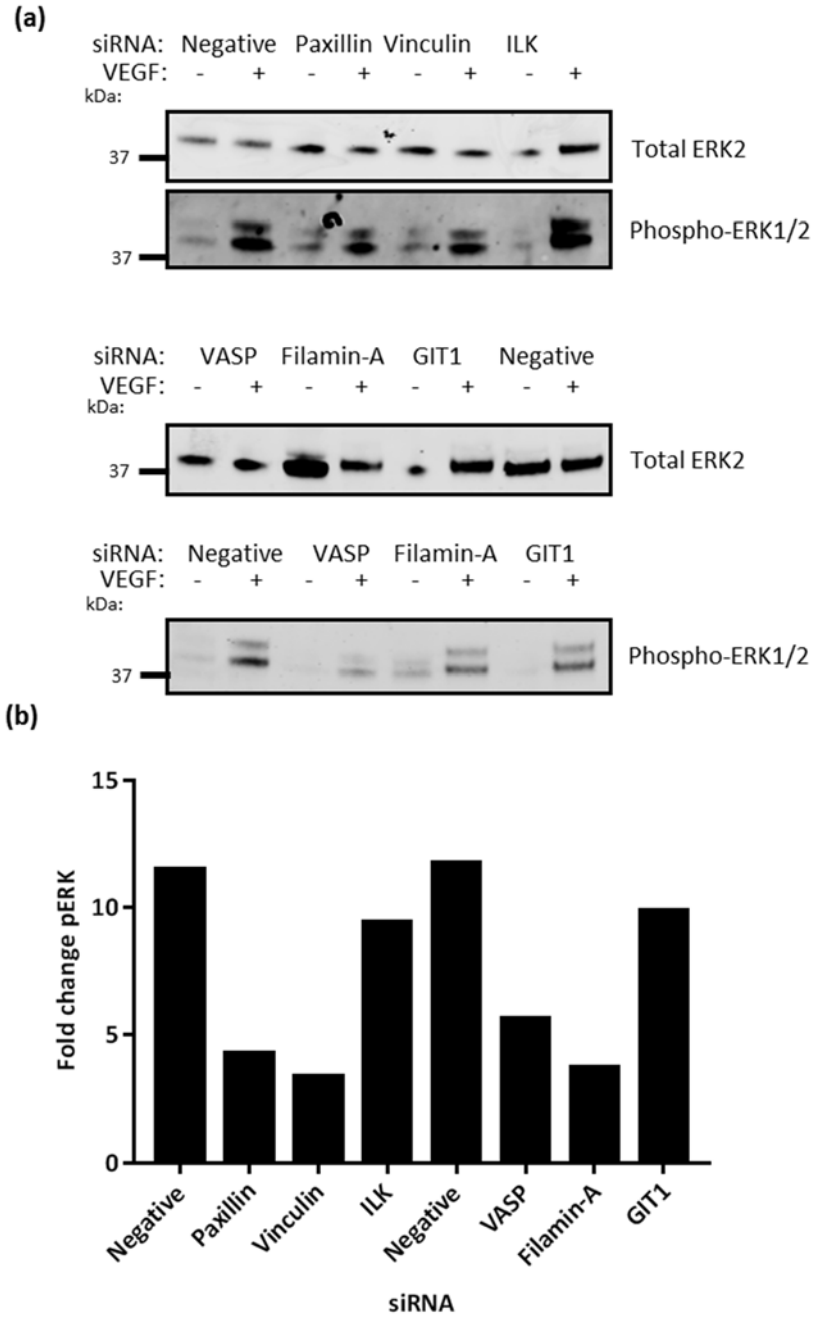

Figure 5.29. Measurement of ERK phosphorylation induced by VEGF in HUVECs with siRNA mediated knockdown of paxillin, vinculin, ILK, VASP, filamin-A and GIT1. HUVECs were treated with the indicated siRNA to reduce protein expression. Following protein knockdown, HUVECs were spread on fibronectin for 2 hours, treated with SFM or VEGF (25 ng/mL) for 7.5 minutes, and total cell lysates collected for analysis. (a) Western blot analysis of total ERK2 and phospho-ERK1/2. Molecular weight values (kDa) are displayed to the left of each blot. (b) Phospho-ERK fold change: phospho-ERK band intensity values were normalised to total ERK band intensity values and fold change calculated [VEGF/SFM]. n=1.

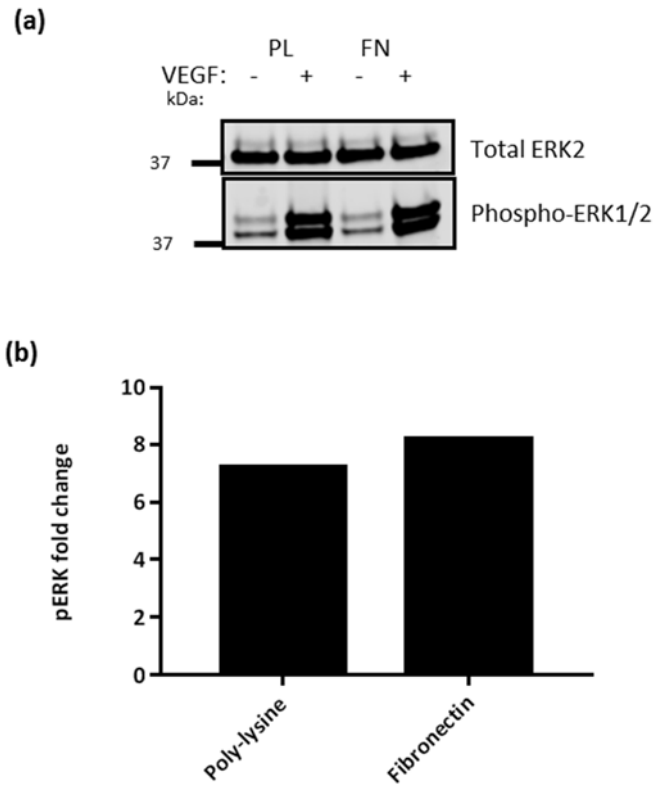

Figure 5.30. Measurement of ERK phosphorylation induced by VEGF in HUVECs plated on fibronectin (FN) and poly-lysine (PL). HUVECs were spread on FN or PL coated plated for 2 hours, treated with SFM or VEGF (25 ng/mL) for 7.5 minutes, and total cell lysates collected for analysis. (a) Western blot analysis of total ERK2 and phospho-ERK1/2. Molecular weight values (kDa) are displayed to the left of each blot. (b) Phospho-ERK fold change: phospho-ERK band intensity values were normalised to total ERK band intensity values and fold change calculated [VEGF/SFM]. n=1.

5.6 FRAP analysis of HUVEC IAC phosphotyrosine dynamics

Combined proteomic and phosphoproteomic experiments have suggested that protein composition of HUVEC IACs remains unchanged with VEGF treatment, while the phosphorylation status of proteins was altered. Previous studies involving proteomic analysis of IACs have observed similar results. For example, minimal changes in protein composition were observed in EGF-induced epithelial cells and FAK inhibitor treated fibroblasts; whist changes in IAC phosphorylation were detected (Horton et al. 2016b;Paul 2014). In the FAK inhibitor study, to investigate how a lack of change in IAC composition could result in altered cell behaviour upon FAK inhibition, the dynamics of core IAC components and SH2 domain–containing proteins using a phosphotyrosine reporter were performed using FRAP, a live cell imaging approach (Horton et al. 2016b). A similar approach could be applied to HUVECs to investigate VEGF-induced changes in HUVEC IAC phosphorylation.

FRAP allows the dynamics of a protein of interest in a specific cell area to be investigated. Briefly, the protein of interest is fluorescently labelled. Once expressed within the cell, the fluorescently labelled proteins that localise to the region of interest, such as the adhesion complex, are irreversibly bleached. Following bleaching, the fluorescence recovery within the selected region of interest is recorded over time. In live cells, most proteins undergo continuous turnover, meaning bleached proteins are replaced by newly recruited fluorescent proteins. This recovery can be quantified and mathematical analysis allows behavioural assessment of the protein of interest. To investigate tyrosine phosphorylation dynamics within HUVEC IACs upon VEGF treatment, a phosphotyrosine reporter was expressed. This reporter (dSH2-YFP) labels SH2 domain–containing proteins within cells, and its fluorescence is proportional to that of tyrosine phosphorylation antibody labelling. The construct was successfully expressed in HUVECs (figure 5.31), with expression representative of adhesion complexes, consistent with previous results showing dSH2-YFP expression co-localised with that of IAC proteins (Ballestrem et al. 2006;Kirchner et al. 2003).

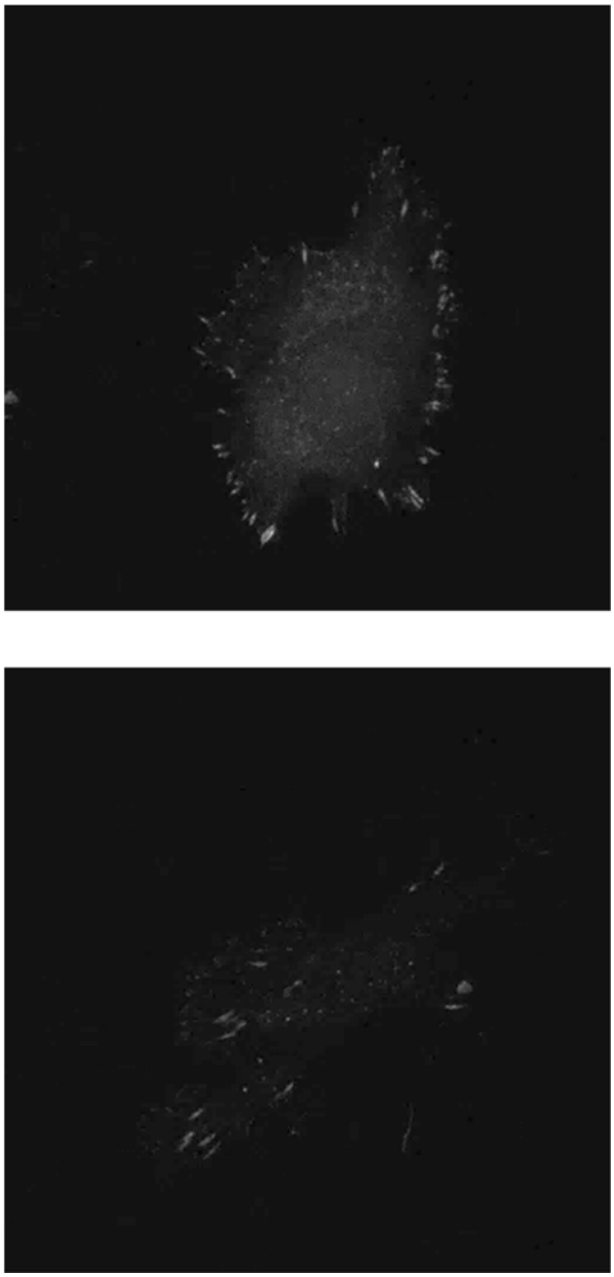

Figure 5.31. SH2 domain containing YFP construct expression in HUVECs. The SH2-YFP DNA construct was expressed in HUVECs by nucleofection. After 24 hours, HUVECs were plated on fibronectin coated glass bottomed plates in SFM for 2 hours, and imaged. Figure shows two representative images.

For FRAP experiments, the dSH2-YFP DNA construct was expressed in HUVECs using nucleofection. After 24 hours, HUVECs were plated on fibronectin-coated plates for two hours. FRAP experiments were then performed to investigate turnover rates of dSH2-YFP domain containing proteins in IACs before and after five minutes of VEGF treatment (figure 5.32). An increase in half-time of recovery of dSH2-YFP was observed upon VEGF treatment (figure 5.32, SFM: mean 26.59 ± 3.903 [SEM], n=14; VEGF: 39.36 ± 5.231 [SEM], n=15; p-value=0.06). These results suggest that phosphotyrosine binding proteins display increased transient residency time within the adhesion complex upon VEGF treatment. The turnover rate has been suggested to depend on the number of interaction partners of the fluorescently labelled protein. In this study, an increased half-time therefore suggests increased SH2 domain binding to phosphotyrosine proteins, and therefore increased levels of phosphotyrosine within IACs (Lele et al. 2008).

In addition, preliminary studies were performed investigating the effects of Src inhibition on turnover rates of dSH2-YFP domain containing proteins in IACs. The recovery curves were similar to the previous experiment involving VEGF treatment (figure 5.32); an overall increase in normalised intensity was observed with Src inhibition. This was similar to results observed with FAK inhibition (Horton et al. 2016b). In contrast, however, an increase in half-time of recovery of dSH2-YFP was observed upon following Src inhibition (figure 5.33, DMSO: 41.62 ± 6.02 [SEM], n=10; Src [i]: 52.22 ± 10.68, n=9; p-value=0.4). This was in contrast to that of previous similar experiments performed with FAK inhibitor, where half-time decreased (Horton et al. 2016b). However, only two experiments were performed here and this difference was non-significant (p-value=0.4). Increasing the number of experiments performed will generate greater confidence in the changes that are occurring in IACs upon Src inhibition treatment.

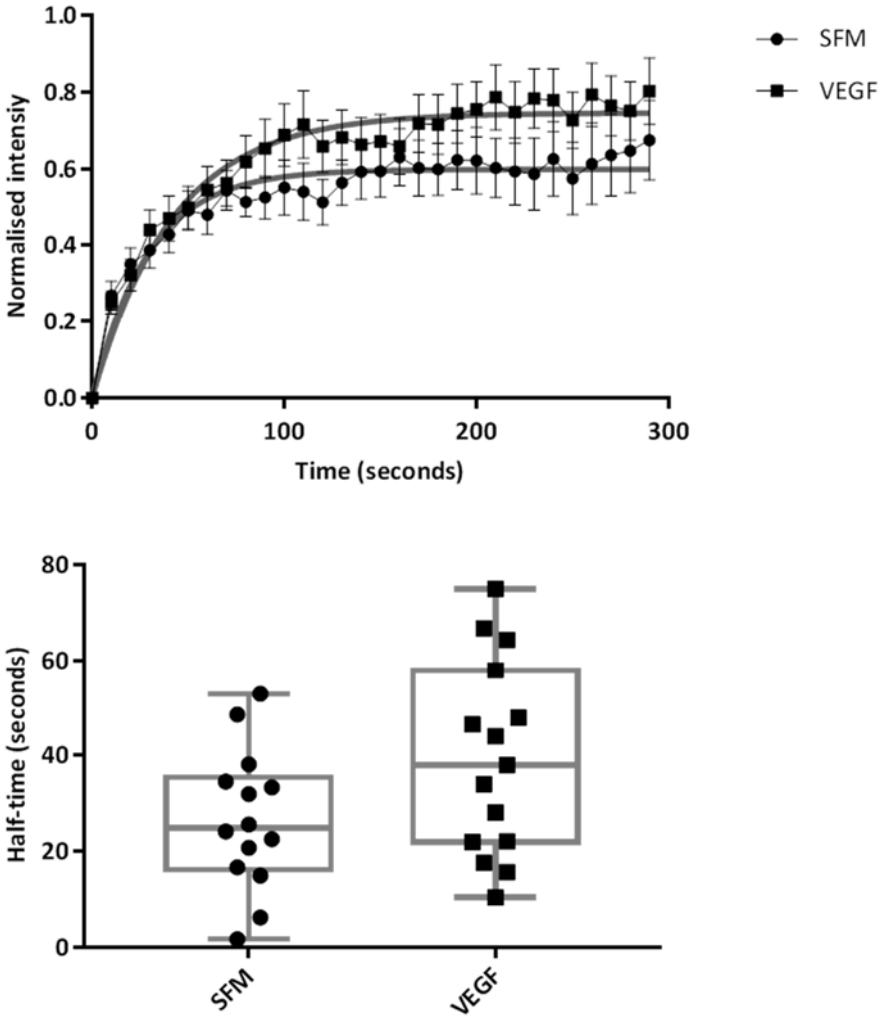

Figure 5.32. FRAP analysis of SH2 domain containing proteins expressed in HUVEC integrin adhesion complexes following VEGF treatment. The dSH2-YFP DNA construct was expressed in HUVECs by nucleofection. After 24 hours, HUVECs were plated on fibronectin coated glass bottomed plates in SFM for 2 hours and imaged according to the FRAP method before and after 5 minutes of VEGF treatment (25 ng/mL). (a) Graphs show the mean fluorescence recovery curves for all recorded adhesions before (SFM) and after VEGF treatment (VEGF), error bars are SEM, and data are fitted to the single exponential equation $F(t) = MF \times (1 - e^{\tau t})$ displayed in grey. (b) Half-time values for each recorded adhesion complex were calculated and plotted. Graph shows mean ± SEM; 14-15 adhesions per condition from three individual cells from three separate experiments. P-value= 0.062, unpaired t-test.

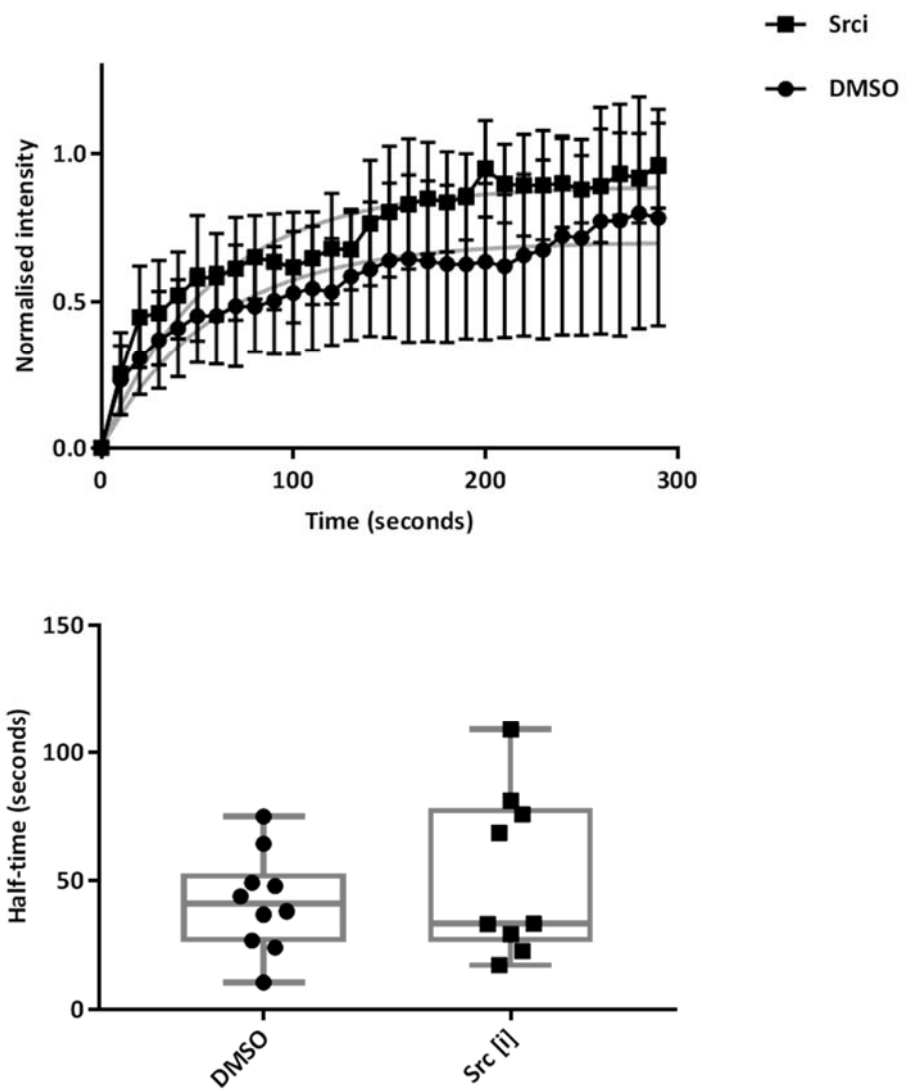

Figure 5.33. FRAP analysis of SH2 domain containing proteins expressed in HUVEC integrin adhesion complexes following Src inhibition. The dSH2-YFP DNA construct was expressed in HUVECs by nucleofection. After 24 hours, HUVECs were plated on fibronectin coated glass bottomed plates in SFM for 1 hour, then treated with DMSO or 10 µg/mL Src [i], and imaged using FRAP. (a) Graphs show the mean fluorescence recovery curves for all recorded adhesions with DMSO and Src [i] treatment, error bars are SEM, and data is fitted to the single exponential equation $F(t) = MF \times (1 - e\tau t)$ displayed in grey. (b) Half-time values for each recorded adhesion complex were calculated and plotted. Graphs show mean ± SEM; 9-10 adhesions per condition from two individual cells from two separate experiments. P-value= 0.4, unpaired t-test.

5.7 Chapter 5 summary

The first aim of this chapter was to perform a range of analyses of the proteomic and phosphoproteomic mass spectrometry datasets generated in chapter 4, to highlight interesting candidates that may be involved in VEGF-adhesion crosstalk. First, a range of protein-protein interaction networks were constructed, statistical analyses of the datasets employed, and detailed kinase prediction analysis performed. Kinase prediction analyses suggested that Src kinase activity in was increased in HUVEC IACs following VEGF treatment. In addition, from the range of analyses performed, six proteins: VASP, filamin-A, GIT1, paxillin, vinculin and ILK were selected for further investigation into their role in VEGF-adhesion crosstalk.

To investigate the role of selected candidates in VEGF-induced cellular processes western blotting was employed to investigate changes in ERK-mediated VEGF signalling, and a HUVEC scratch wound migration assay was developed to investigate adhesion-specific VEGF-induced HUVEC migration. Preliminary migration assays investigating VEGF-induced migration upon kinase Src kinase inhibition were performed. In addition, as FAK has been previously suggested to play a role in VEGF-adhesion crosstalk, FAK inhibition was also performed. These kinase inhibition studies suggested that Src and FAK both play roles in VEGF induced migration, with combined kinase inhibition showing greater effects. In addition, inhibition of MEK and PKC, kinases critical to canonical VEGF signalling pathways, decreased VEGF-induced migration. Further studies of this type, using a combination of kinase inhibitors including Src and FAK inhibitors, along with inhibitors of kinases involved in canonical VEGF signalling pathways, would be useful to further define the pathway by which Src and FAK contribute to VEGF-induced migration.

Initial studies investigating the role of VASP, filamin-A, GIT1, paxillin, vinculin and ILK in VEGF signalling were performed using siRNA silencing of the selected candidates. However, the role of these proteins still remains unclear. Live cell imaging analysis by FRAP was also used to detect VEGF-induced changes in phosphotyrosine binding protein dynamics within IACs, suggesting that VEGF induces changes in the phosphorylation activity of proteins within IACs, as suggested by mass spectrometry analyses in chapter 4 (section 4.4.5). Overall, the dataset analyses highlight many interesting candidates that may be involved in VEGF signalling and VEGF-adhesion crosstalk, and may be used as a starting point, or supporting reference for other studies interested in VEGF-signalling and/or adhesion in ECs. In addition, these analyses have suggested a role for Src in VEGF-adhesion crosstalk, with further functional analyses supporting this hypothesis.

Chapter 6: Discussion

6.1 Summary

Cell adhesion and growth factor signalling are key processes that are both involved in the control of replication and fate, and there is abundant evidence for a number of components and pathways often being shared (Streuli and Akhtar 2009;Eliceiri 2001). However, the mechanisms by which intracellular crosstalk occurs between adhesion complexes and their associated signalling, and growth factor signalling, are yet to be determined. In this study, new methodologies have been developed that permitted enrichment and analysis of HUVEC adhesion complexes, and identification of changes in IAC protein and protein phosphorylation induced by growth factor treatment. A large body of evidence suggests a role for VEGF-adhesion crosstalk in ECs and angiogenesis (see chapter 1); therefore, this investigation focussed on the adhesion and VEGF responses of ECs.

In this study, a number of technical advances have been made. In chapter 3, a method was established for HUVEC IAC protein enrichment and proteomic analysis by LC-MS/MS. This method was used to produce a protein dataset that defined the HUVEC adhesion complex protein composition. In chapter 4, a workflow was established for phosphoproteomic analysis of isolated IAC and TCL samples from HUVECs, both of which permitted the study of phosphorylation events occurring within HUVEC IACs, and associated changes with VEGF treatment. In addition, quantification of protein and peptide data using spectral counting and ion intensity measurements was performed, the data from which were used to perform complex bioinformatic analysis in chapter 5. This analysis was used to hypothesise novel roles for IAC proteins in VEGF-adhesion crosstalk.

These technical advances permitted a range of biological findings. In chapter 3, analysis of HUVEC adhesion complexes identified 297 proteins deemed specific to FN-mediated adhesion complexes. Quantitative proteomic analysis of enriched IACs following VEGF treatment suggested no major structural alterations in the complex. Complementary phosphoproteomic analysis detected changes in IAC protein phosphorylation following VEGF treatment. Kinase predication analysis using phosphoproteomic data provided evidence for a role of Src kinase-mediated protein phosphorylation in VEGF-adhesion crosstalk. This is one of the first studies to perform a global analysis of adhesion complexes in ECs, and the first to address phosphorylation of IAC proteins induced by VEGF treatment at a global level.

6.2 Establishment of a HUVEC adhesion complex enrichment protocol

Adhesion complexes have been isolated from a range of cell types, using a variety of methodologies (Humphries et al. 2009;Horton et al. 2015;Robertson et al. 2015;Ng et al. 2014;Schiller et al. 2011;Schiller and Fässler 2013). However, only one recent study has been performed in ECs (Atkinson et al. 2017), and analysis of IAC protein composition in primary ECs has not been performed. Therefore, it was necessary to establish a methodology for enrichment of IAC proteins that could be used to define the EC IAC protein composition. Most studies involving adhesion complex isolation from cells have used FN as a canonical ligand to induce IAC formation (Horton et al. 2015). In this study, it was important that a biologically relevant ligand was used to induce the formation of adhesion complexes prior to isolation, in addition to a ligand that allowed isolation of IAC proteins in sufficient quantities for mass spectrometry analysis. In addition, it was important to consider that a VEGF treatment step was to be introduced into the protocol at a later point, and hence to optimise a protocol to which a VEGF treatment step could be applied. Collagen, laminin, vitronectin and FN binding integrin heterodimers have been shown to be expressed in ECs in previous studies (Stupack and Cheresh 2002). However, there are limited studies that have assessed adhesion complex formation by ECs on different ligands by immunocytochemistry. In HUVECs plated on FN and collagen, adhesion complexes were detected; in contrast, when plated on laminin, adhesion complexes were not apparent. This is possibly due to the lower expression of laminin-binding integrins, which include the α3 and α6 subunits, as shown by flow cytometry in this study. When isolating IACs from HUVECs plated on fibronectin, an increased quantity of IAC protein was isolated, when compared to collagen. For this reason, along with literature suggesting that fibronectin is a biologically relevant EC ligand with an important role in modulating a range of EC functions associated with angiogenesis and VEGF signalling (section 1.9.2), fibronectin was chosen as the ligand of choice. An additional consideration was incorporation of a negative control ligand into the protocol. To allow a negative control ligand to be used, it was important that plating time was kept short. Plating time was therefore selected as two hours; this would allow time for adhesion complexes to form, whilst minimising the ability of cells to synthesise their own matrix molecules while spreading, which would override the control ligand (Jones et al. 2015;Hayman and Ruoslahti 1979).

6.3 Defining the HUVEC IAC protein composition

The HUVEC IAC isolation workflow established in this study was used to define the HUVEC IAC composition, a network of 297 proteins (enriched ≥two-fold over the poly-lysine negative control). Following generation of this dataset, extensive bioinformatics analyses were performed. This included analysis of the HUVEC dataset alone, and a detailed comparison with previously reported adhesion complex datasets, including the consensus adhesome, meta adhesome and LCA.

Detailed comparison of the HUVEC adhesome dataset with other mass spectrometry-derived IAC datasets confirmed that a high proportion (85%) of proteins identified in the HUVEC adhesion complex dataset are previously reported adhesion complex-associated proteins. However, 15% of identified proteins have not been associated with adhesion complexes previously, and may warrant further investigation. For example, these may represent uncharacterised or endothelial-specific adhesion components for which further validation would be required.

One unexpected observation was that the fibronectin-induced IACs analysed in this study were predominantly α5β1- and not αVβ3 integrin-mediated. This is surprising as (1) αVβ3 was shown to be expressed in HUVECs used in this study by immunofluorescence, and (2) αV was identified in 7/7 meta adhesome datasets and β3 in 5/7 meta adhesome datasets (Horton et al. 2015). This therefore makes the HUVEC IAC dataset defined in this study a FN-α5β1 integrin specific complex. Atkinson et al. 2017, who recently performed a proteomic analysis of IACs on ECs plated on FN for 90 minutes identified α5, β1 αV and β3 integrins, all greater than four-fold enriched over the poly lysine control. However, there are a number of experimental differences this result may be attributed to. For example, whereas primary endothelial cells (HUVECs) were used in this study, Atkinson et al. used immortalised mouse lung microvascular ECs. Differences in both molecular and phenotypic characteristics have been reported in different EC types (Lang et al. 2003;Staton et al. 2007), and so may contribute to the differences observed here. It would be interesting to perform a comparative study of IAC composition of different EC types, to determine which proteins, and in particular integrin subunits, may be present in all EC IACs and if any are specific to individual subsets of ECs. In addition, Atkinson et al. used a shorter plating time, different chemical crosslinker and longer cell lysis incubation, which may contribute differences. This theory is supported by previous comparative studies that suggest that differences in isolation methodology can have an impact on the composition identified by mass spectrometry (Horton et al. 2015).

The HUVEC adhesome dataset generated in this study, in addition to defining the HUVEC adhesome composition, was used to compile an updated consensus adhesome combined with current data (Horton et al. 2015). Two updated consensus adhesome datasets were produced: a refined network (49 proteins in 6/8 datasets, figure 6.1) and an expanded network (101 proteins in 5/8 datasets; figure 6.2). Tables showing the combined datasets are shown in supplementary file 6.1 (appendix). The data validate the selection of consensus adhesome proteins in the HUVEC dataset, and provide confidence in the use of the consensus adhesome to streamline data analysis of future datasets. Hence, as additional datasets are generated, it is important to compile these with datasets such as the meta and consensus adhesome, to continue increasing confidence in adhesome data.

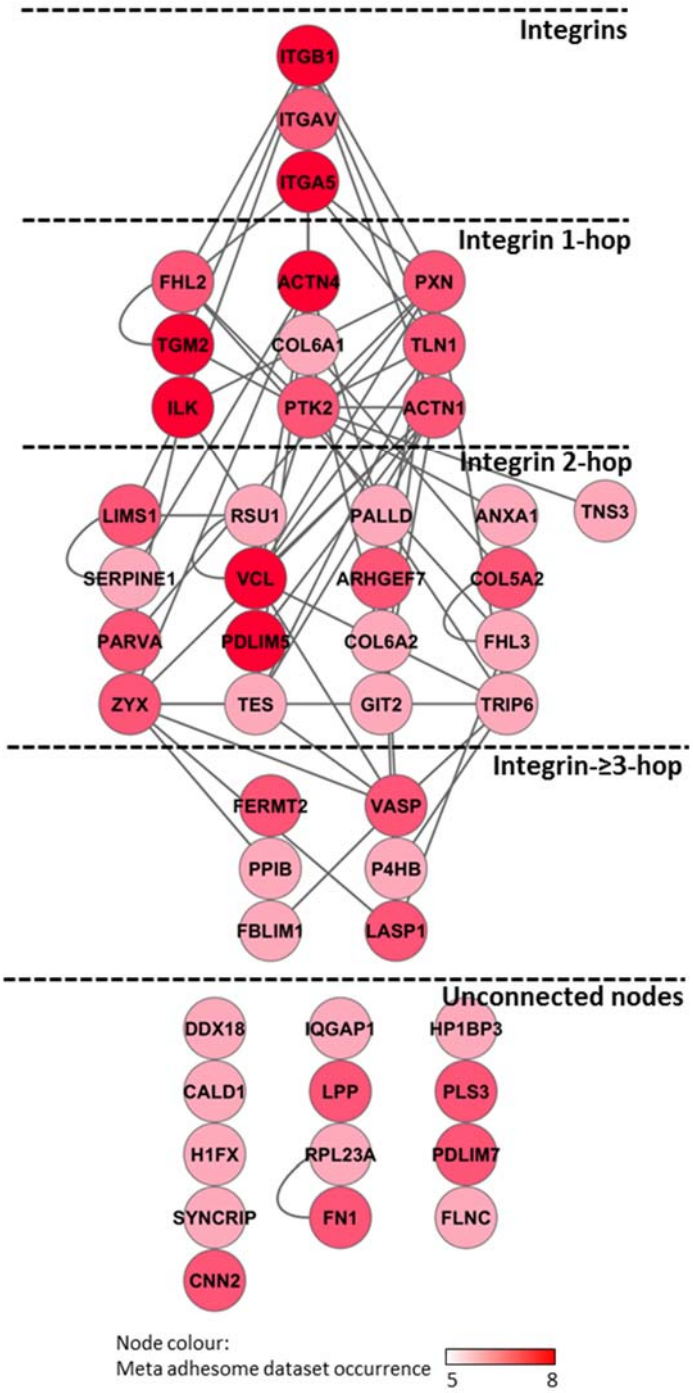

Figure 6.1. Updated consensus adhesome (48 proteins). The 297 proteins determined specific to fibronectin-mediated integrin adhesion complexes in HUVECs (proteins ≥2-fold enriched in the fibronectin compared to poly-lysine and with ≥2 mean spectral count) were combined with the meta adhesome dataset (supplementary table 6.1b; appendix), and those 49 proteins that were identified in 6/8 datasets mapped onto a known human protein-protein interaction network. In total, out of 49 proteins, 48 were mapped onto the network. The network comprises 75 interactions (grey lines; edges) between the 48 proteins (circles; nodes), which are labelled with gene names for clarity. Proteins are shaded according to dataset occurrence and arranged according to their association with integrins.

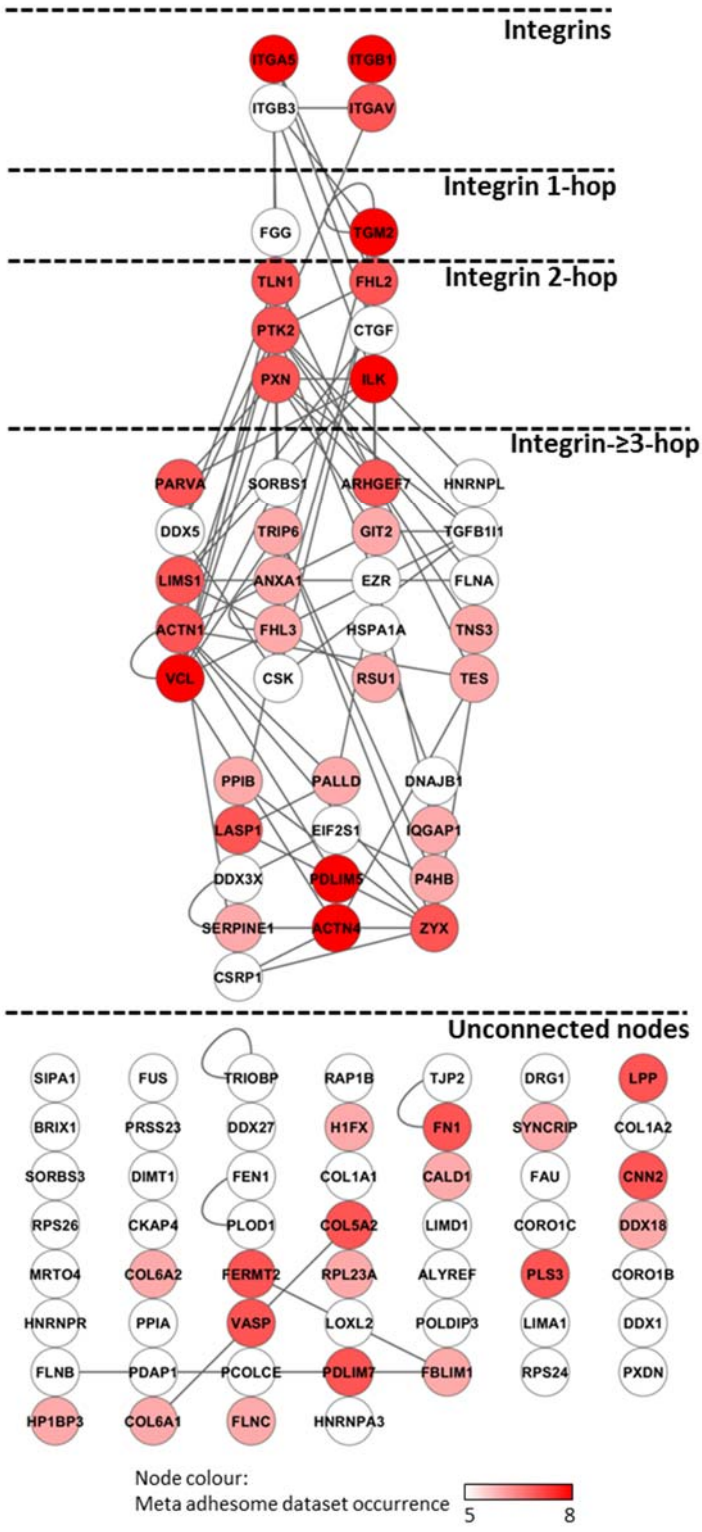

Figure 6.2. Updated consensus adhesome (98 proteins). The 297 proteins determined specific to fibronectin-mediated integrin adhesion complexes in HUVECs (proteins ≥2-fold enriched in the fibronectin compared to poly-lysine and with ≥2 mean spectral count) were combined with the meta adhesome dataset (supplementary table 6.1c; appendix), and those 101 proteins that were identified in 5/8 datasets mapped onto a known human protein-protein interaction network. In total, out of 101 proteins, 98 were mapped onto the network. The network comprises 99 interactions (grey lines; edges) between the 98 proteins (circles; nodes), which are labelled with gene names for clarity. Proteins are shaded according to dataset occurrence and arranged according to their association with integrins.

6.4 Optimisation of the phosphoproteomic workflow

The next aim was to use and further optimise the IAC enrichment workflow (figure 3.8) to perform a global, unbiased analysis of changes in both protein composition and phosphorylation within adhesion complexes upon VEGF treatment. To do this, a VEGF treatment step was introduced, and a workflow for phosphoproteomic analysis of HUVEC adhesion complex proteins developed.

In a typical protein digest, a non-phospho enriched peptide sample has a low proportion of phosphopeptides in comparison to non-phosphorylated peptides (usually less than 0.2%), leading to low signal intensities in the mass spectrometer (Kanshin et al. 2012). To facilitate the detection of naturally low abundant phosphorylated residues within the proteome, phosphorylated protein or peptide enrichment is performed prior to mass spectrometry analysis, for which many methodologies have been developed. In this study, IMAC and TiO_2 approaches were tested and compared. TiO_2 approaches using established solid-bead phospho-affinity reagents have been used successfully in previous studies to enrich phosphopeptides from isolated IAC samples (Robertson et al. 2015). However, in this study, this TiO_2 approach was shown to be less superior to magnetic bead approaches that were tested. A recent study also compared the performance of a range of magnetic IMAC and TiO_2 beads and a non-magnetic bead approach, for phosphopeptide enrichment from TCL samples (Tape et al. 2014). Similarly to this HUVEC study, the magnetic beads tested displayed enhanced results. In addition both studies identified the most unique peptides following enrichment with magnetic Ti-IMAC beads, compared to that of other magnetic bead types. In this study, of the unique phosphopeptides identified with Ti-IMAC and TiO_2 magnetic approaches, only 35% were identified in both. This may suggest that these two approaches may enrich for specific subsets of phosphopeptides or alternatively represent stochastic phosphopeptide enrichment or incomplete peptide detection by the mass spectrometer. A similar observation was previously seen (Tape et al. 2014), with combined use of TiO_2 and Ti-IMAC increasing the number of unique phosphopeptides identified compared to their individual use (Tape et al. 2014). This combination approach was therefore used in this study.

With isolated IAC phosphoproteomic analyses, Robertson et al. 2015 identified an increased coverage of IAC adhesion-associated phosphorylation sites, compared to when using TCL samples. However, this HUVEC study identified a higher number of IAC proteins with phosphoproteomic analysis of TCL samples compared to that of isolated IACs. This provides an alternative approach for the study of VEGF-induced changes in IACs as phosphoproteomic analysis of both isolated IAC and TCL samples could be performed. The difference in coverage observed between the HUVEC and Robertson et al. studies may be due to differences in phosphopeptide enrichment methodology, which can affect the detection of lower abundance adhesion-regulated phosphorylation sites (Fíla and Honys 2012). For example, as discussed previously, different phosphopeptide enrichment

methods can have different preferences, and so enrich for specific subsets of the phosphoproteome. It may therefore be the combination approach used in this HUVEC study that led to a higher coverage (Solari et al. 2015;Tape et al. 2014). In addition, IAC proteins have a high proportion of phosphotyrosine sites compared to the overall proteome (Paul 2014;Robertson 2014;Kirchner et al. 2003). However, the TiO_2 enrichment strategy has been shown to have low affinity for phosphotyrosine residues in comparison to other methods (Sharma et al. 2014). This low affinity of TiO_2 beads for phosphotyrosine may contribute to the low detection of tyrosine phosphorylated IAC peptides in TCL samples (Robertson et al. 2015).

In this HUVEC IAC phosphoproteomic study, optimisation experiments were promising, identifying a high proportion of IAC proteins. However, the final VEGF-induced IAC phosphoproteomic dataset did not contain the proportion of IAC proteins that was expected from previous optimisation experiments. Although the reasoning for this drop in performance is not clear, there are multiple possible explanations. As each isolated IAC sample was checked for quality prior to analysis, it is unlikely due to variability in IAC isolation methodology, and also unlikely due to reduced performance of phosphoenrichment beads, as no decreased performance was observed when phosphoproteomic TCL analysis was performed alongside these samples. One explanation could be problems with buffers used for with IAC or phosphopeptide enrichment processing, which can play an important role in enrichment efficiency (Fíla and Honys 2012). Another problem could be variability of performance of the mass spectrometer, as differences on different days were occasionally observed. Despite this decreased performance, this VEGF-induced IAC dataset still holds valuable information, and together with the VEGF-induced TCL dataset, can be used for analysis. In addition, a global coverage of all previously reported phosphorylation sites was less important in this study. This is because the aim of this study was to identify changes following VEGF-treatment, rather than a comprehensive analysis of adhesion regulated signalling, as was the case in the Robertson et al. 2015 study.

A recent phosphoproteomic study in TCL samples was used to investigate VEGF-induced changes in bovine aortic ECs (Chidiac et al. 2016). Further comparative analysis of this published dataset with adhesome datasets was performed here. Of the 2424 TiO_2-enriched phosphopeptides identified in this phosphoproteomic dataset, 1030 , 60 and 168 were from the meta, consensus and literature-curated adhesome proteins respectively (43%, 2.5% and 6.9% of all phosphopeptides, respectively), (Chidiac et al. 2016). This adhesome coverage is similar to that identified in the HUVEC TCL phosphoproteomic dataset in this study (42%, 1.5% and 5.2%). Therefore, these results support the conclusion that phosphoproteomic analysis of TCL samples may be used to specifically investigate phosphorylation within IACs.

6.5 VEGF-induced adhesion complex changes

Many studies have investigated changes in ECs induced by VEGF, in terms of adhesion-related proteins and signalling pathways (table 1.1), with associated mechanisms mainly indicating changes in protein phosphorylation. However, these studies have mainly used a targeted approach based on genetically modified animals or blocking agents. In this study, using a global proteomic approach, the optimised HUVEC IAC enrichment workflow was used to identify changes in protein composition within HUVEC IACs following VEGF treatment. Few significant changes were observed in terms of protein composition, indicating no major structural alterations in the complex. Combined phosphoproteomic analysis confirmed that whilst there are minimal changes in IAC protein composition, a much higher proportion of phosphorylated peptides changed upon VEGF treatment.

These results led to the hypothesis that VEGF treatment induces changes in IAC protein phosphorylation, whilst protein composition remains unchanged. This fits with a recent proteomic study that has shed light on the nature of FAK and Src signalling in IACs. Inhibition of Src and/or FAK had no effect on IAC composition, as reported by mass spectrometry, although reduced IAC tyrosine phosphorylation. These results illustrated how IAC composition and phosphotyrosine-based signalling could be independently regulated through alterations in the dynamic exchange of signalling proteins (Horton et al. 2016b). Phosphorylation analysis in this inhibitor study was investigated by a combination of western blotting, immunofluorescence and FRAP. This HUVEC study involved a global phosphoproteomic approach, which allows a much more detailed analysis, and aids identification of specific phosphorylation switches and pathways activated in response to VEGF. Overall, phosphoproteomic studies confirmed that changes in IAC protein phosphorylation occur upon VEGF treatment. Additional preliminary FRAP analysis also supports this hypothesis, as results suggested increased levels of phosphotyrosine within IACs following VEGF treatment. For FRAP experiments including VEGF treatment and Src inhibition, in future studies it will be important to perform the same experiments on other IAC proteins that are not expected to change upon VEGF treatment or Src inhibition. This would increase confidence that the changes observed are specific to the phosphotyrosine reporter, and not a general effect observed in all IAC proteins. Taken together, these results provide additional support to the hypothesis that phosphorylation signals are transmitted through the adhesion complex, whilst the composition remains stable.

Further comparative analysis of the Atkinson et al. 2017 EC IAC isolation study proteomic dataset was performed here. Upon VEGF-treatment, 7% (72/1040) of proteins in the isolated IAC sample changed greater than two-fold (38 increased and 35 decreased). This is much greater than the 1% of proteins that changed greater than two-fold upon VEGF-treatment in HUVECs in this study. Of

these 72 proteins, 51 were meta adhesome proteins, whereas only two and three where consensus adhesome and LCA proteins, respectively. Therefore, of the changing proteins, only few are well characterised adhesion complex components. In addition, there are no details of data normalisation and limited details of statistical analysis are provided. This lack of information makes it difficult to assess if the changes observed are real. Furthermore, the differences observed may be due to differences in methodology used to isolate IACs and analyse associated proteomic data, as previously discussed.

A limited number of studies have performed phosphoproteomic analysis of VEGF-induced changes in TCL samples. Chidac et al. 2016 investigated both VEGF- and angiopoietin-induced changes by phosphoproteomic analysis of bovine aortic EC (BAEC) TCL samples. Of the 2424 phosphopeptides identified by this analysis, 179 (7.4%) changed greater than two-fold with 170 increasing. The number changing is a much lower total proportion than that identified in this HUVEC study (34% of identified phosphopeptides). Again, this difference may be due to differences in methodology used. A similar VEGF treatment time was used (10 minutes vs 7.5 minutes in this study); however, the EC are likely to have been treated differently prior to growth factor treatment. For example, BAECs were not plated on an ECM ligand prior to VEGF treatment, and experiments appeared to be performed at a confluent state. In contrast, HUVECs used in this study were plated on fibronectin for two hours prior to VEGF treatment, and were treated in a sparse state. Cell confluence can affect both morphology and biological response of cells, and could contribute to differential EC responses to growth factor. For example, ERK pathway activation is inhibited by cell confluence (Viñals and Pouysségur 1999). In addition, different ECM ligands can trigger distinct cellular responses, for example, different responses to VEGF have been observed when plated on different ECM ligands (Geiger and Yamada 2011;Soldi et al. 1999;Mahabaleshwar and Byzova 2008).

6.6 Phosphoproteomic data analysis: kinase prediction reveals a role for Src kinase activity in VEGF-adhesion crosstalk

Kinase prediction analysis of both IAC and TCL phosphoproteomic datasets was used to assign phosphorylation sites as potential substrates for a particular protein kinase or group/family of protein kinases. A large amount of data was derived from this analysis; however, one of the most interesting outputs was the observation that a number of protein phosphorylation sites predicted to be substrates for Src were increased. These analyses suggested that Src kinase activity is increased in HUVEC IACs following VEGF treatment, and therefore may play a role in VEGF-adhesion crosstalk.

Since kinase prediction analysis led to the hypothesis that Src kinase activity was increased on IAC proteins upon VEGF treatment, previously reported roles for Src in VEGF and/or adhesion signalling

was reviewed. The Src family kinases are required for VEGF-mediated signalling and angiogenesis (Werdich and Penn 2006;Eliceiri et al. 1999). More specifically, Src is essential for VEGF-mediated FAK-Y861 phosphorylation, which plays a role in VEGF-induced migration and anti-apoptosis (Eliceiri et al. 1999;Abu-Ghazaleh et al. 2001). Treatment of ECs with VEGF induced formation of a FAK-αVβ5 complex in a Src-dependent manner (Eliceiri et al. 2002). Src was also reported to mediate VEGF signalling through a pathway involving PLC-γ. These studies suggest an important role for Src and Src-dependent FAK signalling in VEGF-adhesion crosstalk. However, only few studies have begun to understand the mechanisms by which Src is involved in VEGF signalling and VEGF-adhesion crosstalk.

Proteins predicted to have increased levels of Src-mediated phosphorylation upon VEGF treatment included GIT1, Paxillin and FAK. Paxillin and FAK are known substrates of Src (Mitra et al. 2005;Playford and Schaller 2004). More recently, GIT1 has been shown to be a substrate for Src (Yin et al. 2004). Previous studies revealed that a pathway involving Src-GIT1-PLCγ signalling is required for VEGF-mediated podosome formation and cell migration (Wang et al. 2009). However, the GIT1 phosphorylation site identified in this study (Y598) has not been previously identified as a Src substrate. Therefore, this study identified GIT1-Y598 as a novel phosphorylation site predicated to be phosphorylated in response to VEGF. Further investigation into the specific role of GIT1 and GIT1-Y598, in relation to VEGF-Src signalling may provide an insight into Src-mediated mechanisms of VEGF-adhesion crosstalk.

Activated Src leads to phosphorylation of substrates including FAK and paxillin (Mitra et al. 2005;Playford and Schaller 2004), mediating further signalling and interactions with sites of integrin adhesion. In addition evidence suggests a role for FAK and paxillin in VEGF-adhesion crosstalk. For example, previous studies have shown that VEGF increases FAK-Y397, -Y407 and -Y861 phosphorylation (Abu-Ghazaleh et al. 2001;Herzog et al. 2011), FAK-Y407 was also increased in VEGF-treated TCL samples in this study (table 5.7). VEGF also induces FAK-paxillin binding, FAK localisation to nascent adhesions and as previously discussed, formation of a FAK-αVβ5 integrin signalling complex in a Src-dependent manner (Chen et al. 2012;Avraham et al. 2003;Birukova et al. 2009;Eliceiri et al. 2002). In addition to the role of FAK and Src as individual signalling components, these kinases form a FAK-Src signalling complex, determined to be a potential cancer therapeutic target (Brunton and Frame 2008;Kim et al. 2009;Sulzmaier et al. 2014). The complex binds to and phosphorylates IAC molecules such as paxillin and p130-Cas. For this reason, the effects of Src and FAK inhibition on VEGF-induced signalling and migration were investigated in this study.

Src and FAK inhibition both decreased VEGF-induced HUVEC migration, suggesting an important role for these kinases. Consistent with previous studies, the combined effect of Src and FAK inhibition had an increased effect on overall migration (Horton et al. 2016b), with only a small VEGF-induced effect remaining. These results suggest that preventing functioning of both kinases, and hence disrupting the FAK-Src signalling complex, has a greater effect than inhibiting those individually. This suggests that the Src-FAK signalling complex plays an important role in VEGF induced signalling and migration, and in particular VEGF-adhesion crosstalk. This is likely due to prevention of complex specific phosphorylation events mediated by the FAK-Src complex, such as substrates paxillin and p130-Cas which have previously determined to be phosphorylated in response to VEGF, and play a role in VEGF induced processes (table 1.1). It would be interesting to study further the role of Src and FAK in VEGF-adhesion crosstalk, and in particular the mechanisms by which the FAK-Src complex contributes to VEGF-induced HUVEC migration.

6.7 Limitations and future perspectives

The HUVEC IAC isolation protocol and combined proteomic and phosphoproteomic workflow developed here represents a novel approach for the phosphoproteomic analysis of growth factor receptor crosstalk and adhesion receptor signalling. However, the data generated have highlighted some ongoing technical challenges and indicated that further optimisation to the current workflow may achieve improved results.

In this study, VEGF-treatment (7.5 minutes) of HUVECs resulted in minimal changes in IAC protein composition. It may be hypothesised however, that a longer VEGF treatment time may induce changes in protein composition. Growth factor and in particular VEGF treatment time courses performed in previous studies have shown that different treatment times results in differential effects on protein phosphorylation status (Chidiac et al. 2016;Zheng et al. 2013;Reddy et al. 2016). Although VEGF is known to induce changes in phosphorylation rapidly, growth factor-induced effects can still be detected following 60 minutes of stimulation and can induce early and late response genes. Both in vivo and in vitro, these longer-term changes in gene expression may therefore lead to changes in adhesion complex composition over a longer VEGF treatment timeframe than performed in this study (Chidiac et al. 2016;Nagano et al. 2012).

The coverage of phosphorylation sites identified from isolated adhesion complexes in this study may be expanded. Multiple optimisation steps could be considered within the phosphoproteomic workflow. For example, increasing sample amount is likely to improve phosphopeptide detection and reliability of phosphopeptide quantification (Solari et al. 2015); however, further increasing sample amount for IAC samples is impractical without automation. In particular, it would be

interesting to determine whether the use of an alternative protease to trypsin or multiple proteases would increase phosphopeptide detection. Alternative proteases can provide accessibility to areas of the proteome which may be in inaccessible due to generation of too long or too short peptides (Solari et al. 2015).

Another goal for future work will be to consider alternative approaches for both protein and peptide quantification. Spectral counting and ion intensity label-free approaches were used in this study, and although together they provide a reliable method of quantification, both approaches have their disadvantages (section 4.4.1). For example, low spectral count numbers can be unreliable for quantification, and poor alignment prior to ion intensity analysis can decrease precision and accuracy in protein quantification (Ng et al. 2017;Liu et al. 2004). Isotopic labelling approaches such as stable isotope labelling with amino acids in cell culture (SILAC) or isobaric tag for relative and absolute quantitation (iTRAQ) have been used in quantitative proteomic and phosphoproteomic studies. In particular, for low abundance species like phosphopeptides, these labelled approaches can be more accurate and sensitive than spectral counting and ion intensity analysis (Miller et al. 2010). Where practical, performing a combination of quantitative approaches will increase reliability of protein and peptide quantitative data. Overall, improved quantification data may allow interesting candidates to be identified and selected for follow up studies more easily, allowing the proteomics data generated to be of increasing value.

Global proteomic analysis using mass spectrometry generates a huge amount of data; just a small proportion of the potential bioinformatics analysis, validation and follow-up analysis can be performed in a single study. Additional quantification and bioinformatic analysis may aid the identification of interesting candidates to follow up from the large datasets generated. The validation and follow-up analysis performed in this study highlights the potential of the datasets generated, which may be used in future studies to generate further hypotheses involving targets to follow-up relating to VEGF and/or adhesion signalling. However, the impact of proteomic data is greatest when targets such Src have revealed roles in biological processes. Preliminary studies have suggested a role for Src and the FAK-Src complex in VEGF-induced migration. Further studies may be performed to determine the role of Src and the Src/FAK complex in VEGF-adhesion crosstalk. An interesting approach would be to specifically mutate predicted Src phosphorylation sites (for example GIT1-Y598), which would (1) validate novel Src induced phosphorylation sites and (2) identify the specific protein and/or phosphorylation sites involved in VEGF-adhesion crosstalk. Ultimately the contribution of any crosstalk mechanisms revealed would be investigated in relation to angiogenesis and therapeutic targets for angiogenesis related disorders.

In addition to the identification of Src as a potential mediator of VEGF-adhesion crosstalk, kinase predication analysis also highlighted an increase in the IL-1 receptor-associated kinase (IRAK) mediated phosphorylation upon VEGF treatment (Figure 5.14). The IRAK family of kinases play an important role in both positively and negatively regulating the expression of inflammatory molecules. These inflammatory signals are important for the elimination of viruses, bacteria, and cancer cells, as well as for wound healing (Jain et al. 2015). IRAK has not previously been associated with VEGF or adhesion signalling, and so the results of this study may have identified IRAK as a potential mediator of the two systems. However, inflammation has been linked to VEGF receptor signalling, and inflammation is involved in angiogenesis related conditions such as arthritis (McInnes & Schett 2007). It would be interesting to perform follow up studies on IRAK kinases, for example using kinase inhibitors and protein knockdown, to test the effects of adhesion dependent VEGF induced process such as migration.

Any hypotheses generated using the proteomic data generated in this study, would be followed up using a range of biochemical and molecular cell biology techniques. Different techniques may be used to determine the exact mechanisms by which the hypothesised mechanisms may be occurring, and to consider the importance of these mechanisms using assays that are more physiologically relevant in relation to both VEGF signalling and angiogenesis. For example, as performed in preliminary studies here, candidates may be tested by pharmacological inhibition and/or siRNA mediated knockdown, and their effects on cell signalling pathways, and processes such as adhesion and spreading investigated. The mechanistic contributions of these candidates will then be further assessed. For example, the activity of a particular integrin and/or components of growth factor signalling may be blocked, and any effects on activity of the candidate assessed. The effects of manipulating any proteins of interest will be assessed in angiogenesis assays. For example, functional assays that assess key angiogenic functions could be used, such as proliferation and migration. More physiologically relevant cell culture tube formation assays could then be used, such as the matrigel assay, and endothelial–fibroblast organotypic co-culture assay, which recapitulates processes involved in tube formation in vivo, including EC migration, assembly, sprouting and lumen formation (Vailhé et al. 2001;Martin and Murray 2009;Hetheridge et al. 2011). Eventually, upon determination of mechanisms involved and identification of a potential therapeutic target, animal models may be used, for example to test the effect of manipulating the target on angiogenesis and other important in vivo processes. Further experiments may examine if the same effect occurs when HUVECs form adhesion complexes on other substrates, such as collagen, and if growth factors other than VEGF induce similar changes. Any findings will also be validated in other cell types, including different ECs types, to confirm whether the findings are HUVEC, and EC specific. The results from a combination of follow up studies will begin to build a picture of the factors involved

in growth factor-adhesion crosstalk, how they contribute to angiogenesis, and the mechanisms involved.

6.8 Concluding remarks

This study presents one of the first to (1) perform a global proteomic analysis of EC IACs, and (2) investigate VEGF-adhesion crosstalk mechanisms using proteomic and phosphoproteomic workflows. The datasets derived in this study contain a great deal of information, which has been used here to define the HUVEC IAC protein composition and identify candidates that may contribute to VEGF-adhesion crosstalk. For example, Src kinase has been highlighted as a potential mediator of crosstalk, and future studies leading from this data may aid discovery of associated therapeutic targets. This study has the potential to provide a base for many future studies; for example to perform a more complete proteomic and/or phosphoproteomic analysis of VEGF signalling in IACs. In addition, there is unlimited potential for candidate selection and follow-up studies to be performed following on from the proteomic datasets generated here.

References

Abedi, H. & Zachary, I. (1997). Vascular endothelial growth factor stimulates tyrosine phosphorylation and recruitment to new focal adhesions of focal adhesion kinase and paxillin in endothelial cells. *Journal of Biological Chemistry,* 272(24)**,** 15442-15451.

Abu-Ghazaleh, R., Kabir, J., Jia, H., Lobo, M. & Zachary, I. (2001). Src mediates stimulation by vascular endothelial growth factor of the phosphorylation of focal adhesion kinase at tyrosine-861, and migration and anti-apoptosis in endothelial cells. *Biochemical Journal,* 360(Pt 1)**,** 255.

Aebersold, R. & Mann, M. (2003). Mass spectrometry-based proteomics. *Nature,* 422(6928)**,** 198-207.

Akalu, A., Cretu, A. & Brooks, P. C. (2005). Targeting integrins for the control of tumour angiogenesis. *Expert Opinion on Investigational Drugs,* 14(12)**,** 1475-1486.

Anthis, N. J. & Campbell, I. D. (2011). The tail of integrin activation. *Trends in Biochemical Sciences,* 36(4)**,** 191-198.

Askari, J. A., Buckley, P. A., Mould, A. P. & Humphries, M. J. (2009). Linking integrin conformation to function. *Journal of Cell Science,* 122(2)**,** 165-170.

Askari, J. A., Tynan, C. J., Webb, S. E., Martin-Fernandez, M. L., Ballestrem, C. & Humphries, M. J. (2010). Focal adhesions are sites of integrin extension. *The Journal of Cell Biology,* 188(6)**,** 891-903.

Atkinson, S. J., Gontarczyk, A. M., Ellison, T. S., Johnson, R. T., Kirkup, B. M., Alghamdi, A., Fowler, W. J., Silva, B. C., Schneider, J. J. & Weilbaecher, K. N. (2017). The β3-integrin endothelial adhesome regulates microtubule dependent cell migration. *bioRxiv***,** 145839.

Avraamides, C. J., Garmy-Susini, B. & Varner, J. A. (2008). Integrins in angiogenesis and lymphangiogenesis. *Nature Reviews Cancer,* 8(8)**,** 604-617.

Avraham, H. K., Lee, T.-H., Koh, Y., Kim, T.-A., Jiang, S., Sussman, M., Samarel, A. M. & Avraham, S. (2003). Vascular endothelial growth factor regulates focal adhesion assembly in human brain microvascular endothelial cells through activation of the focal adhesion kinase and related adhesion focal tyrosine kinase. *Journal of Biological Chemistry,* 278(38)**,** 36661-36668.

Bader, B. L., Rayburn, H., Crowley, D. & Hynes, R. O. (1998). Extensive vasculogenesis, angiogenesis, and organogenesis precede lethality in mice lacking all αv integrins. *Cell,* 95(4)**,** 507-519.

Ballestrem, C., Erez, N., Kirchner, J., Kam, Z., Bershadsky, A. & Geiger, B. (2006). Molecular mapping of tyrosine-phosphorylated proteins in focal adhesions using fluorescence resonance energy transfer. *Journal of Cell Science,* 119(5)**,** 866-875.

Bantscheff, M., Lemeer, S., Savitski, M. M. & Kuster, B. (2012). Quantitative mass spectrometry in proteomics: critical review update from 2007 to the present. *Analytical and Bioanalytical Chemistry,* 404(4)**,** 939-965.

Beekman, K. W., Colevas, A. D., Cooney, K., DiPaola, R., Dunn, R. L., Gross, M., Keller, E. T., Pienta, K. J., Ryan, C. J. & Smith, D. (2006). Phase II evaluations of cilengitide in asymptomatic patients with androgen-independent prostate cancer: scientific rationale and study design. *Clinical Genitourinary Cancer,* 4(4)**,** 299-302.

Bellou, S., Pentheroudakis, G., Murphy, C. & Fotsis, T. (2013). Anti-angiogenesis in cancer therapy: Hercules and hydra. *Cancer Letters,* 338(2)**,** 219-228.

Bergers, G. & Benjamin, L. E. (2003). Tumorigenesis and the angiogenic switch. *Nature Reviews Cancer,* 3(6)**,** 401-410.

Bergers, G. & Song, S. (2005). The role of pericytes in blood-vessel formation and maintenance. *Neuro-oncology,* 7(4)**,** 452-464.

Birukova, A. A., Cokic, I., Moldobaeva, N. & Birukov, K. G. (2009). Paxillin is involved in the differential regulation of endothelial barrier by HGF and VEGF. *American Journal of Respiratory Cell and Molecular Biology,* 40(1)**,** 99-107.

Bischoff, J. (1997). Cell adhesion and angiogenesis. *Journal of Clinical Investigation,* 99(3)**,** 373.

Blanco, R. & Gerhardt, H. (2013). VEGF and Notch in tip and stalk cell selection. *Cold Spring Harbor Perspectives in Medicine,* 3(1)**,** a006569.

Block, M. R., Badowski, C., Millon-Fremillon, A., Bouvard, D., Bouin, A.-P., Faurobert, E., Gerber-Scokaert, D., Planus, E. & Albiges-Rizo, C. (2008). Podosome-type adhesions and focal adhesions, so alike yet so different. *European Journal of Cell Biology,* 87(8)**,** 491-506.

Brakebusch, C. & Fässler, R. (2003). The integrin–actin connection, an eternal love affair. *The EMBO Journal,* 22(10)**,** 2324-2333.

Brooks, P. C., Clark, R. & Cheresh, D. A. (1994). Requirement of vascular integrin αvβ3 for angiogenesis. *Science,* 264(5158)**,** 569-571.

Brunton, V. G. & Frame, M. C. (2008). Src and focal adhesion kinase as therapeutic targets in cancer. *Current Opinion in Pharmacology,* 8(4)**,** 427-432.

Byron, A., Askari, J. A., Humphries, J. D., Jacquemet, G., Koper, E. J., Warwood, S., Choi, C. K., Stroud, M. J., Chen, C. S. & Knight, D. (2015). A proteomic approach reveals integrin activation state-dependent control of microtubule cortical targeting. *Nature Communications,* 6.

Byron, A., Humphries, J. D., Craig, S. E., Knight, D. & Humphries, M. J. (2012). Proteomic analysis of α4β1 integrin adhesion complexes reveals α-subunit-dependent protein recruitment. *Proteomics,* 12(13)**,** 2107-2114.

Byron, A., Morgan, M. R. & Humphries, M. J. (2010). Adhesion signalling complexes. *Current Biology,* 20(24)**,** R1063-R1067.

Byzova, T. V., Goldman, C. K., Pampori, N., Thomas, K. A., Bett, A., Shattil, S. J. & Plow, E. F. (2000). A mechanism for modulation of cellular responses to VEGF: activation of the integrins. *Molecular Cell,* 6(4)**,** 851-860.

Calderwood, D. A., Campbell, I. D. & Critchley, D. R. (2013). Talins and kindlins; partners in integrin-mediated adhesion. *Nature Reviews Molecular Cell Biology,* 14(8)**,** 503.

Cao, Y. (2016). Future options of anti-angiogenic cancer therapy. *Chinese Journal of Cancer,* 35(1)**,** 21.

Carmeliet, P. (2005). Angiogenesis in life, disease and medicine. *Nature,* 438(7070)**,** 932-936.

Carmeliet, P., Ferreira, V., Breier, G. & Pollefeyt, S. (1996). Abnormal blood vessel development and lethality in embryos lacking a single VEGF allele. *Nature,* 380(6573)**,** 435.

Carmeliet, P. & Jain, R. K. (2000). Angiogenesis in cancer and other diseases. *Nature,* 407(6801)**,** 249.

Chen, T. T., Luque, A., Lee, S., Anderson, S. M., Segura, T. & Iruela-Arispe, M. L. (2010). Anchorage of VEGF to the extracellular matrix conveys differential signaling responses to endothelial cells. *The Journal of Cell Biology,* 188(4)**,** 595-609.

Chen, X. L., Nam, J.-O., Jean, C., Lawson, C., Walsh, C. T., Goka, E., Lim, S.-T., Tomar, A., Tancioni, I. & Uryu, S. (2012). VEGF-induced vascular permeability is mediated by FAK. *Developmental Cell,* 22(1)**,** 146-157.

Cheresh, D. A. & Stupack, D. G. (2002). Integrin-mediated death: an explanation of the integrin-knockout phenotype? *Nature Medicine,* 8(3)**,** 193-194.

Chidiac, R., Zhang, Y., Tessier, S., Faubert, D., Delisle, C. & Gratton, J.-P. (2016). Comparative phosphoproteomics analysis of VEGF and angiopoietin-1 signaling reveals ZO-1 as a critical regulator of endothelial cell proliferation. *Molecular and Cellular Proteomics,* 15(5)**,** 1511-1525.

Chung, A. S. & Ferrara, N. (2011). Developmental and pathological angiogenesis. *Annual Review of Cell and Developmental Biology,* 27**,** 563-584.

Cifuentes, A. (2013). *Foodomics: Advanced mass spectrometry in modern food science and nutrition* (Vol. 52): John Wiley and Sons.

Cline, M. S., Smoot, M., Cerami, E., Kuchinsky, A., Landys, N., Workman, C., Christmas, R., Avila-Campilo, I., Creech, M. & Gross, B. (2007). Integration of biological networks and gene expression data using Cytoscape. *Nature Protocols,* 2(10)**,** 2366.

Cory, G. (2011). Scratch-wound assay. *Cell Migration: Developmental Methods and Protocols***,** 25-30.

Cox, B. D., Natarajan, M., Stettner, M. R. & Gladson, C. L. (2006). New concepts regarding focal adhesion kinase promotion of cell migration and proliferation. *Journal of Cellular Biochemistry,* 99(1)**,** 35-52.

De Palma, M., Biziato, D. & Petrova, T. V. (2017). Microenvironmental regulation of tumour angiogenesis. *Nature Reviews Cancer,* 17(8)**,** 457.

Deakin, N. O. & Turner, C. E. (2008). Paxillin comes of age. *Journal of Cell Science,* 121(15)**,** 2435-2444.

Desgrosellier, J. S. & Cheresh, D. A. (2010). Integrins in cancer: biological implications and therapeutic opportunities. *Nature Reviews Cancer,* 10(1)**,** 9-22.

Domon, B. & Aebersold, R. (2010). Options and considerations when selecting a quantitative proteomics strategy. *Nature Biotechnology,* 28(7)**,** 710-721.

Eberwein, P., Laird, D., Schulz, S., Reinhard, T., Steinberg, T. & Tomakidi, P. (2015). Modulation of focal adhesion constituents and their down-stream events by EGF: on the cross-talk of integrins and growth factor receptors. *Biochimica et Biophysica Acta (BBA)-Molecular Cell Research,* 1853(10)**,** 2183-2198.

Eliceiri, B. P. (2001). Integrin and growth factor receptor crosstalk. *Circulation Research,* 89(12)**,** 1104-1110.

Eliceiri, B. P., Paul, R., Schwartzberg, P. L., Hood, J. D., Leng, J. & Cheresh, D. A. (1999). Selective requirement for Src kinases during VEGF-induced angiogenesis and vascular permeability. *Molecular Cell,* 4(6)**,** 915-924.

Eliceiri, B. P., Puente, X. S., Hood, J. D., Stupack, D. G., Schlaepfer, D. D., Huang, X. Z., Sheppard, D. & Cheresh, D. A. (2002). Src-mediated coupling of focal adhesion kinase to integrin αvβ5 in VEGF signaling. *The Journal of Cell Biology,* 157(1)**,** 149-160.

Evans, I. M., Kennedy, S. A., Paliashvili, K., Santra, T., Yamaji, M., Lovering, R. C., Britton, G., Frankel, P., Kolch, W. & Zachary, I. C. (2017). Vascular endothelial growth factor (VEGF) promotes assembly of the p130Cas interactome to drive endothelial chemotactic signaling and angiogenesis. *Molecular & Cellular Proteomics,* 16(2)**,** 168-180.

Ferrara, N., Gerber, H.-P. & LeCouter, J. (2003). The biology of VEGF and its receptors. *Nature Medicine,* 9(6)**,** 669-676.

Ferrara, N. & Kerbel, R. S. (2005). Angiogenesis as a therapeutic target. *Nature,* 438(7070)**,** 967.

Fíla, J. & Honys, D. (2012). Enrichment techniques employed in phosphoproteomics. *Amino Acids,* 43(3)**,** 1025-1047.

Folkman, J. (2006). Angiogenesis. *Annual Review of Medicine,* 57**,** 1-18.

Folkman, J., Merler, E., Abernathy, C. & Williams, G. (1971). Isolation of a tumor factor responsible for angiogenesis. *Journal of Experimental medicine,* 133(2)**,** 275-288.

Francis, S. E., Goh, K. L., Hodivala-Dilke, K., Bader, B. L., Stark, M., Davidson, D. & Hynes, R. O. (2002). Central roles of α5β1 integrin and fibronectin in vascular development in mouse embryos and embryoid bodies. *Arteriosclerosis Thrombosis and Vascular Biology,* 22(6)**,** 927-933.

Frank, S. R. & Hansen, S. H. (Year). The PIX–GIT complex: AG protein signaling cassette in control of cell shape. *In:* Seminars in Cell and Developmental Biology, 2008. Elsevier, 234-244.

Friedlander, M., Brooks, P. C., Shaffer, R. W., Kincaid, C. M., Varner, J. A. & Cheresh, D. A. (1995). Definition of two angiogenic pathways by distinct αv integrins. *Science,* 270(5241)**,** 1500-1502.

Garmy-Susini, B., Jin, H., Zhu, Y., Sung, R.-J., Hwang, R. & Varner, J. (2005). Integrin α4β1–VCAM-1–mediated adhesion between endothelial and mural cells is required for blood vessel maturation. *Journal of Clinical Investigation,* 115(6)**,** 1542-1551.

Geiger, B. & Yamada, K. M. (2011). Molecular architecture and function of matrix adhesions. *Cold Spring Harbor Perspectives in Biology,* 3(5)**,** a005033.

Geiger, T. & Zaidel-Bar, R. (2012). Opening the floodgates: proteomics and the integrin adhesome. *Current Opinion in Cell Biology,* 24(5)**,** 562-568.

George, E. L., Baldwin, H. S. & Hynes, R. O. (1997). Fibronectins are essential for heart and blood vessel morphogenesis but are dispensable for initial specification of precursor cells. *Blood,* 90(8)**,** 3073-3081.

George, E. L., Georges-Labouesse, E. N., Patel-King, R. S., Rayburn, H. & Hynes, R. O. (1993). Defects in mesoderm, neural tube and vascular development in mouse embryos lacking fibronectin. *Development,* 119(4)**,** 1079-1091.

Georges-Labouesse, E., Messaddeq, N., Yehia, G., Cadalbert, L., Dierich, A. & Le Meur, M. (1996). Absence of integrin α6 leads to epidermolysis bullosa and neonatal death in mice. *Nature Genetics,* 13**,** 370-73.

Gong, Y., Yang, X., He, Q., Gower, L., Prudovsky, I., Vary, C. P., Brooks, P. C. & Friesel, R. E. (2013). Sprouty4 regulates endothelial cell migration via modulating integrin β3 stability through c-Src. *Angiogenesis,* 16(4)**,** 861-875.

Gorman, L., Mercer, L. P. & Hennig, B. (1996). Growth requirements of endothelial cells in culture: variations in serum and amino acid concentrations. *Nutrition,* 12(4)**,** 266-270.

Han, G., Ye, M., Liu, H., Song, C., Sun, D., Wu, Y., Jiang, X., Chen, R., Wang, C. & Wang, L. (2010). Phosphoproteome analysis of human liver tissue by long-gradient nanoflow LC coupled with multiple stage MS analysis. *Electrophoresis,* 31(6)**,** 1080-1089.

Harmey, J. H. & Bouchier-Hayes, D. (2002). Vascular endothelial growth factor (VEGF), a survival factor for tumour cells: Implications for anti-angiogenic therapy. *Bioessays,* 24(3)**,** 280-283.

Hashimoto, A., Hashimoto, S., Ando, R., Noda, K., Ogawa, E., Kotani, H., Hirose, M., Menju, T., Morishige, M. & Manabe, T. (2011). GEP100-Arf6-AMAP1-cortactin pathway frequently used in cancer invasion is activated by VEGFR2 to promote angiogenesis. *PloS one,* 6(8)**,** e23359.

Hayman, E. G. & Ruoslahti, E. (1979). Distribution of fetal bovine serum fibronectin and endogenous rat cell fibronectin in extracellular matrix. *The Journal of Cell biology,* 83(1)**,** 255-259.

Herzog, B., Pellet-Many, C., Britton, G., Hartzoulakis, B. & Zachary, I. C. (2011). VEGF binding to NRP1 is essential for VEGF stimulation of endothelial cell migration, complex formation between NRP1 and VEGFR2, and signaling via FAK Tyr407 phosphorylation. *Molecular Biology of the Cell,* 22(15)**,** 2766-2776.

Hetheridge, C., Mavria, G. & Mellor, H. (2011). Uses of the in vitro endothelial–fibroblast organotypic co-culture assay in angiogenesis research. Portland Press Limited.

Hodivala-Dilke, K. M., McHugh, K. P., Tsakiris, D. A., Rayburn, H., Crowley, D., Ullman-Culleré, M., Ross, F. P., Coller, B. S., Teitelbaum, S. & Hynes, R. O. (1999). β3-integrin–deficient mice are a model for Glanzmann thrombasthenia showing placental defects and reduced survival. *The Journal of Clinical Investigation,* 103(2)**,** 229-238.

Hoffmann, J.-E., Fermin, Y., Stricker, R. L., Ickstadt, K. & Zamir, E. (2014). Symmetric exchange of multi-protein building blocks between stationary focal adhesions and the cytosol. *Elife,* 3**,** e02257.

Horton, E. R., Byron, A., Askari, J. A., Ng, D. H., Millon-Frémillon, A., Robertson, J., Koper, E. J., Paul, N. R., Warwood, S. & Knight, D. (2015). Definition of a consensus integrin adhesome and its dynamics during adhesion complex assembly and disassembly. *Nature Cell Biology,* 17(12)**,** 1577.

Horton, E. R., Humphries, J. D., James, J., Jones, M. C., Askari, J. A. & Humphries, M. J. (2016a). The integrin adhesome network at a glance. *Journal of Cell Science,* 129(22)**,** 4159-4163.

Horton, E. R., Humphries, J. D., Stutchbury, B., Jacquemet, G., Ballestrem, C., Barry, S. T. & Humphries, M. J. (2016b). Modulation of FAK and Src adhesion signaling occurs independently of adhesion complex composition. *Journal of Cell Biology,* 212(3)**,** 349-364.

Hu, P. & Luo, B. H. (2013). Integrin bi-directional signaling across the plasma membrane. *Journal of Cellular Physiology,* 228(2)**,** 306-312.

Huang, C., Liu, J., Haudenschild, C. C. & Zhan, X. (1998). The role of tyrosine phosphorylation of cortactin in the locomotion of endothelial cells. *Journal of Biological Chemistry,* 273(40)**,** 25770-25776.

Huang, D. W., Sherman, B. T. & Lempicki, R. A. (2008). Bioinformatics enrichment tools: paths toward the comprehensive functional analysis of large gene lists. *Nucleic Acids Research,* 37(1)**,** 1-13.

Huang, D. W., Sherman, B. T. & Lempicki, R. A. (2009). Systematic and integrative analysis of large gene lists using DAVID bioinformatics resources. *Nature Protocols,* 4(1)**,** 44.

Huang, I.-H., Hsiao, C.-T., Wu, J.-C., Shen, R.-F., Liu, C.-Y., Wang, Y.-K., Chen, Y.-C., Huang, C.-M., Chang, Z.-F. & Tang, M.-J. (2014). GEF-H1 controls focal adhesion signaling that regulates mesenchymal stem cell lineage commitment. *Journal of Cell Science,* 127(19)**,** 4186-4200.

Huang, P. H. (2012). Phosphoproteomic studies of receptor tyrosine kinases: future perspectives. *Molecular BioSystems,* 8(4)**,** 1100-1107.

Huang, X., Griffiths, M., Wu, J., Farese, R. V. & Sheppard, D. (2000a). Normal development, wound healing, and adenovirus susceptibility in β5-deficient mice. *Molecular and Cellular Biology,* 20(3)**,** 755-759.

Huang, X., Wu, J., Ferrando, R., Lee, J., Wang, Y., Farese, R. & Sheppard, D. (2000b). Fatal bilateral chylothorax in mice lacking the integrin α9β1. *Molecular and Cellular Biology,* 20(14)**,** 5208-5215.

Hughes, J.P., Rees, S., Kalindjian, S.B. and Philpott, K.L. (2011). Principles of early drug discovery. *British Journal of Pharmacology*, 162(6), 1239-1249.

Humphries, J. D., Byron, A., Bass, M. D., Craig, S. E., Pinney, J. W., Knight, D. & Humphries, M. J. (2009). Proteomic analysis of integrin-associated complexes identifies RCC2 as a dual regulator of Rac1 and Arf6. *Science Signaling,* 2(87)**,** ra51.

Humphries, J. D., Byron, A. & Humphries, M. J. (2006). Integrin ligands at a glance. *Journal of Cell Science,* 119(19)**,** 3901-3903.

Humphries, M. (2004). Monoclonal antibodies as probes of integrin priming and activation. *Biochemical Society Transactions,* 32(3)**,** 407-411.

Hurwitz, H., Fehrenbacher, L., Novotny, W., Cartwright, T., Hainsworth, J., Heim, W., Berlin, J., Baron, A., Griffing, S. & Holmgren, E. (2004). Bevacizumab plus irinotecan, fluorouracil, and leucovorin for metastatic colorectal cancer. *New England Journal of Medicine,* 350(23)**,** 2335-2342.

Hynes, R. O. (1992). Integrins: versatility, modulation, and signaling in cell adhesion. *Cell,* 69(1)**,** 11-25.

Hynes, R. O. (1999). Cell adhesion: old and new questions. *Trends in Biochemical Sciences,* 24(12)**,** M33-M37.

Hynes, R. O. (2002a). Integrins: bidirectional, allosteric signaling machines. *Cell,* 110(6)**,** 673-687.

Hynes, R. O. (2002b). A reevaluation of integrins as regulators of angiogenesis. *Nature Medicine,* 8(9)**,** 918-921.

Ishihama, Y. & Imami, K. (2014). Quantitation of cellular phosphorylation dynamics by phosphoproteomics approaches. *Yakugaku Zasshi: Journal of the Pharmaceutical Society of Japan,* 134(4)**,** 521-527.

Ivy, S. P., Wick, J. Y. & Kaufman, B. M. (2009). An overview of small-molecule inhibitors of VEGFR signaling. *Nature Reviews Clinical Oncology,* 6(10)**,** 569-579.

Jain, A., Kaczanowska, S., & Davila, E. (2014). IL-1 receptor-associated kinase signaling and its role in inflammation, cancer progression, and therapy resistance. *Frontiers in Immunology*, *5*, 553.

Jones, M. C., Humphries, J. D., Byron, A., Millon-Frémillon, A., Robertson, J., Paul, N. R., Ng, D. H., Askari, J. A. & Humphries, M. J. (2015). Isolation of integrin-based adhesion complexes. *Current Protocols in Cell Biology***,** 9.8. 1-9.8. 15.

Juliano, R. (2002). Signal transduction by cell adhesion receptors and the cytoskeleton: functions of integrins, cadherins, selectins, and immunoglobulin-superfamily members. *Annual Review of Pharmacology and Toxicology,* 42(1)**,** 283-323.

Kalluri, R. (2003). Basement membranes: structure, assembly and role in tumour angiogenesis. *Nature Reviews Cancer,* 3(6)**,** 422-433.

Kanchanawong, P., Shtengel, G., Pasapera, A. M., Ramko, E. B., Davidson, M. W., Hess, H. F. & Waterman, C. M. (2010). Nanoscale architecture of integrin-based cell adhesions. *Nature,* 468(7323)**,** 580.

Kanshin, E., Michnick, S. & Thibault, P. (Year). Sample preparation and analytical strategies for large-scale phosphoproteomics experiments. *In:* Seminars in Cell and Developmental Biology, 2012. Elsevier, 843-853.

Kelley, L. C., Hayes, K. E., Ammer, A. G., Martin, K. H. & Weed, S. A. (2010). Cortactin phosphorylated by ERK1/2 localizes to sites of dynamic actin regulation and is required for carcinoma lamellipodia persistence. *PloS one,* 5(11)**,** e13847.

Kelstrup, C. D., Young, C., Lavallee, R., Nielsen, M. L. & Olsen, J. V. (2012). Optimized fast and sensitive acquisition methods for shotgun proteomics on a quadrupole orbitrap mass spectrometer. *Journal of Proteome Research,* 11(6)**,** 3487-3497.

Kim, L. C., Song, L. & Haura, E. B. (2009). Src kinases as therapeutic targets for cancer. *Nature reviews Clinical oncology,* 6(10)**,** 587-595.

Kim, S., Bakre, M., Yin, H. & Varner, J. A. (2002). Inhibition of endothelial cell survival and angiogenesis by protein kinase A. *The Journal of Clinical Investigation,* 110(7)**,** 933.

Kim, S., Bell, K., Mousa, S. A. & Varner, J. A. (2000a). Regulation of angiogenesis in vivo by ligation of integrin α5β1 with the central cell-binding domain of fibronectin. *The American Journal of Pathology,* 156(4)**,** 1345-1362.

Kim, S., Harris, M. & Varner, J. A. (2000b). Regulation of integrin αvβ3-mediated endothelial cell migration and angiogenesis by integrin α5β1 and protein kinase A. *Journal of Biological Chemistry,* 275(43)**,** 33920-33928.

Kirchner, J., Kam, Z., Tzur, G., Bershadsky, A. D. & Geiger, B. (2003). Live-cell monitoring of tyrosine phosphorylation in focal adhesions following microtubule disruption. *Journal of Cell Science,* 116(6)**,** 975-986.

Koch, S. & Claesson-Welsh, L. (2012). Signal transduction by vascular endothelial growth factor receptors. *Cold Spring Harbor Perspectives in Medicine,* 2(7)**,** a006502.

Koch, S., Tugues, S., Li, X., Gualandi, L. & Claesson-Welsh, L. (2011). Signal transduction by vascular endothelial growth factor receptors. *Biochemical Journal,* 437(2)**,** 169-183.

Kopec, K. K., Bozyczko-Coyne, D., & Williams, M. (2005). Target identification and validation in drug discovery: the role of proteomics. *Biochemical Pharmacology*, 69(8), 1133-1139.

Kumar, V., Viji, R., Kiran, M. & Sudhakaran, P. R. (2012). Angiogenic response of endothelial cells to fibronectin. *Biochemical Roles of Eukaryotic Cell Surface Macromolecules.* Springer.

Kuo, J.-C., Han, X., Hsiao, C.-T., Yates III, J. R. & Waterman, C. M. (2011). Analysis of the myosin-II-responsive focal adhesion proteome reveals a role for β-Pix in negative regulation of focal adhesion maturation. *Nature Cell Biology,* 13(4)**,** 383-393.

Kuo, J.-C., Han, X., Yates, J. R. & Waterman, C. M. (2012). Isolation of focal adhesion proteins for biochemical and proteomic analysis. *Integrin and Cell Adhesion Molecules: Methods and Protocols***,** 297-323.

Lampugnani, M. G. (1999). Cell migration into a wounded area in vitro. *Adhesion Protein Protocols***,** 177-182.

Lang, I., Pabst, M. A., Hiden, U., Blaschitz, A., Dohr, G., Hahn, T. & Desoye, G. (2003). Heterogeneity of microvascular endothelial cells isolated from human term placenta and macrovascular umbilical vein endothelial cells. *European Journal of Cell Biology,* 82(4)**,** 163-173.

Launay, G., Salza, R., Multedo, D., Thierry-Mieg, N. & Ricard-Blum, S. (2014). MatrixDB, the extracellular matrix interaction database: updated content, a new navigator and expanded functionalities. *Nucleic Acids Research,* 43(D1)**,** D321-D327.

Lee, S. H., Schloss, D. J., Jarvis, L., Krasnow, M. A. & Swain, J. L. (2001). Inhibition of angiogenesis by a mouse sprouty protein. *Journal of Biological Chemistry,* 276(6)**,** 4128-4133.

Lee, T.-H., Seng, S., Li, H., Kennel, S. J., Avraham, H. K. & Avraham, S. (2006). Integrin regulation by VEGF in human brain microvascular endothelial cells: role of α6β1 integrin in angiogenesis. *Journal of Biological Chemistry,* 281(52)**,** 40450-40460.

Legate, K. R. & Fässler, R. (2009). Mechanisms that regulate adaptor binding to β-integrin cytoplasmic tails. *Journal of Cell Science,* 122(2)**,** 187-198.

Legler, D. F., Wiedle, G., Ross, F. P. & Imhof, B. A. (2001). Superactivation of integrin αvβ3 by low antagonist concentrations. *Journal of Cell Science,* 114(8)**,** 1545-1553.

Lele, T. P., Thodeti, C. K., Pendse, J. & Ingber, D. E. (2008). Investigating complexity of protein–protein interactions in focal adhesions. *Biochemical and Biophysical Research Communications,* 369(3)**,** 929-934.

Lesslie III, D., Summy, J., Parikh, N., Fan, F., Trevino, J., Sawyer, T., Metcalf III, C., Shakespeare, W., Hicklin, D. & Ellis, L. (2006). Vascular endothelial growth factor receptor-1 mediates migration of human colorectal carcinoma cells by activation of Src family kinases. *British Journal of Cancer,* 94(11)**,** 1710.

Liu, H., Sadygov, R. G. & Yates, J. R. (2004). A model for random sampling and estimation of relative protein abundance in shotgun proteomics. *Analytical Chemistry,* 76(14)**,** 4193-4201.

Liu, K., Zhang, J., Wang, J., Zhao, L., Peng, X., Jia, W., Ying, W., Zhu, Y., Xie, H. & He, F. (2009). Relationship between sample loading amount and peptide identification and its effects on quantitative proteomics. *Analytical Chemistry,* 81(4)**,** 1307-1314.

Lua, B. L. & Low, B. C. (2005). Cortactin phosphorylation as a switch for actin cytoskeletal network and cell dynamics control. *FEBS Letters,* 579(3)**,** 577-585.

Lundgren, D. H., Hwang, S.-I., Wu, L. & Han, D. K. (2010). Role of spectral counting in quantitative proteomics. *Expert Review of Proteomics,* 7(1)**,** 39-53.

Luo, B.-H. & Springer, T. A. (2006). Integrin structures and conformational signaling. *Current Opinion in Cell Biology,* 18(5)**,** 579-586.

Maeshima, Y., Sudhakar, A., Lively, J. C., Ueki, K., Kharbanda, S., Kahn, C. R., Sonenberg, N., Hynes, R. O. & Kalluri, R. (2002). Tumstatin, an endothelial cell-specific inhibitor of protein synthesis. *Science,* 295**,** 140-143.

Mahabaleshwar, G. H. & Byzova, T. (2008). Regulation of VEGF induced angiogenesis by β3 integrin through recruitment of VEGFR-2 associated protein tyrosine phosphatase. *The FASEB Journal,* 22(1 Supplement)**,** 746.8-746.8.

Mahabeleshwar, G. H., Feng, W., Phillips, D. R. & Byzova, T. V. (2006). Integrin signaling is critical for pathological angiogenesis. *Journal of Experimental Medicine,* 203(11)**,** 2495-2507.

Mahabeleshwar, G. H., Feng, W., Reddy, K., Plow, E. F. & Byzova, T. V. (2007). Mechanisms of integrin–VEGFR cross-activation in angiogenesis. *Circulation Research,* 101(6)**,** 570-580.

Mann, M. (2009). Comparative analysis to guide quality improvements in proteomics. *Nature Methods,* 6(10)**,** 717-719.

Martin, S. & Murray, J. C. (2009). *Angiogenesis protocols*: Springer.

Martino, M. M., Briquez, P. S., Ranga, A., Lutolf, M. P. & Hubbell, J. A. (2013). Heparin-binding domain of fibrin (ogen) binds growth factors and promotes tissue repair when incorporated within a synthetic matrix. *Proceedings of the National Academy of Sciences,* 110(12)**,** 4563-4568.

Martino, M. M., Brkic, S., Bovo, E., Burger, M., Schaefer, D. J., Wolff, T., Gürke, L., Briquez, P. S., Larsson, H. M. & Gianni-Barrera, R. (2015). Extracellular matrix and growth factor engineering for controlled angiogenesis in regenerative medicine. *Frontiers in Bioengineering and Biotechnology,* 3.

Martino, M. M., Tortelli, F., Mochizuki, M., Traub, S., Ben-David, D., Kuhn, G. A., Müller, R., Livne, E., Eming, S. A. & Hubbell, J. A. (2011). Engineering the growth factor microenvironment with fibronectin domains to promote wound and bone tissue healing. *Science Translational Medicine,* 3(100)**,** 100ra89-100ra89.

Mas-Moruno, C., Rechenmacher, F. & Kessler, H. (2010). Cilengitide: the first anti-angiogenic small molecule drug candidate. Design, synthesis and clinical evaluation. *Anti-Cancer Agents in Medicinal Chemistry,* 10(10)**,** 753.

Masson-Gadais, B., Houle, F., Laferrière, J. & Huot, J. (2003). Integrin αvβ3 requirement for VEGFR2-mediated activation of SAPK2/p38 and for Hsp90-dependent phosphorylation of focal adhesion kinase in endothelial cells activated by VEGF. *Cell Stress & Chaperones,* 8(1)**,** 37-52.

Matsui, H., Harada, I. & Sawada, Y. (2012). Src, p130Cas, and mechanotransduction in cancer cells. *Genes & Cancer,* 3(5-6)**,** 394-401.

Maubant, S., Saint-Dizier, D., Boutillon, M., Perron-Sierra, F., Casara, P. J., Hickman, J. A., Tucker, G. C. & Van Obberghen-Schilling, E. (2006). Blockade of αvβ3 and αvβ5 integrins by RGD mimetics induces anoikis and not integrin-mediated death in human endothelial cells. *Blood,* 108(9)**,** 3035-3044.

McInnes, I. B., & Schett, G. (2007). Cytokines in the pathogenesis of rheumatoid arthritis. *Nature Reviews Immunology*, 7(6), 429.

Miles, D. W., Chan, A., Dirix, L. Y., Cortés, J., Pivot, X., Tomczak, P., Delozier, T., Sohn, J. H., Provencher, L. & Puglisi, F. (2010). Phase III study of bevacizumab plus docetaxel compared with placebo plus docetaxel for the first-line treatment of human epidermal growth factor receptor 2–negative metastatic breast cancer. *Journal of Clinical Oncology,* 28(20)**,** 3239-3247.

Miller, M. L., Brunak, S., Olsen, J., Vermeulen, M., Santamaria, A., Kumar, C., Jensen, L., Gnad, F., Cox, J. & Jensen, T. S. (2010). Quantitative phosphoproteomics reveals widespread full phosphorylation site occupancy during mitosis. *Science Signaling,* 3(104).

Mitra, S. K., Hanson, D. A. & Schlaepfer, D. D. (2005). Focal adhesion kinase: in command and control of cell motility. *Nature Reviews Molecular Cell Biology,* 6(1)**,** 56.

Montoya, A., Beltran, L., Casado, P., Rodríguez-Prados, J.-C. & Cutillas, P. R. (2011). Characterization of a TiO2 enrichment method for label-free quantitative phosphoproteomics. *Methods,* 54(4)**,** 370-378.

Morgan, M. R., Humphries, M. J. & Bass, M. D. (2007). Synergistic control of cell adhesion by integrins and syndecans. *Nature Reviews Molecular Cell Biology,* 8(12)**,** 957.

Morris, M. K., Chi, A., Melas, I. N., & Alexopoulos, L. G. (2014). Phosphoproteomics in drug discovery. *Drug Discovery Today*, 19(4), 425-432.

Morse, E. M., Brahme, N. N. & Calderwood, D. A. (2014). Integrin cytoplasmic tail interactions. *Biochemistry,* 53(5)**,** 810-820.

Mould, A., Garratt, A., PUZON-McLAUGHLIN, W., TAKADA, Y. & Humphries, M. (1998). Regulation of integrin function: evidence that bivalent-cation-induced conformational changes lead to the unmasking of ligand-binding sites within integrin α5β1. *Biochemical Journal,* 331**,** 821-828.

Mould, A. P. & Humphries, M. J. (2004). Cell biology: adhesion articulated. *Nature,* 432(7013)**,** 27-28.

Moulton, K. S. (2006). Angiogenesis in atherosclerosis: gathering evidence beyond speculation. *Current Opinion in Lipidology,* 17(5)**,** 548-555.

Muether, P. S., Dell, S., Kociok, N., Zahn, G., Stragies, R., Vossmeyer, D. & Joussen, A. M. (2007). The role of integrin α5β1 in the regulation of corneal neovascularization. *Experimental Eye Research,* 85(3)**,** 356-365.

Munoz-Chapuli, R., Quesada, A. & Medina, M. A. (2004). Angiogenesis and signal transduction in endothelial cells. *Cellular and Molecular Life Sciences,* 61(17)**,** 2224-2243.

Murphy, P. A., Begum, S. & Hynes, R. O. (2015). Tumor Angiogenesis in the Absence of Fibronectin or Its Cognate Integrin Receptors. *PloS one,* 10(3).

Nagano, K., Akpan, A., Warnasuriya, G., Corless, S., Totty, N., Yang, A., Stein, R., Zvelebil, M., Stensballe, A. & Burlingame, A. (2012). Functional proteomic analysis of long-term growth factor stimulation and receptor tyrosine kinase coactivation in Swiss 3T3 fibroblasts. *Molecular & Cellular Proteomics,* 11(12)**,** 1690-1708.

Ng, D. H., Humphries, J. D., Byron, A., Millon-Frémillon, A. & Humphries, M. J. (2014). Microtubule-dependent modulation of adhesion complex composition. *PloS one,* 9(12)**,** e115213.

Ng, D. H., Humphries, J. D., Selley, J. N., Warwood, S., Knight, D., Byron, A. & Humphries, M. J. (2017). Improved LC-MS chromatographic alignment increases the accuracy of label-free quantitative proteomics: Comparison of spectral counting versus ion intensity-based proteomic quantification strategies. *bioRxiv***,** 111476.

Nikolopoulos, S. N., Blaikie, P., Yoshioka, T., Guo, W. & Giancotti, F. G. (2004). Integrin β4 signaling promotes tumor angiogenesis. *Cancer Cell,* 6(5)**,** 471-483.

Niland, S. & Eble, J. A. (2011). Integrin-mediated cell-matrix interaction in physiological and pathological blood vessel formation. *Journal of Oncology,* 2012.

Nussenbaum, F. & Herman, I. M. (2010). Tumor angiogenesis: insights and innovations. *Journal of Oncology,* 2010.

Old, W. M., Meyer-Arendt, K., Aveline-Wolf, L., Pierce, K. G., Mendoza, A., Sevinsky, J. R., Resing, K. A. & Ahn, N. G. (2005). Comparison of label-free methods for quantifying human proteins by shotgun proteomics. *Molecular and Cellular Proteomics,* 4(10)**,** 1487-1502.

Papetti, M. & Herman, I. M. (2002). Mechanisms of normal and tumor-derived angiogenesis. *American Journal of Physiology-Cell Physiology,* 282(5)**,** C947-C970.

Park, H.-J., Zhang, Y., Georgescu, S. P., Johnson, K. L., Kong, D. & Galper, J. B. (2006). Human umbilical vein endothelial cells and human dermal microvascular endothelial cells offer new insights into the relationship between lipid metabolism and angiogenesis. *Stem Cell Reviews and Reports,* 2(2)**,** 93-101.

Paul, N. (2014). Proteomic and phosphoproteomic analysis of signalling by adhesion and growth factor receptors in mammary epithelial cells. *PhD thesis, The University of Manchester,* https://www.escholar.manchester.ac.uk/uk-ac-man-scw:217929.

Playford, M. P. & Schaller, M. D. (2004). The interplay between Src and integrins in normal and tumor biology. *Oncogene,* 23(48)**,** 7928.

Pouwels, J., Nevo, J., Pellinen, T., Ylänne, J. & Ivaska, J. (2012). Negative regulators of integrin activity. *Journal of Cell Science,* 125(14)**,** 3271-3280.

Pozzi, A., Moberg, P. E., Miles, L. A., Wagner, S., Soloway, P. & Gardner, H. A. (2000). Elevated matrix metalloprotease and angiostatin levels in integrin α1 knockout mice cause reduced tumor vascularization. *Proceedings of the National Academy of Sciences,* 97(5)**,** 2202-2207.

Rapisarda, A. & Melillo, G. (2009). Role of the hypoxic tumor microenvironment in the resistance to anti-angiogenic therapies. *Drug Resistance Updates,* 12(3)**,** 74-80.

Ravelli, C., Mitola, S., Corsini, M. & Presta, M. (2013). Involvement of αvβ3 integrin in gremlin-induced angiogenesis. *Angiogenesis,* 16(1)**,** 235-243.

Reck, M., Von Pawel, J., Zatloukal, P. v., Ramlau, R., Gorbounova, V., Hirsh, V., Leighl, N., Mezger, J., Archer, V. & Moore, N. (2010). Overall survival with cisplatin–gemcitabine and bevacizumab or placebo as first-line therapy for nonsquamous non-small-cell lung cancer: results from a randomised phase III trial (AVAiL). *Annals of Oncology,* 21(9)**,** 1804-1809.

Reddy, R. J., Gajadhar, A. S., Swenson, E. J., Rothenberg, D. A., Curran, T. G. & White, F. M. (2016). Early signaling dynamics of the epidermal growth factor receptor. *Proceedings of the National Academy of Sciences,* 113(11)**,** 3114-3119.

Reynolds, A. R., Hart, I. R., Watson, A. R., Welti, J. C., Silva, R. G., Robinson, S. D., Da Violante, G., Gourlaouen, M., Salih, M. & Jones, M. C. (2009). Stimulation of tumor growth and angiogenesis by low concentrations of RGD-mimetic integrin inhibitors. *Nature Medicine,* 15(4)**,** 392.

Reynolds, A. R., Reynolds, L. E., Nagel, T. E., Lively, J. C., Robinson, S. D., Hicklin, D. J., Bodary, S. C. & Hodivala-Dilke, K. M. (2004). Elevated Flk1 (vascular endothelial growth factor receptor 2) signaling mediates enhanced angiogenesis in β3-integrin–deficient mice. *Cancer Research,* 64(23)**,** 8643-8650.

Reynolds, L. E., Wyder, L., Lively, J. C., Taverna, D., Robinson, S. D., Huang, X., Sheppard, D., Hynes, R. O. & Hodivala-Dilke, K. M. (2002). Enhanced pathological angiogenesis in mice lacking β3 integrin or β3 and β5 integrins. *Nature Medicine,* 8(1)**,** 27-34.

Robertson, J. (2014). Phosphoproteomic analysis of adhesion receptor signalling. *PhD thesis, The University of Manchester,* https://www.escholar.manchester.ac.uk/uk-ac-man-scw:217302.

Robertson, J., Humphries, J. D., Paul, N. R., Warwood, S., Knight, D., Byron, A. & Humphries, M. J. (2017). Characterization of the phospho-adhesome by mass spectrometry-based proteomics. *Kinase Signaling Networks.* Springer.

Robertson, J., Jacquemet, G., Byron, A., Jones, M. C., Warwood, S., Selley, J. N., Knight, D., Humphries, J. D. & Humphries, M. J. (2015). Defining the phospho-adhesome through the phosphoproteomic analysis of integrin signalling. *Nature Communications,* 6.

Robinson, S. D., Reynolds, L. E., Wyder, L., Hicklin, D. J. & Hodivala-Dilke, K. M. (2004). β3-Integrin regulates vascular endothelial growth factor-A–dependent permeability. *Arteriosclerosis Thrombosis and Vascular Biology,* 24(11)**,** 2108-2114.

Sadygov, R. G., Cociorva, D. & Yates, J. R. (2004). Large-scale database searching using tandem mass spectra: looking up the answer in the back of the book. *Nature Methods,* 1(3)**,** 195.

Sakurai, T. & Kudo, M. (2011). Signaling pathways governing tumor angiogenesis. *Oncology,* 81(Suppl. 1)**,** 24-29.

Scheltema, R. A., Hauschild, J.-P., Lange, O., Hornburg, D., Denisov, E., Damoc, E., Kuehn, A., Makarov, A. & Mann, M. (2014). The Q Exactive HF, a Benchtop mass spectrometer with a pre-filter, high-performance quadrupole and an ultra-high-field Orbitrap analyzer. *Molecular and Cellular Proteomics,* 13(12)**,** 3698-3708.

Schiller, H. B. & Fässler, R. (2013). Mechanosensitivity and compositional dynamics of cell–matrix adhesions. *European Molecular Biology Organization Reports,* 14(6)**,** 509-519.

Schiller, H. B., Friedel, C. C., Boulegue, C. & Fässler, R. (2011). Quantitative proteomics of the integrin adhesome show a myosin II-dependent recruitment of LIM domain proteins. *European Molecular Biology Organization Reports,* 12(3)**,** 259-266.

Schlessinger, J. (2000). Cell signaling by receptor tyrosine kinases. *Cell,* 103(2)**,** 211-225.

Seaman, S., Stevens, J., Yang, M. Y., Logsdon, D., Graff-Cherry, C. & Croix, B. S. (2007). Genes that distinguish physiological and pathological angiogenesis. *Cancer Cell,* 11(6)**,** 539-554.

Searle, B. C. (2010). Scaffold: a bioinformatic tool for validating MS/MS-based proteomic studies. *Proteomics,* 10(6)**,** 1265-1269.

Senger, D. R., Claffey, K. P., Benes, J. E., Perruzzi, C. A., Sergiou, A. P. & Detmar, M. (1997). Angiogenesis promoted by VEGF: regulation through α1β1 and α2β1 integrins. *Proceedings of the National Academy of Sciences,* 94(25)**,** 13612-13617.

Senger, D. R. & Davis, G. E. (2011). Angiogenesis. *Cold Spring Harbor Perspectives in Biology,* 3(8)**,** a005090.

Sharma, K., D'Souza, R. C., Tyanova, S., Schaab, C., Wiśniewski, J. R., Cox, J. & Mann, M. (2014). Ultradeep human phosphoproteome reveals a distinct regulatory nature of Tyr and Ser/Thr-based signaling. *Cell Reports,* 8(5)**,** 1583-1594.

Sheppard, D. (2002). Endothelial integrins and angiogenesis: not so simple anymore. *The Journal of Clinical Investigation,* 110(7)**,** 913-914.

Shi, L., Fisslthaler, B., Zippel, N., Frömel, T., Hu, J., Elgheznawy, A., Heide, H., Popp, R. & Fleming, I. (2013). MicroRNA-223 antagonizes angiogenesis by targeting β1 integrin and preventing growth factor signaling in endothelial cells. *Circulation Research,* 113(12)**,** 1320-1330.

Shojaei, F. (2012). Anti-angiogenesis therapy in cancer: current challenges and future perspectives. *Cancer Letters,* 320(2)**,** 130-137.

Sieg, D. J., Hauck, C. R., Ilic, D., Klingbeil, C. K., Schaefer, E., Damsky, C. H. & Schlaepfer, D. D. (2000). FAK integrates growth-factor and integrin signals to promote cell migration. *Nature Cell Biology,* 2(5)**,** 249.

Silva, R., D'amico, G., Hodivala-Dilke, K. M. & Reynolds, L. E. (2008). Integrins: the keys to unlocking angiogenesis. *Arteriosclerosis, thrombosis, and vascular biology,* 28(10)**,** 1703-1713.

Simons, M. (2005). Angiogenesis where do we stand now? *Circulation,* 111(12)**,** 1556-1566.

Simons, M., Gordon, E. & Claesson-Welsh, L. (2016). Mechanisms and regulation of endothelial VEGF receptor signalling. *Nature Reviews Molecular Cell Biology,* 17(10)**,** 611-625.

Smith, J. W., Ruggeri, Z., Kunicki, T. & Cheresh, D. (1990). Interaction of integrins alpha v beta 3 and glycoprotein IIb-IIIa with fibrinogen. Differential peptide recognition accounts for distinct binding sites. *Journal of Biological Chemistry,* 265(21)**,** 12267-12271.

Solari, F. A., Dell'Aica, M., Sickmann, A. & Zahedi, R. P. (2015). Why phosphoproteomics is still a challenge. *Molecular BioSystems,* 11(6)**,** 1487-1493.

Soldi, R., Mitola, S., Strasly, M., Defilippi, P., Tarone, G. & Bussolino, F. (1999). Role of αvβ3 integrin in the activation of vascular endothelial growth factor receptor-2. *The EMBO Journal,* 18(4)**,** 882-892.

Somanath, P. R., Ciocea, A. & Byzova, T. V. (2009a). Integrin and growth factor receptor alliance in angiogenesis. *Cell Biochemistry and Biophysics,* 53(2)**,** 53-64.

Somanath, P. R., Malinin, N. L. & Byzova, T. V. (2009b). Cooperation between integrin αvβ3 and VEGFR2 in angiogenesis. *Angiogenesis,* 12(2)**,** 177-185.

Song, C., Ye, M., Liu, Z., Cheng, H., Jiang, X., Han, G., Songyang, Z., Tan, Y., Wang, H. & Ren, J. (2012). Systematic analysis of protein phosphorylation networks from phosphoproteomic data. *Molecular and Cellular Proteomics,* 11(10)**,** 1070-1083.

Staton, C. A., Lewis, C. & Bicknell, R. (2007). *Angiogenesis Assays: A critical appraisal of current techniques*: John Wiley & Sons.

Streuli, C. H. & Akhtar, N. (2009). Signal co-operation between integrins and other receptor systems. *Biochemical Journal,* 418(3)**,** 491-506.

Strömblad, S. & Cheresh, D. A. (1996). Cell adhesion and angiogenesis. *Trends in Cell Biology,* 6(12)**,** 462-468.

Stupack, D. G. & Cheresh, D. A. (2002). ECM remodeling regulates angiogenesis: endothelial integrins look for new ligands. *Science Signalling,* 119(7).

Stupack, D. G. & Cheresh, D. A. (2004). A Bit-role for integrins in apoptosis. *Nature Cell Biology,* 6(5)**,** 388-389.

Sulzmaier, F. J., Jean, C. & Schlaepfer, D. D. (2014). FAK in cancer: mechanistic findings and clinical applications. *Nature Reviews Cancer,* 14(9)**,** 598-610.

Sun, L., Zhu, G. & Dovichi, N. J. (2013). Comparison of the LTQ-Orbitrap Velos and the Q-Exactive for proteomic analysis of 1–1000 ng RAW 264.7 cell lysate digests. *Rapid Communications in Mass Spectrometry,* 27(1)**,** 157-162.

Sun, Z., Lambacher, A. & Fässler, R. (2014). Nascent adhesions: from fluctuations to a hierarchical organization. *Current Biology,* 24(17)**,** R801-R803.

Tadokoro, S., Shattil, S. J., Eto, K., Tai, V., Liddington, R. C., de Pereda, J. M., Ginsberg, M. H. & Calderwood, D. A. (2003). Talin binding to integrin ß tails: a final common step in integrin activation. *Science,* 302(5642)**,** 103-106.

Takahashi, S., Leiss, M., Moser, M., Ohashi, T., Kitao, T., Heckmann, D., Pfeifer, A., Kessler, H., Takagi, J. & Erickson, H. P. (2007). The RGD motif in fibronectin is essential for development but dispensable for fibril assembly. *The Journal of Cell Biology,* 178(1)**,** 167-178.

Takahashi, T., Yamaguchi, S., Chida, K. & Shibuya, M. (2001). A single autophosphorylation site on KDR/Flk-1 is essential for VEGF-A-dependent activation of PLC-γ and DNA synthesis in vascular endothelial cells. *The EMBO Journal,* 20(11)**,** 2768-2778.

Taniguchi, K., Sasaki, K.-i., Watari, K., Yasukawa, H., Imaizumi, T., Ayada, T., Okamoto, F., Ishizaki, T., Kato, R. & Kohno, R.-i. (2009). Suppression of Sproutys has a therapeutic effect for a mouse model of ischemia by enhancing angiogenesis. *PloS one,* 4(5)**,** e5467.

Tanne, J. H. (2011). FDA cancels approval for bevacizumab in advanced breast cancer. *BMJ: British Medical Journal (Online),* 343.

Tape, C. J., Worboys, J. D., Sinclair, J., Gourlay, R., Vogt, J., McMahon, K. M., Trost, M., Lauffenburger, D. A., Lamont, D. J. & Jørgensen, C. (2014). Reproducible automated phosphopeptide enrichment using magnetic TiO2 and Ti-IMAC. *Analytical Chemistry,* 86(20)**,** 10296-10302.

Thingholm, T. E. & Jensen, O. N. (2009). Enrichment and characterization of phosphopeptides by immobilized metal affinity chromatography (IMAC) and mass spectrometry. *Phospho-Proteomics: Methods and Protocols***,** 47-56.

Thingholm, T. E. & Larsen, M. R. (2009). The use of titanium dioxide micro-columns to selectively isolate phosphopeptides from proteolytic digests. *Phospho-Proteomics: Methods and Protocols***,** 57-66.

Tugues, S., Honjo, S., König, C., Padhan, N., Kroon, J., Gualandi, L., Li, X., Barkefors, I., Thijssen, V. L. & Griffioen, A. W. (2013). Tetraspanin CD63 promotes VEGFR2-β1 integrin complex formation, thereby regulating activation and downstream signaling in endothelial cells in vitro and in vivo. *Journal of Biological Chemistry,* 288(26)**,** 19060-19071.

Umeda, N., Kachi, S., Akiyama, H., Zahn, G., Vossmeyer, D., Stragies, R. & Campochiaro, P. A. (2006). Suppression and regression of choroidal neovascularization by systemic administration of an α5β1 integrin antagonist. *Molecular Pharmacology,* 69(6)**,** 1820-1828.

Vachon, P. H. (2011). Integrin signaling, cell survival, and anoikis: distinctions, differences, and differentiation. *Journal of Signal Transduction,* 2011.

Vailhé, B., Vittet, D. & Feige, J.-J. (2001). In vitro models of vasculogenesis and angiogenesis. *Laboratory Investigation,* 81(4)**,** 439.

van der Mijn, J. C., Labots, M., Piersma, S. R., Pham, T. V., Knol, J. C., Broxterman, H. J., Verheul, H. M. & Jiménez, C. R. (2015). Evaluation of different phospho-tyrosine antibodies for label-free phosphoproteomics. *Journal of Proteomics,* 127**,** 259-263.

Van Der Neut, R., Krimpenfort, P., Calafat, J., Niessen, C. M. & Sonnenberg, A. (1996). Epithelial detachment due to absence of hemidesmosomes in integrin β4 null mice. *Nature Genetics,* 13(3)**,** 366-369.

Viñals, F. & Pouysségur, J. (1999). Confluence of vascular endothelial cells induces cell cycle exit by inhibiting p42/p44 mitogen-activated protein kinase activity. *Molecular and Cellular Biology,* 19(4)**,** 2763-2772.

Vlahakis, N. E., Young, B. A., Atakilit, A., Hawkridge, A. E., Issaka, R. B., Boudreau, N. & Sheppard, D. (2007). Integrin α9β1 directly binds to vascular endothelial growth factor VEGF-A and contributes to VEGF-A-induced angiogenesis. *Journal of Biological Chemistry,* 282(20)**,** 15187-15196.

Vuori, K. (1998). Integrin signaling: tyrosine phosphorylation events in focal adhesions. *Journal of Membrane Biology,* 165(3)**,** 191-199.

Walther, T. C. & Mann, M. (2010). Mass spectrometry–based proteomics in cell biology. *The Journal of Cell Biology,* 190(4)**,** 491-500.

Wang, J., Taba, Y., Pang, J., Yin, G., Yan, C. & Berk, B. C. (2009). GIT1 mediates VEGF-induced podosome formation in endothelial cells. *Arteriosclerosis, thrombosis, and vascular biology,* 29(2)**,** 202-208.

Webb, D. J., Mayhew, M. W., Kovalenko, M., Schroeder, M. J., Jeffery, E. D., Whitmore, L., Shabanowitz, J., Hunt, D. F. & Horwitz, A. F. (2006). Identification of phosphorylation sites in GIT1. *Journal of Cell Science,* 119(14)**,** 2847-2850.

Weis, S. M., Lindquist, J. N., Barnes, L. A., Lutu-Fuga, K. M., Cui, J., Wood, M. R. & Cheresh, D. A. (2007). Cooperation between VEGF and β3 integrin during cardiac vascular development. *Blood,* 109(5)**,** 1962-1970.

Werdich, X. Q. & Penn, J. S. (2006). Src, Fyn and Yes play differential roles in VEGF-mediated endothelial cell events. *Angiogenesis,* 8(4)**,** 315-326.

West, X. Z., Meller, N., Malinin, N. L., Deshmukh, L., Meller, J., Mahabeleshwar, G. H., Weber, M. E., Kerr, B. A., Vinogradova, O. & Byzova, T. V. (2012). Integrin β3 crosstalk with VEGFR accommodating tyrosine phosphorylation as a regulatory switch. *Public Library of Science One,* 7(2)**,** e31071.

Wijelath, E. S., Murray, J., Rahman, S., Patel, Y., Ishida, A., Strand, K., Aziz, S., Cardona, C., Hammond, W. P. & Savidge, G. F. (2002). Novel vascular endothelial growth factor binding domains of fibronectin enhance vascular endothelial growth factor biological activity. *Circulation Research,* 91(1)**,** 25-31.

Wijelath, E. S., Rahman, S., Namekata, M., Murray, J., Nishimura, T., Mostafavi-Pour, Z., Patel, Y., Suda, Y., Humphries, M. J. & Sobel, M. (2006). Heparin-II domain of fibronectin is a vascular endothelial growth factor-binding domain. *Circulation Research,* 99(8)**,** 853-860.

Winograd-Katz, S. E., Fässler, R., Geiger, B. & Legate, K. R. (2014). The integrin adhesome: from genes and proteins to human disease. *Nature Reviews Molecular Cell Biology,* 15(4)**,** 273-288.

Wong, B. W., Marsch, E., Treps, L., Baes, M. & Carmeliet, P. (2017). Endothelial cell metabolism in health and disease: impact of hypoxia. *The EMBO Journal,* 36(15)**,** 2187-2203.

Yang, J. T., Bader, B. L., Kreidberg, J. A., Ullman-Culleré, M., Trevithick, J. E. & Hynes, R. O. (1999). Overlapping and independent functions of fibronectin receptor integrins in early mesodermal development. *Developmental Biology,* 215(2)**,** 264-277.

Yang, J. T., Rayburn, H. & Hynes, R. O. (1993). Embryonic mesodermal defects in α5 integrin-deficient mice. *Development,* 119(4)**,** 1093-1105.

Yang, J. T., Rayburn, H. & Hynes, R. O. (1995). Cell adhesion events mediated by α4 integrins are essential in placental and cardiac development. *Development,* 121(2)**,** 549-560.

Yang, W., Zhong, J., Yu, J., Zhao, F. & Xiang, Y. (2017). The structure and functions of paxillin and its roles in neovascularization. *European Review for Medical and Pharmacological Sciences,* 21**,** 1768-1773.

Yang, W. J., Yang, Y. N., Cao, J., Man, Z. H., Li, Y. & Xing, Y. Q. (2015). Paxillin regulates vascular endothelial growth factor A-induced in vitro angiogenesis of human umbilical vein endothelial cells. *Molecular Medicine Reports,* 11(3)**,** 1784-1792.

Yin, G., Haendeler, J., Yan, C. & Berk, B. C. (2004). GIT1 functions as a scaffold for MEK1-extracellular signal-regulated kinase 1 and 2 activation by angiotensin II and epidermal growth factor. *Molecular and Cellular Biology,* 24(2)**,** 875-885.

Zachary, I. & Gliki, G. (2001). Signaling transduction mechanisms mediating biological actions of the vascular endothelial growth factor family. *Cardiovascular research,* 49(3)**,** 568-581.

Zaidel-Bar, R. & Geiger, B. (2010). The switchable integrin adhesome. *Journal of Cell Science,* 123(9)**,** 1385-1388.

Zaidel-Bar, R., Itzkovitz, S., Ma'ayan, A., Iyengar, R. & Geiger, B. (2007). Functional atlas of the integrin adhesome. *Nature Cell Biology,* 9(8)**,** 858-867.

Zamir, E., Katz, B.-Z., Aota, S.-i., Yamada, K. M., Geiger, B. & Kam, Z. (1999). Molecular diversity of cell-matrix adhesions. *Journal of Cell Science,* 112(11)**,** 1655-1669.

Zhang, Z., Ramirez, N. E., Yankeelov, T. E., Li, Z., Ford, L. E., Qi, Y., Pozzi, A. & Zutter, M. M. (2008). α2β1 integrin expression in the tumor microenvironment enhances tumor angiogenesis in a tumor cell–specific manner. *Blood,* 111(4)**,** 1980-1988.

Zheng, Y., Zhang, C., Croucher, D. R., Soliman, M. A., St-Denis, N., Pasculescu, A., Taylor, L., Tate, S. A., Hardy, R. W. & Colwill, K. (2013). Temporal regulation of EGF signaling networks by the scaffold protein Shc1. *Nature,* 499(7457)**,** 166.

Zhou, X., Rowe, R. G., Hiraoka, N., George, J. P., Wirtz, D., Mosher, D. F., Virtanen, I., Chernousov, M. A. & Weiss, S. J. (2008). Fibronectin fibrillogenesis regulates three-dimensional neovessel formation. *Genes & Development,* 22(9)**,** 1231-1243.

Zhuang, G., Yu, K., Jiang, Z., Chung, A., Yao, J., Ha, C., Toy, K., Soriano, R., Haley, B. & Blackwood, E. (2013). Phosphoproteomic analysis implicates the mTORC2-FoxO1 axis in VEGF signaling and feedback activation of receptor tyrosine kinases. *Science Signaling,* 6(271)**,** ra25-ra25.

Appendix- Supplementary CD